ULTRASOUND ASSESSMENT IN GYNECOLOGIC ONCOLOGY

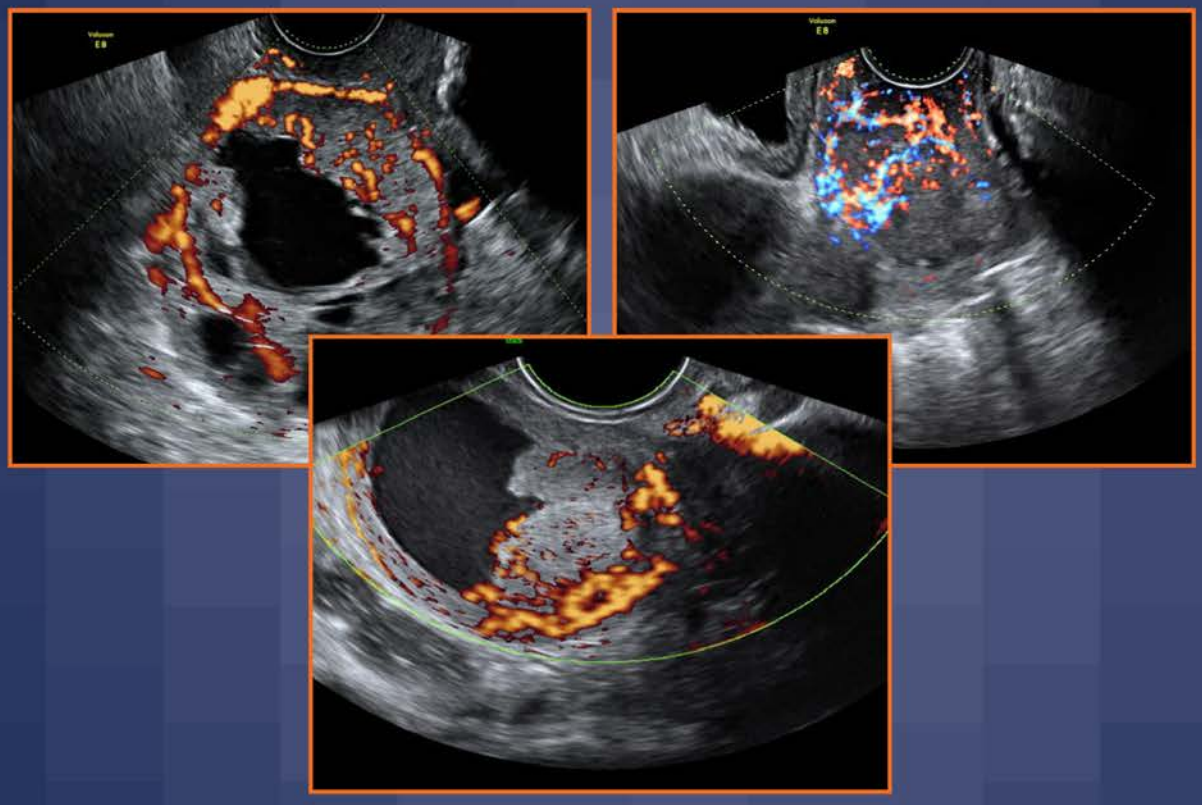

JUAN LUIS ALCÁZAR

CRC Press
Taylor & Francis Group

ULTRASOUND ASSESSMENT IN GYNECOLOGIC ONCOLOGY

Taylor & Francis
Taylor & Francis Group
http://taylorandfrancis.com

ULTRASOUND ASSESSMENT IN GYNECOLOGIC ONCOLOGY

JUAN LUIS ALCÁZAR, MD, PHD
Full Professor and Co-Chairman of the Department of Gynecology and Obstetrics
Medical School of the University of Navarra, Pamplona, Spain

CRC Press
Taylor & Francis Group
Boca Raton London New York

CRC Press is an imprint of the
Taylor & Francis Group, an **informa** business

CRC Press
Taylor & Francis Group
6000 Broken Sound Parkway NW, Suite 300
Boca Raton, FL 33487-2742

Printed on acid-free paper

International Standard Book Number-13: 978-1-138-04432-6 (Pack - Book and Ebook)

Library of Congress Cataloging-in-Publication Data

Names: Alcazar, Juan Luis, author.
Title: Ultrasound assessment in gynecologic oncology / Juan Luis Alcazar.
Description: Boca Raton, FL : CRC Press, 2018. | Includes bibliographical references and index.
Identifiers: LCCN 2017048078| ISBN 9781138044326 (pack- hardback and ebook : alk. paper) | ISBN 9781315172392 (ebook : alk. paper)
Subjects: | MESH: Genital Neoplasms, Female--diagnostic imaging | Ultrasonography
Classification: LCC RC280.G5 | NLM WP 145 | DDC 616.99/46--dc23
LC record available at https://lccn.loc.gov/2017048078

Visit the Taylor & Francis Web site at
http://www.taylorandfrancis.com

and the CRC Press Web site at
http://www.crcpress.com

Contents

Foreword vii
Preface ix

1 Ultrasound Scanning of the Female Pelvis: Normal Findings 1
Introduction 1
Pelvic Wall Structures 1
Nonreproductive Organs 1
Reproductive Organs 3
References 7

2 Ultrasound for Differential Diagnosis of Adnexal Masses 9
Introduction 9
Pattern Recognition 9
Scoring Systems 10
Simple Rules 10
Logistic Regression Models 12
Reporting Ultrasound Findings of Adnexal Masses 12
Other Imaging Techniques for Differential Diagnosis of Adnexal Masses 13
Ultrasound-Based Imaging Techniques 13
Other Imaging Techniques 15
References 16

3 Ultrasound Features of Ovarian Malignancies 17
Introduction 17
Borderline Tumors 17
Primary Epithelial Invasive Ovarian Carcinoma 18
Primary Nonepithelial Ovarian Malignancies 19
Dysgerminoma 20
Sertoli Cell Tumors 20
Granulosa Cell Tumors 21
Other Nonepithelial Ovarian Tumors 21
Metastatic Tumors to the Ovary 22
References 23

4 Ultrasound Assessment of Intra-Abdominal Spread of Ovarian Cancer 25
Introduction 25
Computed Tomography (CT) Scan 25
Magnetic Resonance Imaging (MRI) 25
Positron Emission Tomography (PET) 26
Ultrasound 26
References 29

5 Ultrasound Features of Endometrial Cancer 31
Introduction 31
Ultrasound for Diagnosing Endometrial Cancer 31
Ultrasound Features of Endometrial Cancer 35
References 36

6 Ultrasound Features of Uterine Sarcomas 39
Introduction 39
Ultrasound Features of Uterine Sarcomas 39
Ultrasound Features of Uterine LMS 39

Ultrasound Features of EES 40
Other Imaging Techniques for the Diagnosis of Uterine Sarcomas 42
References 43

7 Ultrasound Assessment of Locoregional Spread of Endometrial Cancer 45
Introduction 45
Ultrasound for Assessing Myometrial and Cervical Infiltration in Endometrial Cancer 45
Two-Dimensional Ultrasound 45
Three-Dimensional Ultrasound 49
Other Imaging Techniques 49
References 49

8 Ultrasound Features of Uterine Cervical Cancer 51
Introduction 51
Ultrasound Features of Uterine Cervical Cancer 51
Ultrasound for Assessing Locoregional Spread of Cervical Cancer 52
Tumor Size and Stromal Invasion 52
Parametrial Infiltration 53
Ultrasound for Assessing Treatment Response in Locally Advanced Cervical Cancer 57
References 57

9 Ultrasound Features of Gestational Trophoblastic Disease 61
Introduction 61
Hydatiform Mole 61
Gestational Trophoblastic Neoplasia 63
The Role of Doppler Ultrasound in GTD 65
Role of Other Imaging Techniques for Assessing GTD 65
References 65

10 Ultrasound-Guided Procedures in Gynecologic Oncology 67
Introduction 67
Tru-Cut Biopsy 67
Fine Needle Aspiration (FNA) Biopsy 68
Drainage 68
Other Ultrasound-Guided Procedures 69
References 69

11 Ultrasound in Vulvar and Vaginal Cancer 71
Introduction 71
Role of Ultrasound in Vulvar Cancer 71
Role of Ultrasound in Vaginal Cancer 73
References 76

Index 79

Foreword

I thank Dr. Alcázar for giving me the opportunity to write the Foreword to his fine book on the role of ultrasound in gynecologic oncology: *Ultrasound Assessment in Gynecologic Oncology*. The combination of both his experience as a gynecologist treating gynecological cancer and his long and exceptional experience in ultrasonography make this book a real opportunity to learn about this matter in a comprehensive way. Coherent from beginning to end, this book is one of the first published in this field; it includes an extensive set of clinical images that will be invaluable to both the general gynecologist and gynecologist–oncologist in the management of this pathology.

I know Dr. Alcázar personally and have been fortunate to be able to follow his scientific, professional, and teaching careers. He completed his residency in the Department of Gynecology and Obstetrics at the Clinica Universidad de Navarra in Pamplona, Spain, where I met him as a resident. He began his training in the field of ultrasound under the mentoring of Dr. Mercé, who is world renowned in gynecological ultrasonography and who worked with us for several years. Dr. Alcázar's numerous publications, his brilliant collaboration in the national and international ultrasound societies, and his more than remarkable participation in scientific forums have given him exceptional credentials for a work of this type.

I was privileged to be his mentor in his training in Gynecologic Oncology, and I have enjoyed his personal assistance for many years. I shared with him many ideas regarding the "crossover" between gynecological oncology and ultrasound that have been transformed into a reality with his research. It is also fair to mention the great many gynecologists, both from within our country and from overseas, who have come here to train with him.

More than merely an elucidation of theory, this book combines qualities that make it of great practical use, as well as an invaluable reference. It includes all of the important topics for daily practice, from an exhaustive description of the normal anatomy of the pelvic contents to comprehensive discussions of those less common topics in which more recent definitive experience has been gained, such as adnexal masses and endometrial cancer. This book also includes chapters on a novel staging system for ovarian, endometrial, and cervical uterine neoplasms; a number of preliminary studies, among them those published by Dr. Alcázar, support its application in the very near future. Finally, it also includes some chapters on invasive diagnostic procedures guided by ultrasound and the treatment of more infrequent tumors such as cancer of the vulva or vagina.

I would like to conclude by thanking Dr. Alcázar for his generosity and continued support in the treatment of so many oncological patients to whose healing or improvement he has contributed. The excellence that routinely characterizes his professional work has made successful therapy possible. It is gratifying to see the product of years of training and dedicated practice and research made available to all of us in this challenging discipline.

Prof. Dr. Matías Jurado
Professor of Gynecology and Obstetrics
Director of the Gynecologic Oncology Section
Clinica Universidad de Navarra
Pamplona, Spain

Taylor & Francis
Taylor & Francis Group
http://taylorandfrancis.com

Preface

Gynecologic oncology is one of the most important specialties in the field of gynecology. Gynecologic oncology focuses on the diagnosis and treatment of cancers developed from the female reproductive system. The clinical relevance of this specialty is highlighted by the fact that three gynecological cancers are among the top six most frequent malignancies suffered by women around the world, namely, cancer of the uterine cervix, endometrial cancer, and ovarian cancer.

For more than 30 years, ultrasound has been an imaging technique frequently used in gynecological practice. It has become an essential diagnostic tool for most clinicians.

The main role of ultrasound in the field of gynecologic oncology has been the differential diagnosis of uterine and ovarian lesions, with good performance. However, in the last decade, significant advances have been achieved in the use of ultrasound in the assessment of gynecological cancers, not only for diagnosis but also for staging.

After many years of practicing and teaching both ultrasound and gynecologic oncology, I realized the lack of a dedicated handbook about this topic: the use of ultrasound in gynecologic oncology practice. This text aims to summarize current state-of-the-art use of ultrasound in the field of gynecologic oncology, providing to the reader both theoretical knowledge and practical tips, adding a brief description about the role of other diagnostic imaging techniques such as computed tomography scan, magnetic resonance imaging, and positron emission tomography scan. I intend to address not only the most frequent cancers from the female genital tract but also those less common.

Juan Luis Alcázar
Pamplona, Spain

Taylor & Francis
Taylor & Francis Group
http://taylorandfrancis.com

1

Ultrasound Scanning of the Female Pelvis: Normal Findings

Introduction

Transvaginal ultrasound is currently considered as the first-line technique for imaging the female pelvis, especially for assessing the uterus and the adnexa. Transabdominal ultrasound is needed in some circumstances for assessing the entire pelvis or the abdomen for evaluating large structures or disease that spread intra-abdominally. Certainly, ultrasound has become an essential diagnostic tool for most clinicians involved in the clinical management of gynecological diseases, specifically tumoral entities.

In this chapter, we review the normal findings of the female pelvic organs as scanned by transvaginal ultrasound.

When assessing the female pelvis by ultrasound, we must clearly identify the anatomical landmarks to be assessed, especially when we focus on gynecological malignancies. From a practical perspective, the female pelvis can be divided into three parts: reproductive organs, nonreproductive organs, and pelvic wall structures.

Pelvic wall structures refer to the pelvic great vessels, muscles, and bones. Nonreproductive organs refer mainly to the bladder, ureter, recto-sigmoid, and bowel. Reproductive organs refer to the uterus, fallopian tubes, and ovaries. We should also include vaginal fornices, recto-vaginal septum, cardinal ligaments, or parametria and utero-sacral ligaments.

Pelvic Wall Structures

When assessing pelvic wall structures, we should image the great pelvic vessels, muscles, and bones. We focus on the pelvic vessels, as they are the main landmarks for pelvic scan in a gynecological oncological setting.

Pelvic vessels assessable by transvaginal ultrasound are mainly external iliac vessels (artery and vein), internal iliac vessels (artery and vein), and the uterine vessels (artery and venous plexus). Other vessels less frequently assessed by transvaginal ultrasound are the ovarian vessels. Due to the limitation of depth when using a high-frequency transvaginal probe, ovarian vessels are more difficult to assess. The identification of the great iliac vessels is essential for evaluating the presence of lymph nodes.

External iliac vessels are easily identified running parallel to the pelvic wall (Figure 1.1). The vein is larger than the artery and is located over the artery. The latter is clearly seen beating in virtually all women. It is important to insonate the vessels parallel to them in order to obtain a sagittal view of the vessels. This can be achieved by moving the endovaginal probe laterally and anteriorly.

The internal iliac vessels are visible displacing the probe medially and posteriorly (Figure 1.2). Color Doppler may help in identifying these vessels.

Finally, the uterine vessels can be identified laterally to the cervix, either in the longitudinal or axial planes (Figure 1.3).

Nonreproductive Organs

The bladder is easily identified as a central cystic structure located between the uterus and the abdominal wall (Figure 1.4). Bladder wall thickness can be measured, and the internal wall

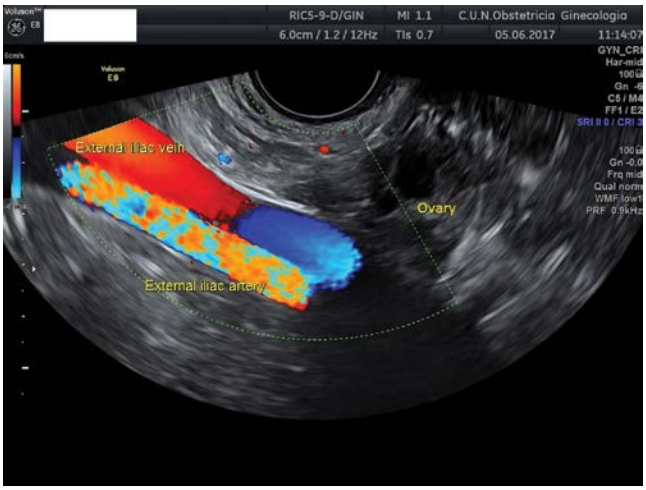

FIGURE 1.1 Transvaginal ultrasound showing right external iliac vessels. The ovary is seen lying over these vessels.

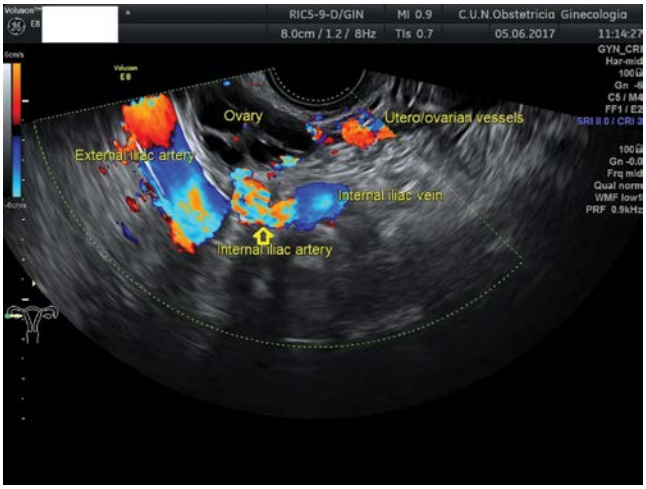

FIGURE 1.2 Transvaginal ultrasound depicting internal iliac vessels and utero-ovarian vessels.

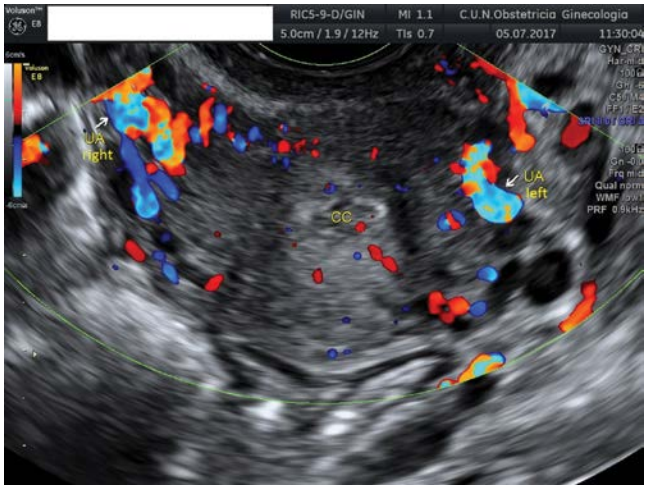

FIGURE 1.3 Transvaginal ultrasound showing both uterine arteries (UAs) at both sides of the cervix. The cervical canal (CC) can be observed.

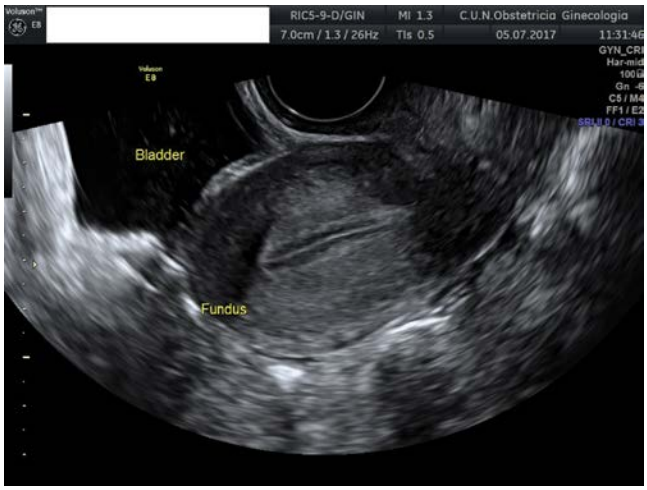

FIGURE 1.4 Transvaginal ultrasound showing the uterus in the longitudinal plane. The bladder can be seen as an anechoic structure located anteriorly to the uterus.

surface may be evaluated. It is a common finding to observe some irregularities of the bladder mucosa. When scanning an oncological patient, it is quite important to determine the presence of sliding of the bladder wall over the cervix, since this is a sign that indicates that the bladder wall is not involved, for example, in a case of cervical carcinoma.

The ureters can be seen passing through the bladder wall, and the ureteral meatus can be identified in both sides (Figure 1.5a). They are commonly identified as a hypoechoic creeping structure within the bladder wall (Figure 1.5b). More laterally, they can be observed crossing under the uterine artery (Figure 1.5c).

The recto-sigmoid is also easily identified as a central pelvic structure located between the uterus and the sacrum. Sometimes it can be seen as a straight structure (Figure 1.6a), but most of the time it is observed as a snaky structure (Figure 1.6b). The

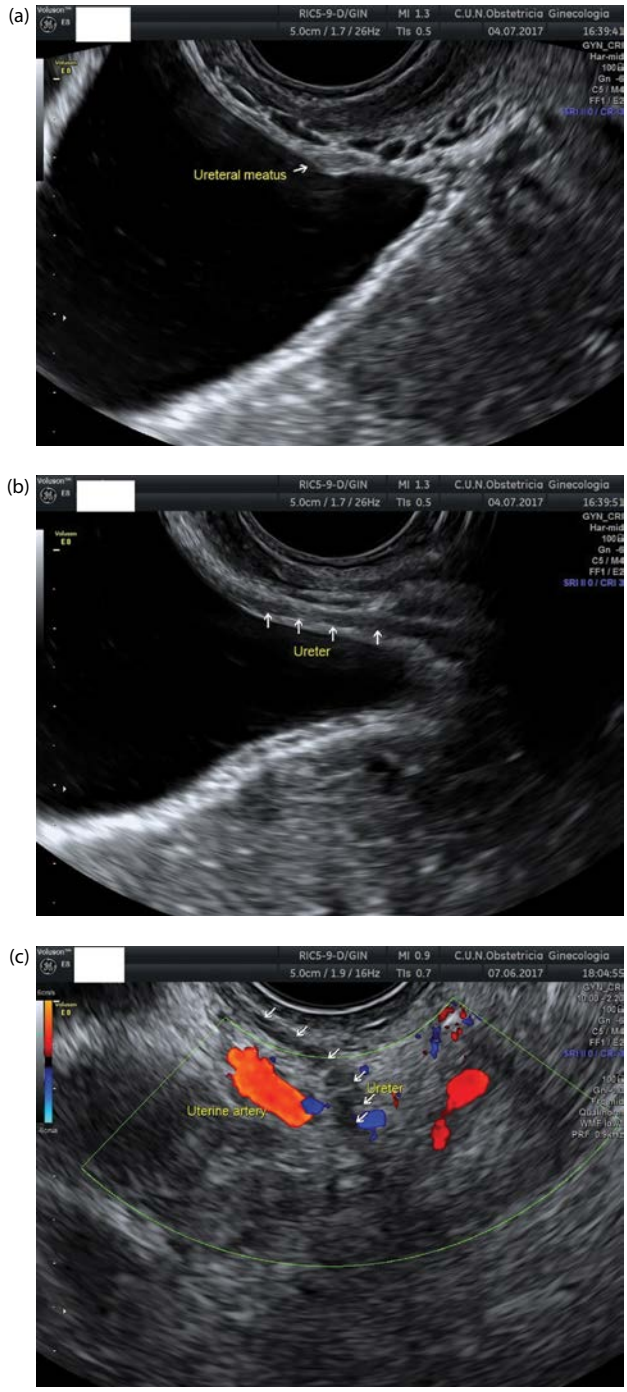

FIGURE 1.5 (a) Transvaginal ultrasound showing the bladder. The ureteral meatus can be observed in the longitudinal plane moving the endovaginal transducer laterally. (b) The transmural portion of the ureter can be observed here as a hypoechogenic structure (arrows). In real-time ultrasound, a creeping movement can be seen. (c) Displacing the endovaginal transducer laterally and a little bit anteriorly, the ureter (arrows) can be seen crossing under the uterine artery.

recto-sigmoid wall layers can be identified when it is empty (Figure 1.6a). Sliding of the rectum over the posterior surface of the uterus is important to observe, and this is a good sign for assessing whether the Douglas pouch is obliterated or not.

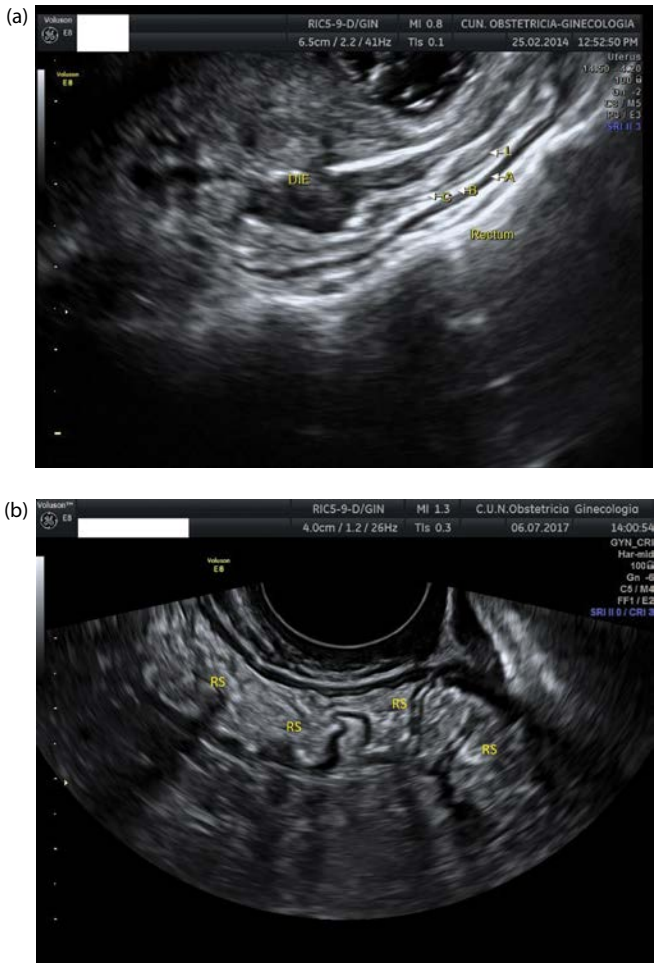

FIGURE 1.6 (a) Transvaginal ultrasound depicting the recto-sigmoid colon. The layers of recto-sigmoid can be visualized (A, muscularis propria; B, submucosa; C, mucosa; L, lumen). A deep infiltrating endometriosis (DIE) is observed. (b) The recto-sigmoid (RS) is seen as a snaky structure.

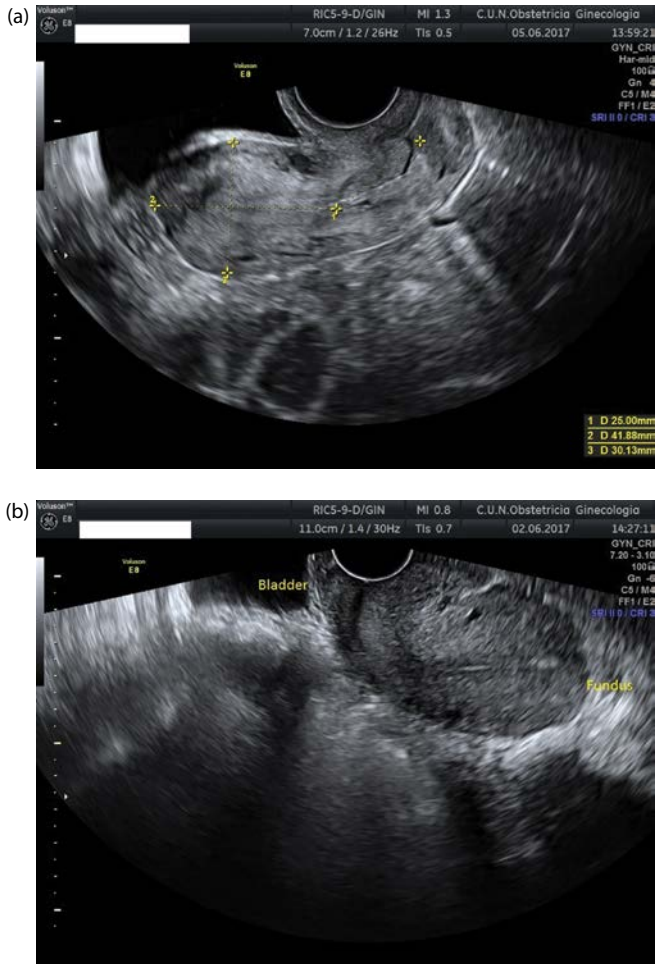

FIGURE 1.7 (a) Transvaginal ultrasound showing a uterus in its longitudinal plane. This uterus is anteverted. Measurements of the cervical length, corpus uteri length, and corpus uteri anterior-posterior diameter can be observed. (b) Transvaginal ultrasound showing a retroverted uterus. The fundus is located away from the bladder, to the rectum.

Reproductive Organs

The uterus is located between the bladder anteriorly and the recto-sigmoid posteriorly, and it can be divided into two parts: the body, or corpus, and the cervix.

The uterus is usually anteverted (the fundus of the corpus tends to lie over the bladder) (Figure 1.7a), but it may be retroverted (the fundus is positioned to the rectum or even the cul-de-sac) (Figure 1.7b). Therefore, the corpus is mobile, but the cervix is fixed in the midline.

The shape and size of the uterus vary depending mainly on a woman's age and parity. In reproductive-age, nongravid women, the uterus is an ellipsoid structure with regular contour (Figure 1.7a). It can be accurately measured by ultrasound, and normal size ranges between 7.5 and 9 cm in length, 4.5–6 cm in width, and 2.5–4 cm in thickness (Figure 1.7a) (1). Parity increases size by 1–2 cm in all three orthogonal planes (1).

In menopause, uterine size decreases to 3.5–6.5 cm in length, and 1.2–1.8 cm in thickness (1). When evaluating the uterus by ultrasound, two distinct structures should be assessed: the myometrium and the endometrium.

The myometrium is constituted by the uterine muscle, limited externally by the uterine serosa and internally by the endometrium (2) (Figure 1.8). The myometrium is divided into three layers. The inner layer, adjacent to the endometrium, is observed by ultrasound as a thin hypoechoic stripe, it is also called the *functional zone* (Figure 1.8). The border between this layer and the endometrium is the *myometrial-endometrial interphase*. The middle layer, which corresponds to the uterine muscle, is the thickest part and it is also called the *uterine wall*. This layer is seen by ultrasound as a homogeneously echodense structure (Figure 1.8). The outer layer corresponds to the uterine serosa, and it appears as an extremely thin echogenic line. Immediately beneath this layer and located in the most outer aspect of the middle layer, the arcuate vessels can be seen.

The cervix length is measured from the internal cervical os to the external cervical os in the longitudinal plane (Figure 1.7a). The cervix measures about 2.5 cm in length, 2.5 cm in width, and 1.5–2 cm in thickness (1).

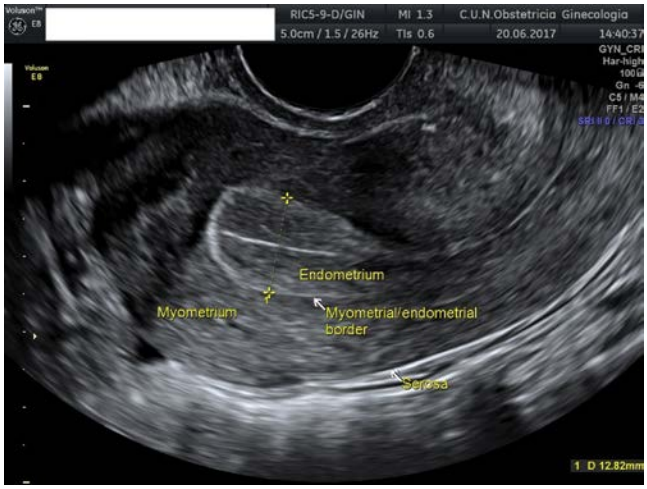

FIGURE 1.8 Transvaginal sonography showing the different structures of the corpus uteri (endometrium and myometrium). Endometrial thickness is 12.8 mm. The uterine serosa and myometrial-endometrial border can also be visualized. The endometrium appears as a three-layer structure.

The cervical canal is easily visible, and the endocervical mucosa may be observed as a hyperechoic structure. The surrounding cervical stroma is hypoechoic. The endocervical mucosa is continuous with the endometrium. In premenopausal women, cervical mucous can be seen within the cervical canal during the periovulatory phase (Figure 1.9a). Another common finding is the nabothian cysts, visualized as rounded cystic areas within the cervical stroma (Figure 1.9b).

The cervix is attached to the pelvic wall by the parametria. The proximal parametrium can be assessed by transvaginal ultrasound. It can be visualized as an echogenic structure at both sides of the cervix in the axial plane (Figure 1.10). The uterine vessels may help to identify this structure.

The utero-sacral ligaments can be visualized in the axial plane running as an echogenic band in the posterior aspect of the cervix (Figure 1.11).

The endometrium corresponds to the endometrial mucosa, and it is located in the inner part of the uterus, surrounding the endometrial cavity. In most instances, the anterior and posterior layers are faced one to the other making the uterine cavity a virtual cavity (3). When any content, such as blood, mucous, or serous liquid, distends the uterine cavity, both layers can be assessed distinctly (Figure 1.12).

The endometrium should be measured in the longitudinal plane, including both layers (anterior and posterior), at the thickest part (Figure 1.8). When there is some fluid within the uterine cavity, each layer should be measured separately (Figure 1.12).

Endometrial thickness varies during the menstrual cycle in reproductive age, from 4–5 mm during menstruation to 16–18 mm during midluteal phase (4). After menopause the endometrium becomes thin, with a median thickness of 3.2 mm (±1 mm), and echogenic (Figure 1.13).

The echogenicity of the endometrium also changes throughout the menstrual cycle, appearing as a three-layer structure during the proliferative phase (Figure 1.8) and becoming homogenously echogenic during the secretory phase.

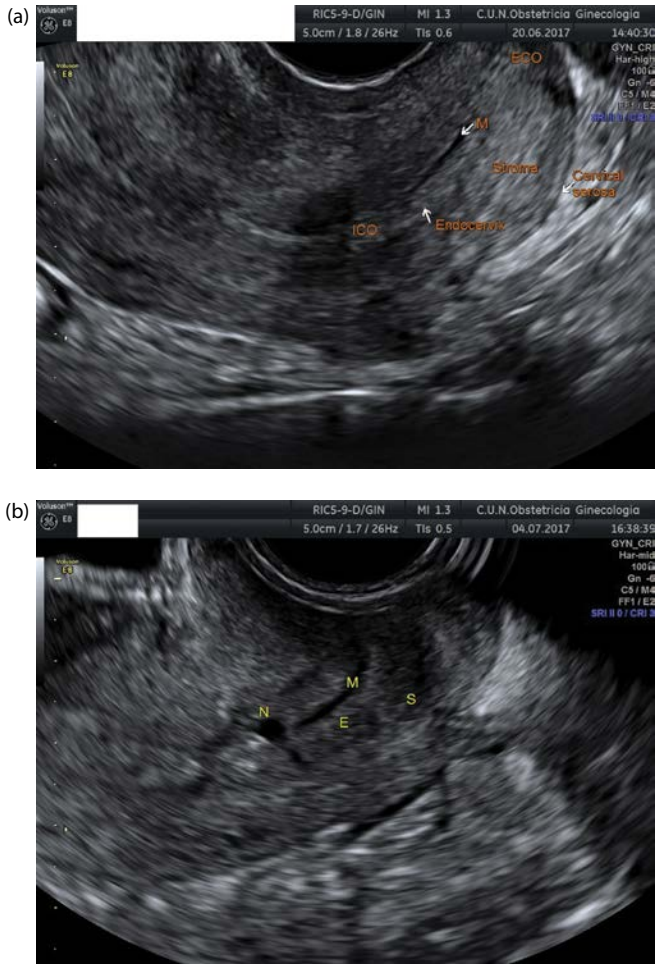

FIGURE 1.9 (a) The cervix. Several landmarks can be observed: the external cervical os (ECO), the internal cervical os (ICO), the cervical serosa, the stroma, and the endocervix. The lumen (M) of the cervical canal can also be visualized. (b) In some cases, nabothian cysts (N) can be observed. (E, endocervix; S, cervical stroma; M, cervical canal lumen.)

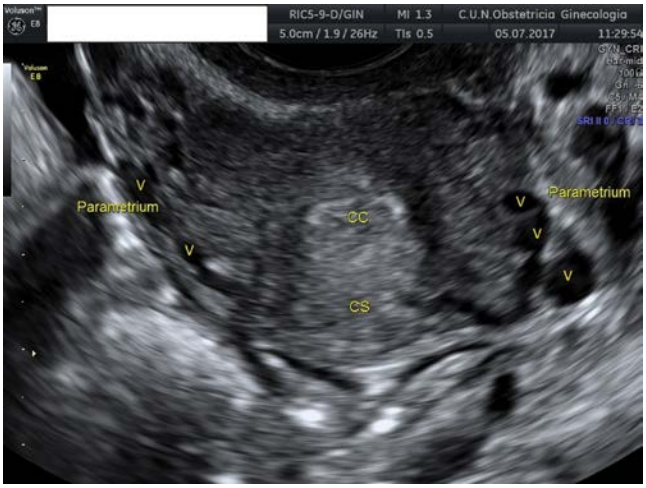

FIGURE 1.10 Transvaginal ultrasound showing a transverse plane view of the cervix. Cervical stroma (CS) and cervical canal (CC) are seen as anatomical landmarks. Both parametria with uterine venous vessels (V) are depicted.

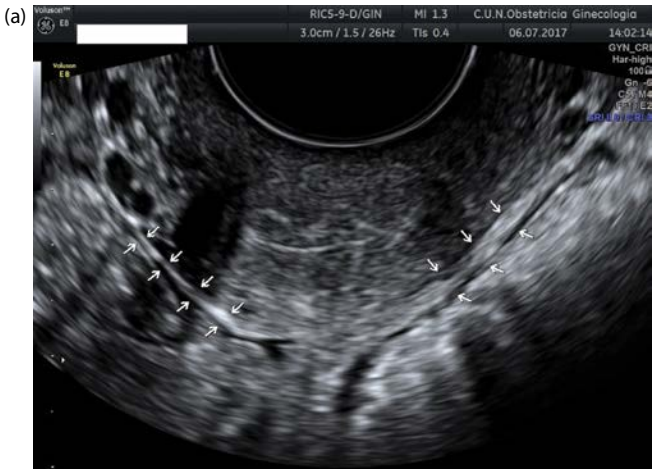

FIGURE 1.11 (a) Transverse view of the cervix showing the utero-sacral ligaments (in between arrows) as echogenic lines running through the posterior-lateral aspects of the cervix. (b) When some amount of fluid is present in the cul-de-sac, the utero-sacral ligament (arrows) can be visualized running from the cervix to the rectum. (The vaginal probe is orientated laterally to the cervix in the sagittal plane.)

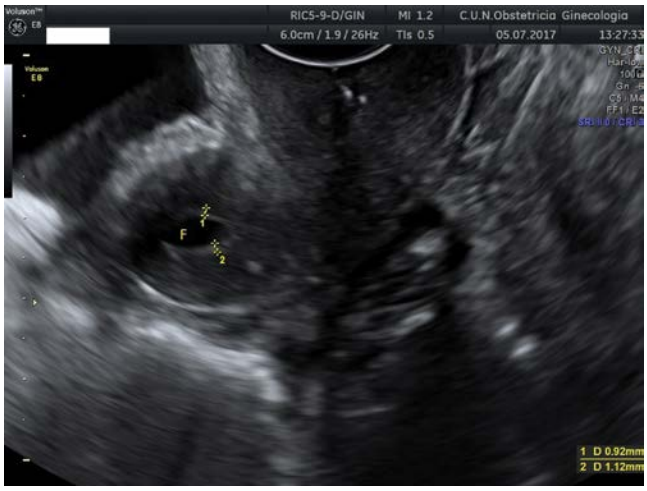

FIGURE 1.12 Transvaginal ultrasound of a uterus in a postmenopausal woman. A small amount of fluid is present within the uterine cavity (F). Both endometrial layers should be measured separately.

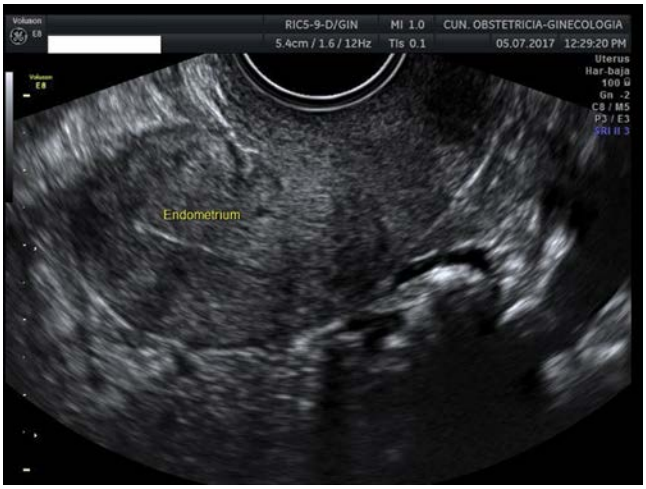

FIGURE 1.13 Transvaginal ultrasound of a uterus in a postmenopausal woman. The endometrium is depicted as a thin hyperechoic stripe.

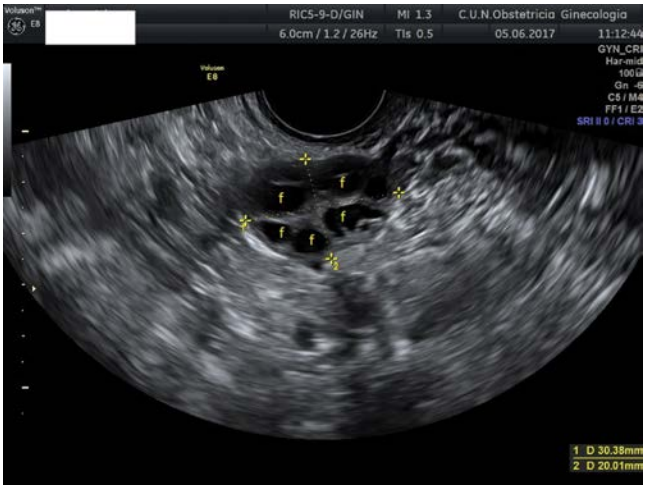

FIGURE 1.14 Transvaginal ultrasound depicting a normal ovary with follicles (f) in a premenopausal woman.

The ovaries can be detected in the *ovarian fossa*, between the uterus and the external iliac vessels (Figure 1.14). However, due to the mobility of the infundibulopelvic and utero-ovarian ligaments, sometimes they are found behind the uterus or in the cul-de-sac.

Sonographically, the ovaries are seen as oval echogenic structures. During reproductive age, the follicles can be seen within the ovaries (Figure 1.14). The size of the ovary in premenopausal women is about 3 × 2 cm. The preovulatory follicle may reach 20–25 mm in size, whereas the corpus luteum formed after ovulation may reach 25–30 mm (3). Blood flow can be observed within the ovarian stroma and surrounding the dominant and preovulatory follicles. After ovulation, a significant angiogenic phenomenon happens, and the corpus luteum appears surrounded by a rich color Doppler halo (Figure 1.15).

After menopause, the ovary decreases (2 × 1 cm) and becomes an oval well-defined echogenic structure (3) (Figure 1.16). At this time, stromal vascularization is hardly detectable.

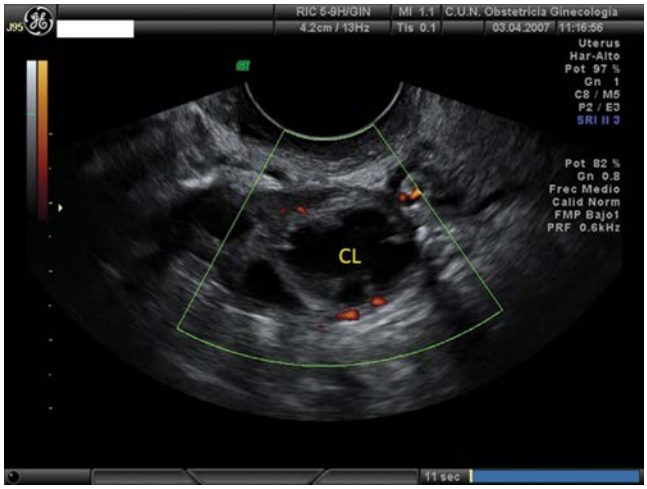

FIGURE 1.15 Transvaginal ultrasound showing a corpus luteum (CL) in the left ovary, after ovulation.

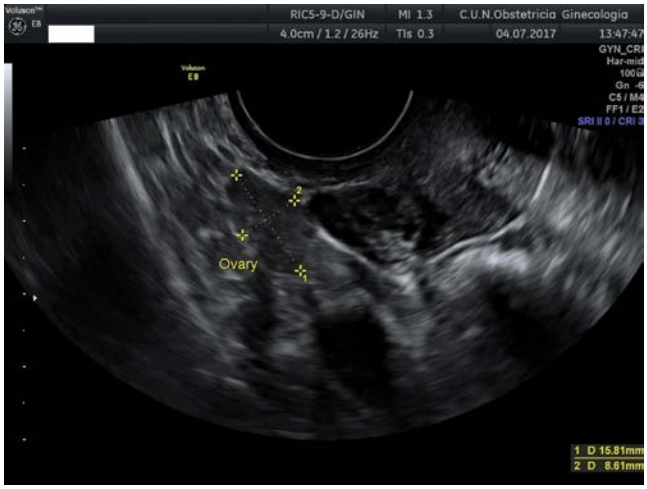

FIGURE 1.16 Transvaginal ultrasound showing a normal ovary in a postmenopausal woman. No follicles can be seen.

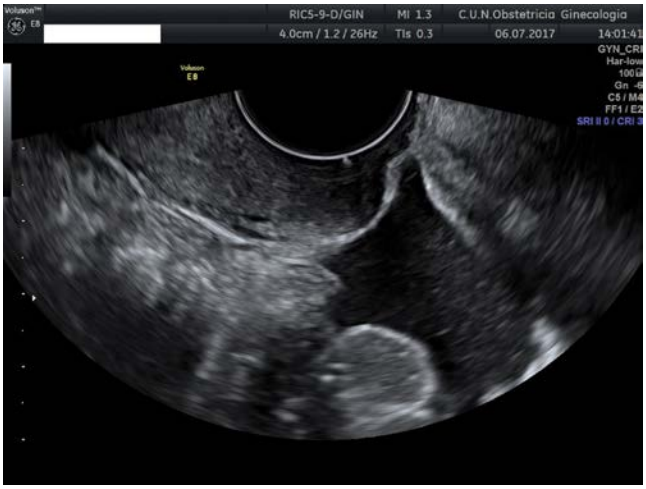

FIGURE 1.18 Pouch of Douglas with free fluid as depicted by transvaginal ultrasound in a sagittal plane.

Finally, the fallopian tubes can be visualized as a thin echogenic structure (Figure 1.17), especially when there is some fluid in the adnexal regions or in the pouch of Douglas (Figure 1.18). The presence of a paratubal cyst is a relatively common finding.

The recto-vaginal septum can also be visualized by transvaginal ultrasound. It is visualized as a hypoechoic line between the posterior vaginal wall and the anterior aspect of the lowest part of the rectum and anal canal (Figure 1.19).

Transvaginal ultrasound allows for assessment of the sliding between the vaginal wall and the rectum, indicating the integrity of the recto-vaginal septum.

Finally, the vaginal fornices are difficult to assess by transvaginal ultrasound. Using some gel into the vagina may help for assessing the vaginal fornices (Figure 1.20).

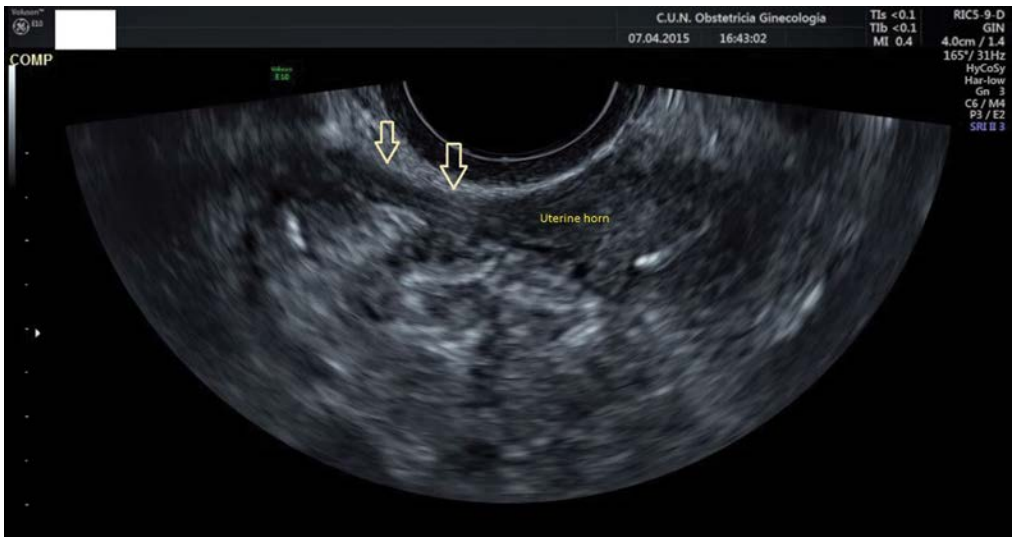

FIGURE 1.17 Transvaginal ultrasound depicting the right fallopian tube (arrows) as a hypoechoic structure arising from the uterine horn.

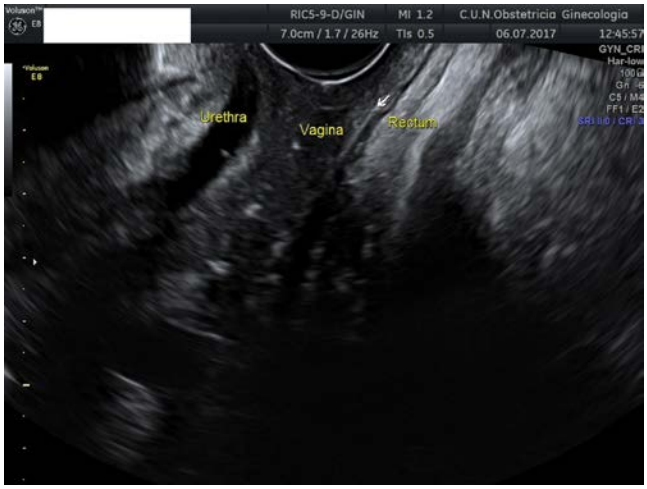

FIGURE 1.19 Transvaginal ultrasound depicting the recto-vaginal septum (arrow) as an echogenic line, lying between the posterior vaginal wall and the anterior wall of the rectum.

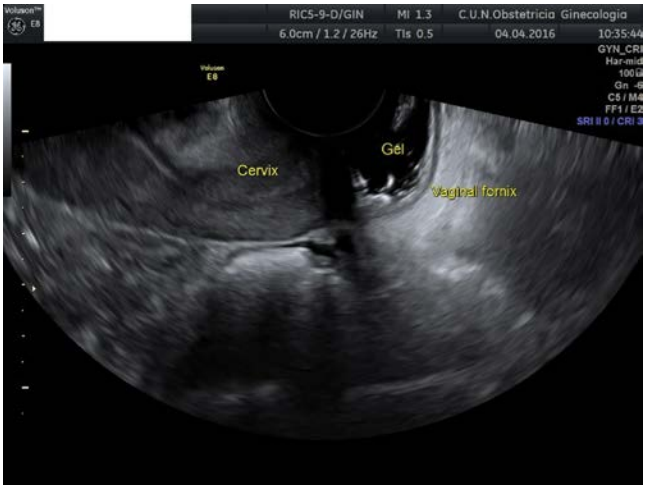

FIGURE 1.20 Transvaginal ultrasound with some gel in the vagina (sonovaginography). Using this technique, the vaginal fornices can be assessed more accurately.

REFERENCES

1. Kupesic S, Honemeyer U, Kurjak A. Normal female reproductive anatomy. In: *Donald School Textbook of Ultrasound in Obstetrics and Gynecology*, 4th edition (Kurjak A, Chervenak FA, eds), Jaypee, London, 2017, pp. 822–837.
2. Van den Bosch T, Dueholm M, Leone FP et al. Terms, definitions and measurements to describe sonographic features of myometrium and uterine masses: A consensus opinion from the Morphological Uterus Sonographic Assessment (MUSA) group. *Ultrasound Obstet Gynecol*. 2015;46:284–298.
3. Langer JE. Normal anatomy of the female pelvis and transvaginal sonography. In: *Callen's Ultrasonography in Obstetrics and Gynecology*, 6th edition (Norton M, Scoutt L, Feldstein V, eds), Elsevier, New York, 2017, pp. 805–824.
4. Leone FP, Timmerman D, Bourne T et al. Terms, definitions and measurements to describe the sonographic features of the endometrium and intrauterine lesions: A consensus opinion from the International Endometrial Tumor Analysis (IETA) group. *Ultrasound Obstet Gynecol*. 2010; 35:103–112.

Taylor & Francis
Taylor & Francis Group
http://taylorandfrancis.com

2

Ultrasound for Differential Diagnosis of Adnexal Masses

Introduction

Adnexal masses represent one of the most frequent problems in clinical practice. Accurate diagnosis is essential to establish the optimal management for these patients. Benign adnexal masses can be treated conservatively or by minimally invasive surgical procedures (1,2). However, suspicious masses should be referred to tertiary care centers that specialize in gynecological oncology and may offer appropriate resources and experienced surgeons (3).

Ultrasound is considered as the first-line imaging technique for the differential diagnosis of adnexal masses (4).

Ultrasound correlates morphologic images with the gross macroscopic pathology of adnexal tumors, and it has been shown that this correlation is high (5). Therefore, diagnosis is mainly based on grayscale ultrasound assessment.

The use of Doppler allows the assessment of tumor vascularization, looking for vascular changes derived from the angiogenic phenomena that occur mainly in malignant tumors. The assessments of velocimetric indexes and velocities by pulsed Doppler are currently disregarded in the differential diagnosis of adnexal masses due to low reproducibility and significant overlap between benign and malignant lesions (6). However, the assessment of the location and the amount of flow within the tumor may contribute to this differential diagnosis (6).

The International Ovarian Tumor Analysis (IOTA) group has reported a consensus paper on how adnexal masses should be evaluated and described (7).

The differential diagnosis of adnexal masses by ultrasound may be performed using different approaches.

Pattern Recognition

To date the best approach is based on the subjective impression of the examiner, the *pattern recognition* (6). This approach is based on the fact that many adnexal masses have a typical grayscale ultrasound related to the macroscopic pathology, such as endometrioma (Figure 2.1), serous or simple cyst (Figure 2.2), dermoid cyst (Figure 2.3), mucinous cyst (Figure 2.4), hydrosalpinx (Figure 2.5), or para-ovarian cyst (Figure 2.6).

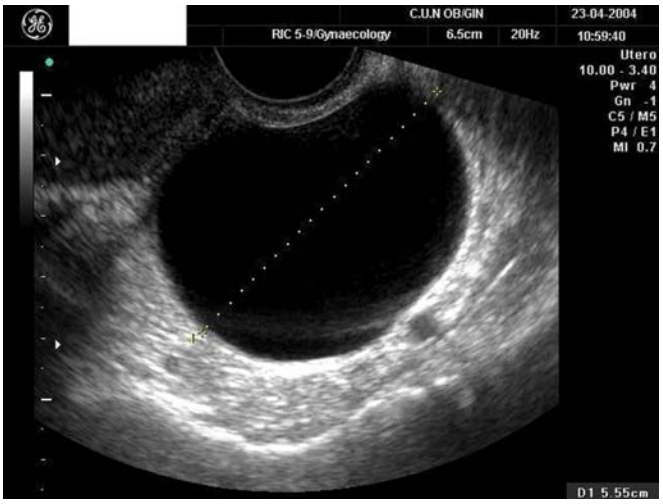

FIGURE 2.2 Typical appearance of an ovarian unilocular anechoic simple cyst.

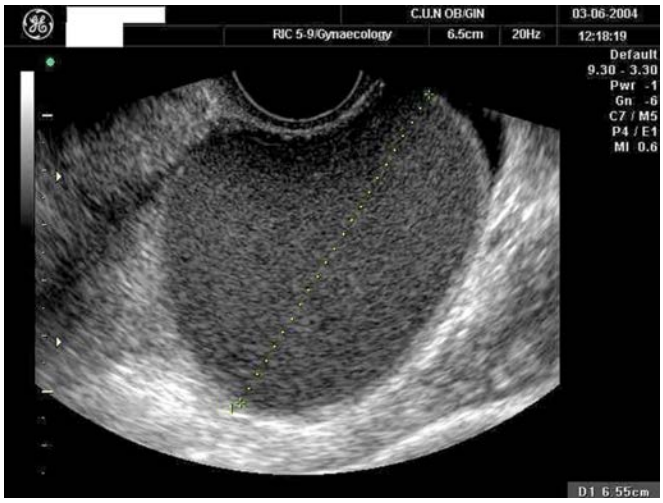

FIGURE 2.1 Transvaginal ultrasound showing an ovarian cyst with the typical appearance of ovarian endometrioma: unilocular cyst with ground-glass echogenic content.

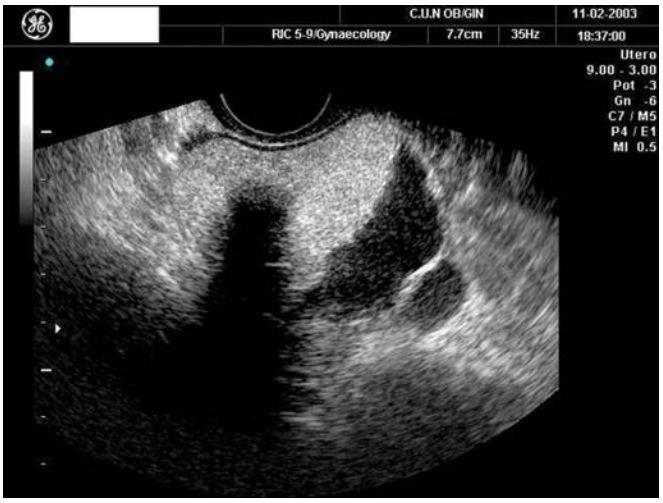

FIGURE 2.3 An ovarian lesion with the characteristic findings of a mature teratoma: unilocular cyst with mixed echogenicity and acoustic shadowing.

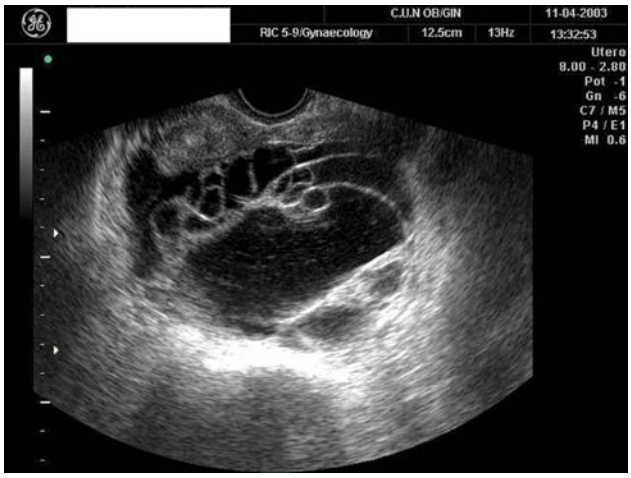

FIGURE 2.4 Transvaginal ultrasound showing a multilocular cyst with no solid components and more than 10 locules. Typical appearance of a mucinous cyst.

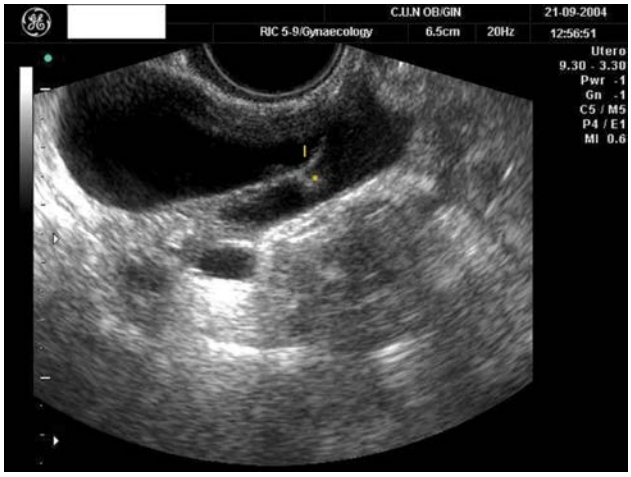

FIGURE 2.5 Adnexal mass showing the characteristic appearance of hydrosalpinx, an elongated cystic lesion with incomplete septation (I) and small irregularity in cyst wall (*).

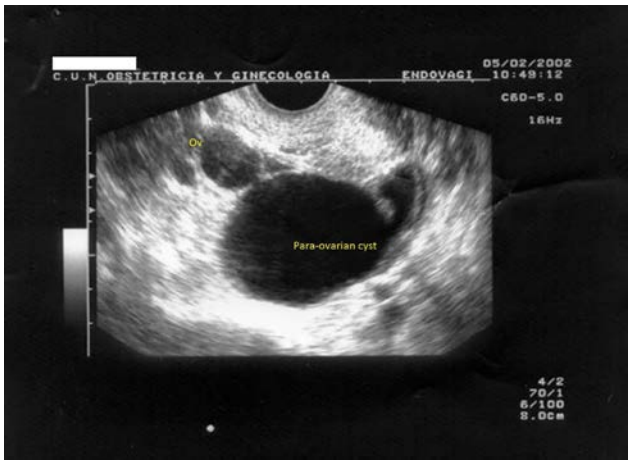

FIGURE 2.6 Transvaginal ultrasound depicting a para-ovarian cyst, located close to the ovary (Ov).

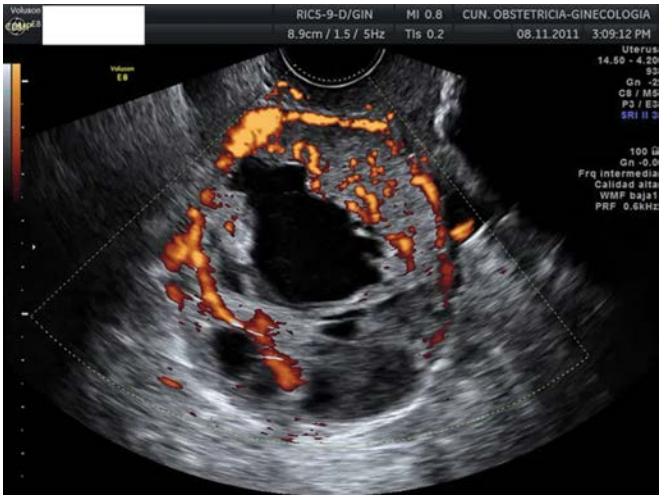

FIGURE 2.7 Transvaginal sonography of an adnexal mass highly suspicious for malignancy (large solid component and abundant vascularization).

Malignant invasive and borderline tumors commonly exhibit solid areas, most of the times with blood vessels detectable by color/power Doppler ultrasound (Figure 2.7). We address the specific features of borderline and invasive ovarian tumors in the next chapter.

Using pattern recognition, the sensitivity and specificity for malignancy are 93% and 89%, respectively (8).

However, the reproducibility and diagnostic performance of this approach are highly dependent on the examiner's experience (9,10). Because of this, different approaches have been proposed in order to allow less experienced examiners to have similar results as those obtained by expert examiners.

Scoring Systems

Since the early 1990s, different scoring systems have been proposed (11). Certainly, the use of these scoring systems may render optimal results in the hands of less experienced examiners (12) and may be useful for triaging women with adnexal masses (13), but they are not superior to the examiner's subjective impression (14).

Simple Rules

In 2008, the IOTA group proposed the use of the ultrasound-based simple rules (SRs) for the diagnosis of ovarian malignancy (15). These rules are based on the identification of some mass's features on ultrasound, some of which are characteristic of malignant lesions (M features) and others of benign lesions (B features) (Table 2.1, Figure 2.8).

When a mass exhibits at least one M feature in the absence of B features, it is classified as malignant. When a mass exhibits at least a B feature in the absence of M features, the mass is classified as benign. When a mass exhibits M and B features, or it exhibits no M features and no B features, it is classified as inconclusive.

TABLE 2.1

IOTA Simple Rules Description

Benign Feature	Description
B1	Unilocular
B2	Presence of solid components where the largest solid component has a largest diameter <7 mm
B3	Presence of acoustic shadows
B4	Smooth multilocular tumor with largest diameter <100 mm
B5	No blood flow (color score 1)
Malignant Feature	
M1	Irregular solid tumor
M2	Presence of ascites
M3	At least four papillary structures
M4	Irregular multilocular solid tumor with largest diameter ≥100 mm
M5	Very strong blood flow (color score 4)

Source: Adapted from Timmerman D et al. *Ultrasound Obstet Gynecol.* 2008;31:681–690.

This approach based on the SRs has been externally validated in several studies (8,11). SRs can be applied in 78%–89% of adnexal masses. Two recent meta-analyses have shown that this approach is superior to scoring systems and to logistic repression models (11) but not to examiner's subjective impression (8).

Because the simple rules cannot be applied to all masses, the IOTA group proposed a risk of malignancy estimation based on the combination of M and B features (16). Using this risk estimation, all adnexal masses could be classified using SRs. However, this new approach needs to be validated.

The IOTA group has also proposed a sequential approach based on the "easy" descriptors followed by the use of SRs and finally the use of the expert examiner's impression (17) (Figure 2.9). The easy descriptors are based on ultrasound information and measurements of CA-125: four describe the typical findings of benign tumors, and two describe probable malignancies (Table 2.2). Several studies have validated this three-step approach, in the hands of both experts and nonexperts, reporting good results in terms of sensitivity (92%–94%) and specificity (87%–95%) (18,19).

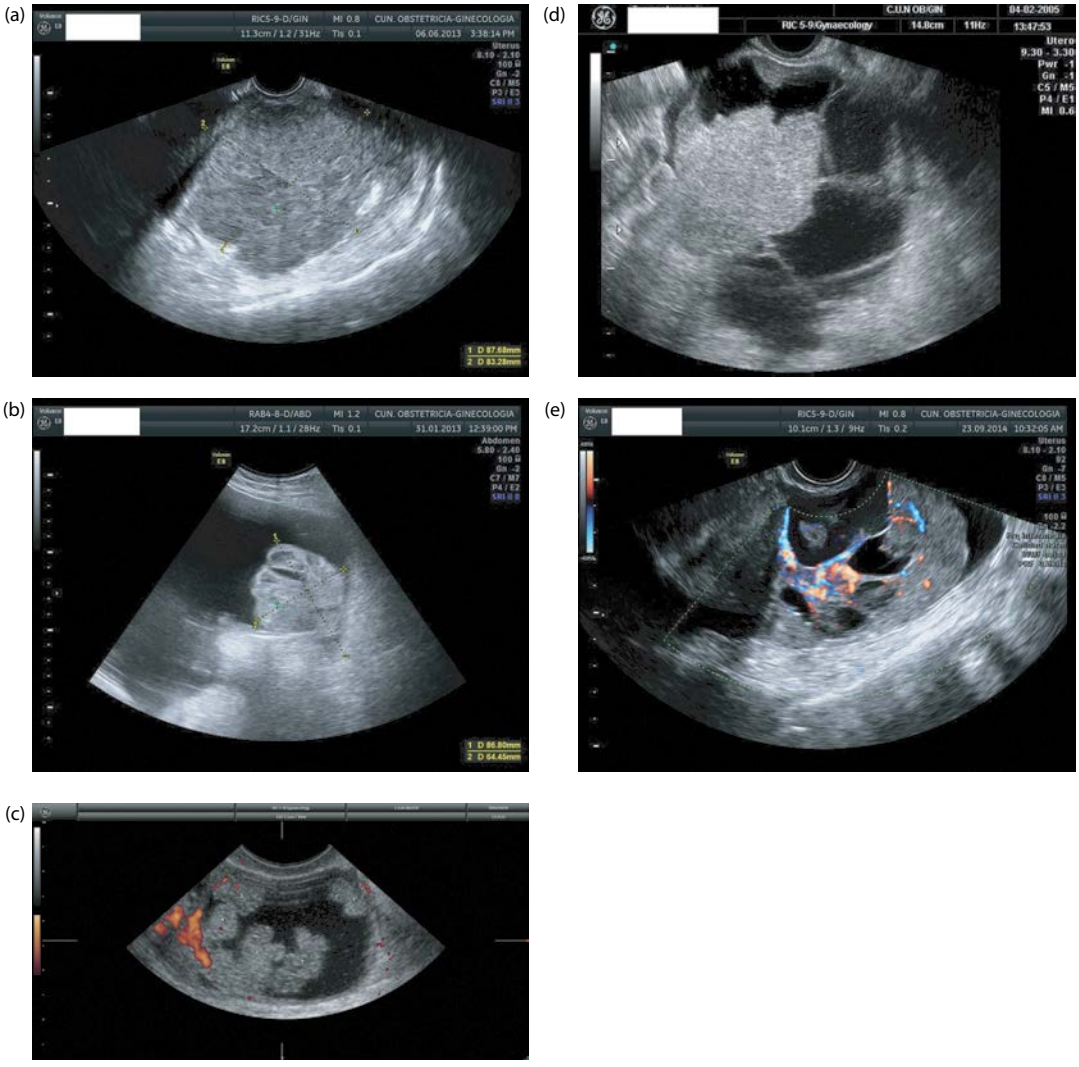

FIGURE 2.8 Examples of ultrasound features of IOTA simple rules. (a) M1 (irregular solid tumor); (b) M2 (presence of ascites); (c) M3 (at least four papillary projections); (d) M4 (irregular multilocular-solid tumor >100 mm); (e) M5 (color score 4). (*Continued*)

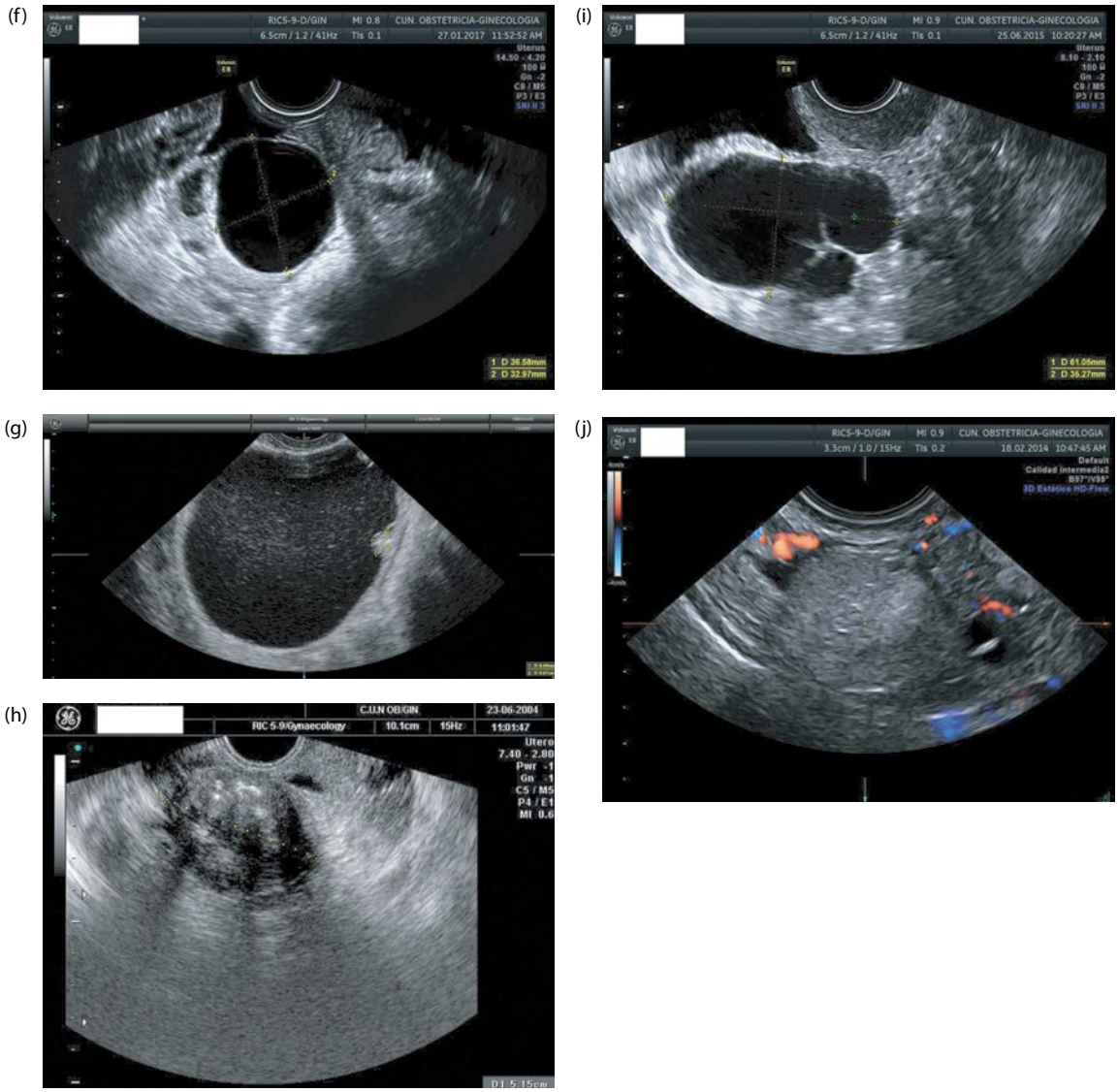

FIGURE 2.8 (Continued) Examples of ultrasound features of IOTA simple rules. (f) B1 (unilocular cyst); (g) B2 (presence of solid components less than 7 mm); (h) B3 (presence of acoustic shadowing); (i) B4 (smooth multilocular tumor <100 mm); (j) B5 (color score 1).

Logistic Regression Models

The use of logistic models is appealing since this approach allows an individualized malignancy risk estimation. Many logistic models have been published (11). Probably, the most used is the Risk of Malignancy Index (RMI) (20). A recent meta-analysis has shown that these models, especially the RMI, are not superior to examiner's subjective impression or to SRs (8).

The IOTA group has also proposed the use of two different logistic models (LR1 and LR2) (11). However, two meta-analyses have shown that these models are not better than an examiner's subjective impression and SRs (8,11). Therefore, the use of these logistic models has not gained acceptance in clinical practice.

More recently, the IOTA group proposed a new logistic model, the ADNEX model (21). This model allows estimation of not only the risk of benignity or malignancy, but also the risk of the tumor being a borderline tumor, early stage invasive cancer, advanced-stage invasive cancer, or metastatic cancer to the ovary. This model is, therefore, quite interesting. However, the results of studies aiming to validate this model are controversial (22,23).

Reporting Ultrasound Findings of Adnexal Masses

One problem commonly found in clinical practice is reporting findings. This may lead to problems in the transmission of information about findings from the sonologist to the clinician who makes the final decisions concerning patient management.

For this reason, Amor et al. proposed the Gynecologic Imaging Reporting and Data System (GI-RADS) (24). This reporting

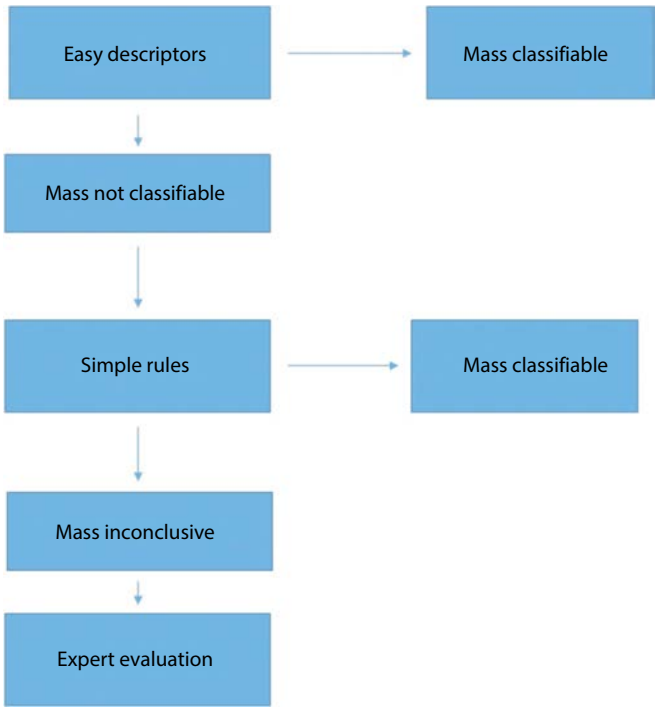

FIGURE 2.9 The sequential use of the IOTA three-step strategy for ultrasound evaluation of adnexal masses.

TABLE 2.2

IOTA Simple Descriptors

Benign Simple Descriptor	Presumed Diagnosis	Correct Outcome (Benign or Malignant) (%)
Unilocular tumor with ground glass echogenicity in a premenopausal woman	Endometrioma	99.5
Unilocular tumor with mixed echogenicity and acoustic shadows in a premenopausal woman	Teratoma	100
Unilocular anechoic tumor with regular walls and maximum diameter of lesion <10 cm	Simple cyst/ Serous cyst	98.8
Unilocular tumor with regular walls	Other benign	98.6
Malignant Simple Descriptor		
Tumor with ascites and at least moderate color Doppler blood flow in a postmenopausal woman	Cancer	95.6
Age >50 years and CA-125 > 100 U/mL	Cancer	93.2

Source: Adapted from Ameye L et al. *Ultrasound Obstet Gynecol.* 2012;40:582–591.

system follows the concept of the Breast Imaging, Reporting and Data System (BI-RADS). It is based on a risk estimation of malignancy and suggests management of the adnexal mass (Table 2.3, Figure 2.10).

TABLE 2.3

GI-RADS

GI-RADS Grade	Diagnosis	Estimated Probability of Malignancy (%)	Description
1	Definitive benign	0	Normal ovaries identified and no adnexal mass seen
2	Very probably benign	<1	Adnexal lesions thought to be of functional origin, for example, follicles, corpora lutea, hemorrhagic cysts
3	Probably benign	1–4	Neoplastic adnexal lesions thought to be benign, such as endometrioma, teratoma, simple cyst, hydrosalpinx, para-ovarian cyst, peritoneal pseudocyst, pedunculated myoma, or findings suggestive of pelvic inflammatory disease
4	Probably malignant	5–20	Any adnexal lesion not included in GI-RADS 1–3 and with one or two findings suggestive of malignancy[a]
5	Very probably malignant	>20	Adnexal masses with three or more findings suggestive of malignancy[a]

Source: Adapted from Amor F et al. *Ultrasound Obstet Gynecol.* 2011;38:450–455.

[a] Thick papillary projections, thick septations, solid areas, or ascites, defined according to IOTA criteria, and vascularization within solid areas, papillary projections, or central area of a solid tumor on color or power Doppler.

There is some evidence that GI-RADS may be of help to referral clinicians not involved in the ultrasound examination but involved in patient management (25).

Other Imaging Techniques for Differential Diagnosis of Adnexal Masses

Ultrasound-Based Imaging Techniques

Contrast-enhanced ultrasound (CEUS) has been proposed as an ultrasound-based technique for the characterization of adnexal tumors. This technique is based on assessment of the vascularization of the tumor after an intravenous injection of a contrast agent. Using this contrast agent, microvascularity can be assessed as well as the kinetics of the contrast agent within the vessels of the tumor. A recent meta-analysis showed that this approach has a 89% pooled sensitivity and 92% pooled specificity for discriminating benign from malignant ovarian tumors (26). These figures are similar to those of grayscale and Doppler ultrasound.

Three-dimensional (3D) ultrasound has also been proposed as an ultrasound-based technique for the differential diagnosis of adnexal masses. Using this technique renders adnexal cysts and allows a clearer image of this internal surface (Figure 2.11).

(a)

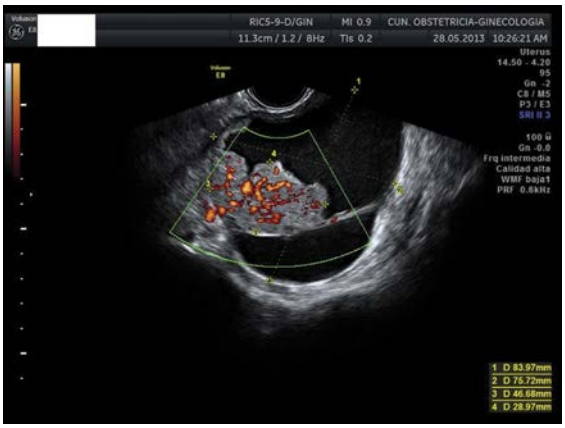

(b)

Gin Informe *Pàg. 1/2* **CUN. OBSTETRICIA-GINECOLOGIA**

Información del paciente/examen				*Fecha examen:*	**28.05.2013**
Nombre:	**Ovario**			*Eje. Méd:*	
ID paciente:	**715632**	*FDN:*		*Ref. Méd:*	
		Edad:		*Ecografista:*	
Indicación:		*Sexo:*	**Mujer**	*Tipo de examen:*	

FUR

FUR	*Dia del ciclo*	*Grávida*	*AB*
Dia de estim.	*Ovulación previst*	*Para*	*Ectópico*

2D genérico	*Valor*	*m1*	*m2*	*m3*	*m4*	*m5*	*m6*	*Mét.*
Dist.								
D	**53.71 mm**	**51.65**	**35.26**	**83.97**	**75.72**	**46.68**	**28.97**	**med.**

Coment.

Findings: Multilocular-solid adnexal mass, with two locules with anechoic content and a thin septum. One single solid area of 46x29mm with irregular contourOne single . Color score 4. No ascites. No carcinomatosis. Regular contour. No acoustic shadowing.
Presumptive diagnosis: Borderline tumor
GI-RADS 4: Probably malignant

FIGURE 2.10 Example of GI-RADS reporting system. (a) A multilocular solid mass with abundant vascularization can be observed. (b) The corresponding GI-RADS report describing the mass and providing a presumptive diagnosis and GI-RADS classification.

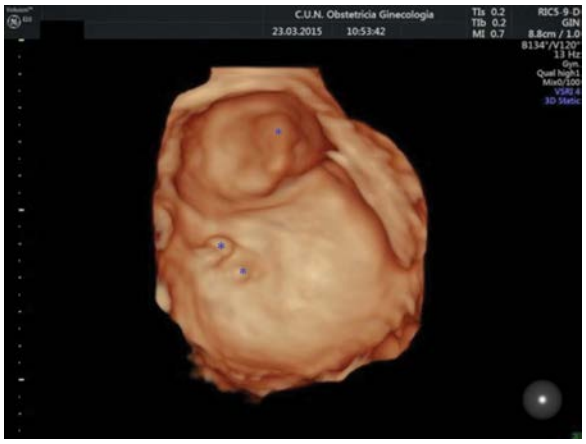

FIGURE 2.11 Three-dimensional ultrasound in surface rendering mode. We can observe the internal surface of a cyst's wall, depicting two locules with papillary projections (*).

However, some studies have shown that 3D ultrasound has no diagnostic advantage over two-dimensional (2D) ultrasound for most adnexal masses (27).

Another interesting characteristic of 3D ultrasound is the way this technique can assess tumor vascularization. Three-dimensional power Doppler ultrasound allows a 3D reconstruction of the tumor's vascular network (Figure 2.12). However, current evidence suggests that the assessment of a 3D vascular network is moderately reproducible among observers and does not significantly improve the diagnostic performance of 2D ultrasound (28).

Three-dimensional power Doppler ultrasound also allows an objective quantification of the amount of color content (vascularization) of ovarian tumors by estimating the 3D vascular indices (Figure 2.13). Although initial reports were encouraging (29), recent studies have shown that this technique does not improve the diagnostic performance of conventional 2D grayscale and Doppler ultrasound (30).

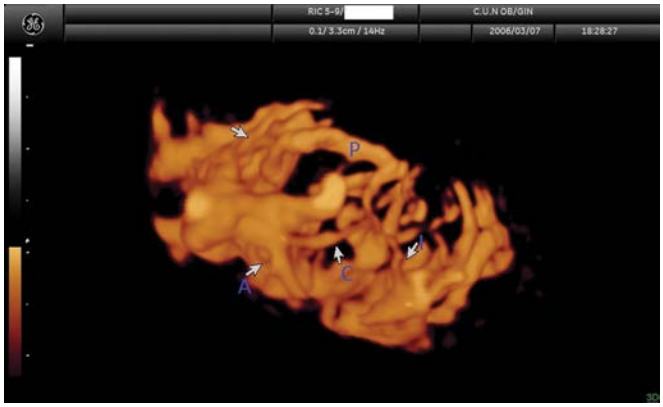

FIGURE 2.12 Three-dimensional ultrasound depicting a 3D reconstruction of the vascular tree of an ovarian tumor. Some suspicious features, such as irregular branching (I), vessel caliber change (C), shunt connections (A), and pseudoaneurysms (P) can be observed.

Other Imaging Techniques

Current evidence shows that other imaging techniques, such as computed tomography (CT), magnetic resonance imaging (MRI), or positron emission tomography (PET) can be useful for discriminating benign from adnexal masses (4). However, none of them is superior to ultrasound in terms of diagnostic performance, and all of them are more expensive and less available. For this reason, as stated earlier in this chapter, ultrasound should be the first-line imaging technique for distinguishing benign from malignant adnexal masses.

However, ultrasound cannot reliably determine the nature of adnexal masses in about 15% of the cases. These masses are deemed as *indeterminate masses*. There is evidence that MRI may be very helpful in this subset of adnexal masses, since it can correctly discriminate up to 92% of indeterminate masses at ultrasound examination (31). The CT scan and PET scan are not superior to MRI and should be considered for evaluating tumor spread in cases of ovarian cancer (see Chapter 4).

(a)

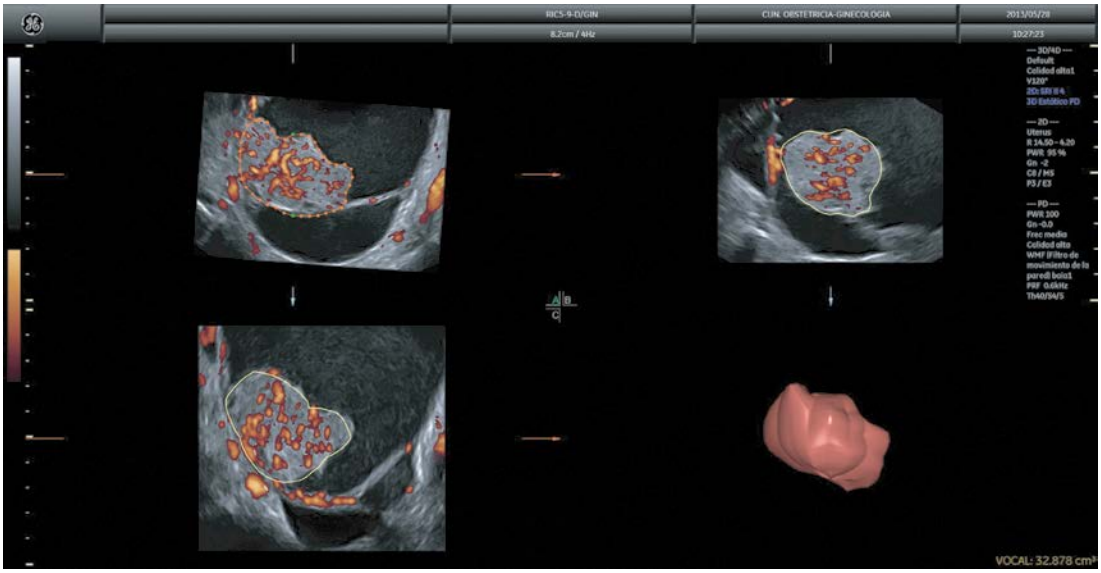

(b)

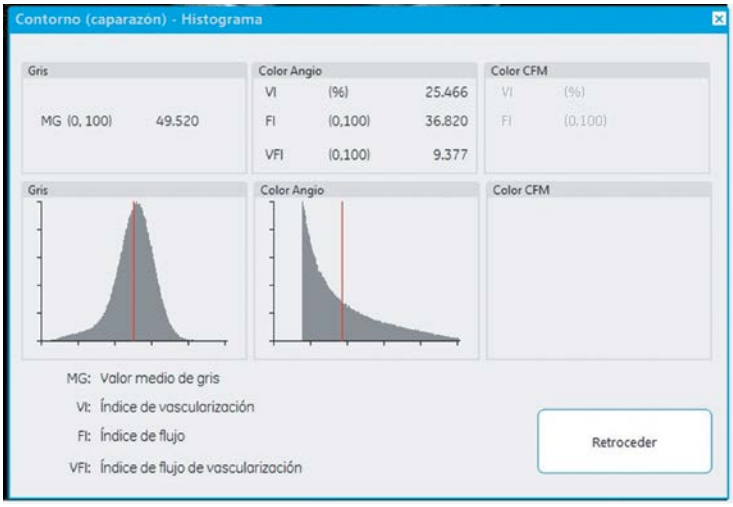

FIGURE 2.13 Three-dimensional ultrasound of a multilocular-solid mass. The solid component volume has been calculated (a), and within this solid component, the 3D vascular indices can be calculated (b).

REFERENCES

1. Canis M, Rabischong B, Houlle C et al. Laparoscopic management of adnexal masses: A gold standard? *Curr Opin Obstet Gynecol*. 2002;14:423–428.
2. Alcázar JL, Olartecoechea B, Guerriero S, Jurado M. Expectant management of adnexal masses in selected premenopausal women: A prospective observational study. *Ultrasound Obstet Gynecol*. 2013;41:582–588.
3. Vernooij F, Heintz P, Witteveen E, van der Graaf Y. The outcomes of ovarian cancer treatment are better when provided by gynecologic oncologists and in specialized hospitals: A systematic review. *Gynecol Oncol*. 2007;105:801–812.
4. American College of Obstetricians and Gynecologists' Committee on Practice Bulletins—Gynecology. Practice bulletin no. 174: Evaluation and management of adnexal masses. *Obstet Gynecol*. 2016;128:e210–e226.
5. Asch E, Levine D, Kim Y, Hecht JL. Histologic, surgical, and imaging correlations of adnexal masses. *J Ultrasound Med*. 2008;27:327–342.
6. Glanc P, Benacerraf B, Bourne T et al. First International Consensus Report on Adnexal Masses: Management recommendations. *J Ultrasound Med*. 2017;36:849–863.
7. Timmerman D, Valentin L, Bourne TH, Collins WP, Verrelst H, Vergote I; International Ovarian Tumor Analysis (IOTA) Group. Terms, definitions and measurements to describe the sonographic features of adnexal tumors: A consensus opinion from the International Ovarian Tumor Analysis (IOTA) group. *Ultrasound Obstet Gynecol*. 2000;16:500–505.
8. Meys EM, Kaijser J, Kruitwagen RF et al. Subjective assessment versus ultrasound models to diagnose ovarian cancer: A systematic review and meta-analysis. *Eur J Cancer*. 2016;58:17–29.
9. Guerriero S, Alcázar JL, Pascual MA et al. Intraobserver and interobserver agreement of grayscale typical ultrasonographic patterns for the diagnosis of ovarian cancer. *Ultrasound Med Biol*. 2008;34:1711–1716.
10. Van Holsbeke C, Daemen A, Yazbek J et al. Ultrasound experience substantially impacts on diagnostic performance and confidence when adnexal masses are classified using pattern recognition. *Gynecol Obstet Invest*. 2010;69:160–168.
11. Kaijser J, Sayasneh A, Van Hoorde K et al. Presurgical diagnosis of adnexal tumours using mathematical models and scoring systems: A systematic review and meta-analysis. *Hum Reprod Update*. 2014;20:449–462.
12. Lee TS, Kim JW, Park NH, Song YS, Kang SB, Lee HP. Assessing clinical performance of gynecology residents: Sonographic evaluation of adnexal masses based on morphological scoring systems. *Ultrasound Obstet Gynecol*. 2005;26:776–779.
13. Alcázar JL, Royo P, Jurado M et al. Triage for surgical management of ovarian tumors in asymptomatic women: Assessment of an ultrasound-based scoring system. *Ultrasound Obstet Gynecol*. 2008;32:220–225.
14. Myers ER, Bastian LA, Havrilesky LJ et al. Management of Adnexal Mass. Rockville, MD: Agency for Healthcare Research and Quality; 2006. *Evidence Report/Technology Assessment 130*.
15. Timmerman D, Testa AC, Bourne T et al. Simple ultrasound-based rules for the diagnosis of ovarian cancer. *Ultrasound Obstet Gynecol*. 2008;31:681–690.
16. Timmerman D, Van Calster B, Testa A et al. Predicting the risk of malignancy in adnexal masses based on the Simple Rules from the International Ovarian Tumor Analysis group. *Am J Obstet Gynecol*. 2016;214:424–437.
17. Ameye L, Timmerman D, Valentin L et al. Clinically oriented three-step strategy for assessment of adnexal pathology. *Ultrasound Obstet Gynecol*. 2012;40:582–591.
18. Alcázar JL, Pascual MA, Graupera B et al. External validation of IOTA simple descriptors and simple rules for classifying adnexal masses. *Ultrasound Obstet Gynecol*. 2016;48:397–402.
19. Sayasneh A, Kaijser J, Preisler J et al. A multicenter prospective external validation of the diagnostic performance of IOTA simple descriptors and rules to characterize ovarian masses. *Gynecol Oncol*. 2013;130:140–146.
20. Jacobs I, Oram D, Fairbanks J, Turner J, Frost C, Grudzinskas JG. A risk of malignancy index incorporating CA 125, ultrasound and menopausal status for the accurate preoperative diagnosis of ovarian cancer. *Br J Obstet Gynaecol*. 1990;97:922–929.
21. Van Calster B, Van Hoorde K, Valentin L et al. Evaluating the risk of ovarian cancer before surgery using the ADNEX model to differentiate between benign, borderline, early and advanced stage invasive, and secondary metastatic tumours: Prospective multicentre diagnostic study. *BMJ*. 2014;349:g5920.
22. Szubert S, Wojtowicz A, Moszynski R et al. External validation of the IOTA ADNEX model performed by two independent gynecologic centers. *Gynecol Oncol*. 2016;142:490–495.
23. Araujo KG, Jales RM, Pereira PN et al. Performance of the IOTA ADNEX model in preoperative discrimination of adnexal masses in a gynecological oncology center. *Ultrasound Obstet Gynecol*. 2017;49:778–783.
24. Amor F, Vaccaro H, Alcázar JL, León M, Craig JM, Martinez J. Gynecologic imaging reporting and data system: A new proposal for classifying adnexal masses on the basis of sonographic findings. *J Ultrasound Med*. 2009;28:285–291.
25. Amor F, Alcázar JL, Vaccaro H, León M, Iturra A. GI-RADS reporting system for ultrasound evaluation of adnexal masses in clinical practice: A prospective multicenter study. *Ultrasound Obstet Gynecol*. 2011;38:450–455.
26. Wu Y, Peng H, Zhao X. Contrast-enhanced ultrasound for differential diagnosis of malignant and benign ovarian tumors: Systematic review and meta-analysis. *Ultrasound Obstet Gynecol*. 2015;46:277–283.
27. Alcázar JL, Iturra A, Sedda F, Aubá M, Ajossa S, Guerriero S, Jurado M. Three-dimensional volume off-line analysis as compared to real-time ultrasound for assessing adnexal masses. *Eur J Obstet Gynecol Reprod Biol*. 2012;161:92–95.
28. Alcázar JL, Cabrera C, Galván R, Guerriero S. Three-dimensional power Doppler vascular network assessment of adnexal masses: Intraobserver and interobserver agreement analysis. *J Ultrasound Med*. 2008;27:997–1001.
29. Alcázar JL, Mercé LT, García Manero M. Three-dimensional power Doppler vascular sampling: A new method for predicting ovarian cancer in vascularized complex adnexal masses. *J Ultrasound Med*. 2005;24:689–696.
30. Utrilla-Layna J, Alcázar JL, Aubá M et al. Performance of three-dimensional power Doppler angiography as third-step assessment in differential diagnosis of adnexal masses. *Ultrasound Obstet Gynecol*. 2015;45:613–617.
31. Anthoulakis C, Nikoloudis N. Pelvic MRI as the "gold standard" in the subsequent evaluation of ultrasound-indeterminate adnexal lesions: A systematic review. *Gynecol Oncol*. 2014;132:661–668.

3

Ultrasound Features of Ovarian Malignancies

Introduction

Ovarian cancer represents the sixth most common cancer among women worldwide. The age-adjusted incidence is about 11.7 per 100,000 women per year (1). This disease is the most lethal gynecologic malignancy, with a global 5-year survival of 30%–45%. Most women are diagnosed in an advanced stage, and there is no effective method for screening (1). According to the International Federation of Gynecology and Obstetrics (FIGO), staging should be performed surgically (2) (Table 3.1).

Histologically, the World Health Organization (WHO) classifies ovarian malignancies into two main groups: epithelial and nonepithelial cancers (3). Within the epithelial tumors, a particular subset is constituted by the borderline tumors or low malignant potential tumors. These tumors are characterized by the presence, in the epithelium of the ovary, of noninvasive neoplastic cells.

It has been presumed that fallopian tube malignancies were rare. However, histologic, molecular, and genetic evidence shows that around 50% of tumors classified as high-grade serous carcinomas of the ovary may have their origin in the fimbrial end of the fallopian tube (4). Therefore, the incidence of fallopian tube cancers may have been substantially underestimated. These new data support the view that high-grade serous ovarian, fallopian tube, and peritoneal cancers should be considered collectively.

In this chapter, we review the ultrasound features of different ovarian malignancies, including metastatic tumors to the ovary, and considering fallopian tube carcinomas and primary peritoneal carcinomas as the same entity together with ovarian carcinomas when describing high-grade serous carcinomas.

Borderline Tumors

Borderline tumors (BOTs) are epithelial tumors of a noninvasive nature but that show neoplastic cells within the ovarian epithelium. They constitute about 15% of all epithelial ovarian tumors (3).

TABLE 3.1

FIGO Ovarian, Fallopian Tube, and Peritoneal Cancer Staging

Stage	Description
Stage I	Tumor confined to ovaries or fallopian tube(s)
IA	Tumor limited to one ovary (capsule intact) or fallopian tube; no tumor on ovarian or fallopian tube surface; no malignant cells in the ascites or peritoneal washings
IB	Tumor limited to both ovaries (capsules intact) or fallopian tubes; no tumor on ovarian or fallopian tube surface; no malignant cells in the ascites or peritoneal washings
IC	Tumor limited to one or both ovaries or fallopian tubes, with any of the following:
IC1	Surgical spill
IC2	Capsule ruptured before surgery or tumor on ovarian or fallopian tube surface
IC3	Malignant cells in the ascites or peritoneal washings
Stage II	Tumor involves one or both ovaries or fallopian tubes with pelvic extension (below pelvic brim) or primary peritoneal cancer
IIA	Extension and/or implants on uterus and/or fallopian tubes and/or ovaries
IIB	Extension to other pelvic intraperitoneal tissues
Stage III	Tumor involves one or both ovaries or fallopian tubes, or primary peritoneal cancer, with cytologically or histologically confirmed spread to the peritoneum outside the pelvis and/or metastasis to the retroperitoneal lymph nodes
IIIA1	Positive retroperitoneal lymph nodes only (cytologically or histologically proven):
IIIA1(i)	Metastasis up to 10 mm in greatest dimension
IIIA1(ii)	Metastasis more than 10 mm in greatest dimension
IIIA2	Microscopic extrapelvic (above the pelvic brim) peritoneal involvement with or without positive retroperitoneal lymph nodes
IIIB	Macroscopic peritoneal metastasis beyond the pelvis up to 2 cm in greatest dimension, with or without metastasis to the retroperitoneal lymph nodes
IIIC	Macroscopic peritoneal metastasis beyond the pelvis more than 2 cm in greatest dimension, with or without metastasis to the retroperitoneal lymph nodes (includes extension of tumor to capsule of liver and spleen without parenchymal involvement of either organ)
Stage IV	Distant metastasis excluding peritoneal metastases
IVA	Pleural effusion with positive cytology
IVB	Parenchymal metastases and metastases to extra-abdominal organs (including inguinal lymph nodes and lymph nodes outside of the abdominal cavity)

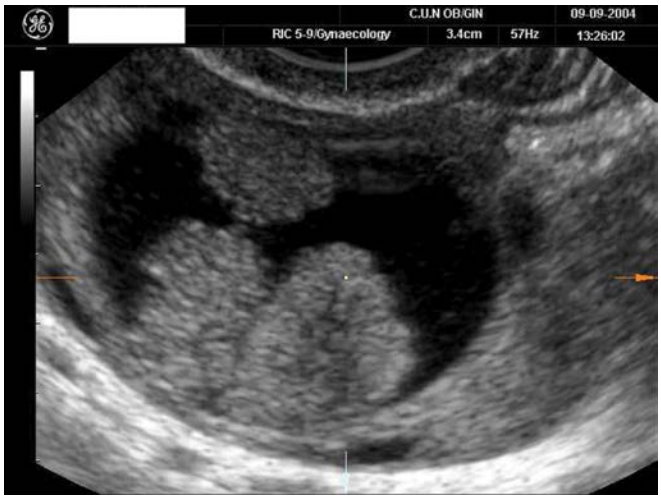

FIGURE 3.1 Unilocular-solid ovarian lesion. At least three papillary projections can be observed. Note the irregular surface of these papillary projections. Histologic analysis revealed a serous borderline tumor.

There are different histotypes. The most frequent is serous BOT (65%–70% of all BOTs), followed by mucinous BOT (15%), endometrioid BOT (5%), and transitional cell BOT (5%) (3).

Serous BOTs occur in the fourth and fifth decades of life and may be bilateral in 30%–50% of the cases (3). The typical ultrasound appearance of serous BOT is unilocular-solid or multilocular-solid adnexal (Figures 3.1 and 3.2), usually with three to five vascularized papillary projections with irregular surfaces (5). When they exhibit a multilocular appearance, the number of locules used is less than 10. Sometimes serous BOTs appear as a solid lesion with an irregular surface (Figure 3.3). Rarely, these tumors appear as a unilocular or multilocular lesion without solid components.

Mucinous BOTs tend to occur in the fifth and sixth decades. There are two different subhistotypes: intestinal (90% of all mucinous BOTs, rarely bilateral) and endocervical (10% of all mucinous BOTs and bilateral in up to 40% of cases).

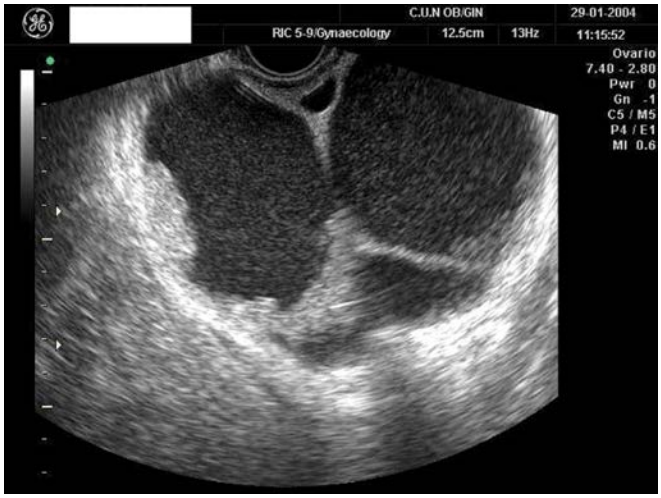

FIGURE 3.2 A multilocular-solid ovarian lesion, showing solid components arising from the internal surface of the cyst's wall. Histology confirmed this lesion as a serous borderline tumor.

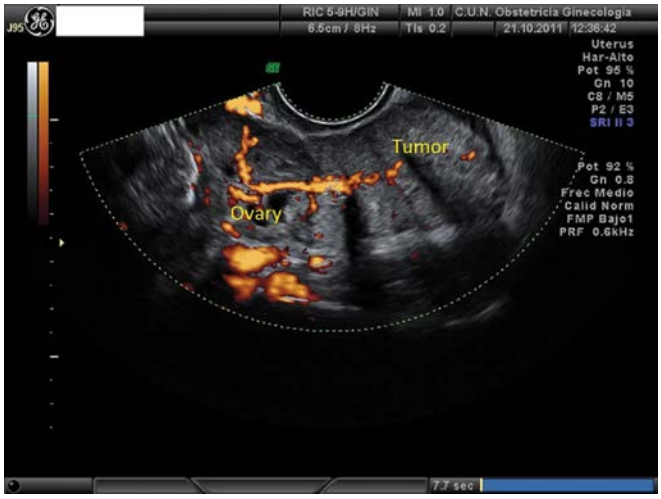

FIGURE 3.3 Transvaginal ultrasound showing a solid tumor arising from the ovarian surface. A large feeding vessel can be seen running from the ovarian stroma into the tumor. Histological analysis after tumor removal revealed a serous borderline tumor.

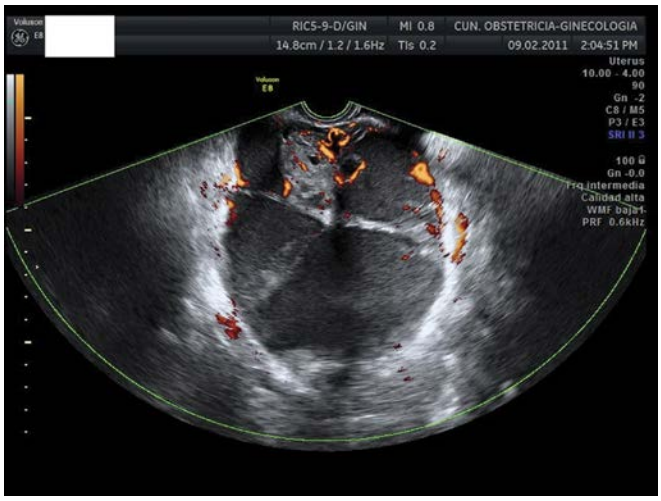

FIGURE 3.4 A multilocular-solid tumor with abundant vascularization within the solid component. This lesion was proven as an intestinal-type mucinous borderline tumor after surgical removal.

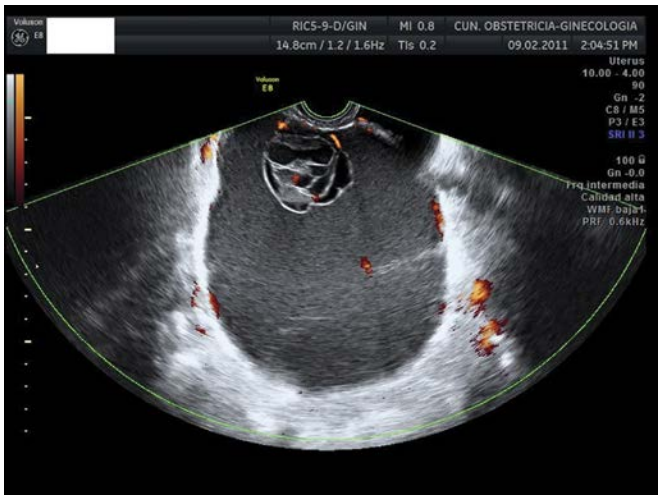

FIGURE 3.5 This is the same case as in Figure 3.4, in a different plane. Adjacent to the solid component, there is a multilocular area. Please note different echogenicities of the locules as typical from a mucinous tumor.

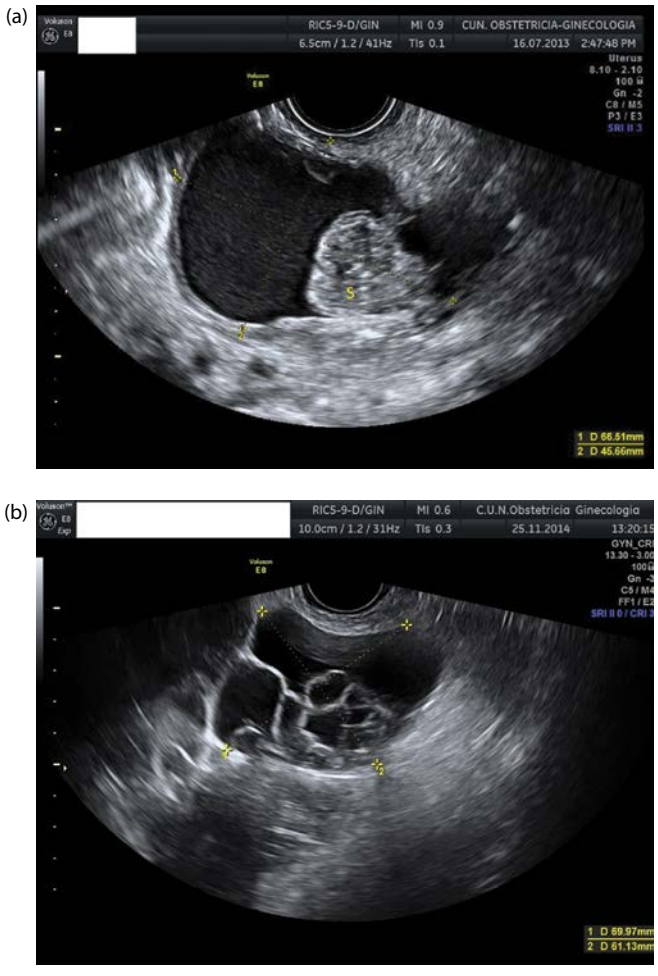

FIGURE 3.6 Transvaginal ultrasound showing a unilocular cyst (a). There is an area that appears to be solid. However, this area actually corresponds to a multicystic area with many tiny locules. This is characteristic of an endocervical-type mucinous borderline tumor. These tumors may also appear as multilocular cysts (b).

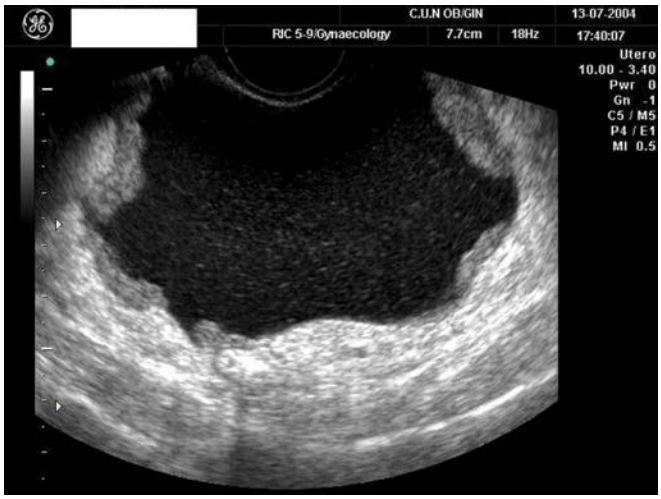

FIGURE 3.7 Transvaginal ultrasound showing a unilocular cyst with a rather low-level echogenic content and irregular walls. Histological analysis confirmed this lesion as an endometrioid borderline tumor.

An intestinal-type mucinous BOT appears commonly as a large unilateral multilocular cyst with some solid components (5). The number of locules uses to be more than 10 (Figure 3.4). Color score uses to be moderate. The echogenicities of locules' content may vary (Figure 3.5).

The endocervical-type mucinous BOT appears as a unilocular cyst with an area of grouped microcysts, like a "grape bunch" (Figure 3.6). Solid components are rare.

Endometrioid BOTs are uncommon. The most frequent ultrasound appearance of them is as a unilocular cyst with irregular walls and ground-glass content (Figure 3.7).

Primary Epithelial Invasive Ovarian Carcinoma

Epithelial invasive cancer is the most frequent ovarian malignancy. It accounts for 80% of all ovarian malignancies (3). Most of these tumors appear in the sixth and seventh decades. Currently, it is accepted that there are two types of primary epithelial ovarian cancer (EOC): type I and type II (4).

Type I EOC accounts for 30% of all EOCs. This type includes low-grade serous carcinomas, low-grade endometrioid carcinomas, clear cell carcinomas, and mucinous carcinomas, as well as malignant transitional cell tumors. These tumors are indolent, are usually diagnosed in an early stage, and are characterized by specific mutations, such as k-RAS, PTEN, and ARID1A (4). Their origin seems to be the epithelium of the ovarian surface, and it seems there is a transition from a benign epithelium to a borderline lesion that turns into invasive cancer (6).

Type II EOC constitutes about 70% of all EOCs. They include high-grade serous carcinomas, high-grade endometrioid carcinomas, carcinosarcomas, and undifferentiated carcinomas. These tumors are aggressive and in most cases are in an advanced stage at diagnosis. These EOCs are associated with mutations of the oncogenes p53 and BRCA. These tumors seem to originate in the epithelium of the fimbria, from the fallopian tube in most cases, and do not have a BOT precursor.

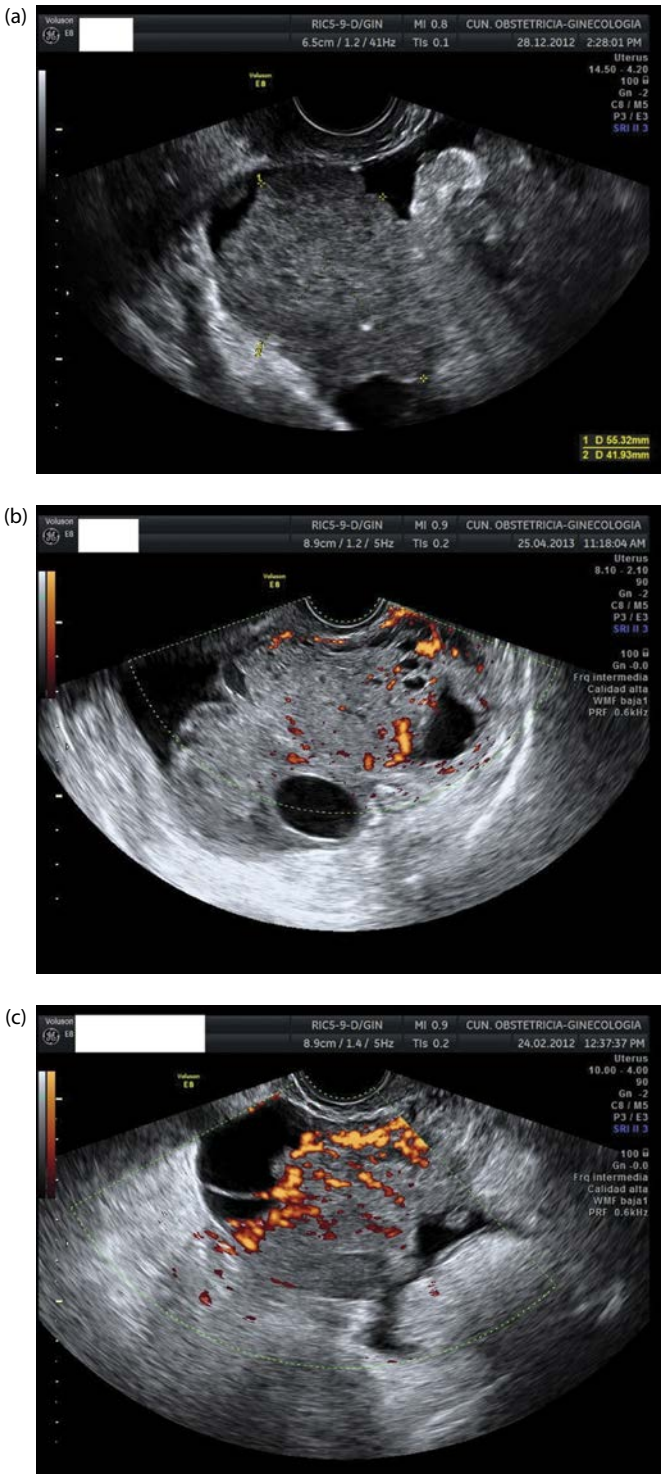

FIGURE 3.8 Some examples of primary invasive epithelial ovarian carcinomas. (a) Irregular purely solid tumor. (b) Solid tumor with cystic content and abundant vascularization. (c) Unilocular-solid tumor with large solid component and abundant vascularization.

Sonographically, types I and II EOCs share many features. The most common findings are the presence of unilocular-solid, multilocular-solid, or solid lesions, with a highly vascularized large solid component (Figure 3.8).

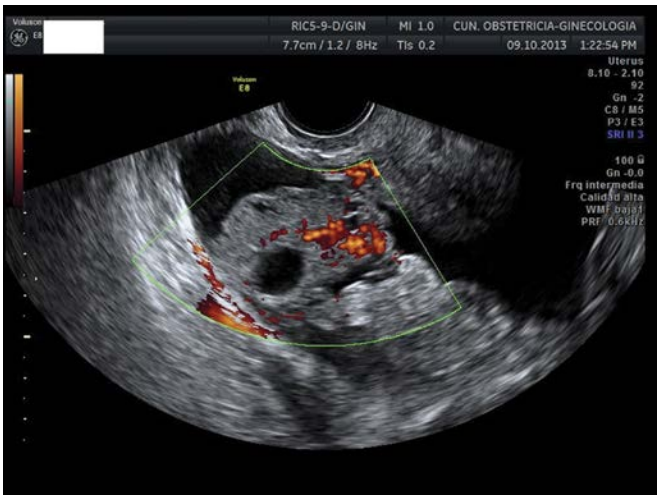

FIGURE 3.9 Transvaginal ultrasonography showing an example of type II epithelial ovarian cancer in a postmenopausal woman. The ovary is almost normal in size, but the surface is irregular, internal echogenicity is not homogeneous, and vascularization is abundant. Ascites can also be noted.

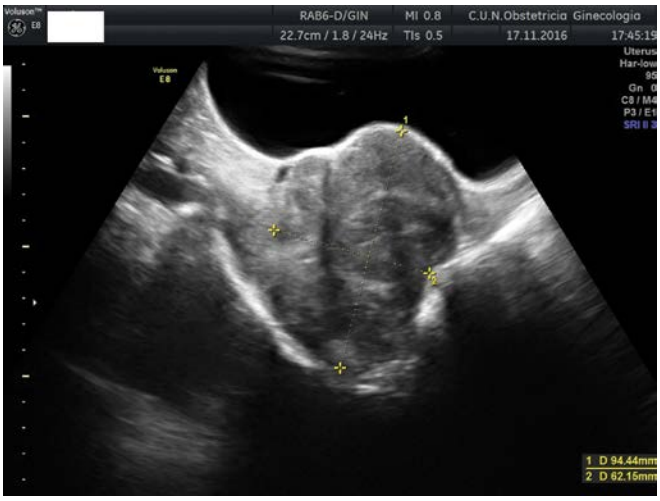

FIGURE 3.10 Transabdominal ultrasound in a 15-year-old girl, showing a large, multilobulated, solid adnexal tumor. Histology revealed an ovarian dysgerminoma.

Ascites and sonographic signs of carcinomatosis are a common finding, especially in type II EOCs (7). Bilateral presentation is also more frequent in type II EOCs (7). Type II EOCs tend to be smaller than type I EOCs (Figure 3.9).

Sonographically, it is almost impossible to discriminate among the different histotypes of EOCs.

Primary Nonepithelial Ovarian Malignancies

Nonepithelial ovarian malignancies are relatively uncommon tumors. They include germ cell tumors, sex-cord stromal tumors, mesenchymal malignant tumors, and lymphoid tumors. We review the most frequent types of these tumors.

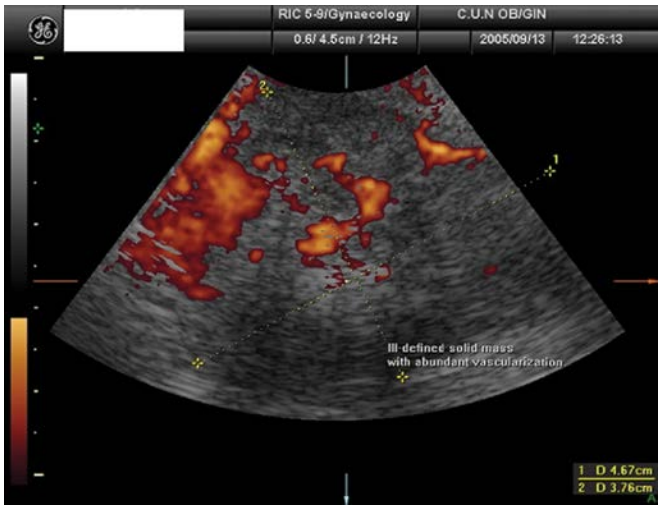

FIGURE 3.11 Transvaginal ultrasound showing an irregular solid tumor with abundant vascularization in a postmenopausal woman. Histology revealed a Sertoli-Leydig cell tumor.

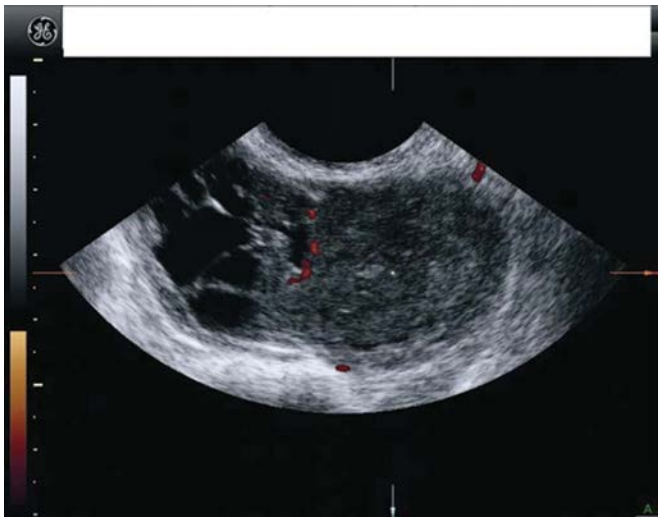

FIGURE 3.12 Transvaginal ultrasound in a 52-year-old woman showing an adnexal mass with a solid component and a multilocular cystic area. Histological analysis showed a granulosa-cell tumor.

Dysgerminoma

Dysgerminomas comprise 1%–2% of all malignant ovarian tumors. These tumors occur most commonly in the second and third decades of life (3).

The typical ultrasound appearance of ovarian dysgerminoma is a large unilateral moderately or highly vascularized purely solid lesion with irregular internal echogenicity and multilobulated appearance (8) (Figure 3.10). Ascites is uncommon.

Sertoli Cell Tumors

Sertoli cell tumors, Leydig cell tumors, and Sertoli-Leydig cell tumors account for less than 1% of all ovarian tumors. Sertoli cell tumors and Sertoli-Leydig cell tumors occur in young women (usually less than 30 years old), whereas Leydig cell tumors appear in postmenopausal women (3).

The typical ultrasound features of these tumors are a unilateral multilocular solid or solid tumor with irregular contour (9) (Figure 3.11). Tumor size may vary significantly. Vascularization is high or moderate. Ascites is uncommon.

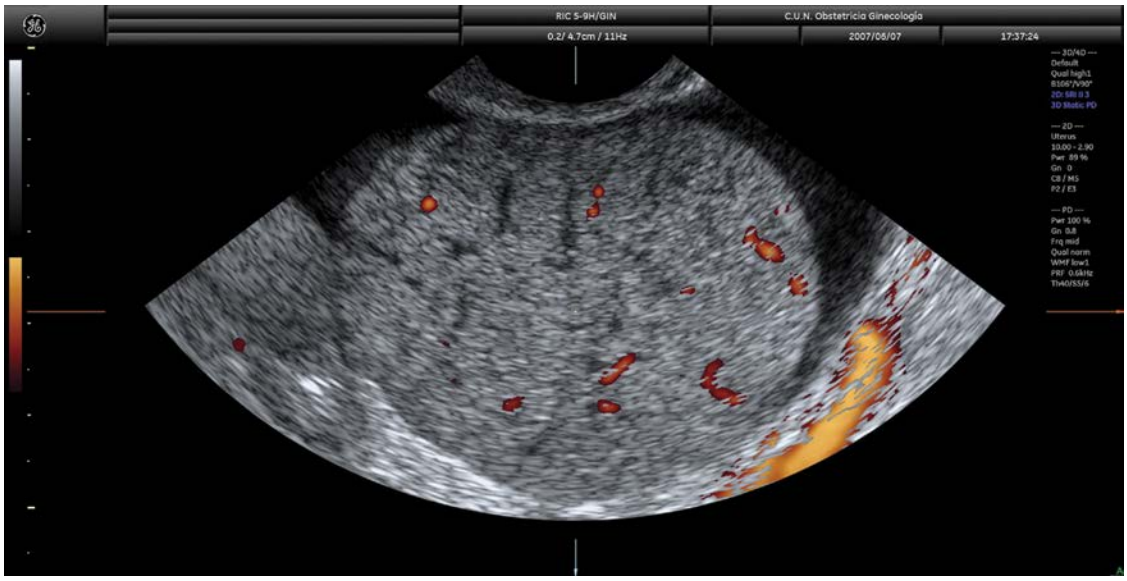

FIGURE 3.13 Transvaginal ultrasound in a 23-year-old woman. A well-defined solid tumor with nonhomogeneous echogenicity and moderate vascularization is observed. Histology confirmed a yolk-sac tumor.

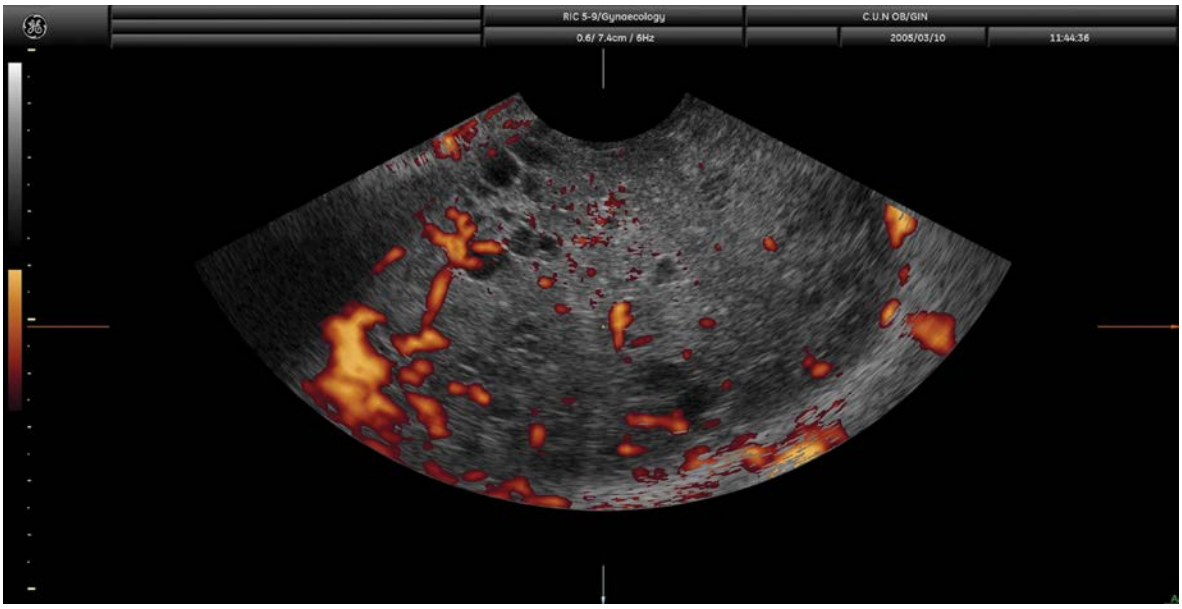

FIGURE 3.14 Transvaginal ultrasound from an immature teratoma in a 26-year-old woman. A solid tumor with some small cystic areas and abundant vascularization is observed.

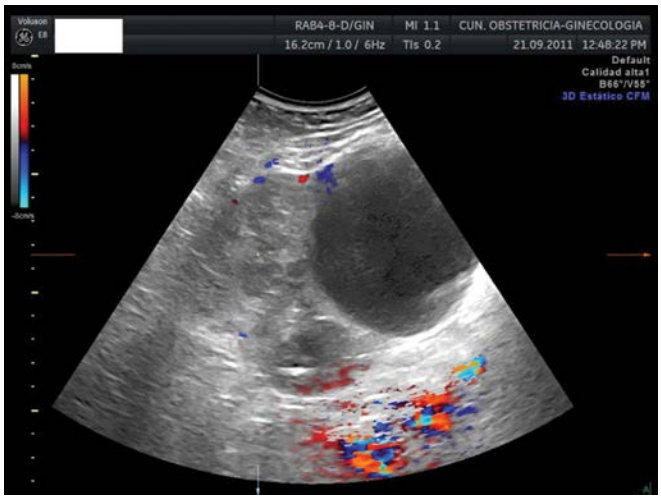

FIGURE 3.15 Transabdominal ultrasound showing a large multilocular-solid adnexal mass. Histology revealed a malignant struma ovarii.

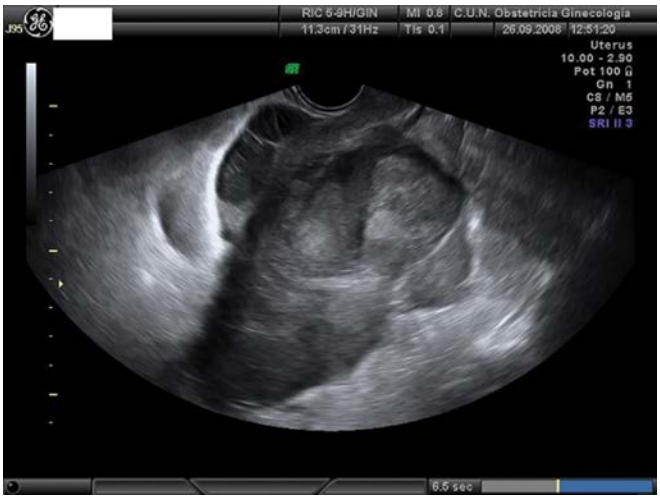

FIGURE 3.16 Transvaginal ultrasound depicting a large, irregular, solid adnexal mass with heterogeneous internal echogenicity. Histological analysis after tumor removal demonstrated this lesion as a primary ovarian angiosarcoma.

Granulosa Cell Tumors

Granulosa cell tumors account for approximately 3% of all ovarian malignancies. Histologically there are two different types: adult (90%) and juvenile (10%) (3). The juvenile type is most commonly found in prepuberal girls or young women. The adult type is more common in postmenopausal women.

Typical ultrasound findings of granulosa cell tumors are the presence of a multilocular-solid or solid lesion with moderate or high vascularization. Most lesions have a size $\geq$8 cm (10) (Figure 3.12). When a multilocular lesion appears, the number of locules is more than 10 in most cases.

Other Nonepithelial Ovarian Tumors

There are few reports about the ultrasound features of other types of nonepithelial ovarian malignancies.

Yolk-sac tumors account for less than 1% of all ovarian malignancies. They appear in prepuberal girls or young women (3). In our experience, yolk-sac tumors appear as a large, highly vascularized, solid unilateral lesion with some tiny cystic content (Figure 3.13).

Immature teratomas account for less than 1% of all ovarian malignancies and commonly appear in young women (3). In our experience, an immature teratoma appears as a large, purely

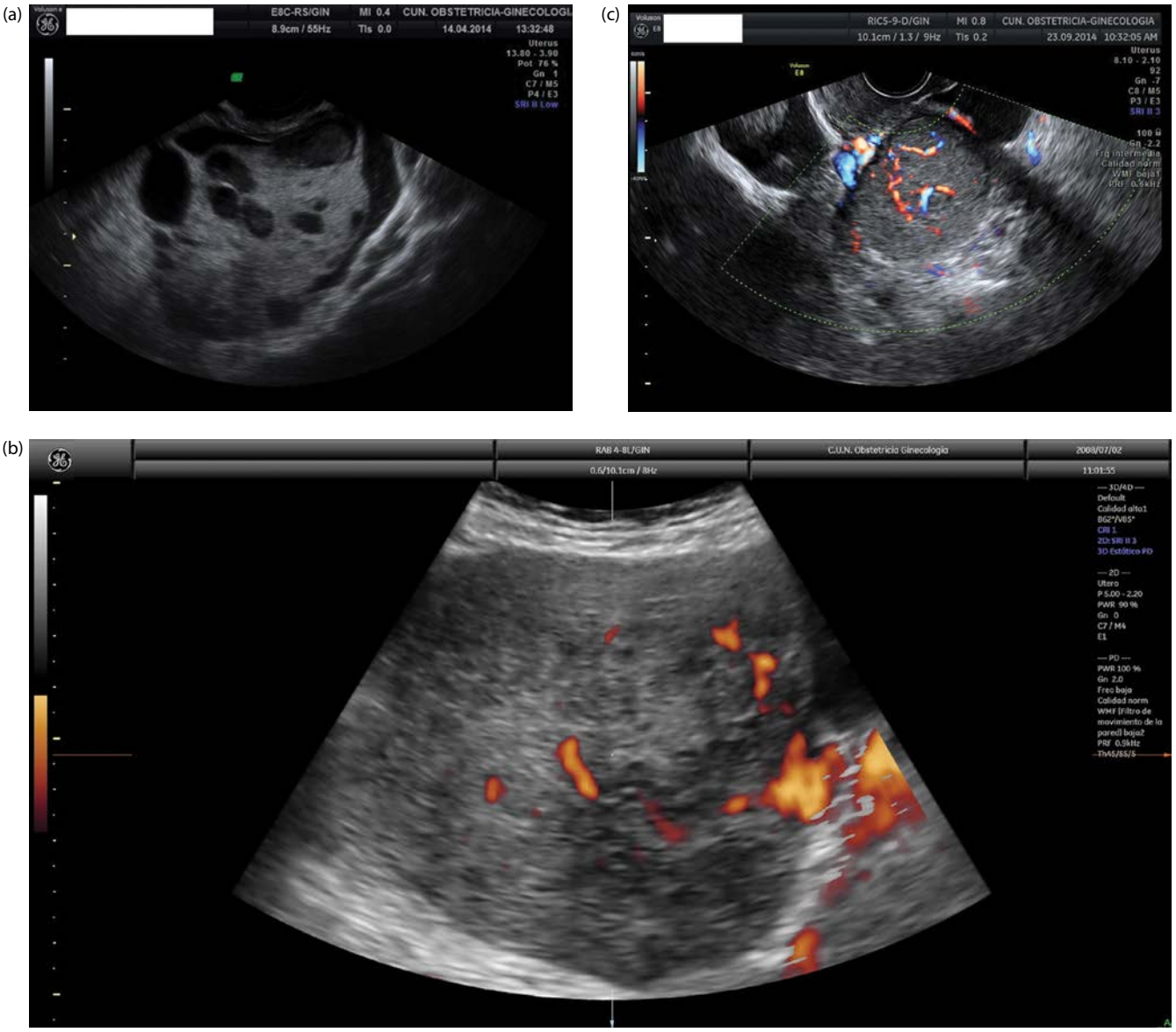

FIGURE 3.17 Ultrasound images from metastatic tumors to the ovary. (a) Metastasis from a colorectal carcinoma showing a solid mass with cystic areas. (b) Metastasis from a gastric cancer showing a large, solid mass with abundant vascularization. (c) Metastasis from a breast cancer showing a small, solid mass with abundant vascularization.

solid, irregular tumor with heterogeneous internal echogenicity (Figure 3.14).

Malignant struma ovarii is a rare ovarian malignancy. Its typical ultrasound appearance is a multilocular-solid, moderately vascularized lesion (11) (Figure 3.15).

Malignant mesenchymal tumors are mainly constituted by primary ovarian sarcomas. They may be pure, soft tissue sarcomas or sarcomas derived from ovarian teratomas (3). They include leiomyosarcoma, angiosarcoma, osteosarcoma, fibrosarcoma, chondrosarcoma, rhabdomyosarcoma, and malignant fibrous histiocytoma (3).

Sonographically, these tumors appear as large solid lesions with heterogeneous internal echogenicity (Figure 3.16).

Metastatic Tumors to the Ovary

Metastatic tumors to the ovary account for up to 5%–8% of all ovarian malignancies (3,12). Most metastatic tumors to the ovary originate from the gastrointestinal tract (colon-rectum and stomach), the uterus, or the breast (3).

Metastasis from a colon-rectum carcinoma appears as a large multilocular-solid or solid lesion with moderate or high vascularization and irregular contours (12,13) (Figure 3.17a).

Metastasis from a stomach carcinoma also appears as a large solid or less commonly multilocular-solid tumor with regular contour and moderate or high vascularization (12,13). (Figure 3.17b).

Metastasis from a breast carcinoma usually appears as a small, bilateral, highly vascularized, solid lesion with sharp contours (12,13) (Figure 3.17c).

REFERENCES

1. Webb PM, Jordan SJ. Epidemiology of epithelial ovarian cancer. *Best Pract Res Clin Obstet Gynaecol*. 2017;41:3–14.
2. Berek JS, Crum C, Friedlander M. Cancer of the ovary, fallopian tube, and peritoneum. *Int J Gynaecol Obstet*. 2015;131(Suppl 2):S111–S122.
3. Tavassoli FA and Devilee P. (Eds.). WHO Classification of Tumors. *Tumors of the Breast and Female Genital Organs*. IARC Press, Lyon, France, 2003.
4. Kurman RJ, Shih IeM. Molecular pathogenesis and extraovarian origin of epithelial ovarian cancer—Shifting the paradigm. *Hum Pathol*. 2011;42:918–931.
5. Fruscella E, Testa AC, Ferrandina G et al. Ultrasound features of different histopathological subtypes of borderline ovarian tumors. *Ultrasound Obstet Gynecol*. 2005;26:644–650.
6. Jordan S, Green A, Webb P. Benign epithelial ovarian tumours—Cancer precursors or markers for ovarian cancer risk? *Cancer Causes Control*. 2006;17:623–632.
7. Alcázar JL, Utrilla-Layna J, Mínguez JÁ, Jurado M. Clinical and ultrasound features of type I and type II epithelial ovarian cancer. *Int J Gynecol Cancer*. 2013;23:680–684.
8. Guerriero S, Testa AC, Timmerman D et al. Imaging of gynecological disease (6): Clinical and ultrasound characteristics of ovarian dysgerminoma. *Ultrasound Obstet Gynecol*. 2011;37:596–602.
9. Demidov VN, Lipatenkova J, Vikhareva O, Van Holsbeke C, Timmerman D, Valentin L. Imaging of gynecological disease (2): Clinical and ultrasound characteristics of Sertoli cell tumors, Sertoli-Leydig cell tumors and Leydig cell tumors. *Ultrasound Obstet Gynecol*. 2008;31:85–91.
10. Van Holsbeke C, Domali E, Holland TK et al. Imaging of gynecological disease (3): Clinical and ultrasound characteristics of granulosa cell tumors of the ovary. *Ultrasound Obstet Gynecol*. 2008;31:450–456.
11. Savelli L, Testa AC, Timmerman D, Paladini D, Ljungberg O, Valentin L. Imaging of gynecological disease (4): Clinical and ultrasound characteristics of struma ovarii. *Ultrasound Obstet Gynecol*. 2008;32:210–219.
12. Guerriero S, Alcázar JL, Pascual MA, Ajossa S, Olartecoechea B, Hereter L. Preoperative diagnosis of metastatic ovarian cancer is related to origin of primary tumor. *Ultrasound Obstet Gynecol*. 2012;39:581–586.
13. Testa AC, Ferrandina G, Timmerman D et al. Imaging in gynecological disease (1): Ultrasound features of metastases in the ovaries differ depending on the origin of the primary tumor. *Ultrasound Obstet Gynecol*. 2007;29:505–511.

4

Ultrasound Assessment of Intra-Abdominal Spread of Ovarian Cancer

Introduction

As stated in Chapter 3, ovarian cancer should be staged surgically (1). About 65%–75% of women who receive a diagnosis of ovarian cancer present with advanced disease (stage III or IV) at diagnosis (2).

Contemporary management of advanced ovarian cancer includes exploratory laparotomy with tumor cytoreduction followed by taxane-/platinum-based chemotherapy (3).

Optimal cytoreduction (less than 0.5 cm size of residual tumor nodules) or complete cytoreduction (no macroscopic residual disease) is consistently associated with a better response to chemotherapy and prolonged survival (4). On the contrary, suboptimal cytoreduction has no beneficial effect on survival and may be associated with significant morbidity and mortality (5).

The reported rate of optimal cytoreduction from centers with adequate resources, volume, and experience ranges from 60% to 90% (6). Optimal cytoreduction cannot be achieved in all women even in an adequate surgical setting.

Women with advanced-stage disease may also benefit from neoadjuvant chemotherapy (NACT) followed by internal cytoreduction; primary cytoreduction is recommended over NACT (7). Therefore, selecting women who may benefit from either primary cytoreduction or NACT is a relevant clinical issue.

From the oncological surgical point of view, accepted criteria for noncomplete cytoreduction are as follows: the presence of extensive parenchymatous liver disease, root of mesentery involvement, massive involvement of bowel serosa that should lead to extensive bowel resection, lymph node involvement cranially to renal vessels, and large-volume diaphragmatic involvement with disease penetrating the thoracic cavity (8). Extra-abdominal disease might be considered as criteria for nonoperability.

In order to achieve optimal cytoreduction, ovarian cancer surgery could be considered as a multivisceral and peritoneal surgery that needs to be tailored for every single woman with this disease.

Considering all these issues, it is understood that preoperative assessment of tumor spread by imaging techniques is recommended.

Computed Tomography (CT) Scan

CT scan may be considered as the first-line imaging technique for assessing tumor spread in advanced ovarian cancer. The sensitivity and specificity of this technique for detecting disease in different anatomic areas vary significantly according to different studies (9–12) (Table 4.1).

Several models based on CT scan findings have been developed for predicting optimal cytoreduction in advanced ovarian cancer (9,10,13,14). However, a recent meta-analysis has shown that these models have rather poor predictive performance on validation studies, with sensitivity ranging from 15% to 79% and specificity ranging from 32% to 64% (15).

TABLE 4.1

Diagnostic Performance of CT Scan to Detect Disease Spread in Ovarian Cancer

Anatomic Area	Sensitivity (%)	Specificity (%)
Ascites	38–44	90–100
Major omentum	72–79	65–71
Rectosigmoid	20–54	100
Colon	20–29	91–95
Spleen	100	96
Liver surface	14–100	90–93
Liver	61–100	64–100
Mesentery root	19–75	44–100
Hepatic hilum	14–20	100
Suprarenal lymph nodes	10–24	46–100
Miliary carcinomatosis	14–71	100
Diaphragm	43–61	75–100

Magnetic Resonance Imaging (MRI)

MRI has also been proposed as an imaging technique for preoperative assessment of advanced ovarian cancer. The reported diagnostic performance also varies significantly among studies (Table 4.2) (16,17). Studies comparing CT scan and MRI for predicting optimal cytoreduction report controversial results (18,19).

TABLE 4.2

Diagnostic Performance of MRI to Detect Disease Spread in Ovarian Cancer

Anatomic Area	Sensitivity (%)	Specificity (%)
Ascites	50	92
Major omentum	85–88	85–92
Rectosigmoid	28	98
Spleen	19–100	100
Liver	44–80	82–83
Mesentery root	22–100	85–95
Hepatic hilum	25–80	83–95
Suprarenal lymph nodes	47–100	86–94
Miliary carcinomatosis	88–92	88–92
Diaphragm	53–80	93–97

Positron Emission Tomography (PET)

PET or PET-CT scan have been compared with CT scan for preoperative staging in ovarian cancer (20,21). PET-CT scan seems to be better than CT scan for detecting lymph node involvement, but there is no difference for evaluating intra-abdominal disease. Additional potential benefits of PET-CT scan are the detection of other concomitant primary cancers and the assessment of extra-abdominal disease.

There are few reports about the utility of PET-CT scan for predicting suboptimal cytoreduction, with poor results (22).

Ultrasound

Ultrasound has been traditionally considered as a poor technique for assessing tumor extension in ovarian cancer (23). However, in the mid-2000s, some studies reported that this technique could reliably evaluate the presence of omental involvement (24) as well as the presence of carcinomatosis (25).

The technique for assessing tumor spread in ovarian cancer has been well described by Fischerova (26). Both transvaginal and transabdominal ultrasound must be performed. Transvaginal ultrasound is the optimal approach for examining the pelvis. Using this route, the presence of disease involving the pelvic peritoneum can be evaluated, such as lateral pelvic walls (Figure 4.1), peritoneum of Douglas pouch (Figure 4.2), or peritoneum of the vesicouterine plica (Figure 4.3), as well as the involvement of uterine serosa (Figure 4.4). These tumoral implants usually manifest as hypoechogenic lesions.

The involvement of the rectosigmoid (Figure 4.5) as well as the presence of pelvic lymph nodes (Figure 4.6) can also be evaluated by transvaginal ultrasound. When a lymph node is involved, the size increases (lymph nodes larger than 1 cm are considered as suspicious). The shape of an infiltrated lymph node is round, with loss of the hilum sign and inhomogeneous echogenicity

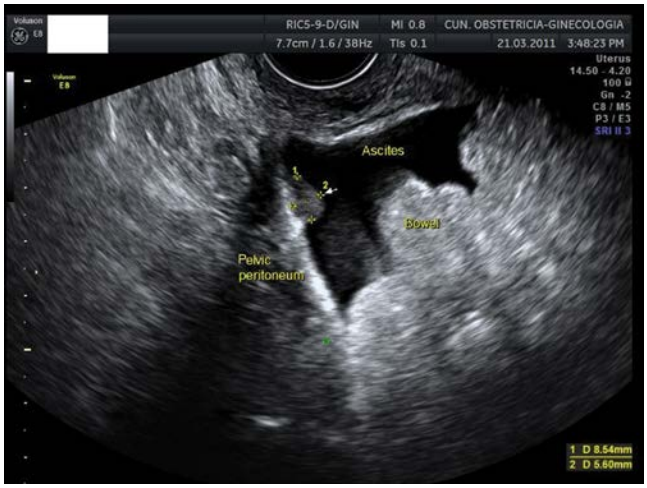

FIGURE 4.1 Transvaginal ultrasound from a 63-year-old woman who presented with abdominal swelling. Carcinomatosis was observed on ultrasound examination. A peritoneal implant on the right pelvic wall peritoneum is observed.

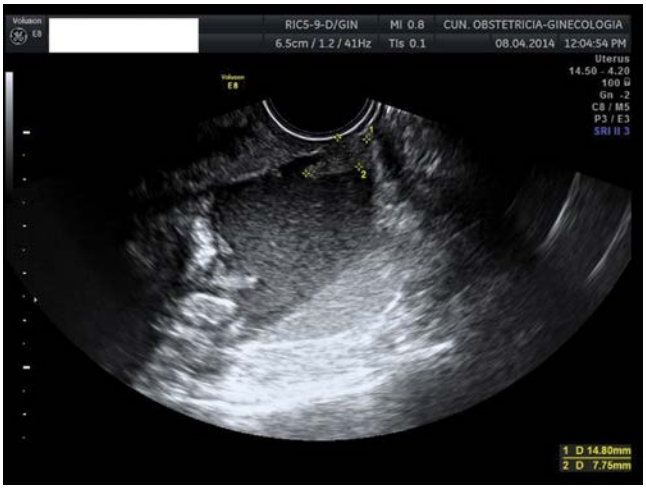

FIGURE 4.2 Similar case to that in Figure 4.1. A metastatic nodule is seen on the peritoneum of the Douglas pouch.

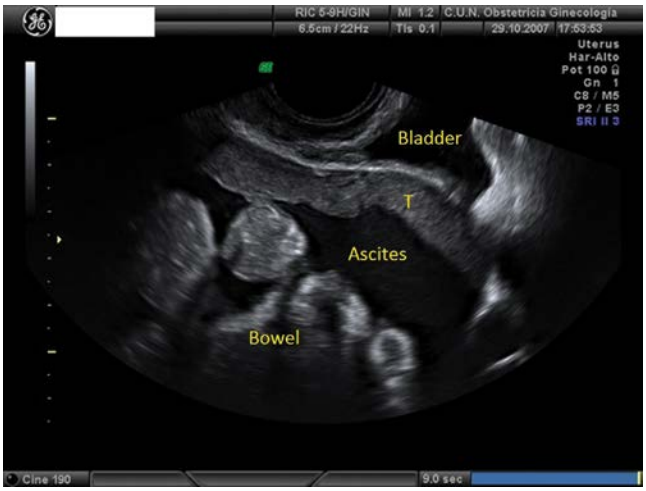

FIGURE 4.3 Transvaginal ultrasound in a case of pelvic carcinomatosis secondary to an epithelial ovarian carcinoma. A tumoral area (T) can be observed over the peritoneum of the bladder dome.

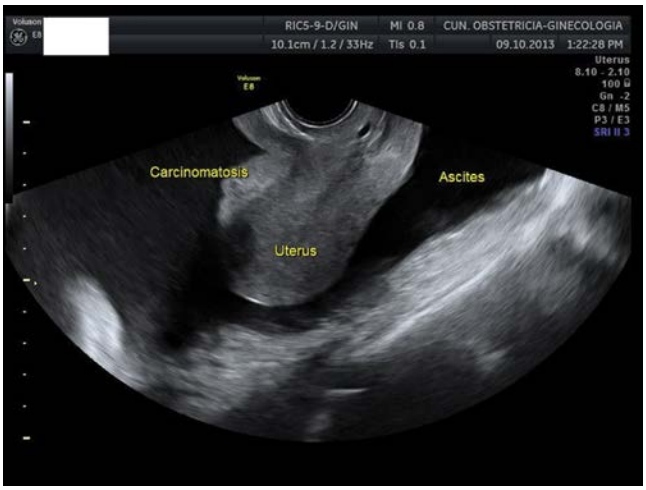

FIGURE 4.4 Transvaginal ultrasound showing a significant amount of ascites surrounding the uterus and a tumoral carcinomatosis over the uterine serosa.

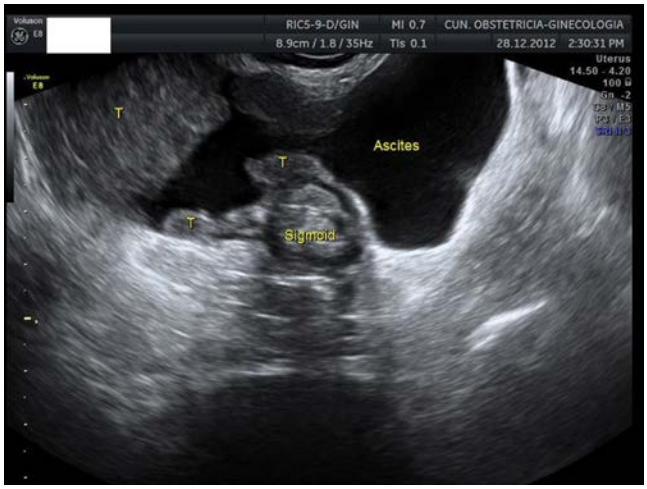

FIGURE 4.5 Transvaginal ultrasound showing tumoral implants T over the serosa of the sigmoid colon.

(26). Bulky lymph nodes may show extracapsular growth with irregular margins.

Transabdominal ultrasound allows assessment of the middle and upper abdomen. An ultrasound examination of the abdominal cavity has to be performed systematically, and the entire anatomy has to be evaluated in both sagittal and transverse sections, which is accomplished by rotating the probe 90°. Attention should be paid first to the visceral organs in the upper abdomen (such as the kidneys and adrenal glands, spleen, liver, and pancreas); their size and structure must be evaluated and possible intraparenchymatous focal or diffuse lesions, capsular infiltration, or visceral lymphadenopathy described (26). Then, the parietal, visceral, mesenteric peritoneum, and omentum should be evaluated, as there is potential for tumor spread in the form of parietal (lateral paracolic gutters, diaphragm, anterior abdominal wall), omental, visceral (intestinal carcinomatosis, organ surfaces), or mesenteric (mesentery of small intestine or mesocolon) carcinomatosis. Finally, the retroperitoneal lymph nodes should be evaluated.

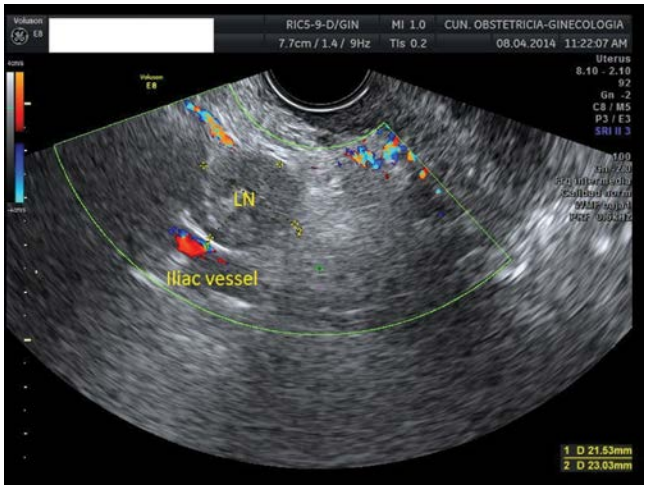

FIGURE 4.6 Transvaginal ultrasound showing a suspicious (>1 cm) pelvic lymph node (LN).

Regarding the assessment of carcinomatosis, miliary dissemination cannot be detected as easily when evaluating the upper abdomen, as it would be with a transvaginal or transrectal examination. The presence of ascites may improve the image quality, but when there are matted loops of intestine or when tumors are advanced and the borders of omental infiltration become indistinguishable from intestinal and/or parietal carcinomatosis, the assessment of carcinomatosis involving the peritoneal or bowel surfaces is very difficult (26).

Ultrasonography is a dynamic technique that can provide important information; for example, it can detect bowel movements, which allows metastatic nodules to be differentiated from the actual bowel. The peristaltic movements of pelvic intestinal loops that are affected by carcinomatosis may remain normal or become sluggish. In the case of sluggish peristalsis due to carcinomatosis, movement of condensed intestinal content, dilatation of the intestinal lumen (over 30 mm), and thickening of the intestinal wall may be observed (26). Additionally, evaluating the mobility of organs allows detection or exclusion of adhesions of a given organ to other peritoneal surfaces.

The examination should be systematic, and the examiner should be expert. In experienced hands, the usual duration of a systematically performed combination of transvaginal (or transrectal) and transabdominal scans to define the clinical stage of disease is approximately 15 minutes (26).

Using this systematic approach, the presence of ascites can be determined (Figure 4.7), as well as the involvement of greater omentum (Figure 4.8), the presence of tumor involving the bowel (Figure 4.9), stomach (Figure 4.10), retroperitoneal lymph nodes (Figure 4.11), hepatic hilum (Figure 4.12), diaphragmatic peritoneum or liver surface (Figure 4.13), or liver parenchyma (Figure 4.14). There are some limitations to this evaluation such as the absence of ascites or the presence of intestinal gas. The patient's obesity may be another limitation.

There are some studies that have shown that ultrasound may have good sensitivity for detecting rectosigmoid involvement (25,27,28) as well as pelvic carcinomatosis (25,28,29). The

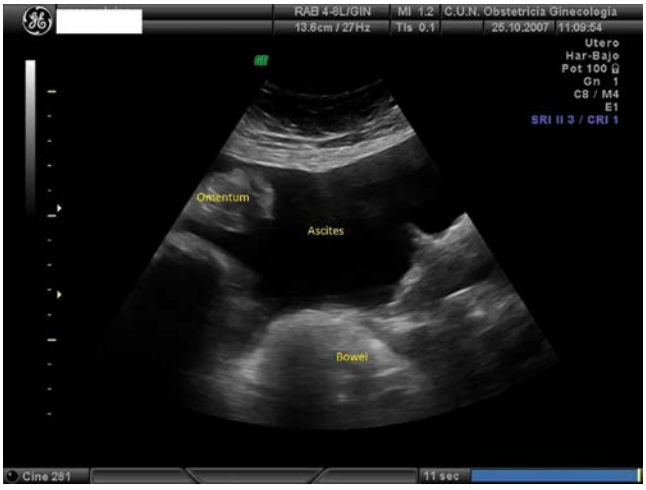

FIGURE 4.7 Transabdominal ultrasound in sagittal plane depicting abundant ascites. The greater omentum can be visualized, involved by tumor. In real-time ultrasound, it is easy to differentiate from bowel loops since the latter move and the omentum do not.

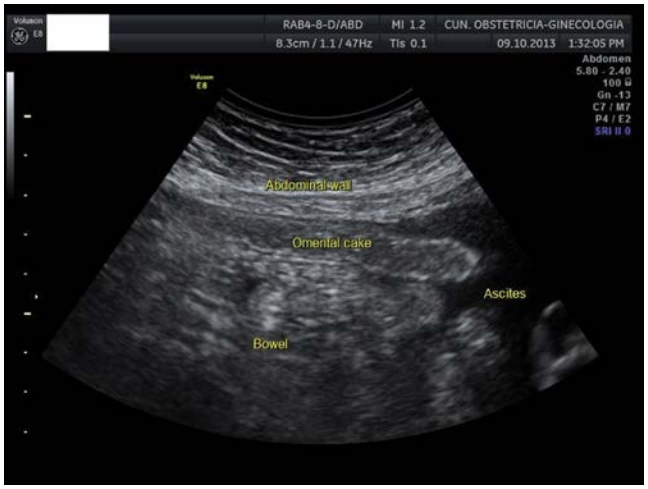

FIGURE 4.8 Transabdominal ultrasound showing an omental cake in cases of abdominal carcinomatosis secondary to epithelial ovarian carcinoma.

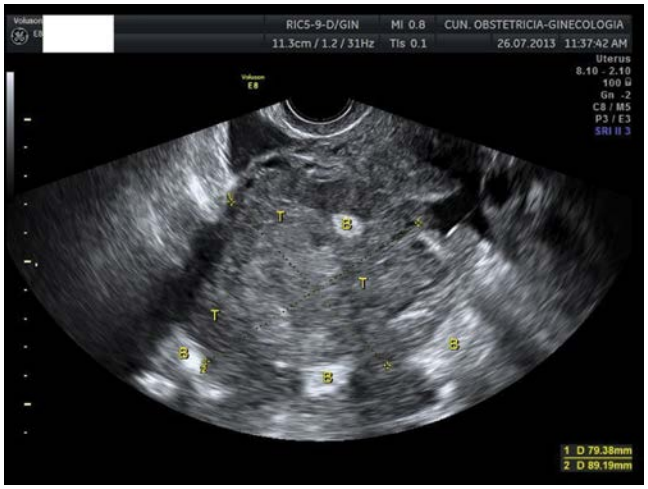

FIGURE 4.9 Transvaginal ultrasound showing massive involvement of bowel loops (B), trapped within large tumor implants (T).

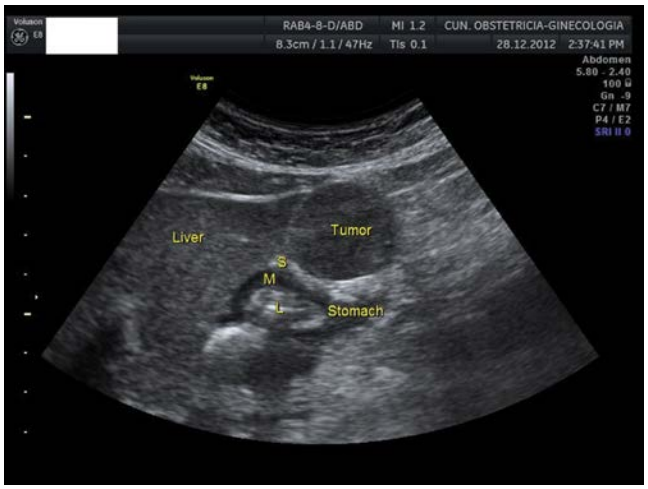

FIGURE 4.10 Transabdominal ultrasound depicting a tumoral implant over the gastric surface. Stomach wall can be assessed. (S, serosa; M, muscularis; L, lumen.)

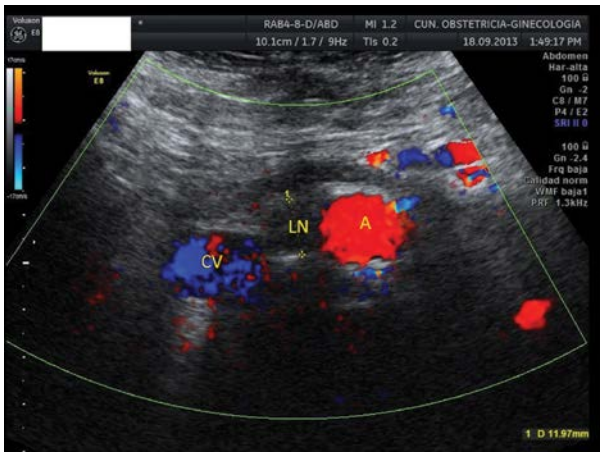

FIGURE 4.11 Transabdominal ultrasound showing a suspicious lymph node (LN) in para-aortic area. The lymph node is located between the aorta (A) and the inferior vena cava (ICV).

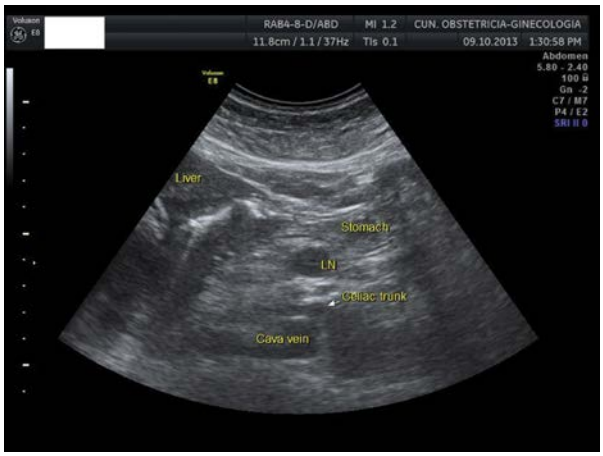

FIGURE 4.12 Transabdominal ultrasound showing a suspicious lymph node (LN) behind the stomach and close to the celiac trunk. Sometimes they are difficult to differentiate from tumoral implants in the omental sac.

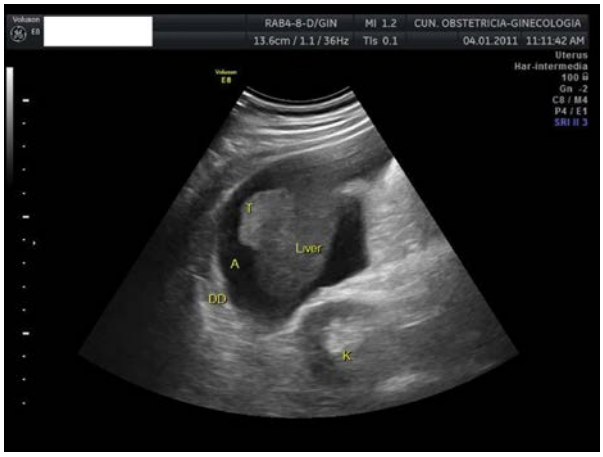

FIGURE 4.13 Transabdominal ultrasound showing a tumoral implant over the liver's surface. The kidney is visible (K). The presence of ascites (A) also allows the surface of the peritoneum of the right diaphragm (DD) to be assessed. In this case, the peritoneum is thickened, suggesting the presence of carcinomatosis at this site.

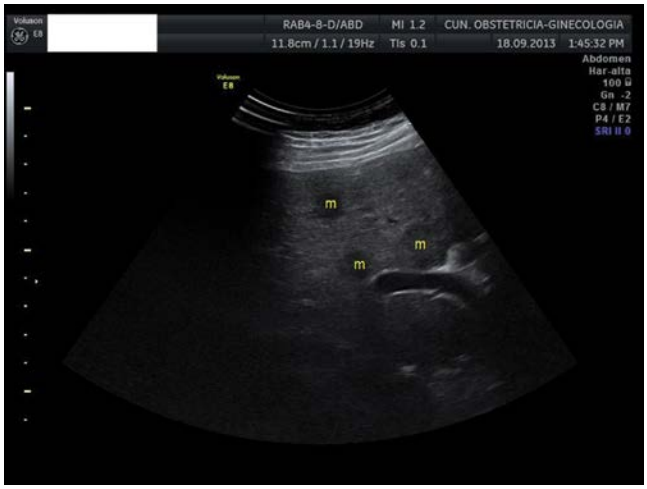

FIGURE 4.14 Transabdominal ultrasound showing three liver metastases (m) in a case of primary epithelial ovarian cancer.

TABLE 4.3

Diagnostic Performance of Ultrasound to Detect Disease Spread in Ovarian Cancer

Anatomic Area	Sensitivity (%)	Specificity (%)
Ascites	98	97
Major omentum	67–94	90–94
Rectosigmoid	83	97
Spleen	75	98
Liver surface	21	99
Liver	93	98
Mesentery root	23	98
Hepatic hilum	14–20	100
Any lymph nodes	34	99
Diaphragm	31	98
Peritoneal carcinomatosis	32–88	92–93

diagnostic performance of ultrasound for detecting the involvement of lymph nodes, root of mesentery, miliary carcinomatosis, and liver or splenic surface is limited (28,29) (Table 4.3). However, the data are encouraging enough to support research in this field.

Only one study has evaluated the role of ultrasound for predicting optimal cytoreduction in advanced ovarian cancer (29). This study showed that the use of an ultrasound-based score had a sensitivity of 72% and a specificity of 68% for predicting optimal cytoreduction.

REFERENCES

1. Berek JS, Crum C, Friedlander M. Cancer of the ovary, fallopian tube, and peritoneum. *Int J Gynaecol Obstet*. 2015;131(Suppl 2):S111–S122.
2. Webb PM, Jordan SJ. Epidemiology of epithelial ovarian cancer. *Best Pract Res Clin Obstet Gynaecol*. 2017;41:3–14.
3. Bookman MA. Optimal primary therapy of ovarian cancer. *Ann Oncol*. 2016;27(Suppl 1):i58–i62.
4. Bristow RE, Tomacruz RS, Armstrong DK et al. Survival effect of maximal cytoreductive surgery for advanced ovarian carcinoma during the platinum era: A meta-analysis. *J Clin Oncol*. 2002;20:1248–1259.
5. Salani R, Bristow RE. Surgical management of epithelial ovarian cancer. *Clin Obstet Gynecol*. 2012;55:75–95.
6. Vernooij F, Heintz P, Witteveen E, van der Graaf Y. The outcomes of ovarian cancer treatment are better when provided by gynecologic oncologists and in specialized hospitals: A systematic review. *Gynecol Oncol*. 2007;105:801–812.
7. Vergote I, Tropé CG, Amant F et al., European Organization for Research and Treatment of Cancer-Gynaecological Cancer Group; NCIC Clinical Trials Group. Neoadjuvant chemotherapy or primary surgery in stage IIIC or IV ovarian cancer. *N Engl J Med*. 2010;363:943–953.
8. Salani R, Axtell A, Gerardi M, Holschneider C, Bristow RE. Limited utility of conventional criteria for predicting unresectable disease in patients with advanced stage epithelial ovarian cancer. *Gynecol Oncol*. 2008;108:271–275.
9. Nelson BE, Rosenfield AT, Schwartz PE. Preoperative abdominopelvic computed tomographic prediction of optimal cytoreduction in epithelial ovarian carcinoma. *J Clin Oncol*. 1993;11:166–172.
10. Bristow RE, Duska LR, Lambrou NC et al. A model for predicting surgical outcome in patients with advanced ovarian carcinoma using computed tomography. *Cancer*. 2000;89:1532–1540.
11. Glaser G, Torres M, Kim B et al. The use of CT findings to predict extent of tumor at primary surgery for ovarian cancer. *Gynecol Oncol*. 2013;130:280–283.
12. Hynninen J, Kemppainen J, Lavonius M et al. A prospective comparison of integrated FDG-PET/contrast-enhanced CT and contrast-enhanced CT for pretreatment imaging of advanced epithelial ovarian cancer. *Gynecol Oncol*. 2013;131:389–394.
13. Dowdy SC, Mullany SA, Brandt KR et al. The utility of computed tomography scans in predicting suboptimal cytoreductive surgery in women with advanced ovarian carcinoma. *Cancer*. 2004;101:346–352.
14. Qayyum A, Coakley FV, Westphalen AC, Hricak H, Okuno WT, Powell B. Role of CT and MR imaging in predicting optimal cytoreduction of newly diagnosed primary epithelial ovarian cancer. *Gynecol Oncol*. 2005;96:301–306.
15. Rutten MJ, van de Vrie R, Bruining A et al. Predicting surgical outcome in patients with International Federation of Gynecology and Obstetrics stage III or IV ovarian cancer using computed tomography: A systematic review of prediction models. *Int J Gynecol Cancer*. 2015;25:407–415.
16. Espada M, Garcia-Flores JR, Jimenez M et al. Diffusion-weighted magnetic resonance imaging evaluation of intra-abdominal sites of implants to predict likelihood of suboptimal cytoreductive surgery in patients with ovarian carcinoma. *Eur Radiol*. 2013;23:2636–2642.
17. Kasper SM, Dueholm M, Marinovskij E, Blaakær J. Imaging diagnostics in ovarian cancer: Magnetic resonance imaging and a scoring system guiding choice of primary treatment. *Eur J Obstet Gynecol Reprod Biol*. 2017;210:83–89.
18. Qayyum A, Coakley FV, Westphalen AC, Hricak H, Okuno WT, Powell B. Role of CT and MR imaging in predicting optimal cytoreduction of newly diagnosed primary epithelial ovarian cancer. *Gynecol Oncol*. 2005;96:301–306.

19. Low RN, Barone RM, Lucero J. Comparison of MRI and CT for predicting the Peritoneal Cancer Index (PCI) preoperatively in patients being considered for cytoreductive surgical procedures. *Ann Surg Oncol*. 2015;22:1708–1715.
20. Drieskens O, Stroobants S, Gysen M, Vandenbosch G, Mortelmans L, Vergote I. Positron emission tomography with FDG in the detection of peritoneal and retroperitoneal metastases of ovarian cancer. *Gynecol Obstet Invest*. 2003;55:130–134.
21. Kitajima K, Murakami K, Yamasaki E et al. Diagnostic accuracy of integrated FDG-PET/contrast-enhanced CT in staging ovarian cancer: Comparison with enhanced CT. *Eur J Nucl Med Mol Imaging*. 2008;35:1439–1448.
22. Risum S, Høgdall C, Loft A et al. Prediction of suboptimal primary cytoreduction in primary ovarian cancer with combined positron emission tomography/computed tomography—A prospective study. *Gynecol Oncol*. 2008;108:265–270.
23. Tempany CM, Zou KH, Silverman SG, Brown DL, Kurtz AB, McNeil BJ. Staging of advanced ovarian cancer: Comparison of imaging modalities—Report from the Radiological Diagnostic Oncology Group. *Radiology*. 2000;215:761–767.
24. Testa AC, Ludovisi M, Savelli L et al. Ultrasound and color power Doppler in the detection of metastatic omentum: A prospective study. *Ultrasound Obstet Gynecol*. 2006;27:65–70.
25. Savelli L, De Iaco P, Ceccaroni M et al. Transvaginal sonographic features of peritoneal carcinomatosis. *Ultrasound Obstet Gynecol*. 2005;26:552–557.
26. Fischerova D. Ultrasound scanning of the pelvis and abdomen for staging of gynecological tumors: A review. *Ultrasound Obstet Gynecol*. 2011;38:246–266.
27. Zikan M, Fischerova D, Semeradova I et al. A prospective evaluation of ultrasound accuracy in the prediction of rectosigmoid infiltration in patients with epithelial ovarian cancer. *Ultrasound Obstet Gynecol*. 2016. doi:10.1002/uog.17363.
28. Fischerova D, Zikan M, Semeradova I et al. Ultrasound in preoperative assessment of pelvic and abdominal spread in patients with ovarian cancer: A prospective study. *Ultrasound Obstet Gynecol*. 2017;49:263–274.
29. Testa AC, Ludovisi M, Mascilini F et al. Ultrasound evaluation of intra-abdominal sites of disease to predict likelihood of suboptimal cytoreduction in advanced ovarian cancer: A prospective study. *Ultrasound Obstet Gynecol*. 2012;39:99–105.

5

Ultrasound Features of Endometrial Cancer

Introduction

Endometrial cancer is the most frequent gynecologic malignancy in the developed world, with an age-adjusted incidence of 24.7 per 100,000 women (1). More than 90% of endometrial cancers occur in postmenopausal women with a mean age of 63 years (1).

Histologically, endometrial cancer has been classified into two types according to clinicopathological and molecular features: type I and type II. Type I endometrial carcinomas include endometrioid carcinomas (adenocarcinoma, adenoacanthoma, and serous squamous) and associate genetic alterations in *PTEN*, *KRAS*, *CTBNNB1*, and *PIK3CA* genes. This type comprises 80%–90% of all endometrial cancers. Type II endometrial cancers include clear cell papillary-serous and undifferentiated carcinomas, as well as carcinosarcoma or malignant mixed Müllerian tumor (MMMT). This type is more frequently associated with mutations of p53 gene and accounts for 10%–20% of all endometrial cancers (1).

Tumor grade is another important histologic feature. Usually endometrioid carcinomas can be classified into three groups according to tumor grade, which is based on the proportion of nonsquamous solid growth pattern observed within the tumor. These tumors can be well differentiated (G1 $\leq$5% of solid growth pattern), moderately differentiated (G2, 6%–50% of solid growth pattern), or poorly differentiated (G3 $>$ 50% of solid growth pattern) (1). All Type II cancers are considered as G3 for grading.

Ultrasound for Diagnosing Endometrial Cancer

The definitive diagnosis of endometrial cancer must be based on endometrial biopsy and histologic evaluation. The risk of endometrial cancer in asymptomatic women is less than 1% (2,3), and there is no effective method for screening (1).

The main clinical scenario for suspecting endometrial cancer is the presence of uterine bleeding in a postmenopausal woman. However, only 10% of women with postmenopausal bleeding will have an endometrial cancer (1). For this reason, systematic endometrial sampling in all these women will render a high number of unnecessary biopsies.

Pelvic examination followed by a transvaginal ultrasound has been demonstrated as the most cost-effective strategy for evaluating symptomatic postmenopausal women (4,5).

The main ultrasound feature associated with the presence of an endometrial cancer is a thickened endometrium in a postmenopausal woman who presents with uterine bleeding (Figure 5.1). An endometrial thickness $\geq$4–5 mm should prompt the performance of an endometrial sampling (6,7). The risk of endometrial cancer when endometrial thickness is <4–5 mm is low, ranging from 0.5% to 4% (6–9) (Figure 5.2).

Some studies have shown that in case of rebleeding, the risk of endometrial cancer remains low if the endometrium remains thin (10). However, other studies have challenged this point (11). It should be kept in mind that cancer may occur in women with postmenopausal bleeding and thin endometrium, specifically

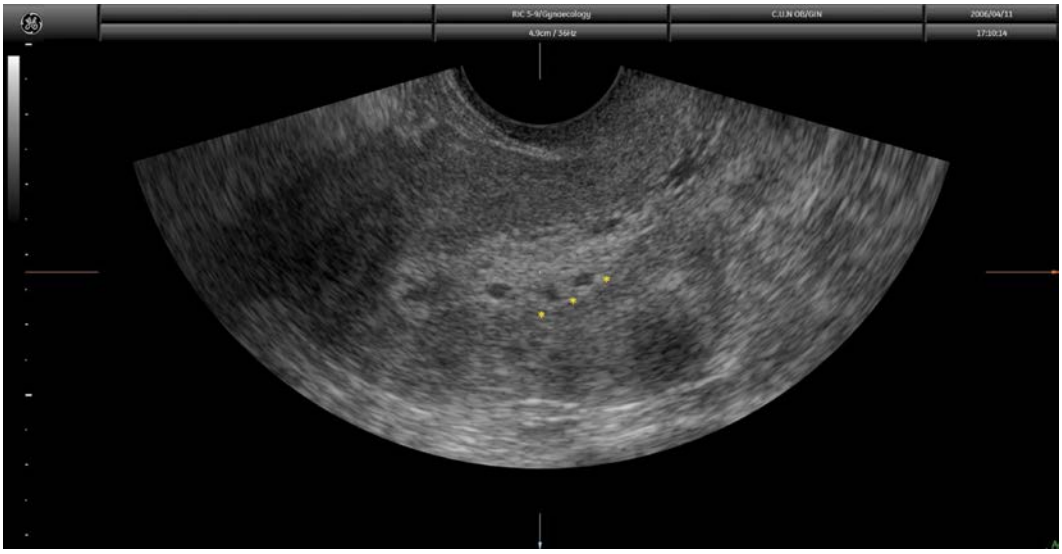

FIGURE 5.1 Transvaginal ultrasound showing a thickened endometrium in a 59-year-old woman presenting with postmenopausal bleeding. We observe some cystic areas, and it seems that the posterior endometrium is protruding into the myometrial wall (*) suggesting some degree of infiltration. Endometrial sampling proved the existence of a G2 endometrioid carcinoma.

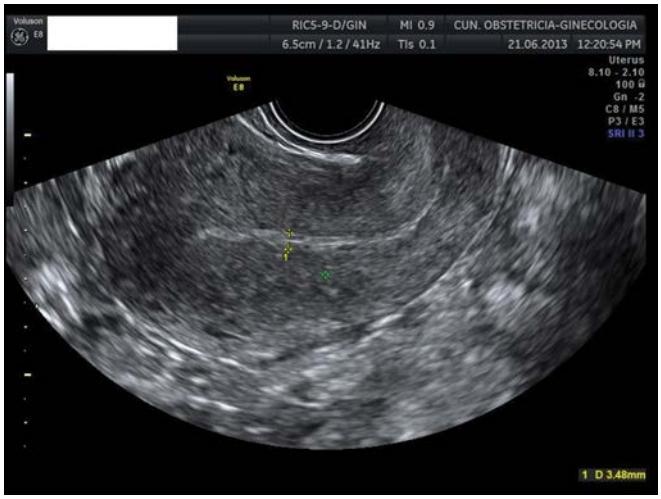

FIGURE 5.2 Transvaginal ultrasound in a case of serous-papillary adenocarcinoma of endometrium (type II carcinoma). The endometrial stripe is thin (3.5 mm).

women with endometrial cancer type II, that tend to arise from atrophic endometrium (12). But if the endometrium is not assessable, hysteroscopy should be performed (Figure 5.3) (13).

Transvaginal measurement of endometrial thickness has shown high sensitivity (>95%–98%) for detecting endoemtrial cancer, but it is not specific (6), since many benign lesions may thicken the endometrium in a postmenopausal woman, such as endometrial polyps (Figure 5.4), endometrial hyperplasia (Figure 5.5), endometritis, or cystic atrophy (Figures 5.6 and 5.7).

One interesting question is whether endometrial biopsy should be performed in asymptomatic women with a thickened endometrium and what should be considered as "thickened" in this setting. Smith-Bindman and colleagues performed a retrospective analysis and concluded that the risk for endometrial cancer in women without bleeding with an endometrial thickness ≥11 mm was similar to that in women with bleeding and endometrial thickness ≥5 mm, suggesting that endometrial sampling should

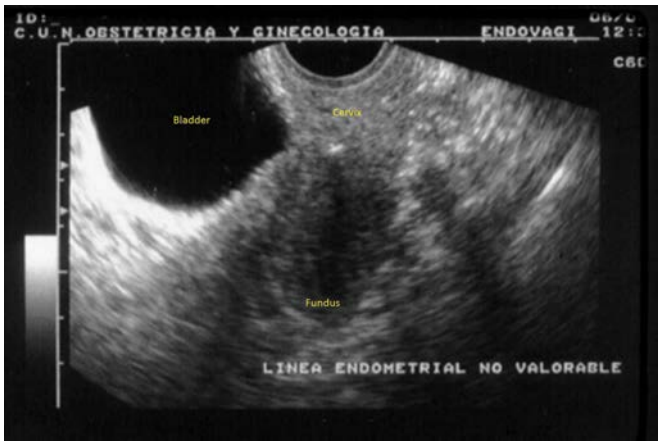

FIGURE 5.3 Transvaginal ultrasound in a 74-year-old woman who presented with vaginal bleeding. The endometrium cannot be assessed due to the uterine position. A gentle pressure either with the vaginal probe or over the hypogastrium with the free hand may solve this problem. Patient voiding may also be useful.

(a)

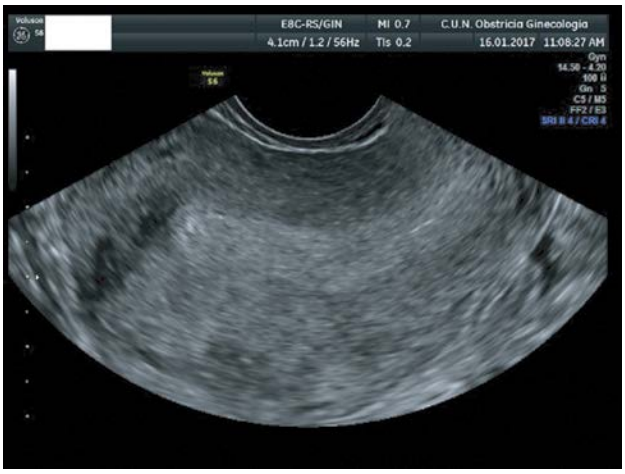

(b)

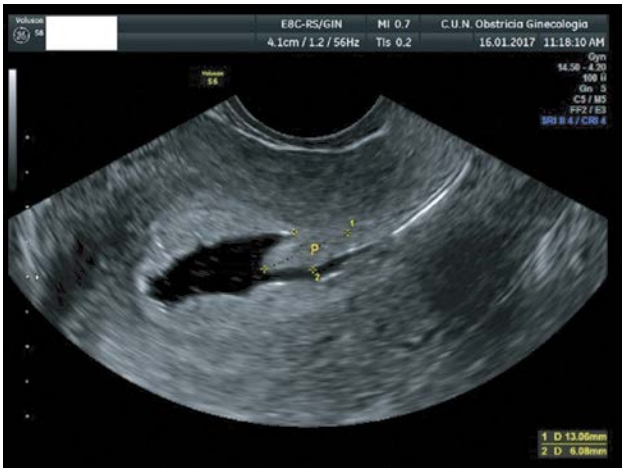

FIGURE 5.4 Transvaginal ultrasound showing a thickened endometrium (a) in a postmenopausal woman who presented with vaginal spotting. This finding is not specific. Saline infusion sonohysterography (b) allows detection of the cause of endometrial thickening: an endometrial polyp (P).

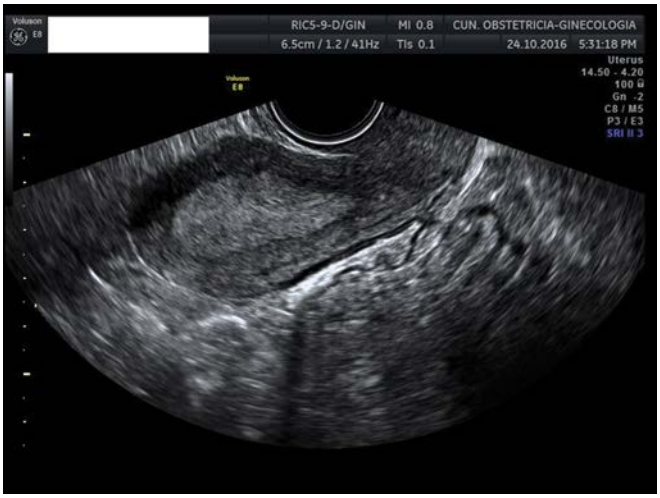

FIGURE 5.5 Transvaginal ultrasound in a postmenopausal woman presenting with bleeding. A thickened endometrium is observed. In this case endometrial sampling showed the presence of simple endometrial hyperplasia.

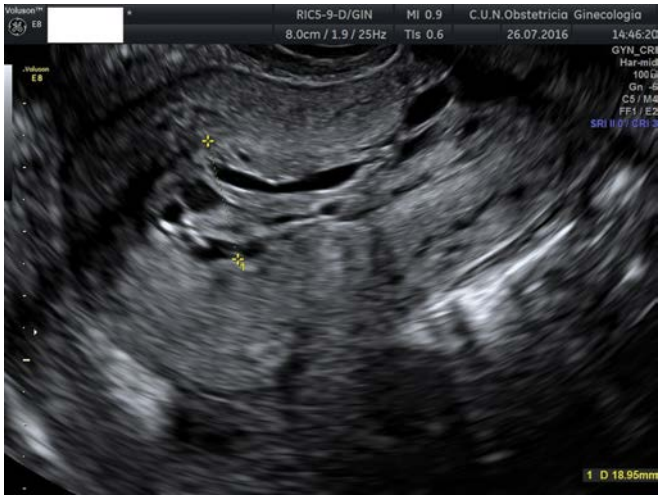

FIGURE 5.6 A thickened endometrium with cystic areas in a 55-year-old postmenopausal woman taking tamoxifen. This is a typical finding of endometrial cystic atrophy secondary to tamoxifen.

be performed in asymptomatic women with an endometrium thicker than 11 mm (14). However, this criterion has not been validated in large prospective studies. A meta-analysis by Alcázar and coworkers showed that the risk for endometrial cancer or endometrial hyperplasia with atypia in asymptomatic women with endometrium thickness ≥11 mm is three times higher than the risk in women with endometrial thickness <11 mm. The absolute risk for endometrial cancer or endometrial hyperplasia with atypia was 5% for the former group, as compared to 1.5% for the latter group (15).

However, when deciding whether to obtain an endometrial sampling in asymptomatic women, it should be considered that there is no apparent benefit in terms of overall survival if the endometrial cancer is detected in asymptomatic women or soon after the first episode of bleeding (16).

Other ultrasound features associated with endometrial cancer are the presence of an ill-defined myometrial-endometrial

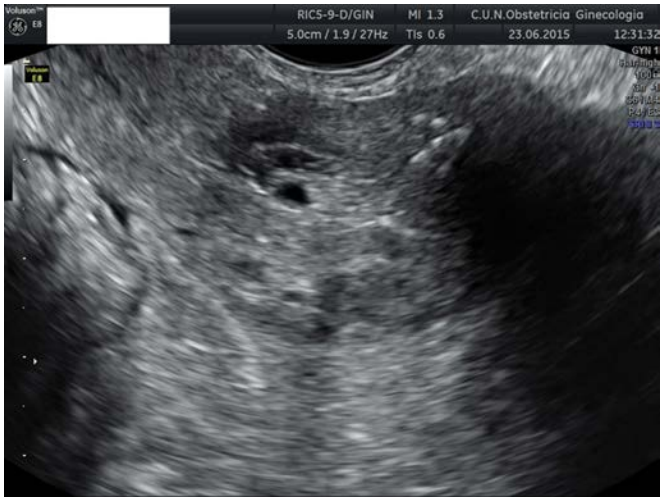

FIGURE 5.7 Transvaginal ultrasound in a 62-year-old asymptomatic postmenopausal woman who was taking antihypertensive drugs. A thickened endometrium with cystic areas is observed. Endometrial sampling revealed a cystic atrophy of the endometrium.

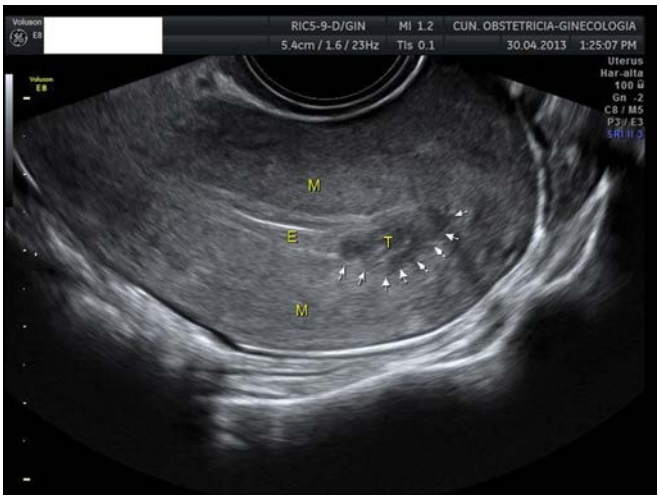

FIGURE 5.8 An endometrial carcinoma (T) in a perimenopausal woman. The endometrium (E) and myometrium (M) are observed. The tumor is located in the fundus, and it is infiltrating the myometrium (arrows).

interphase (suggesting myometrial infiltration) (Figure 5.8) and the presence of a heterogeneous endometrium (Figure 5.9).

The use of Doppler ultrasound has been advocated for diagnosing endometrial cancer. Regarding the use of pulsed Doppler, early reports during the 1990s were encouraging, since malignant endometrial lesions tended to show lower velocimetric indices as compared with benign lesions (17,18). However, subsequent studies did not confirm these findings (19,20). Furthermore, a significant overlap for velocimetric indices between malignant and benign endometrial lesions was found, and reproducibility of this technique was questionable (21). For this reason, the use of pulsed Doppler is not currently recommended in clinical practice.

Alcázar and coworkers proposed the use of color/power Doppler mapping for discriminating between benign and malignant endometrial lesions in women with postmenopausal bleeding and thickened endometrium (>5 mm) (22). They found that the presence of abundant vascularization within the endometrium

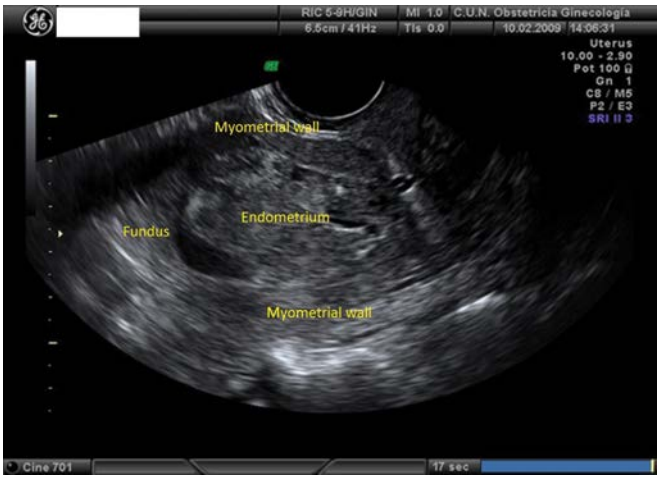

FIGURE 5.9 Transvaginal ultrasound showing a heterogeneous and thickened endometrium in a 60-year-old woman presenting with postmenopausal bleeding. These findings are highly suspicious for endometrial cancer.

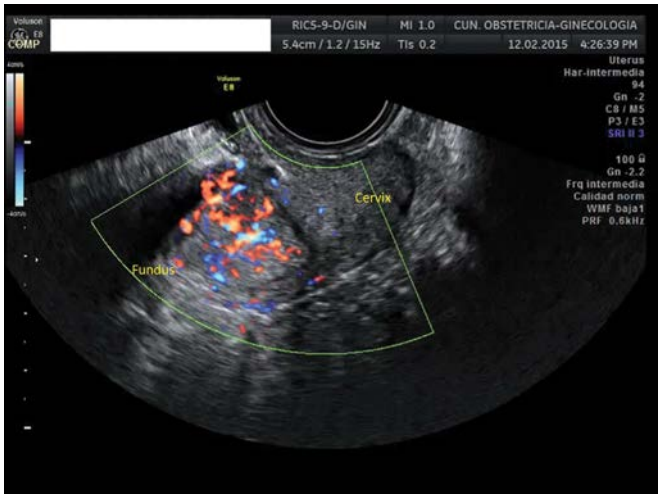

FIGURE 5.10 Transvaginal ultrasound showing a highly vascularized endometrium in a case of endometrial carcinoma.

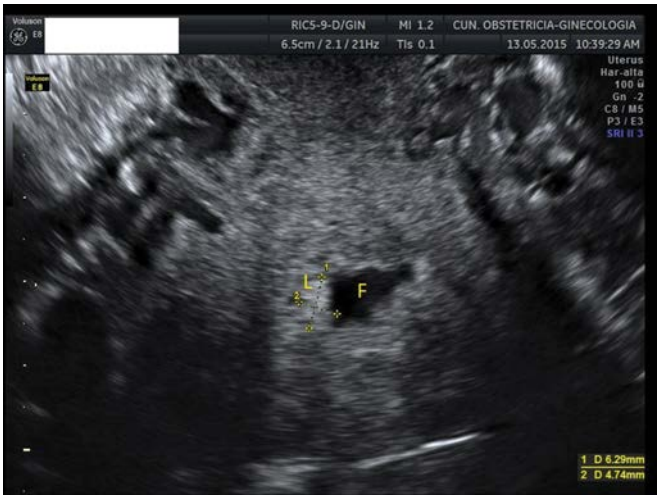

FIGURE 5.12 Transvaginal ultrasound showing a small amount of fluid (F) within the uterine cavity. This fluid allows detection of a small polypoid lesion (L) that turned out to be an endometrial carcinoma.

was highly predictive for endometrial cancer (Figure 5.10), although some endometrial cancers may not exhibit vascularization at color Doppler interrogation (Figure 5.11). Other authors also observed these findings (23). Alcázar et al. also demonstrated that this approach has good reproducibility among expert examiners (24).

A study has shown that the use of an algorithm that combines grayscale and color mapping features may have a high diagnostic performance for the identification of endometrial cancer by ultrasound, with a sensitivity of 91% and a specificity of 94% (25).

The presence of intrauterine fluid may be a common finding in some cases of endometrial cancer. However, this finding does not increase the risk of endometrial cancer. If intrauterine fluid is present, attention should be paid to the endometrium. A diffuse, irregular thickening or irregular polypoid mass are suspicious for endometrial cancer (Figure 5.12).

Some authors have proposed the use of sonohysterography with saline infusion to increase the specificity of ultrasound for diagnosing endometrial cancer by ultrasound (26). Findings suspicious for malignancy are similar to those observed when fluid is present: irregular thickening and polypoid mass (Figure 5.13). An additional finding suggestive of endometrial cancer is the difficulty to distend the uterine cavity when instilling the fluid (27). It should be kept in mind that a small risk of spreading malignant cells into the pelvic cavity exists when performing sonohysterography in women with endometrial cancer (28). However, the clinical implications of this spreading might be inconsequential.

Three-dimensional (3D) ultrasound has been evaluated as an ultrasound-based technique for diagnosing endometrial cancer. Three-dimensional ultrasound allows the calculation of endometrial volume as well as an objective estimation of the amount of power Doppler signals within the endometrium by calculating the 3D vascular indices (29) (Figure 5.14). This technique seems to be reproducible among different observers (30).

Several studies have assessed the role of endometrial volume as estimated by 3D ultrasound for diagnosing endometrial

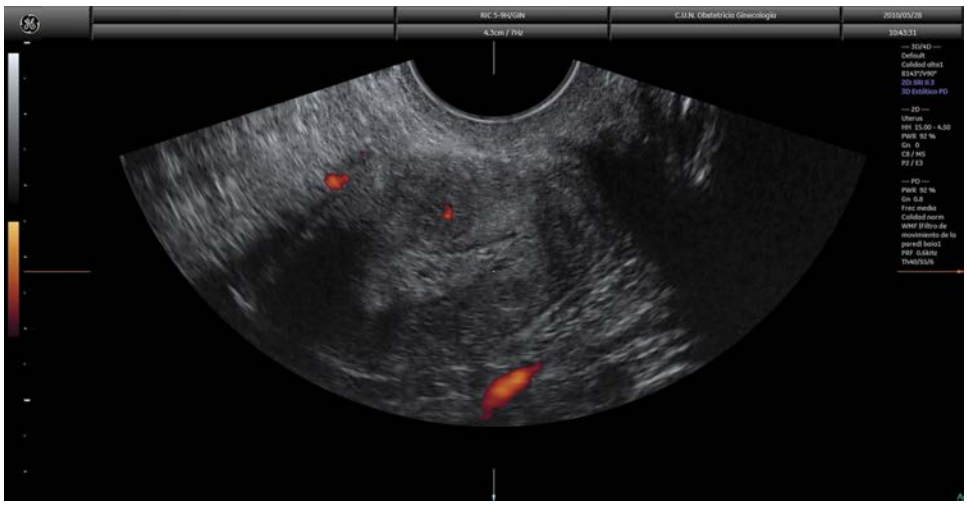

FIGURE 5.11 Endometrial carcinoma. Note the absence of any power Doppler signal with the endometrium.

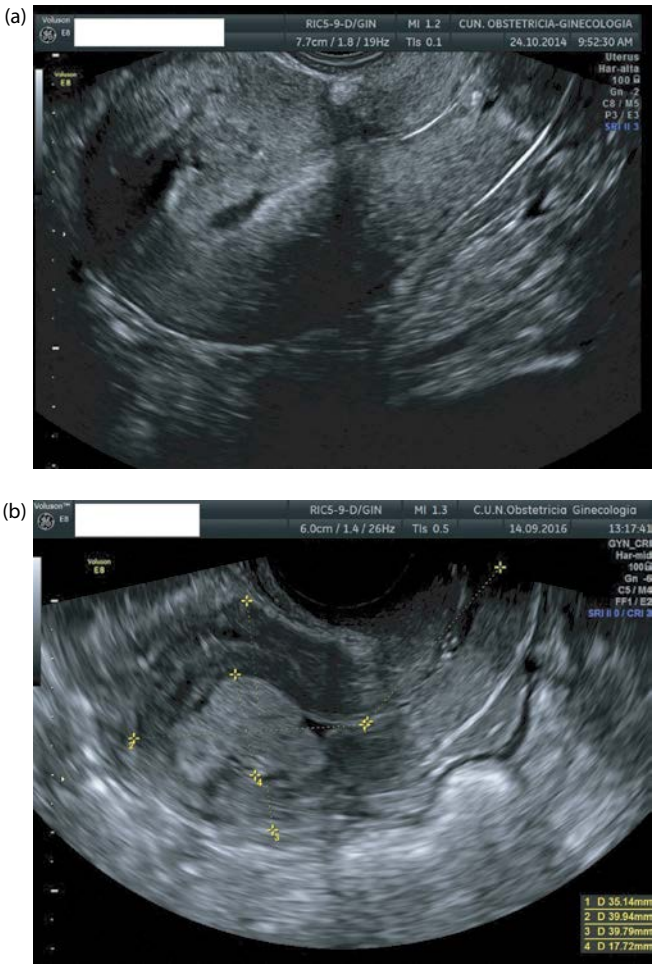

FIGURE 5.13 Saline infusion sonohysterography in two different cases of postmenopausal bleeding. In case (a), a diffuse asymmetric thickening involving the anterior endometrial layer is observed. In case (b), a polypoid lesion is shown. In both cases endometrial carcinoma was confirmed after endometrial sampling.

cancer. Most of these studies have shown that endometrial volume is more specific than endometrial thickness in women with postmenopausal bleeding (31,32). However, series were small, and there is no consensus regarding the cut-off for endometrial volume to be used.

Regarding the use of 3D vascular indices, the results of studies reported are controversial (32,33). This could be explained by the fact that this technique has not been standardized (34). Therefore, more research is needed in this field to determine the role of 3D ultrasound.

Ultrasound Features of Endometrial Cancer

Few studies have been reported correlating ultrasound findings with histologic type and grade in endometrial cancer.

Epstein et al. (35) reported that grade 1 and grade 2 endometrioid carcinomas were more frequently hyperechoic than grade 3 endometrioid or nonendometrioid carcinomas (Figure 5.15).

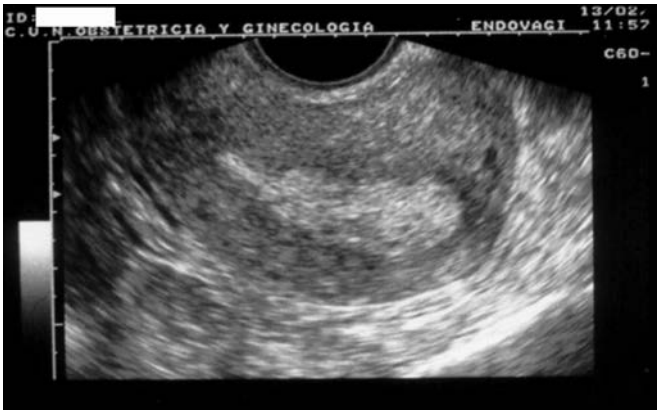

FIGURE 5.15 Transvaginal ultrasound showing a hyperechoic endometrium in case of a well-differentiated carcinoma in a postmenopausal woman.

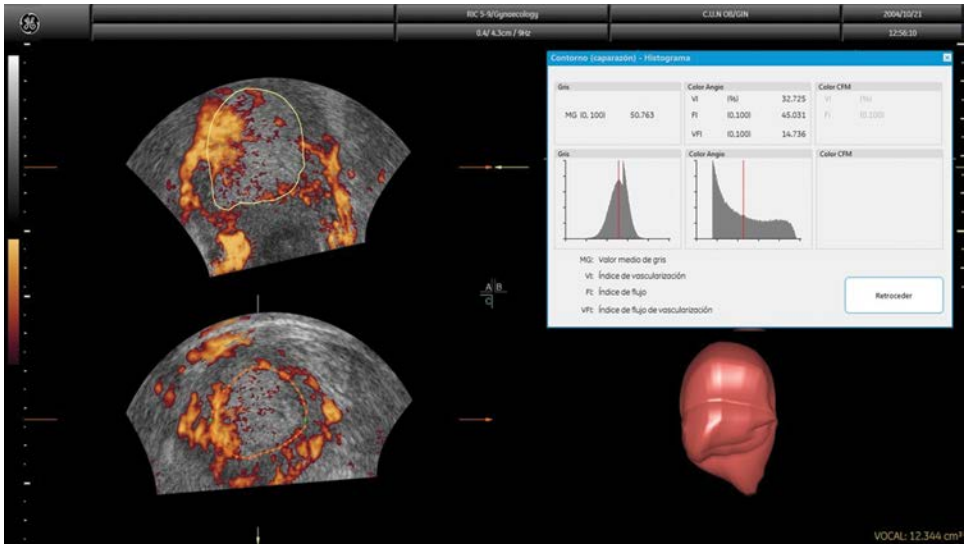

FIGURE 5.14 Endometrial volume and 3D vascular indices calculation using 3D ultrasound in a case of endometrial carcinoma.

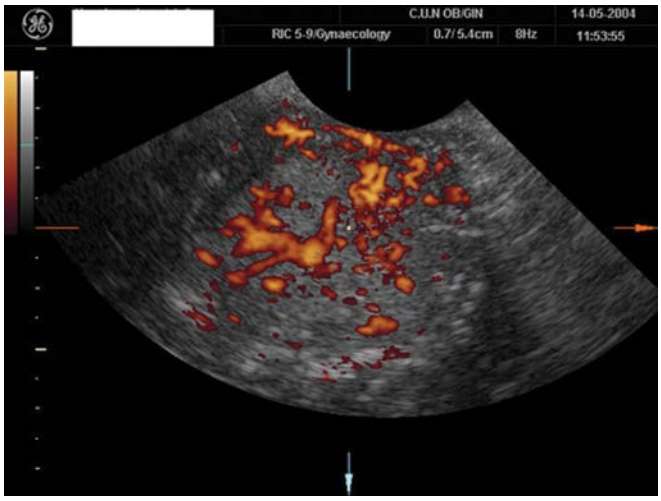

FIGURE 5.16 Transvaginal ultrasound showing an ill-defined, thickened endometrium in a case of a poorly differentiated endometrioid carcinoma. Multiple vessels within the endometrium may be seen.

However, the presence of multiple global vessels within the tumor was more frequent in grade 3 and nonendometrioid carcinomas as compared to grade 1 or grade 2 endometrioid carcinomas (Figure 5.16). There are no differences regarding the amount of vessels according to histologic type or grade.

Other studies have shown that grade 3 tumors, tumors with lymphovascular space involvement, deep myometrial infiltration, cervical involvement, or lymph node metastasis, are more vascularized than their counterparts according to pulsed Doppler velocimetric indices (36) or three-dimensional vascular indices (37). However, these studies have not been confirmed by other researchers; therefore, these data should not be used in clinical practice.

REFERENCES

1. Amant F, Moerman P, Neven P, Timmerman D, Van Limbergen E, Vergote I. Endometrial cancer. *Lancet*. 2005;366:491–505.
2. Martínez-Rubio MP, Alcázar JL. Ultrasonographic and pathological endometrial findings in asymptomatic postmenopausal women taking antihypertensive drugs. *Maturitas*. 2003;46:27–32.
3. Famuyide AO, Breitkopf DM, Hopkins MR, Laughlin-Tommaso SK. Asymptomatic thickened endometrium in postmenopausal women: Malignancy risk. *J Minim Invasive Gynecol*. 2014;21:782–786.
4. Clark TJ, Barton PM, Coomarasamy A, Gupta JK, Khan KS. Investigating postmenopausal bleeding for endometrial cancer: Cost-effectiveness of initial diagnostic strategies. *BJOG*. 2006;113:502–510.
5. Breijer MC, Van Doorn HC, Clark TJ et al. Diagnostic strategies for endometrial cancer in women with postmenopausal bleeding: Cost-effectiveness of individualized strategies. *Eur J Obstet Gynecol Reprod Biol*. 2012;163:91–96.
6. Smith-Bindman R, Kerlikowske K, Feldstein VA et al. Endovaginal ultrasound to exclude endometrial cancer and other endometrial abnormalities. *JAMA*. 1998;280:1510–1517.
7. Timmermans A, Opmeer BC, Khan KS et al. Endometrial thickness measurement for detecting endometrial cancer in women with postmenopausal bleeding: A systematic review and meta-analysis. *Obstet Gynecol*. 2010;116:160–167.
8. Van den Bosch T, Van Schoubroeck D, Domali E et al. A thin and regular endometrium on ultrasound is very unlikely in patients with endometrial malignancy. *Ultrasound Obstet Gynecol*. 2007;29:674–679.
9. Gupta JK, Chien PF, Voit D, Clark TJ, Khan KS. Ultrasonographic endometrial thickness for diagnosing endometrial pathology in women with postmenopausal bleeding: A meta-analysis. *Acta Obstet Gynecol Scand*. 2002;81:799–816.
10. Epstein E, Valentin L. Rebleeding and endometrial growth in women with postmenopausal bleeding and endometrial thickness <5 mm managed by dilatation and curettage or ultrasound follow-up: A randomized controlled study. *Ultrasound Obstet Gynecol*. 2001;18:499–504.
11. Van Doorn HC, Timmermans A, Opmeer BC et al. What is the recurrence rate of postmenopausal bleeding in women who have a thin endometrium during a first episode of postmenopausal bleeding? *Acta Obstet Gynecol Scand*. 2008;87:89–93.
12. Billingsley CC, Kenne KA, Cansino CD et al. The use of transvaginal ultrasound in type II endometrial cancer. *Int J Gynecol Cancer*. 2015;25:858–862.
13. Ragupathy K, Cawley N, Ridout A, Iqbal P, Alloub M. Non-assessable endometrium in women with post-menopausal bleeding: To investigate or ignore. *Arch Gynecol Obstet*. 2013;288:375–378.
14. Smith-Bindman R, Weiss E, Feldstein V. How thick is too thick? When endometrial thickness should prompt biopsy in postmenopausal women without vaginal bleeding. *Ultrasound Obstet Gynecol*. 2004;24:558–565.
15. Alcázar J, Salas R, Navarro B, Chacon E, Errasti T, Olartecoechea B, Guerriero S, Pascual M, Jurado M. Risk of endometrial cancer in asymptomatic postmenopausal women with endometrial thickness ≥11mm: Systematic review and meta-analysis. *Ultrasound Obstet Gynecol*. 2017;50:35. doi:10.1002/uog.17659.
16. Gerber B, Krause A, Müller H et al. Ultrasonographic detection of asymptomatic endometrial cancer in postmenopausal patients offers no prognostic advantage over symptomatic disease discovered by uterine bleeding. *Eur J Cancer*. 2001;37:64–71.
17. Kupesic-Urek S, Shalan H, Kurjak A. Early detection of endometrial cancer by transvaginal color Doppler. *Eur J Obstet Gynecol Reprod Biol*. 1993 Apr;49(1–2):46–49.
18. Campbell S, Bourne T, Crayford T, Pittrof R. The early detection and assessment of endometrial cancer by transvaginal colour Doppler ultrasonography. *Eur J Obstet Gynecol Reprod Biol*. 1993;49:44–45.
19. Conoscenti G, Meir YJ, Fischer-Tamaro L et al. Endometrial assessment by transvaginal sonography and histological findings after D&C in women with postmenopausal bleeding. *Ultrasound Obstet Gynecol*. 1995;6:108–115.
20. Sladkevicius P, Valentin L, Marsál K. Endometrial thickness and Doppler velocimetry of the uterine arteries as discriminators of endometrial status in women with postmenopausal bleeding: A comparative study. *Am J Obstet Gynecol*. 1994;171:722–728.
21. Tekay A, Järvelä I, Jouppila P. Reproducibility of transvaginal Doppler velocimetry measurements in the uterine arteries of postmenopausal women. *Ultrasound Obstet Gynecol*. 1997;10:198–204.

22. Alcázar JL, Castillo G, Mínguez JA, Galán MJ. Endometrial blood flow mapping using transvaginal power Doppler sonography in women with postmenopausal bleeding and thickened endometrium. *Ultrasound Obstet Gynecol*. 2003;21:583–588.
23. Dueholm M, Christensen JW, Rydbjerg S, Hansen ES, Ørtoft G. Two- and three-dimensional transvaginal ultrasound with power Doppler angiography and gel infusion sonography for diagnosis of endometrial malignancy. *Ultrasound Obstet Gynecol*. 2015;45:734–743.
24. Alcázar JL, Ajossa S, Floris S, Bargellini R, Gerada M, Guerriero S. Reproducibility of endometrial vascular patterns in endometrial disease as assessed by transvaginal power Doppler sonography in women with postmenopausal bleeding. *J Ultrasound Med*. 2006;25:159–163.
25. Dueholm M, Møller C, Rydbjerg S, Hansen ES, Ørtoft G. An ultrasound algorithm for identification of endometrial cancer. *Ultrasound Obstet Gynecol*. 2014;43:557–568.
26. O'Connell LP, Fries MH, Zeringue E, Brehm W. Triage of abnormal postmenopausal bleeding: A comparison of endometrial biopsy and transvaginal sonohysterography versus fractional curettage with hysteroscopy. *Am J Obstet Gynecol*. 1998;178:956–961.
27. Epstein E, Ramirez A, Skoog L, Valentin L. Transvaginal sonography, saline contrast sonohysterography and hysteroscopy for the investigation of women with postmenopausal bleeding and endometrium >5 mm. *Ultrasound Obstet Gynecol*. 2001;18:157–162.
28. Alcázar JL, Errasti T, Zornoza A. Saline infusion sonohysterography in endometrial cancer: Assessment of malignant cells dissemination risk. *Acta Obstet Gynecol Scand*. 2000;79:321–322.
29. Alcázar JL, Jurado M. Three-dimensional ultrasound for assessing women with gynecological cancer: A systematic review. *Gynecol Oncol*. 2011;120:340–346.
30. Alcázar JL, Mercé LT, Manero MG, Bau S, López-García G. Endometrial volume and vascularity measurements by transvaginal 3-dimensional ultrasonography and power Doppler angiography in stimulated and tumoral endometria: An interobserver reproducibility study. *J Ultrasound Med*. 2005;24:1091–1098.
31. Mansour GM, El-Lamie IK, El-Kady MA, El-Mekkawi SF, Laban M, Abou-Gabal AI. Endometrial volume as predictor of malignancy in women with postmenopausal bleeding. *Int J Gynaecol Obstet*. 2007;99:206–210.
32. Alcázar JL, Galvan R. Three-dimensional power Doppler ultrasound scanning for the prediction of endometrial cancer in women with postmenopausal bleeding and thickened endometrium. *Am J Obstet Gynecol*. 2009;200:44.e1–e6.
33. Rossi A, Forzano L, Romanello I, Fachechi G, Marchesoni D. Assessment of endometrial volume and vascularization using transvaginal 3D power Doppler angiography in women with postmenopausal bleeding. *Int J Gynaecol Obstet*. 2012;119:14–17.
34. Alcázar JL. Three-dimensional power Doppler derived vascular indices: What are we measuring and how are we doing it? *Ultrasound Obstet Gynecol*. 2008;32:485–487.
35. Epstein E, Van Holsbeke C, Mascilini F et al. Gray-scale and color Doppler ultrasound characteristics of endometrial cancer in relation to stage, grade and tumor size. *Ultrasound Obstet Gynecol*. 2011;38:586–593.
36. Alcázar JL, Galán MJ, Jurado M, López-García G. Intratumoral blood flow analysis in endometrial carcinoma: Correlation with tumor characteristics and risk for recurrence. *Gynecol Oncol*. 2002;84:258–262.
37. Galván R, Mercé L, Jurado M, Mínguez JA, López-García G, Alcázar JL. Three-dimensional power Doppler angiography in endometrial cancer: Correlation with tumor characteristics. *Ultrasound Obstet Gynecol*. 2010;35:723–729.

Taylor & Francis
Taylor & Francis Group
http://taylorandfrancis.com

6

Ultrasound Features of Uterine Sarcomas

Introduction

Uterine sarcomas constitute only 3% of all uterine malignancies (1). The World Health Organization (WHO) classifies uterine sarcomas into two main groups: mesenchymal tumors and mixed epithelial and mesenchymal tumors (2).

Mesenchymal tumors include leiomyosarcoma (LMS), endometrial stromal sarcoma (ESS), undifferentiated endometrial sarcoma, and smooth muscle tumors of uncertain malignant potential (STUMP).

Mixed epithelial and mesenchymal tumors include Müllerian adenosarcomas and carcinosarcomas. Uterine carcinosarcoma is now considered as a high-grade endometrioid carcinoma; therefore, it is considered as an epithelial cancer (1). LMS is the most frequent uterine sarcoma, followed by ESS. We focus on these two types of uterine sarcomas.

The International Federation of Gynecology and Obstetrics (FIGO) recommended surgical staging using a similar system as that for endometrial cancer (3) (Table 6.1). LMS accounts for approximately 63% of all uterine sarcomas (4). LMS presents with symptoms similar to those of benign uterine leiomyoma, such as bleeding, pelvic pain, increase of abdominal girth, uterine palpable mass, or pelvic pressure. Most cases of LMS appear in postmenopausal women (5).

Traditionally, a sign for suspicion is a rapidly growing "myoma." However, evidence suggests that the probability of uterine sarcoma in this clinical setting is very low (0.23%) (6).

EES accounts for approximately 20% of all uterine sarcomas. About 50% of them appear in premenopausal women. Like LMS, the main symptom associated with EES is abnormal uterine bleeding. Pelvic or abdominal discomfort is another common complaint (7). Endometrial stromal sarcomas can be divided into low-grade EES or undifferentiated endometrial sarcoma (2).

Most patients with uterine LMS have no identifiable risk factors. No imaging modality can offer a reliable preoperative diagnosis. Most uterine sarcomas are diagnosed by permanent frozen section analysis after hysterectomy or myomectomy. The estimated incidence of uterine sarcoma in hysterectomy specimens is 0.2%–0.5% (8,9).

TABLE 6.1

FIGO Staging for Uterine Sarcoma

Stage	Description
Stage I	Tumor limited to uterus
IA	Tumor size <5 cm
IB	Tumor size ≥5 cm
Stage II	Tumor extends to the pelvis
IIA	Adnexal involvement
IIB	Tumor extends to extrauterine pelvic tissue
Stage III	Tumor invades abdominal tissues (not just protruding into the abdomen)
IIIA	One site
IIIB	More than one site
IIIC	Metastasis to pelvic and/or para-aortic lymph nodes
Stage IV	
IVA	Tumor invades bladder and/or rectum
IVB	Distant metastasis

Ultrasound Features of Uterine Sarcomas

The specific diagnosis of uterine sarcoma is difficult and represents a real clinical challenge (1). The introduction of morcellation as a surgical technique for laparoscopic removal of uterine leiomyomas has made this challenge more problematic, since prognosis seems to worsen in women with occult uterine sarcoma and morcellated uterus (8).

Most reports analyzing ultrasound features of uterine sarcomas did not distinguish between LMS and EES. In general, they are reported as a single mass with nonmyometrial origin, no acoustic shadowing, and a thickened endometrium or an intracavitary process (10). However, some reports attempt to define the characteristics on imaging of leiomyosarcomas and endometrial stromal sarcomas. However, it has been reported that considerable overlap exists between uterine benign leiomyomas and sarcomas (10).

Ultrasound Features of Uterine LMS

There are scanty data about the specific ultrasound appearance of uterine LMS. On ultrasound, uterine leiomyosarcomas are reportedly large, oval-shaped tumors, with an inhomogeneous content owing to tumor tissue and central necrosis and hemorrhage, leading to a "bizarre" internal echo pattern (11,12).

A recent report comprising 116 LMS from 13 centers has shown that the most typical finding in uterine LMS is the presence of a large heterogeneous mass with irregular contours (13) (Figure 6.1). The median largest diameter was 106 mm, ranging from 30 to 321 mm. Irregular cystic areas within the lesion appear in 82% of the cases (Figure 6.2), and shadowing is present in only 30% of the lesions (Figure 6.3). In about 20% of the cases, the uterus cannot be reliably identified (Figure 6.4).

Tumors were moderately or highly vascularized in 68% of the cases (Figure 6.5). However, the absence of vascularization cannot exclude malignancy (Figure 6.6). These data regarding vascularization are in agreement with previous data reported in a smaller series (12).

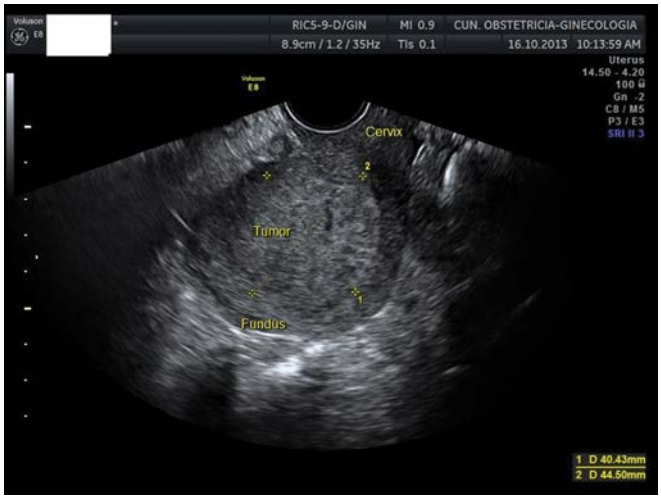

FIGURE 6.1 Transvaginal sonography showing a heterogeneous ill-defined lesion apparently located within the uterine cavity in a 60-year-old woman presenting with postmenopausal bleeding. Hysteroscopy revealed a submucous lesion. Endometrial sampling was negative. The woman was submitted to hysterectomy, and pathological analysis demonstrated the existence of a uterine leiomyosarcoma.

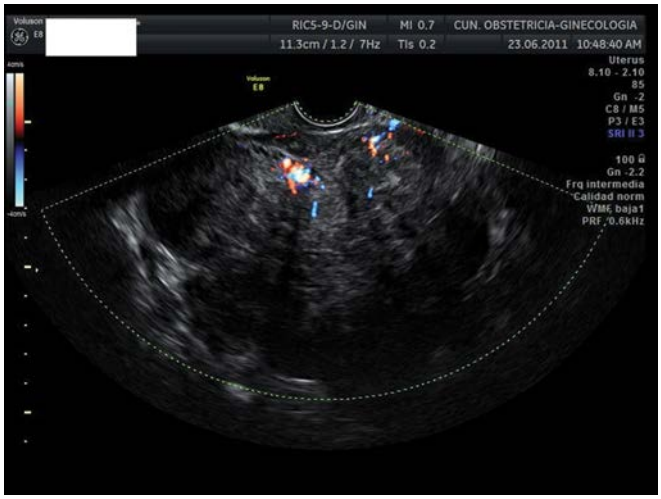

FIGURE 6.3 Transvaginal ultrasound in a 52-year-old woman who presented with pelvic pain and vaginal spotting. The mass is heterogeneous, and acoustic shadowings are present. A polymyomatous uterus was presumed. However, pathologic analysis after hysterectomy showed a leiomyosarcoma.

The use of pulsed Doppler and velocimetric indices, such as resistance index or pulsatility index, was advocated for discriminating benign myomas from LMS.

Kurjak et al. reported that uterine artery and myometrial vessels showed a significantly lower resistance index in cases of LMS as compared with normal uteri and uteri with benign leiomyomas (14). However, the series for uterine sarcomas was small ($n = 10$).

Hata et al. reported that the resistance indices from uterine vessels were not significantly different in cases of LMS ($n = 5$) as compared with cases of benign uterine leiomyomas (15). However, these authors found that peak systolic velocity was significantly higher in cases of leiomyosarcomas. A cut-off >41 cm/s showed a sensitivity of 80% and a specificity of 98%.

However, other authors did not find significant differences in pulsed Doppler velocimetric indices between LMS and benign myomas (16,17). Due to these controversial results, the use of pulsed Doppler is not currently recommended.

Notwithstanding, as stated above, in many circumstances the ultrasound appearance of LMS is not significantly different from that of a benign uterine leiomyoma (Figure 6.7).

Ultrasound Features of EES

Kim et al. reported sonographic findings in a series of 10 cases of endometrial stromal sarcomas (18). They reported that endometrial stromal sarcoma presents with four patterns of its

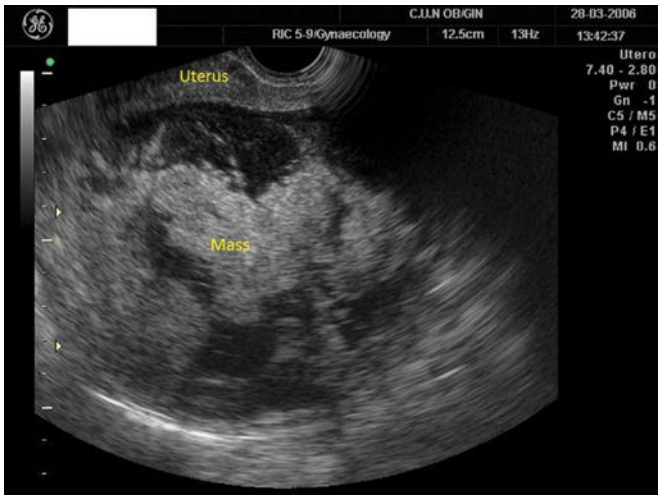

FIGURE 6.2 Transvaginal ultrasound depicting an ill-defined uterine mass. The uterus can be observed flattened and displaced anteriorly. The mass exhibits cystic irregular areas. After hysterectomy, a leiomyosarcoma was found on histological analysis.

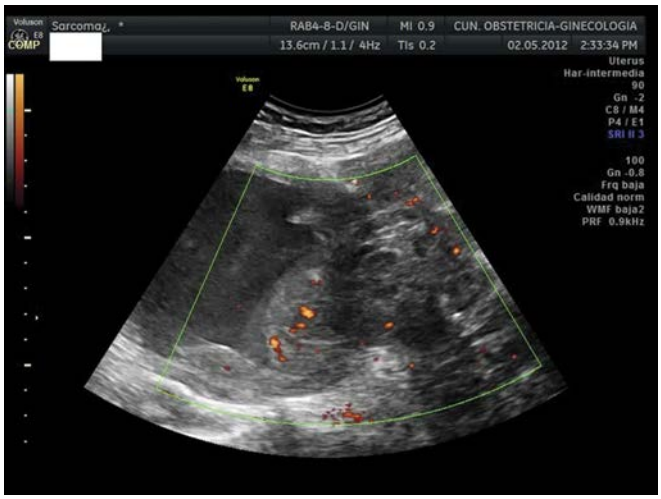

FIGURE 6.4 Transabdominal ultrasound showing a pelvic mass with cystic areas and moderate vascularization. Contours are irregular. The uterus cannot be recognized. A uterine sarcoma was suspected and confirmed after hysterectomy.

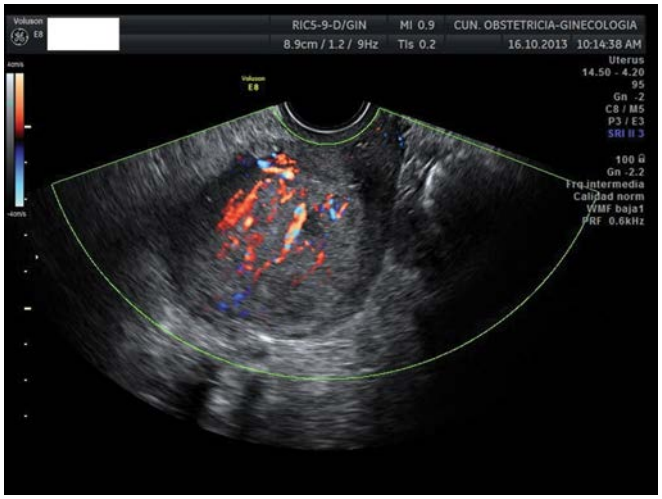

FIGURE 6.5 The same case from Figure 6.1. A rich vascularization can be observed within the lesion.

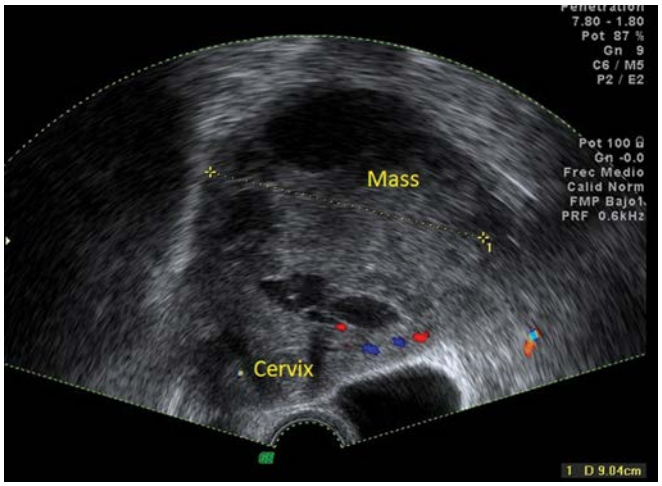

FIGURE 6.6 Uterine leiomyosarcoma. The mass is located in the uterine fundus. There are some cystic areas, but vascularization is absent. (Courtesy of Dr. M.A. Pascual, Institute University Dexeus, Barcelona, Spain.)

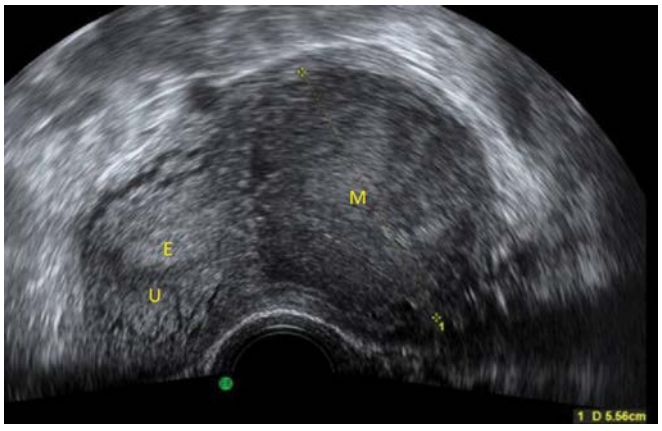

FIGURE 6.7 Transvaginal ultrasound showing a uterine mass (M) in the left lateral of the uterus (U). The endometrium is visible (E). The mass is homogeneous and well defined. A myoma was suspected. However, histological analysis revealed a uterine leiomyosarcoma. (Courtesy of Dr. M.A. Pascual, Institute University Dexeus, Barcelona, Spain.)

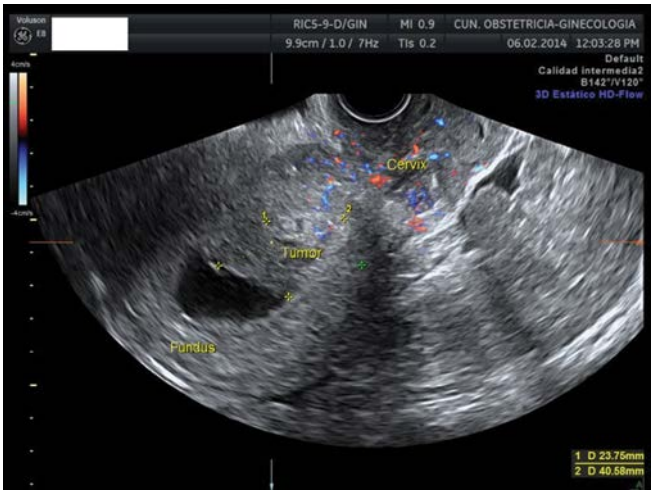

FIGURE 6.8 Transvaginal ultrasound showing an intracavitary lesion that turned out to be an endometrial stromal sarcoma.

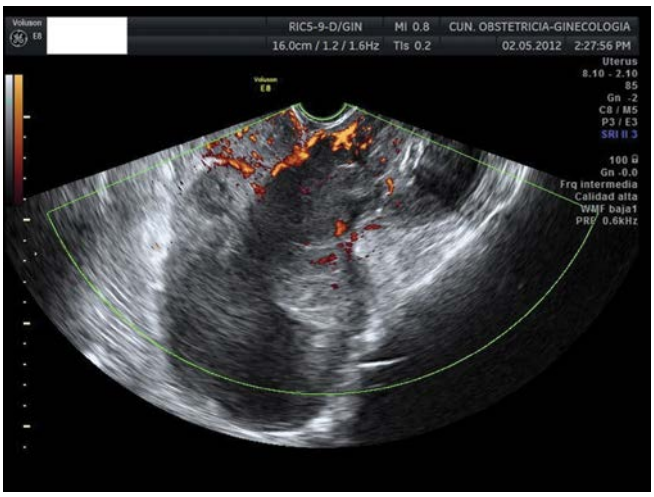

FIGURE 6.9 Transvaginal ultrasound in a case of endometrial stromal sarcoma. The uterus is hardly recognizable.

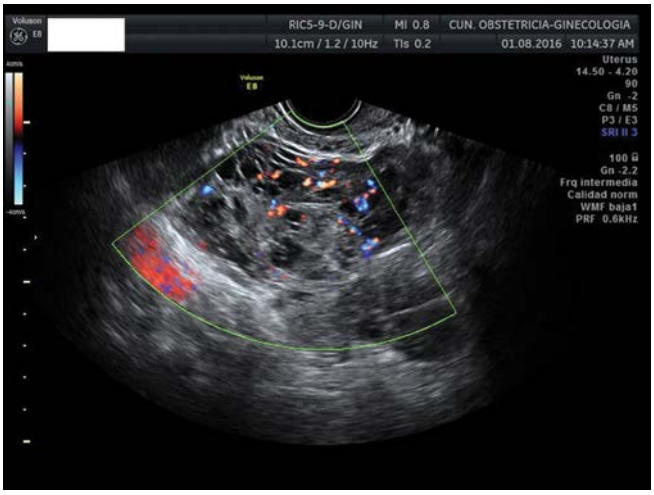

FIGURE 6.10 Transvaginal ultrasound in another case of endometrial stromal sarcoma. We can observe an irregular mass with cystic areas and moderate vascularization.

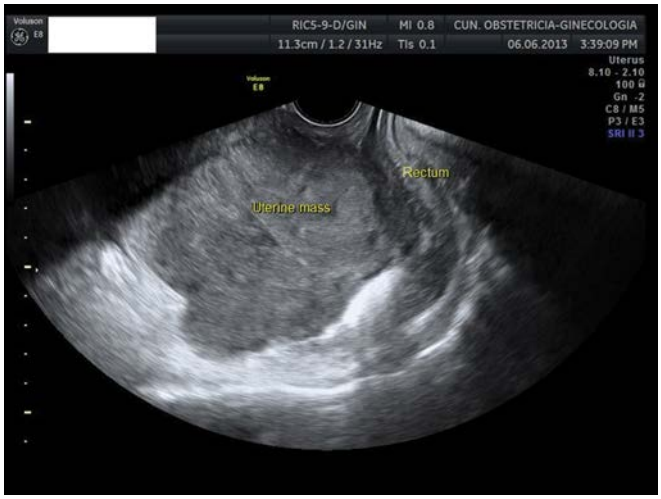

FIGURE 6.11 Transvaginal ultrasound in a case of endometrial stromal sarcoma showing an irregular uterine mass.

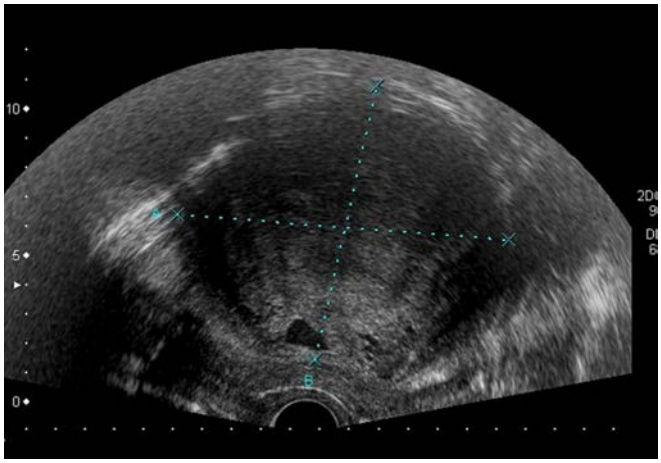

FIGURE 6.12 Transvaginal ultrasound in a case of endometrial stromal sarcoma. Acoustic shadowing can be observed. (Courtesy of Dr. M.A. Pascual, Institute University Dexeus, Barcelona, Spain.)

sonographic appearance: a polypoid mass with nodular myometrial extension, an intramural mass with an ill-defined margin and heterogeneous echogenicity, an ill-defined large central cavity mass, or diffuse myometrial thickening.

A recent report comprising 79 EESs has shown that the most typical appearance of EES is the presence of an intracavitary uterine heterogeneous mass (Figure 6.8) (19). The median largest diameter is 68 mm, ranging from 7 mm to 250 mm. In some cases, the uterus cannot be recognized because of the presence of a large mass (Figure 6.9).

Irregular cyst areas within the mass appear in 70% of the cases (Figure 6.10). An irregular contour appears in only 40% of low-grade EESs but up to 75% of undifferentiated endometrial sarcomas (Figure 6.11). Acoustic shadowing appears in only 20% of the cases (Figure 6.12), and vascularization may be absent or scanty in up to 40% of the lesions (Figure 6.13).

Similar to LMSs, EESs may exhibit ultrasound findings no different from benign uterine leiomyomas (Figure 6.14).

Other Imaging Techniques for the Diagnosis of Uterine Sarcomas

Computed tomography is not specific in discriminating benign myoma and leiomyosarcoma (11,20). This technique is preferred for staging, assessment of distant metastases, and follow-up (20).

On T1-weighted images, leiomyosarcomas demonstrate heterogeneous low to intermediate signal intensity with foci of high signal, whereas on T2-weighted images, they have intermediate to high signal intensity. Necrosis is seen as cystic areas on T2-weighted images (21). The presence of high signal intensity on T2-weighted images and irregular margins and hyperintense areas on T1-weighted images are some objective criteria reported in the literature to distinguish leiomyosarcomas and atypical leiomyomas. However, the accuracy of these objective criteria is debatable and depends on the experience of the reader (22).

More recently, the application of diffusion-weighted imaging–magnetic resonance imaging (DWI-MRI) has been reported. Uterine leiomyosarcomas tend to exhibit high or intermediate signal intensity on DWI on T2-weighted images and lower

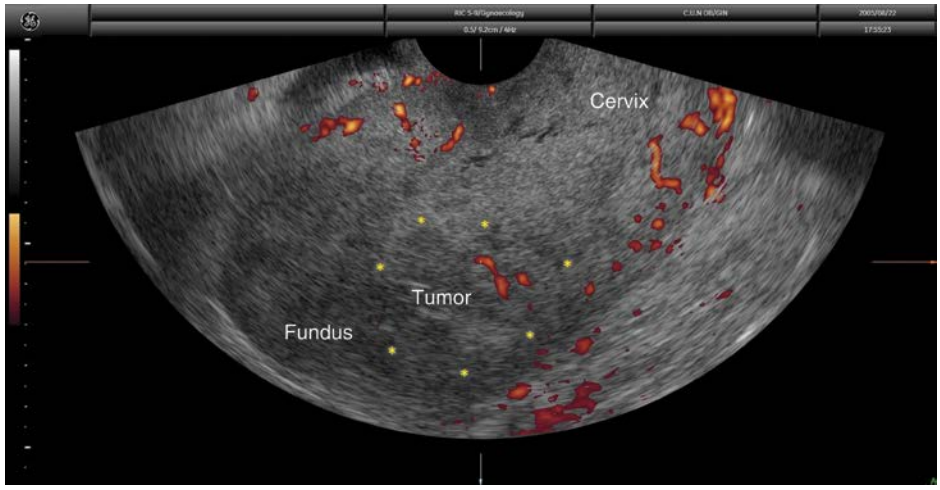

FIGURE 6.13 Transvaginal ultrasounds showing an ill-defined mass (*) located in the myometrial wall. Vascularization is limited. Histology revealed an undifferentiated endometrial stromal sarcoma.

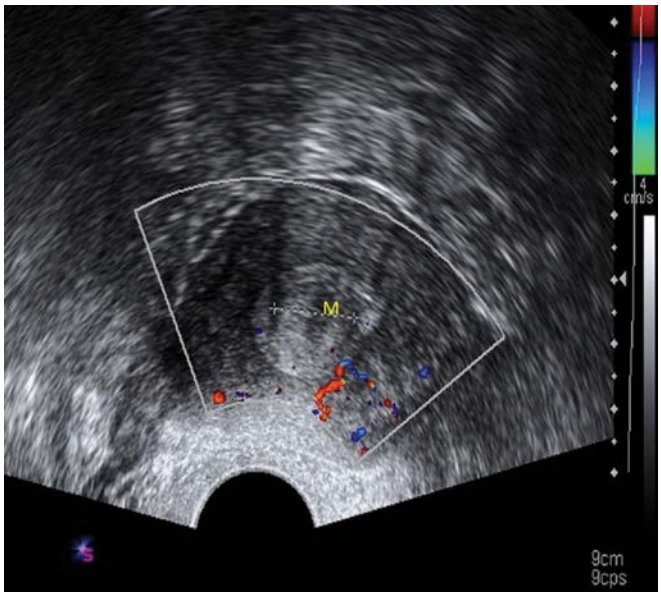

FIGURE 6.14 Transvaginal ultrasound showing an intracavitary mass (M) surrounded by endometrium. A benign leiomyoma was suspected. However, histologic diagnosis after hysteroscopic removal revealed an endometrial stromal sarcoma. (Courtesy of Dr. M.A. Pascual, Institute University Dexeus, Barcelona, Spain.)

apparent diffusion coefficient (ADC) values. The combination of signal intensity on DWI and the ADC seems to be 92%–95% accurate to discriminate benign leiomyomas from leiomyosarcomas (23,24).

Finally, positron emission tomography combined with computed tomography (PET-CT) has also been used for discriminating benign uterine leiomyomas from uterine sarcomas. Results from some reports have shown that PET-CT may be highly accurate. Umesaki et al. reported that PET-CT scan was 100% accurate, MRI was 80% accurate, and ultrasound was 40% accurate (25). However, it should be taken into account that studies analyzing the role of MRI and PET-CT are still limited; most studies are retrospective and include a small number of uterine sarcomas in each series.

A recent meta-analysis including 7 studies using MRI and 11 studies using PET-CT showed that DWI-MRI has a high sensitivity but low specificity for detecting uterine sarcomas. Regarding PET-CT scan, this technique seems to be promising, but current available data do not allow the role of this technique in the diagnosis of uterine sarcomas (26).

REFERENCES

1. Amant F, Coosemans A, Debiec-Rychter M, Timmerman D, Vergote I. Clinical management of uterine sarcomas. *Lancet Oncol*. 2009;10:1188–1198.
2. WHO Classification of Tumors. *Tumors of the Breast and Female Genital Organs*. Tavassoli FA and Devilee P. IARC Press, Lyon, France, 2003.
3. Prat J. FIGO staging for uterine sarcomas. *Int J Gynaecol Obstet*. 2009;104:177–178.
4. Abeler VM, Royne O, Thoresen S et al. Uterine sarcomas in Norway. A histopathological and prognostic survey of a total population from 1970 to 2000 including 419 patients. *Histopathology*. 2009;54:355–364.
5. Hensley ML, Barrette BA, Baumann K et al. Gynecologic Cancer InterGroup (GCIG) consensus review: Uterine and ovarian leiomyosarcomas. *Int J Gynecol Cancer*. 2014;24:S61–S66.
6. Parker WH, Fu YS, Berek JS. Uterine sarcoma in patients operated on for presumed leiomyoma and rapidly growing leiomyoma. *Obstet Gynecol*. 1994;83:414–418.
7. Amant F, Floquet A, Friedlander M et al. Gynecologic Cancer InterGroup (GCIG) consensus review for endometrial stromal sarcoma. *Int J Gynecol Cancer*. 2014;24:S67–S72.
8. Raine-Bennett T, Tucker LY, Zaritsky E et al. Occult uterine sarcoma and leiomyosarcoma: Incidence of and survival associated with morcellation. *Obstet Gynecol*. 2016;127:29–39.
9. Pritts EA, Vanness DJ, Berek JS et al. The prevalence of occult leiomyosarcoma at surgery for presumed uterine fibroids: A meta-analysis. *Gynecol Surg*. 2015;12:165–177.
10. Bonneau C, Thomassin-Naggara I, Dechoux S, Cortez A, Darai E, Rouzier R. Value of ultrasonography and magnetic resonance imaging for the characterization of uterine mesenchymal tumors. *Acta Obstet Gynecol Scand*. 2014;93:261–268.
11. Van den Bosch T, Coosemans A, Morina M, Timmerman D, Amant F. Screening for uterine tumours. *Best Pract Res Clin Obstet Gynaecol*. 2012;26:257–266.
12. Exacoustos C, Romanini ME, Amadio A et al. Can gray-scale and color Doppler sonography differentiate between uterine leiomyosarcoma and leiomyoma? *J Clin Ultrasound*. 2007;35:449–457.
13. Ludovisi M, Giunchi S, Savelli L, Franchi D, Mancari R, Di Noi S, Pasciuto T et al. OP20.05: Ultrasound features of uterine leiomyosarcomas. *Ultrasound Obstet Gynecol*. 2017;50:114. doi:10.1002/uog.17886.
14. Kurjak A, Kupesic S, Shalan H, Jukic S, Kosuta D, Ilijas M. Uterine sarcoma: A report of 10 cases studied by transvaginal color and pulsed Doppler sonography. *Gynecol Oncol*. 1995;59:342–346.
15. Hata K, Hata T, Maruyama R, Hirai M. Uterine sarcoma: Can it be differentiated from uterine leiomyoma with Doppler ultrasonography? A preliminary report. *Ultrasound Obstet Gynecol*. 1997;9:101–104.
16. Szabó I, Szánthó A, Csabay L, Csapó Z, Szirmai K, Papp Z. Color Doppler ultrasonography in the differentiation of uterine sarcomas from uterine leiomyomas. *Eur J Gynaecol Oncol*. 2002;23:29–34.
17. Aviram R, Ochshorn Y, Markovitch O et al. Uterine sarcomas versus leiomyomas: Gray-scale and Doppler sonographic findings. *J Clin Ultrasound*. 2005;33:10–13.
18. Kim JA, Lee MS, Choi JS. Sonographic findings of uterine endometrial stromal sarcoma. *Korean J Radiol*. 2006;7:281–286.
19. Ludovisi M, Giunchi S, Moruzzi M, Savelli L, Mancari R, Pasciuto T, Franchi D, Sladkevicius P et al. OP20.03: Ultrasound features of endometrial stromal sarcomas. *Ultrasound Obstet Gynecol*. 2017;50:113. doi:10.1002/uog.17884.
20. Shah SH, Jagannathan JP, Krajewski K, O'Regan KN, George S, Ramaiya NH. Uterine sarcomas: Then and now. *AJR Am J Roentgenol*. 2012;199:213–223.
21. Tirumani SH, Ojili V, Shanbhogue AK, Fasih N, Ryan JG, Reinhold C. Current concepts in the imaging of uterine sarcoma. *Abdom Imaging*. 2013;38:397–411.

22. Cornfield D, Israel G, Martel M et al. MRI appearance of mesenchymal tumors of the uterus. *Eur J Radiol*. 2010;74:241–249.
23. Sato K, Yuasa N, Fujita M, Fukushima Y. Clinical application of diffusion-weighted imaging for preoperative differentiation between uterine leiomyoma and leiomyosarcoma. *Am J Obstet Gynecol*. 2014;210:368.e1–e8.
24. Thomassin-Naggara I, Dechoux S, Bonneau C et al. How to differentiate benign from malignant myometrial tumours using MR imaging. *Eur Radiol*. 2013;23:2306–2314.
25. Umesaki N, Tanaka T, Miyama M et al. Positron emission tomography with (18)F-fluorodeoxyglucose of uterine sarcoma: A comparison with magnetic resonance imaging and power Doppler imaging. *Gynecol Oncol*. 2001;80:372–377.
26. Dubreuil J, Tordo J, Rubello D, Giammarile F, Skanjeti A. Diffusion-weighted MRI and 18F-FDG-PET/CT imaging: Competition or synergy as diagnostic methods to manage sarcoma of the uterus? A systematic review of the literature. *Nucl Med Commun*. 2017;38:84–90.

7

Ultrasound Assessment of Locoregional Spread of Endometrial Cancer

Introduction

Staging of endometrial cancer should be surgical (1) (Table 7.1). The standard surgical procedure should include total hysterectomy with bilateral salpingo-oophorectomy, peritoneal washings. Pelvic and para-aortic lymphadenectomy should be carried out (1). However, lymphadenectomy remains controversial (2). In patients with high-intermediate risk for lymph node metastases, lymphadenectomy should be performed, whereas in women with low-risk endometrial cancer, the role of lymphadenectomy is arguable (3).

The main factors associated with lymph node metastasis are tumor histology, tumor grade, myometrial infiltration depth, cervical involvement, and lymphovascular space involvement (4). Women at high risk for lymph node involvement are those with tumors with nonendometrioid histology and poorly differentiated endometrioid cancers (2). Well-differentiated or moderately differentiated endometrioid carcinoma with less than 50% myometrial infiltration indicates a low risk for lymph node metastases (0.3%–5%) (2).

Therefore, for clinical decision making, tumor histology, tumor grade, and myometrial infiltration are the main factors to be assessed, since the decision to perform lymphadenectomy should be made before or during the surgery to avoid a second surgery for restaging.

Tumor histology and tumor grade can be determined reliably in the preoperative endometrial biopsy (5). However, myometrial infiltration can only be determined after permanent frozen section assessment of the uterus after surgical removal.

In many oncological centers, intraoperative gross examination (IGE) or intraoperative frozen section (IFS) is used to assess myometrial infiltration. Two recent meta-analyses have shown that IGE has a sensitivity of 71%–75% and a specificity of 91%–95% for detecting deep myometrial infiltration (6,7), whereas IFS has a sensitivity of 85% and a specificity of 97% (7). However, these techniques may be time consuming during surgery and are not available in all hospitals.

Therefore, preoperative assessment of myometrial infiltration by imaging techniques may be clinically relevant.

TABLE 7.1

FIGO Staging Endometrial Cancer

Stage	Description
Stage I	Tumor confined to the corpus uteri[a]
IA	No or less than half myometrial invasion
IB	Invasion equal to or more than half of the myometrium
Stage II	Tumor invades cervical stroma but does not extend beyond the uterus[a,b]
Stage III	Local and/or regional spread of the tumor
IIIA	Tumor invades the serosa of the corpus uteri and/or adnexae[c]
IIIB	Vaginal involvement and/or parametrial involvement[c]
IIIC	Metastases to pelvic and/or para-aortic lymph nodes[a,c]
IIIC1	Positive pelvic node
IIIC2	Positive para-aortic nodes with or without positive pelvic lymph nodes
Stage IV	Tumor invades bladder and/or bowel mucosa, and/or distant metastases[a]
IVA	Tumor invasion of bladder and/or bowel mucosa
IVB	Distant metastasis, including intra-abdominal metastases and/or inguinal nodes

[a] Either G1, G2, or G3.

[b] Endocervical glandular involvement only should be considered as stage I and no longer as stage II.

[c] Positive cytology has to be reported separately without changing the stage.

Ultrasound for Assessing Myometrial and Cervical Infiltration in Endometrial Cancer

Two-Dimensional Ultrasound

Transvaginal or transrectal ultrasound should be used for assessing myometrial and cervical involvement in women with endometrial cancer.

For assessing myometrial infiltration, three approaches have been described: subjective assessment, Karlsson's approach, and Gordon's approach (8–10).

Subjective approach is based on the examiner's subjective impression. The main feature is the presence of disruption of the endometrial-myometrial interphase and the impression of how deep the tumor invades the myometrium (Figures 7.1 through 7.3). A meta-analysis has shown that this approach has a sensitivity and specificity for detecting deep myometrial infiltration of 78% and 81%, respectively (11).

Body mass index, uterus position, and uterine size do not affect the accuracy of the method. However, infra-estimation may occur in well-differentiated tumors, small tumors, or tumors with limited vascularization. On the contrary, overestimation may happen in G3, large, and highly vascularized tumors (12).

Despite being a subjective assessment, reproducibility among observers seems to be good (13).

Karlsson's method consists of calculating the ratio between endometrial thickness and anterior-posterior uterine diameter (9) (Figures 7.4 and 7.5). A ratio of endometrial thickness/anterior-posterior uterine diameter greater than or equal to 0.5 indicates deep myometrial infiltration, whereas a ratio of endometrial thickness/

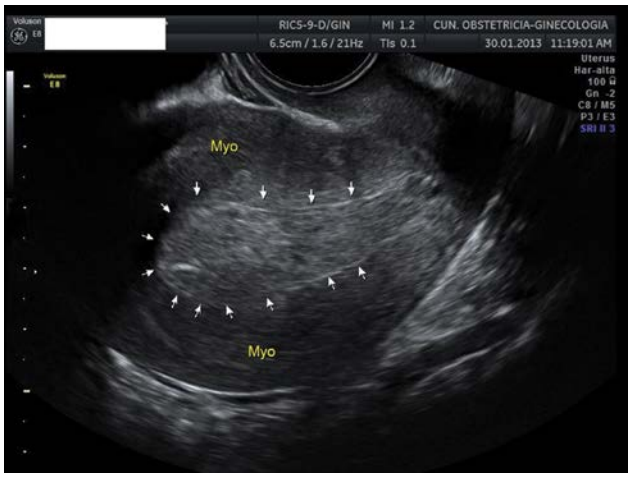

FIGURE 7.1 Transvaginal ultrasound in a case of endometrial cancer. The endometrial-myometrial border is well defined and preserved (arrows), suggesting no myometrial (Myo) infiltration.

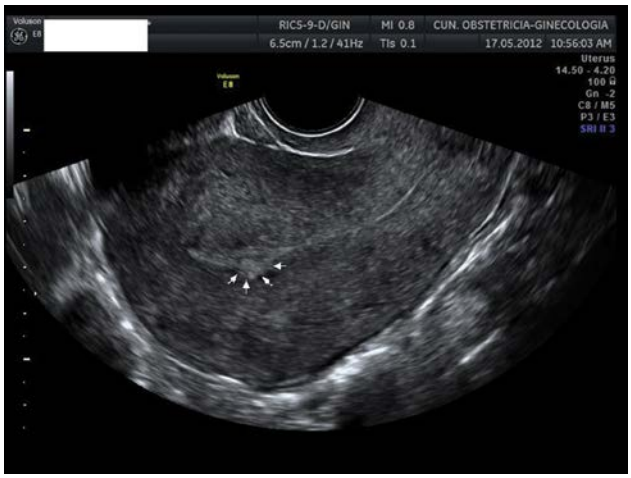

FIGURE 7.2 Transvaginal ultrasound in a case of endometrial carcinoma. The endometrium is thin; however, in the posterior wall, there is a small lesion protruding into the myometrium (arrows) suggesting superficial infiltration.

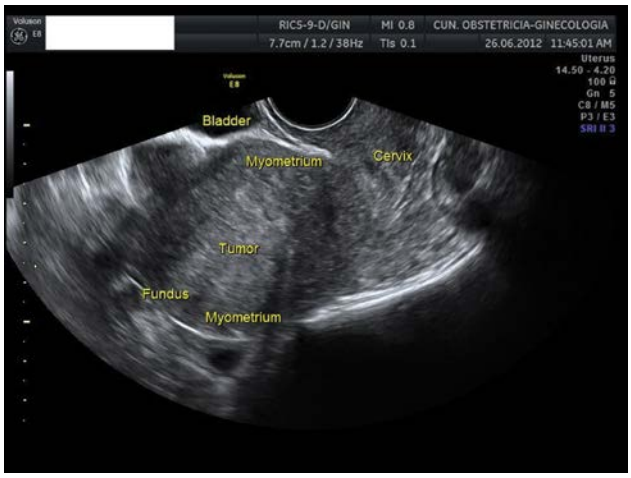

FIGURE 7.3 Transvaginal ultrasound showing a large endometrial lesion corresponding to an endometrial carcinoma (tumor). The tumor invades deeply the myometrial wall at the level of the fundus and posterior wall.

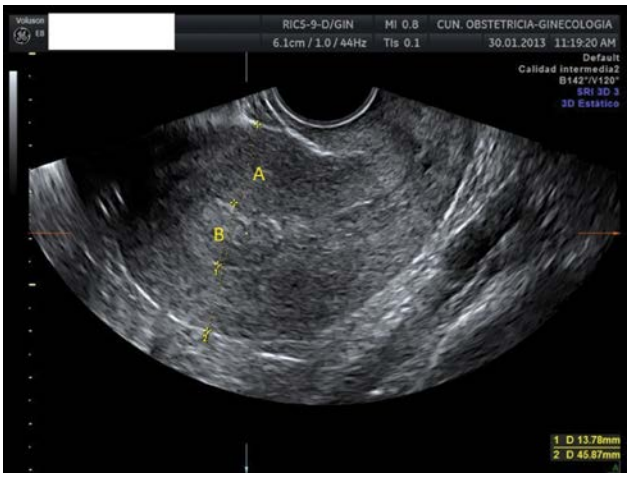

FIGURE 7.4 Transvaginal ultrasound showing the Karlsson's method for assessing myometrial infiltration in endometrial cancer. In this case the ratio B/A is 0.30, suggesting a less than 50% infiltration.

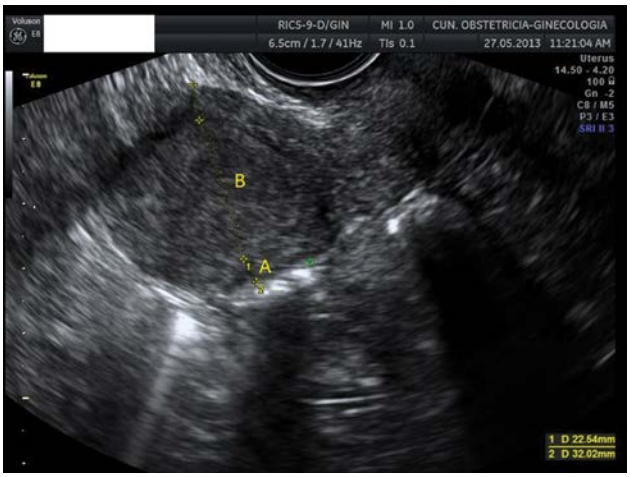

FIGURE 7.5 In this case, according to Karlsson's method, the ratio B/A is 0.70, suggesting more than 50% infiltration.

anterior-posterior uterine diameter less than 0.5 indicates superficial or no myometrial infiltration. This approach is easy to apply, and it has a sensitivity and specificity of 84% and 82%, respectively (11).

Gordon's methods consist of tracing an imaginary line dividing the uterus in two parts in the longitudinal plane and then measuring the distance from this line to the uterine serosa (A), and from this line to the deepest point of myometrial infiltration according to the examiner's impression (B). A ratio B/A greater than or equal to 50% suggests deep myometrial infiltration (8) (Figures 7.6 and 7.7). This approach has a sensitivity and a specificity of 85% and 80%, respectively (11).

There are no differences in terms of diagnostic performance among all three methods.

In all cases, the presence of a poor-quality image, adenomyosis, and uterine myomas may affect the results of the approach used (Figures 7.8 and 7.9).

However, the vast majority of studies assessing myometrial infiltration have the same study's design flaw: they include low- and high-risk cases. From the oncological point of view, in

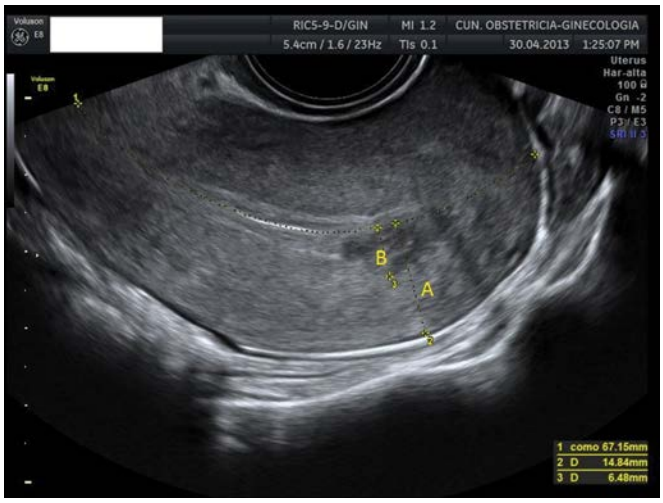

FIGURE 7.6 Transvaginal ultrasound showing the Gordon method for assessing myometrial infiltration in endometrial cancer. In this case, the ratio B/A is 0.44, suggesting superficial infiltration (<50%).

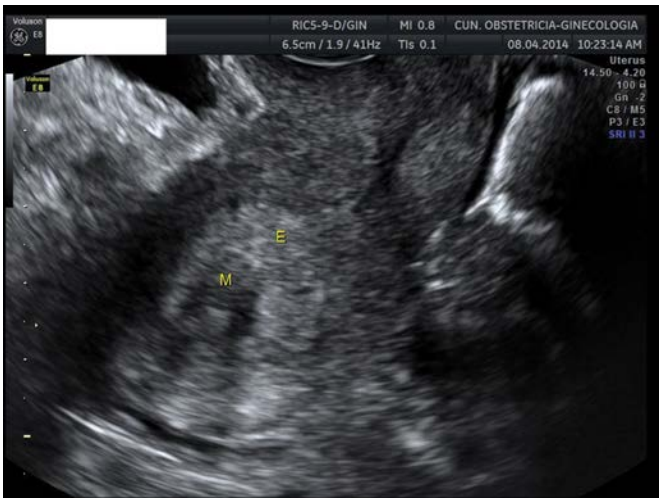

FIGURE 7.8 Transvaginal ultrasound in a case of endometrial carcinoma. There is an intracavitary myoma (M) that may affect our ability to assess myometrial infiltration.

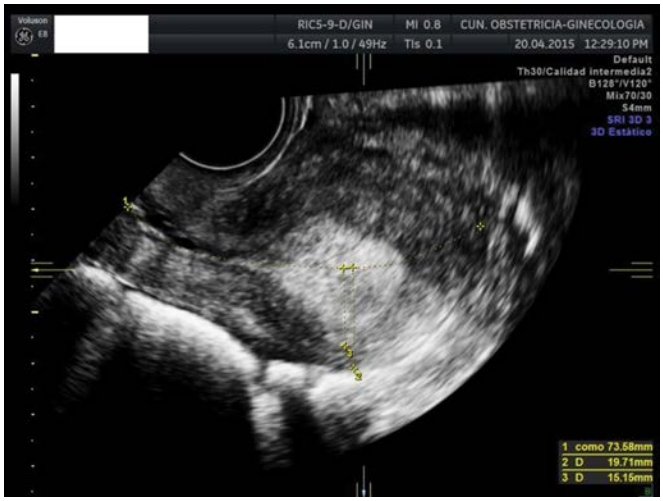

FIGURE 7.7 In this case, according to Gordon's method, the ratio B/A is 0.77, suggesting a deep infiltration (>50%).

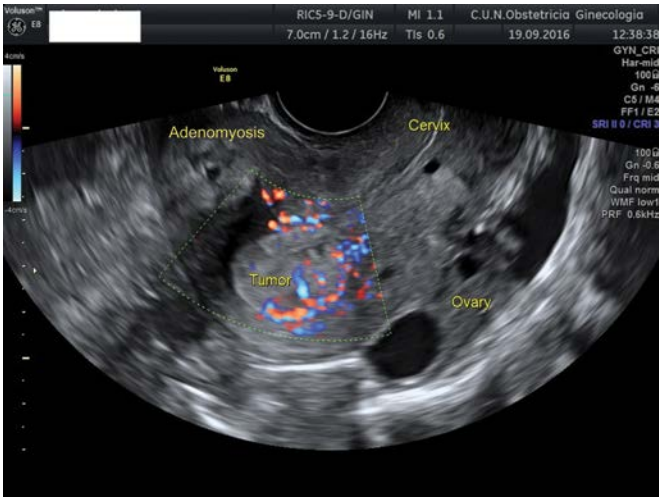

FIGURE 7.9 In this case, we can observe an adenomyotic nodule in the anterior myometrial wall. This finding may also affect the accuracy for estimating myometrial infiltration.

high-risk cases (nonendometrioid histology or poorly differentiated endometrioid carcinomas) preoperative imaging is much less relevant, since lymph node dissection must be performed as part of the staging surgical procedure. This flaw implies that the diagnostic performance of ultrasound might be overestimated when we take into consideration only those cases that make sense to assess preoperatively the myometrial infiltration: well- or moderately differentiated endometrioid carcinomas (2).

Therefore, there is a need to determine the diagnostic performance of ultrasound in this set of cases. Only two studies have focused on low-risk cases (14,15).

Van Holsbeke et al. reported a prospective study on 163 cases of well- or moderately differentiated endometrioid carcinomas (14). They estimated myometrial infiltration according to the examiner's subjective impression and to Karlsson's approach. Sensitivity and specificity for the examiner's subjective impression to detect deep myometrial infiltration were 73% and 74%, respectively. Sensitivity and specificity for Karlsson's approach to detect deep myometrial infiltration were 47% and 78%, respectively. They developed two different mathematical prediction models, but none of them was superior to the examiner's subjective impression.

Pineda et al. reported a prospective study on 152 cases of well- or moderately differentiated endometrioid carcinomas (15) comparing ultrasound assessment and intraoperative gross examination to detect deep myometrial infiltration. They estimated myometrial infiltration according to the examiner's subjective impression. They found that sensitivity and specificity for the examiner's subjective impression to detect deep myometrial infiltration were 82% and 89%, respectively. Sensitivity and specificity for intraoperative gross examination were 79% and 90%, respectively. There were no significant statistical differences between both methods.

Alcázar et al. reported a study aimed to detect actual high-risk cases for lymph node involvement, according to myometrial

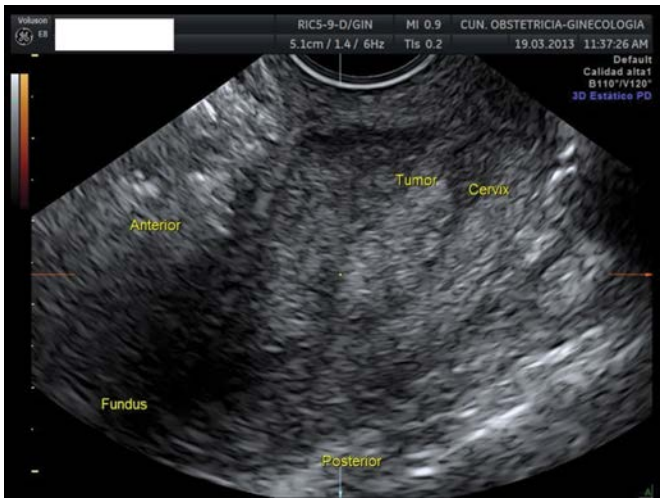

FIGURE 7.10 Transvaginal ultrasound showing cervical involvement in a case of endometrial cancer.

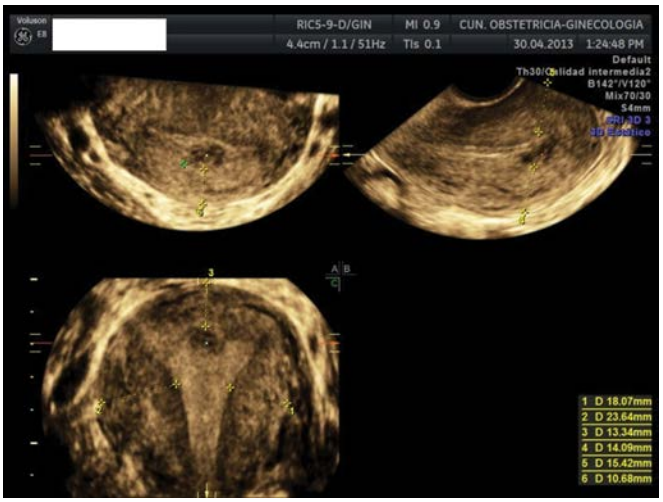

FIGURE 7.12 In this case, the shortest distance to serosa is 10.68 mm (measurement 6) in posterior wall, suggesting less than 50% infiltration.

infiltration, cervical involvement, and adnexal metastasis, in women considered as low-risk cases due to a diagnosis of G1/G2 endometrioid carcinoma prior to surgery (16). They included 169 cases; 50 out of these 169 cases were high-risk cases after surgical staging was performed. These authors reported that ultrasound was able to detect preoperatively 78% of those high-risk cases with a false-positive rate of 11%.

This group also compared the examiner's subjective impression to Karlsson's approach in G1/G2 endometrioid carcinomas according to preoperative endometrial biopsy (17). As in Van Holsbeke's study, they found that an examiner's subjective impression had higher sensitivity than Karlsson's approach (79% versus 32%) with similar specificity (84% versus 94%).

Cervical involvement of endometrial cancer should be suspected when the tumor invades the cervix, disrupting the cervical canal (Figure 7.10). The diagnostic performance of ultrasound

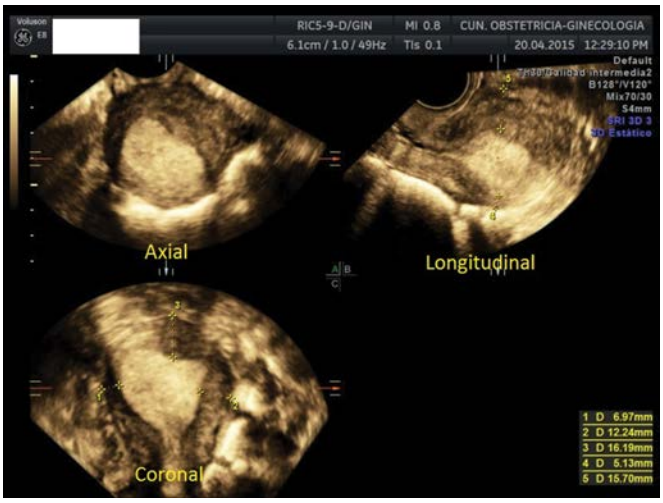

FIGURE 7.11 Myometrial infiltration estimated using virtual navigation with 3D ultrasound. Five measurements of myometrial wall thickness are performed in the anterior and posterior walls (longitudinal plane) and lateral and fundal walls (coronal plane). The shortest distance to serosa is 5.13 mm (measurement 4). This finding suggests deep myometrial infiltration at this site.

(a)

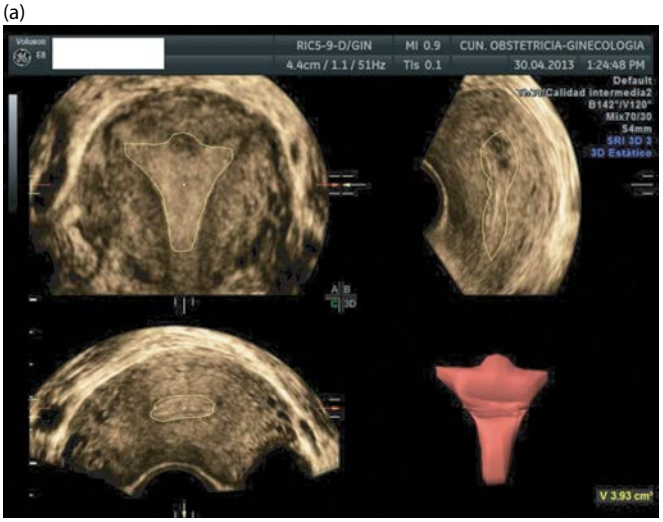

(b)

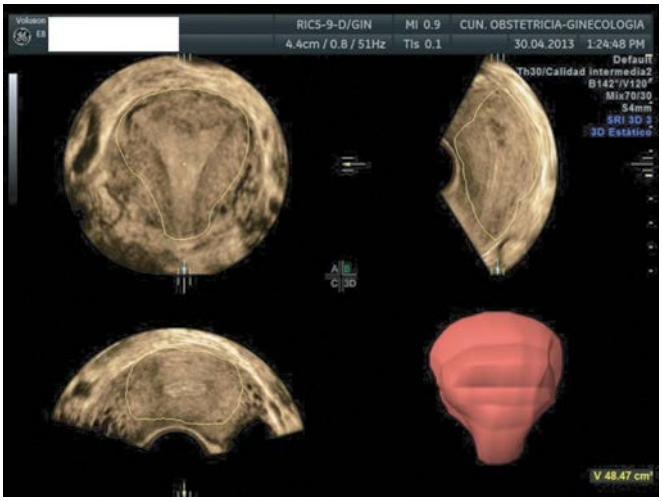

FIGURE 7.13 Estimation of myometrial infiltration using 3D ultrasound and the tumor/uterine volume ratio. We can calculate tumor volume (a) and uterine volume (b) and calculate a ratio (in this case, 0.08). As stated in the text, this method is not accurate.

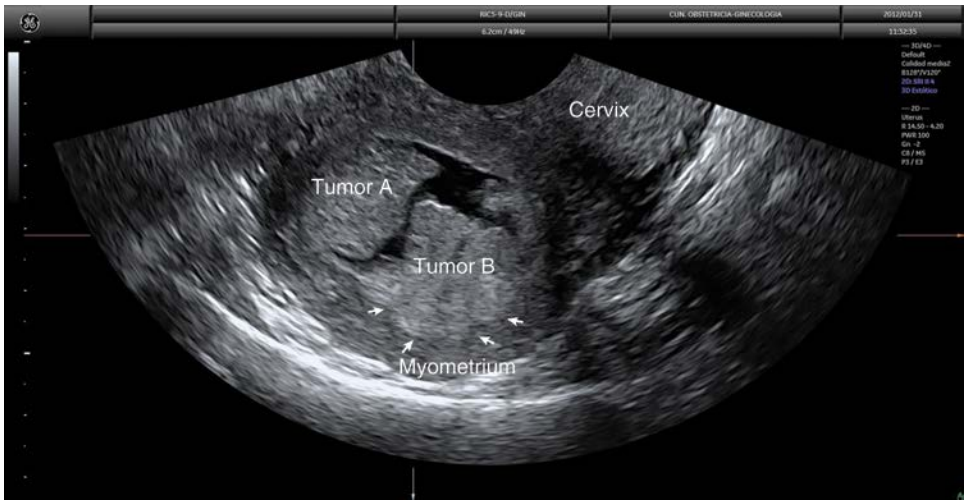

FIGURE 7.14 Ultrasound findings after sonohysterography in a case of endometrial cancer. We can observe two different polypoid lesions. In the case of tumor B, myometrial infiltration seems to be present.

for detecting cervical involvement is similar to that for detecting deep myometrial infiltration (18,19).

Three-Dimensional Ultrasound

Few studies have assessed the role of three-dimensional ultrasound (3D-US) for evaluating myometrial infiltration.

Alcázar et al. proposed a virtual navigation through a 3D stored volume of the uterus (20). This approach consists of navigating through the uterus in the longitudinal and coronal planes using an offline dedicated software and measuring the thickness of the myometrial wall in both uterine lateral walls, anterior and posterior uterine walls, and the uterine fundus. The shortest distance is taken as reference, and this is called "tumor distance to serosa" (TDS) (Figures 7.11 and 7.12). A TDS $\geq$9 mm has a negative predictive valve of 100% for deep infiltration.

Two studies performing an external validation of this approach have been published. Rodriguez-Trujillo et al. reported a negative predictive value of 84% (21), whereas Ergenoglu et al. found that this approach had a negative predictive value of 96% (22).

Interestingly, in Alcázar's and Ergenoglu's studies, the correlation between TDS measured by ultrasound and TDS measured histologically was good (20,22).

Jantarasaengaram et al. used virtual navigation with volume contrast imaging to detect myometrial and cervical infiltration on 3D stored volumes (23). They used subjective assessment. Their results were impressive. For deep myometrial infiltration, sensitivity and specificity reported were 100% and 89%, respectively. For cervical involvement, these figures were 100% and 86%.

Mascilini proposed an interesting approach, the use of 3D volume endometrial/uterine ratio (24) (Figure 7.13). However, their results were poor, with sensitivity and specificity of 75% and 49%, respectively. Similar results were reported by Alcázar et al. (17).

However, recent reports have shown that when compared to 2D ultrasound, 3D ultrasound seems to offer no diagnostic advantage when using virtual navigation and subjective assessment to determine myometrial infiltration (25,26).

Other Imaging Techniques

Computed tomography (CT) scan is considered as a poor technique for assessing myometrial infiltration (27).

Saline infusion sonography has been proposed as an adjuvant to conventional 2D ultrasound for assessing myometrial infiltration with apparent good results (28) (Figure 7.14). However, it should be taken into account that a small risk of malignant cell dissemination through the fallopian tubes to the pelvic cavity exists (29,30).

Magnetic resonance imaging (MRI) is considered as the standard technique for assessing myometrial infiltration in many institutions. At least four different meta-analyses have shown that the sensitivity and the specificity of this technique for detecting deep myometrial infiltration are high, 86%–90% and 86%–89%, respectively, for diffusion-weighted imaging–magnetic resonance imaging (DWI-MRI) (31–34).

However, a recent meta-analysis comparing MRI and transvaginal ultrasound did not find statistical differences between both techniques (35).

REFERENCES

1. Amant F, Mirza MR, Koskas M, Creutzberg CL. Cancer of the corpus uteri. *Int J Gynaecol Obstet*. 2015;131(Suppl 2):S96–S104.
2. Bogani G, Dowdy SC, Cliby WA, Ghezzi F, Rossetti D, Mariani A. Role of pelvic and para-aortic lymphadenectomy in endometrial cancer: Current evidence. *J Obstet Gynaecol Res*. 2014;40:301–311.
3. Neubauer NL, Lurain JR. The role of lymphadenectomy in surgical staging of endometrial cancer. *Int J Surg Oncol*. 2011;2011:814–849.
4. Creasman WT, Morrow CP, Bundy BN, Homesley HD, Graham JE, Heller PB. Surgical pathologic spread patterns of endometrial cancer. *A Gynecologic Oncology Group Study. Cancer*. 1987;60:2035–2041.
5. Sany O, Singh K, Jha S. Correlation between preoperative endometrial sampling and final endometrial cancer histology. *Eur J Gynaecol Oncol*. 2012;33:142–144.

6. Mavromatis ID, Antonopoulos CN, Matsoukis IL et al. Validity of intraoperative gross examination of myometrial invasion in patients with endometrial cancer: A meta-analysis. *Acta Obstet Gynecol Scand*. 2012;91:779–793.
7. Alcázar JL, Dominguez-Piriz J, Juez L, Caparros M, Jurado M. Intraoperative gross examination and intraoperative frozen section in patients with endometrial cancer for detecting deep myometrial invasion: A systematic review and meta-analysis. *Int J Gynecol Cancer.* 2016;26:407–415.
8. Gordon AN, Fleischer AC, Reed GW. Depth of myometrial invasion in endometrial cancer: Preoperative assessment by transvaginal ultrasonography. *Gynecol Oncol*. 1990;39:321–327.
9. Karlsson B, Norström A, Granberg S, Wikland M. The use of endovaginal ultrasound to diagnose invasion of endometrial carcinoma. *Ultrasound Obstet Gynecol*. 1992;2:35–39.
10. Van Doorn HC, Van Der Zee AGJ, Peeters PHM, Kroeks MVAM, Van Eijkeren MA. Preoperative selection of patients with low-stage endometrial cancer at high risk of pelvic lymph node metastases. *Int J Gynecol Cancer.* 2002;12:144–148.
11. Alcázar JL, Orozco R, Martinez-Astorquiza Corral T et al. Transvaginal ultrasound for preoperative assessment of myometrial invasion in patients with endometrial cancer: A systematic review and meta-analysis. *Ultrasound Obstet Gynecol*. 2015;46:405–413.
12. Fischerova D, Frühauf F, Zikan M et al. Factors affecting sonographic preoperative local staging of endometrial cancer. *Ultrasound Obstet Gynecol*. 2014;43:575–585.
13. Eriksson LS, Lindqvist PG, Flöter Rådestad A et al. Transvaginal ultrasound assessment of myometrial and cervical stromal invasion in women with endometrial cancer: Interobserver reproducibility among ultrasound experts and gynecologists. *Ultrasound Obstet Gynecol*. 2015;45:476–482.
14. Van Holsbeke C, Ameye L, Testa AC et al. Development and external validation of new ultrasound-based mathematical models for preoperative prediction of high-risk endometrial cancer. *Ultrasound Obstet Gynecol*. 2014;43:586–589.
15. Pineda L, Alcázar JL, Caparrós M et al. Agreement between preoperative transvaginal ultrasound and intraoperative macroscopic examination for assessing myometrial infiltration in low-risk endometrioid carcinoma. *Ultrasound Obstet Gynecol*. 2016;47:369–373.
16. Alcázar JL, Pineda L, Caparrós M et al. Transvaginal/transrectal ultrasound for preoperative identification of high-risk cases in well- or moderately differentiated endometrioid carcinoma. *Ultrasound Obstet Gynecol*. 2016;47:374–379.
17. Alcázar JL, Pineda L, Martinez-Astorquiza Corral T et al. Transvaginal/transrectal ultrasound for assessing myometrial invasion in endometrial cancer: A comparison of six different approaches. *J Gynecol Oncol*. 2015;26:201–207.
18. Köse G, Aka N, Api M. Preoperative assessment of myometrial invasion and cervical involvement of endometrial cancer by transvaginal ultrasonography. *Gynecol Obstet Invest*. 2003;56:70–76.
19. Akbayir O, Corbacioglu A, Numanoglu C et al. Preoperative assessment of myometrial and cervical invasion in endometrial carcinoma by transvaginal ultrasound. *Gynecol Oncol*. 2011;122:600–603.
20. Alcázar JL, Galván R, Albela S et al. Assessing myometrial infiltration by endometrial cancer: Uterine virtual navigation with three-dimensional US. *Radiology.* 2009;250:776–783.
21. Rodríguez-Trujillo A, Martínez-Serrano MJ, Martínez-Román S et al. Preoperative assessment of myometrial invasion in endometrial cancer by 3D ultrasound and diffusion-weighted magnetic resonance imaging: A comparative study. *Int J Gynecol Cancer.* 2016;26:1105–1110.
22. Ergenoglu M, Akman L, Terek MC et al. The prediction of myometrial infiltration by three-dimensional ultrasonography in patients with endometrial carcinoma: A validation study from Ege university hospital. *Med Ultrason*. 2016;18:201–206.
23. Jantarasaengaram S, Praditphol N, Tansathit T, Vipupinyo C, Vairojanavong K. Three-dimensional ultrasound with volume contrast imaging for preoperative assessment of myometrial invasion and cervical involvement in women with endometrial cancer. *Ultrasound Obstet Gynecol*. 2014;43:569–574.
24. Mascilini F, Testa AC, Van Holsbeke C, Ameye L, Timmerman D, Epstein E. Evaluating myometrial and cervical invasion in women with endometrial cancer: Comparing subjective assessment with objective measurement techniques. *Ultrasound Obstet Gynecol*. 2013;42:353–358.
25. Saarelainen SK, Kööbi L, Järvenpää R, Laurila M, Mäenpää JU. The preoperative assessment of deep myometrial invasion by three-dimensional ultrasound versus MRI in endometrial carcinoma. *Acta Obstet Gynecol Scand*. 2012;91:983–990.
26. Christensen JW, Dueholm M, Hansen ES, Marinovskij E, Lundorf E, Ørtoft G. Assessment of myometrial invasion in endometrial cancer using three-dimensional ultrasound and magnetic resonance imaging. *Acta Obstet Gynecol Scand*. 2016;95:55–64.
27. Haldorsen IS, Salvesen HB. What is the best preoperative imaging for endometrial cancer? *Curr Oncol Rep*. 2016;18:25.
28. Takac I. Transvaginal ultrasonography with and without saline infusion in assessment of myometrial invasion of endometrial cancer. *J Ultrasound Med*. 2007;26:949–955.
29. Alcázar JL, Errasti T, Zornoza A. Saline infusion sonohysterography in endometrial cancer: Assessment of malignant cells dissemination risk. *Acta Obstet Gynecol Scand*. 2000;79:321–322.
30. Dessole S, Rubattu G, Farina M et al. Risks and usefulness of sonohysterography in patients with endometrial carcinoma. *Am J Obstet Gynecol*. 2006;194:362–368.
31. Andreano A, Rechichi G, Rebora P, Sironi S, Valsecchi MG, Galimberti S. MR diffusion imaging for preoperative staging of myometrial invasion in patients with endometrial cancer: A systematic review and meta-analysis. *Eur Radiology*. 2014;24:1327–1338.
32. Das SK, Niu XK, Wang JL et al. Usefulness of DWI in preoperative assessment of deep myometrial invasion in patients with endometrial carcinoma: A systematic review and meta-analysis. *Cancer Imaging.* 2014;14:32.
33. Luomaranta A, Leminen A, Loukovaara M. Magnetic resonance imaging in the assessment of high-risk features of endometrial carcinoma: A meta-analysis. *Int J Gynecol Cancer.* 2015;25:837–842.
34. Deng L, Wang QP, Chen X, Duan XY, Wang W, Guo YM. The combination of diffusion- and T2-weighted imaging in predicting deep myometrial invasion of endometrial cancer: A systematic review and meta-analysis. *J Comput Assist Tomogr.* 2015;39:661–673.
35. Alcázar JL, Gastón B, Navarro B, Salas R, Aranda J, Guerriero S. Transvaginal ultrasound versus magnetic resonance imaging for preoperative assessment of myometrial infiltration in patients with endometrial cancer: A systematic review and meta-analysis. *J Gynecol Oncol*. 2017;28:e86.

8

Ultrasound Features of Uterine Cervical Cancer

Introduction

Uterine cervical cancer is the second most common gynecological malignancy worldwide (1). The incidence has declined in the past 30–40 years in developed countries due to the introduction of cervical screening programs. Human papilloma virus infection is a necessary event, and it is considered as the main etiological factor (1).

Clinically, many early cervical cancers may be asymptomatic. When the tumor grows, abnormal vaginal bleeding and discharge are the two most frequent symptoms. The diagnosis of cervical cancer is based on colposcopic and pelvic examination and biopsy from the lesion.

Histologically, the most frequent types are squamous cell carcinoma (70%) and adenocarcinoma (25%) (2). Cervical tumors may have exophytic or endophytic growth.

According to the International Federation of Gynecology and Obstetrics (FIGO), staging should be clinically performed based on pelvic examination, chest x-ray, cystoscopy, and proctoscopy (3) (Table 8.1). However, discrepancies between clinical staging and surgical findings may occur in up to 48% of the cases (4), especially in stages IB2 and II (3). One of the most problematic issues is the assessment of parametrium, since clinical staging may underestimates parametrial involvement in 20%–30% of stages IB–IIA (5).

This may be relevant because primary treatment for early stages (IA–IB1) is surgery, whereas for advanced stages primary treatment should be concomitant chemoradiation (6).

Because of this discrepancy between clinical staging and pathological results, surgical staging and pretreatment imaging assessment have been encouraged (2,7).

The main imaging techniques proposed for pretreatment staging are magnetic resonance imaging (MRI) and positron emission tomography–computed tomography (PET-CT) scan (7).

MRI has shown good sensitivity (84%) and specificity (92%) for detecting parametrial involvement (8). However, this technique has a low sensitivity to detect lymph node involvement (9). For detecting lymph node involvement, PET-CT scan is superior to MRI (sensitivity of 82% for PET-CT scan as compared to 56% for MRI) (9).

The role of ultrasound for assessing uterine cervical cancer has been considered as very limited (10). However, in the last 10 years, significant research has been performed, and ultrasound has gained attention as an imaging technique for evaluating women with cervical cancer.

Ultrasound Features of Uterine Cervical Cancer

Cancer of the uterine cervix may be assessed by transvaginal ultrasound. An important trick is to use some gel in the vagina to obtain an acoustic window that would allow better assessment of the cervix, especially in exophytic tumors, and the vaginal fornices (Figure 8.1).

As previously stated, cervical cancer may exhibit an exophytic or an endophytic growth pattern. Exophytic tumors commonly appear as an irregular heterogeneous mass located within the cervix, involving the anterior lip, the posterior lip, or the whole cervix, and protruding into the vagina (Figures 8.2 and 8.3).

Endophytic tumors may appear as a homogeneous or heterogeneous mass, usually well defined and located within the cervix but not protruding into the vagina (Figure 8.4).

In large tumors, the cervical canal is usually distorted and in many cases cannot be clearly defined (Figure 8.5). However, in small tumors, the cervical canal can be identified (Figure 8.6).

It has been reported that adenocarcinomas are usually isoechoic or hyperechoic (Figure 8.7), whereas squamous cell carcinomas are hypoechoic (Figure 8.8) (11).

Most uterine cervical cancers exhibit moderate or abundant vascularization (Figure 8.9). However, in some cases vascularization may be limited (Figure 8.10).

TABLE 8.1

FIGO Staging for Cervical Carcinoma

Stage I	Carcinoma strictly confined to the cervix
IA	Invasive cancer identified only microscopically. Invasion is limited to measured stromal invasion with a maximum depth of 5 mm and no wider than 7 mm.
IA1	Measured invasion of the stroma no greater than 3 mm in depth and no wider than 7 mm diameter.
IA2	Measured invasion of stroma greater than 3 mm but no greater than 5 mm in depth and no wider than 7 mm in diameter.
IB	Clinical lesions confined to the cervix or preclinical lesions greater than stage IA. All gross lesions even with superficial invasion are stage IB cancers.
IB1	Clinical lesions no greater than 4 cm in size.
IB2	Clinical lesions greater than 4 cm in size.
Stage II	Carcinoma that extends beyond the cervix, but does not extend into the pelvic wall. The carcinoma involves the vagina, but not as far as the lower third.
IIA	No obvious parametrial involvement. Involvement of up to the upper two-thirds of the vagina.
IIB	Obvious parametrial involvement, but not into the pelvic sidewall.
Stage III	Carcinoma that has extended into the pelvic sidewall.
IIIA	No extension into the pelvic sidewall but involvement of the lower third of the vagina.
IIIB	Extension into the pelvic sidewall or hydronephrosis or non-functioning kidney.
Stage IV	Carcinoma that has extended beyond the true pelvis or has clinically involved the mucosa of the bladder and/or rectum.
IVA	Spread of the tumor into adjacent pelvic organs.
IVB	Spread to distant organs.

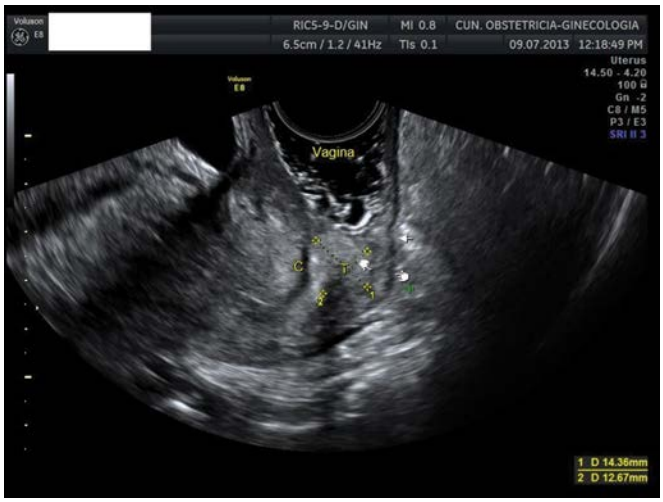

FIGURE 8.1 Transvaginal ultrasound with gel in the vagina (*vaginosonography*) depicting a cervical cancer (T) located in the posterior cervical lip. The cervical canal (C) is visible. The use of gel generates an acoustic window that allows assessment of the posterior vaginal fornix (hands). This area appears as irregular (arrow), suggesting involvement of the vagina.

Some studies have evaluated whether tumor vascularization is correlated with some histoprognostic factors. Most studies found a correlation between the amount of blood flow as assessed by color/pulsed Doppler and tumor size, lymph node involvement, stromal invasion depth, and tumor stage (12–15). However, the series were small, and the Doppler criteria used varied significantly among studies. Additionally, the assessment of tumor blood flow by Doppler has the inherent bias of subjectivity, limiting the potential use of this technique in a clinical setting.

Three-dimensional (3D) vascular indices are not related to tumor characteristics (14,16).

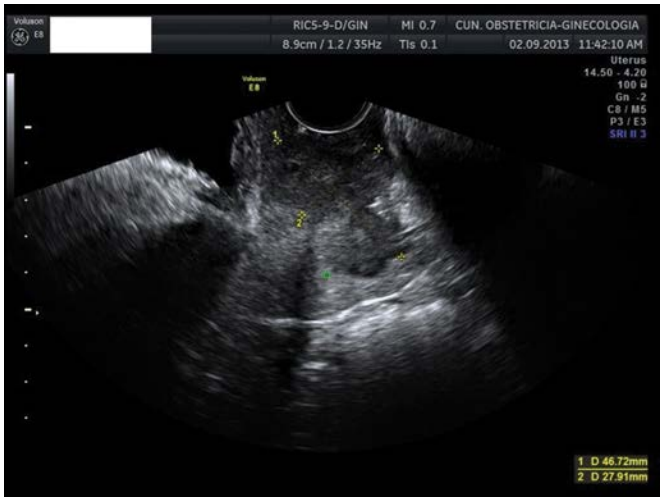

FIGURE 8.2 Transvaginal ultrasound showing an exophytic cervical carcinoma. The lesion is irregular and hypoechoic. It seems to protrude into the vagina.

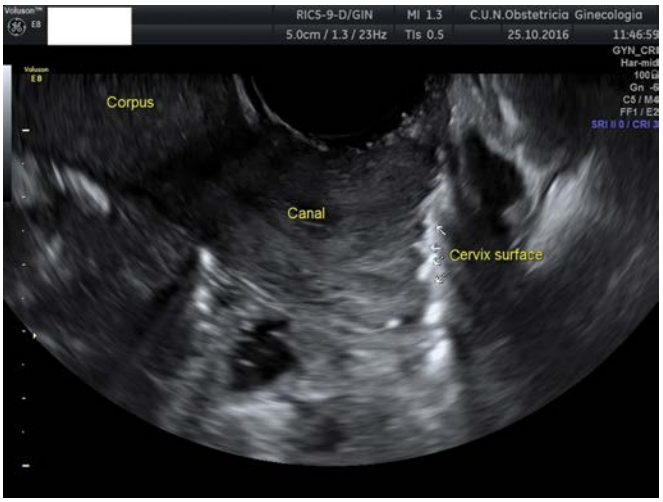

FIGURE 8.3 An exophytic cervical carcinoma. The "cervical" surface is irregular (arrows). The lesion is isoechoic, and it is difficult to ascertain its limits. The cervical canal seems to be free of disease.

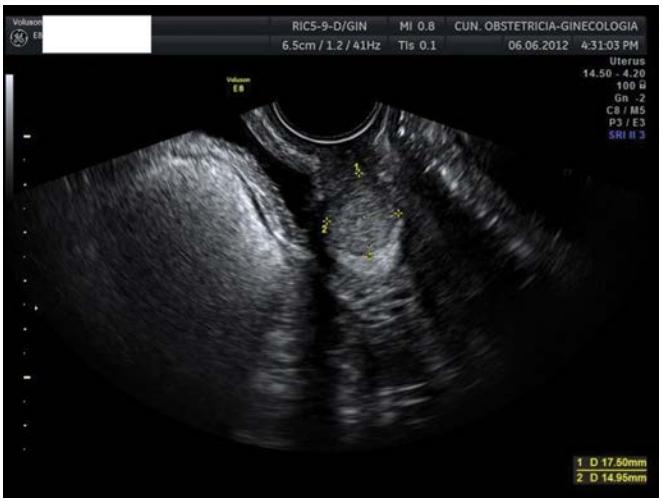

FIGURE 8.4 Transvaginal ultrasound showing a small endophytic cervical carcinoma located in the anterior lip of the cervix. The tumor is well defined and isoechoic.

Ultrasound for Assessing Locoregional Spread of Cervical Cancer

Tumor Size and Stromal Invasion

Transvaginal ultrasound is highly accurate for measuring tumor size (17). However, when considering tumor volume estimation, 3D ultrasound is more accurate than two-dimensional (2D) ultrasound (18).

Cervical stromal invasion can also be estimated using transvaginal ultrasound (Figure 8.11). Some studies have shown that this technique offers good diagnostic performance for detecting deep stromal invasion, with sensitivity and specificity of 88%–90% and 65%–93%, respectively (19,20).

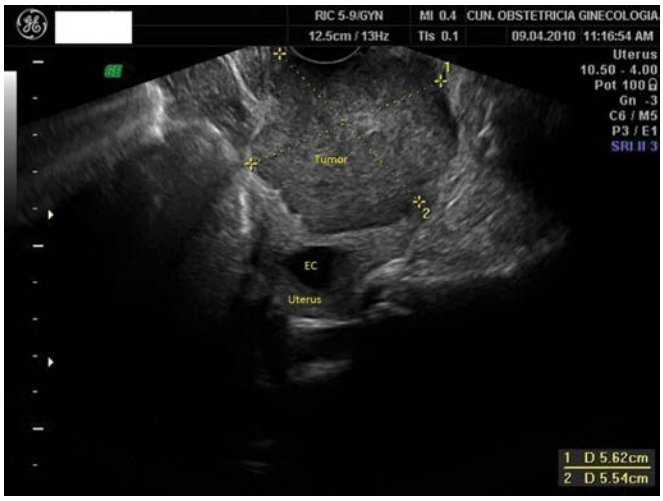

FIGURE 8.5 Transvaginal sonography showing a large, irregular cervical cancer. The uterus is small, and there is some fluid within the uterine cavity (EC), probably secondary to cervical canal distortion and obstruction. In fact, the cervical canal is not visible.

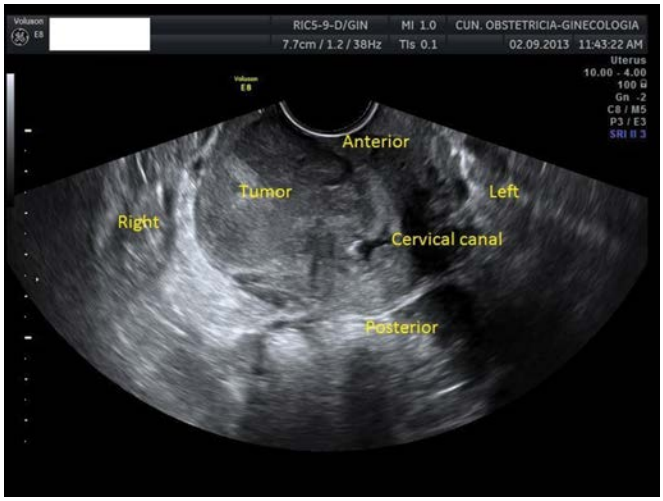

FIGURE 8.6 A transverse view of the cervix shows a cervical cancer located in the right side of the cervix. The lesion is endophytic and expands laterally and anteriorly. The cervical canal is clearly seen.

Parametrial Infiltration

Reports from the early 1990s showed that transrectal ultrasound was able to detect parametrial infiltration in cervical cancer, even more accurately than physical examination (sensitivity 78% versus 52%, respectively) (21).

Parametrial infiltration can be assessed by 2D ultrasound in the transverse plane of the cervix, analyzing the integrity of the pericervical fascia (a dense hyperechoic tissue surrounding the cervix) (22). When this fascia is disrupted, parametrial involvement should be suspected (Figure 8.12).

Several studies have compared transrectal or transvaginal ultrasound with MRI for assessing parametrial involvement. Although the sensitivity of transvaginal ultrasound varied significantly among studies, these studies consistently have shown that ultrasound has a similar diagnostic performance as MRI (Table 8.2) (19,22–24).

(a)

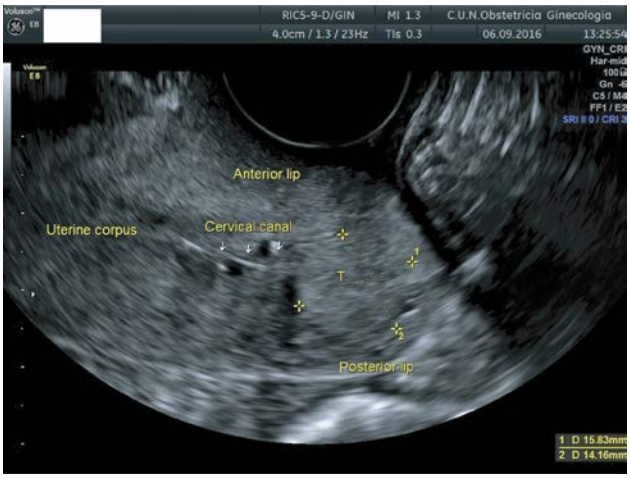

(b)

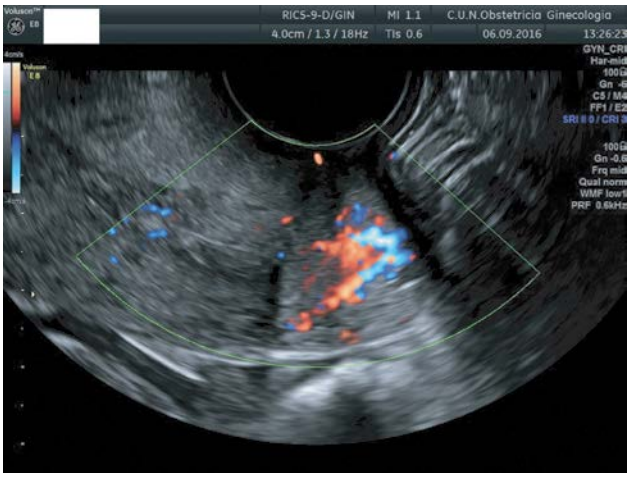

FIGURE 8.7 Transvaginal ultrasound showing an isoechoic cervical cancer (T) involving the posterior lip of the cervix. The cervical canal can be observed. However, the tumor limits are difficult to identify (a). The use of color Doppler allows a better definition of the tumor's location (b).

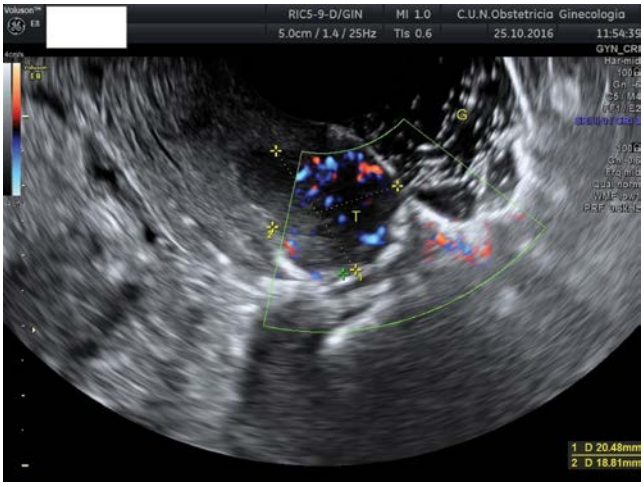

FIGURE 8.8 Transvaginal ultrasound showing a cervical cancer (T). The lesion is irregular and hypoechoic. The use of gel (G) in the vagina allows the assessment of cervical and vaginal surfaces.

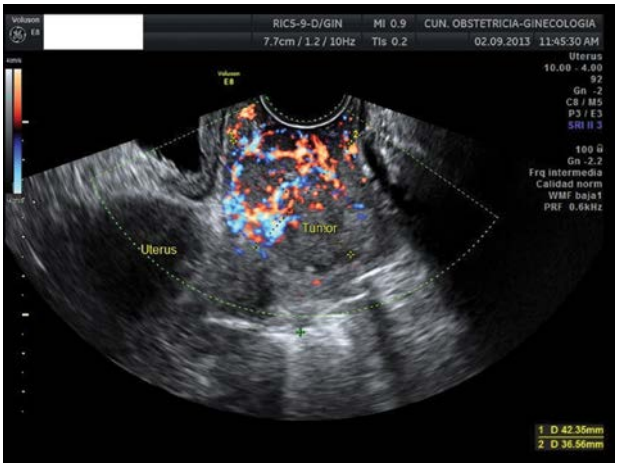

FIGURE 8.9 Transvaginal color Doppler ultrasonography showing the typical Doppler findings in cervical cancer. An abundant vascularization can be observed surrounding and in the tumor.

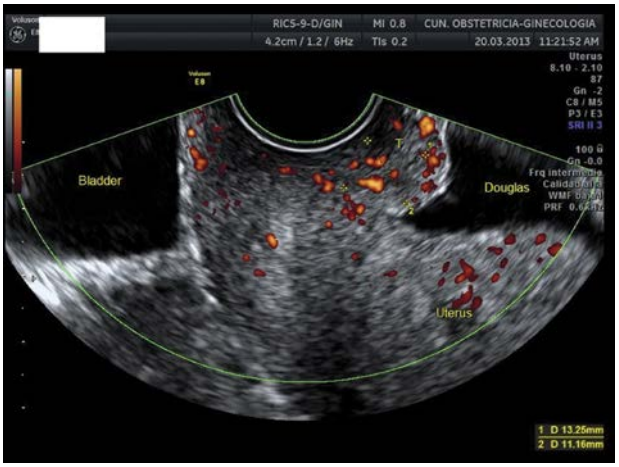

FIGURE 8.10 In some cases of cervical cancer, like that shown here (T), vascularization is limited or moderate.

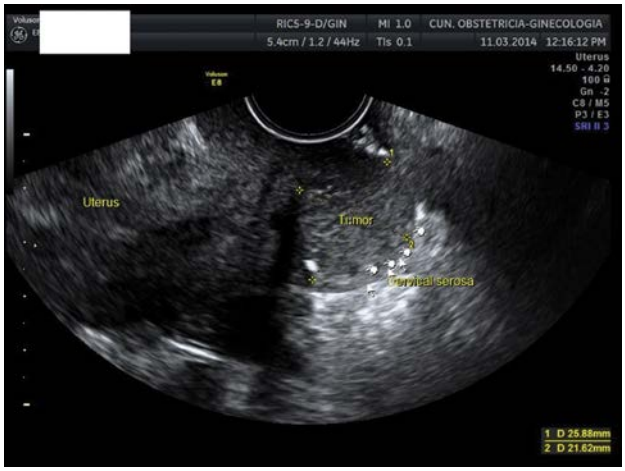

FIGURE 8.11 In cases of cervical carcinoma, cervical stromal infiltration can be assessed using transvaginal ultrasound. In this case, the tumor deeply infiltrates the cervical stroma. The borders of the tumor (hands) almost reach cervical serosa (arrows).

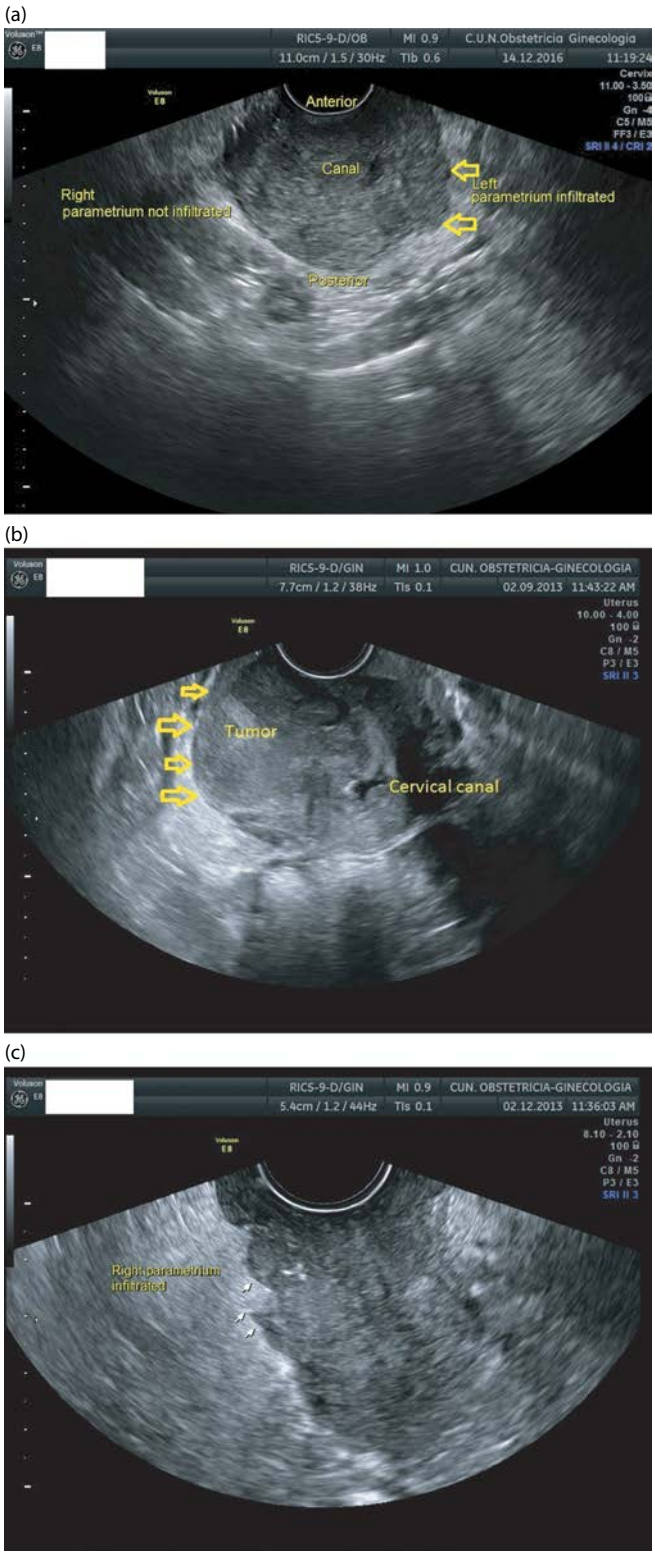

FIGURE 8.12 Transverse view of the cervix by transvaginal ultrasound. This view allows the assessment of parametrial infiltration. Case (a) shows how the left parametrium is infiltrated. The cervical contour is irregular as the tumor infiltrates the proximal parametrium (arrows). When the borders of the cervix remain smooth (arrows), no infiltration is suggested (b). In case (c), there is an infiltration of the right parametrium.

TABLE 8.2

Diagnostic Performance of Transvaginal Ultrasound (TVS) and Magnetic Resonance Imaging (MRI) for Detecting Parametrial Infiltration in Cervical Cancer

	TVS		MRI	
Author	**Sensitivity (%)**	**Specificity (%)**	**Sensitivity (%)**	**Specificity (%)**
Fischerova (22)	83	100	50	97
Testa (23)	60	89	40	89
Epstein (19)	77	98	69	92
Moloney (24)	20	86	40	89

Bladder and rectal involvement can also be assessed by transvaginal ultrasound (Figure 8.13). The possibility of performing a dynamic assessment with real-time ultrasound may be very helpful for assessing bladder or rectal infiltration. The sliding of the cervix over the bladder and/or the rectum suggests that these structures are not affected. On the contrary, the absence of sliding suggests infiltration. Small series have shown that transvaginal ultrasound can accurately detect bladder infiltration (25).

Some studies have assessed the role of ultrasound for detecting pelvic lymph node involvement in uterine cervical cancer (20,26). Lymph nodes can be detected by transvaginal ultrasound (Figure 8.14), but the results of these studies have shown that diagnostic performance of transvaginal ultrasound is poor in terms of sensitivity (23%–43%) but shows high specificity (96%–98%).

There are few reports about the role of 3D ultrasound for local staging of cervical cancer. At least four studies have found a good correlation between 3D ultrasound and MRI with similar diagnostic performance for detecting parametrial infiltration (27–30)

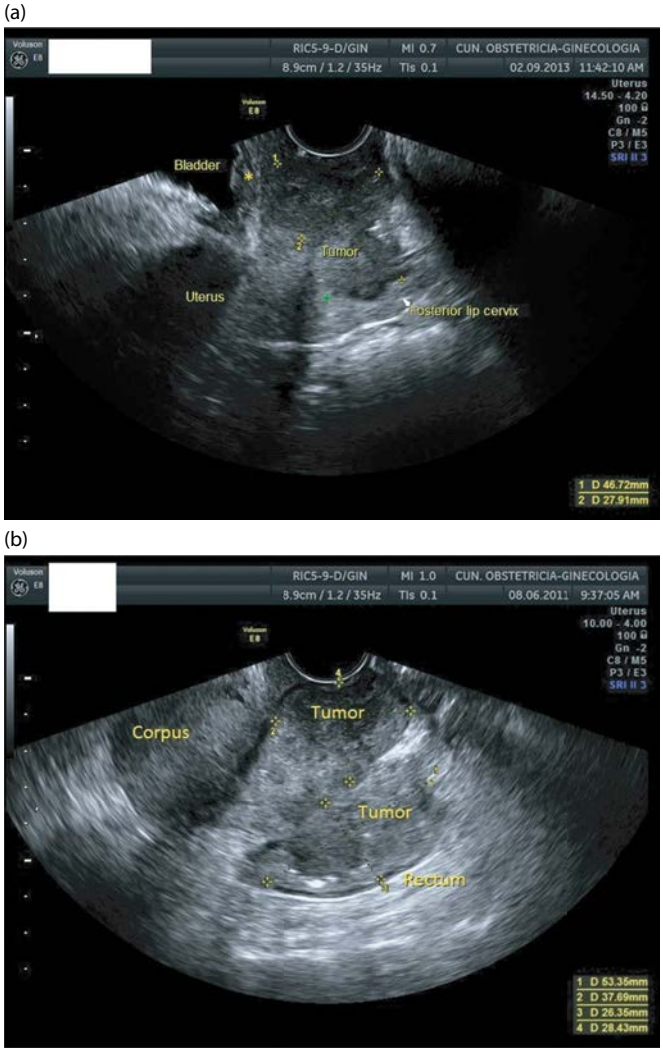

FIGURE 8.13 Two examples of bladder involvement (a) and rectal involvement (b) in cases of cervical cancer as depicted by transvaginal ultrasound. In case (a), the tumor reaches the bladder wall. We can observe the thickening and irregularity of bladder wall at the point the tumor is infiltrating (*). In case (b), the tumor expands posteriorly, reaching and infiltrating the anterior rectal wall.

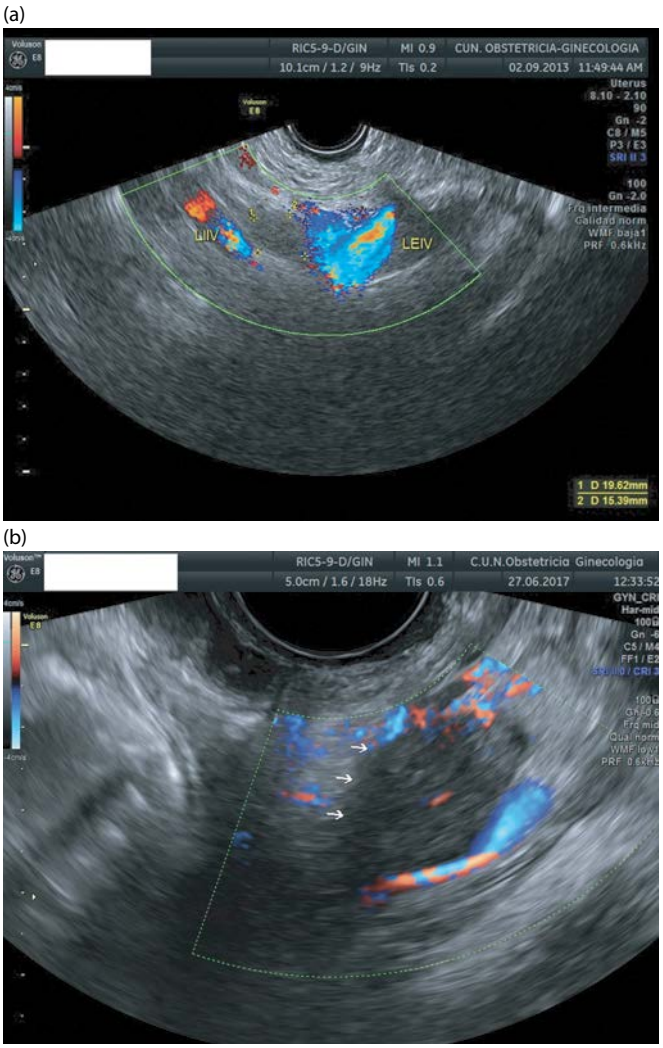

FIGURE 8.14 Transvaginal ultrasound showing lymph node assessment in cases of cervical cancer. In (a), the lymph node is located between the left internal iliac vein (LIIV). In case (b), the lymph node is located lying over the left external iliac artery (LEIV).

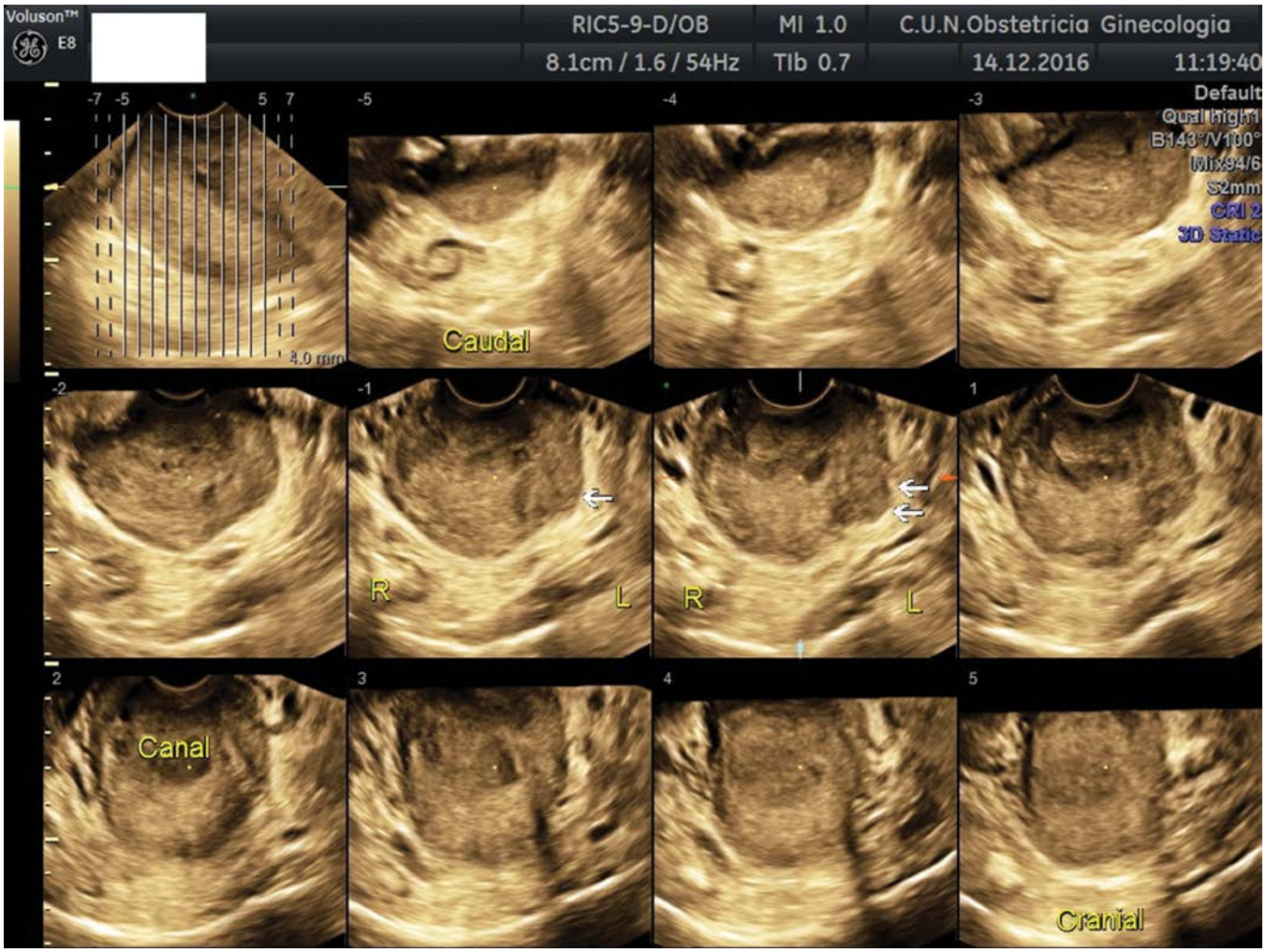

FIGURE 8.15 Three-dimensional ultrasound in a case of cervical cancer using the tomographic ultrasound imaging (TUI) display. A transverse view is shown with multislice display depicted from the external cervical os (caudal) to the internal cervical os (cranial). Observed in the middle slices is a left-sided parametrial infiltration (arrows).

(Figure 8.15). However, the technique for assessing parametrial infiltration using 3D ultrasound needs to be standardized.

There are some recent reports about the potential role of elastography for assessing women with cervical cancer (Figure 8.16). Sun et al. described that cervical cancer exhibits a higher hardness (higher strain ratio) than benign tissue (31). Ma and colleagues assessed the use of elastography for detecting parametrial infiltration and compared this technique with MRI. They reported a similar diagnostic performance for transvaginal elastography (sensitivity 72% and specificity 79%) and MRI (sensitivity 72% and specificity 82%) in a series of 59 women with cervical cancer (32). Mabuchi et al. reported encouraging preliminary results about the use of real-time elastography to assess treatment response in a series of 14 women with cervical cancer. They reported that the strain ratio decreases significantly in women who responded to treatment, whereas there was no significant change in women who did not respond (33).

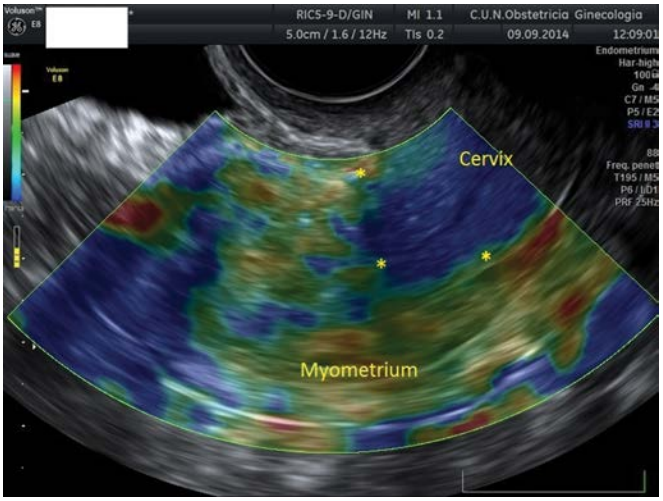

FIGURE 8.16 Transvaginal ultrasound elastography showing the cervical tumor (*) colored as dark blue (high strain ratio).

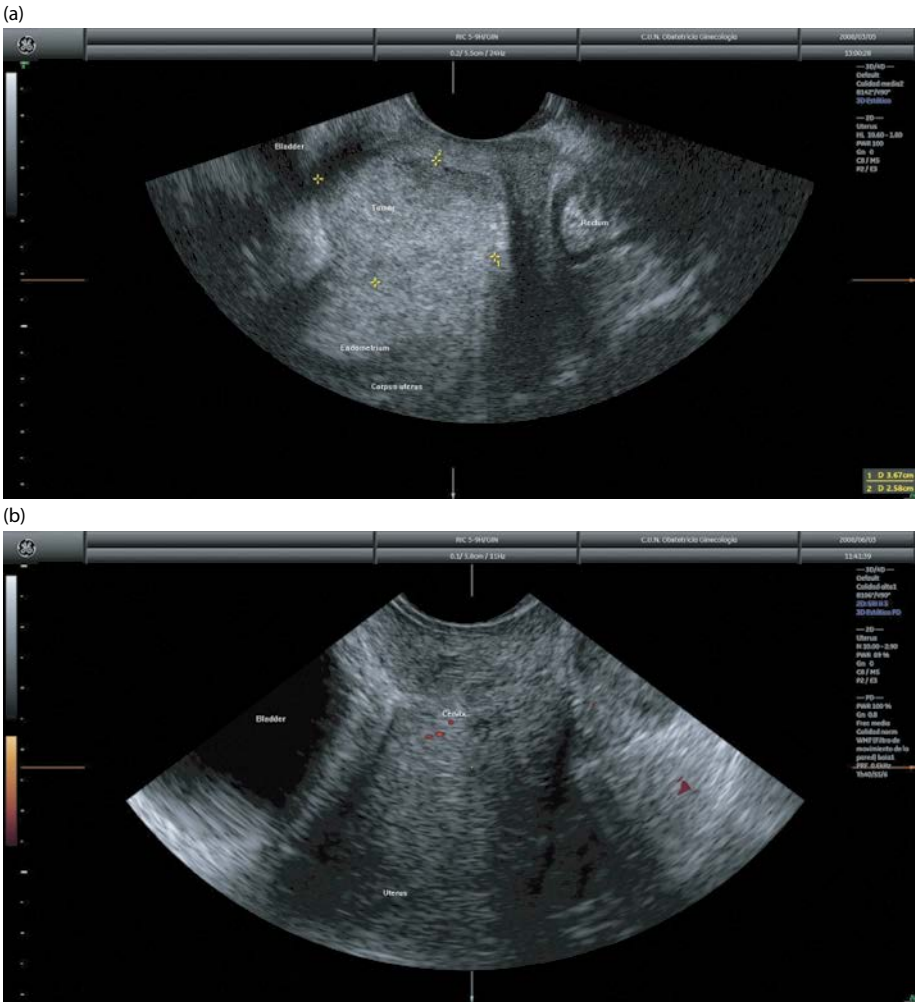

FIGURE 8.17 Transvaginal ultrasound in a case of cervical cancer, prior to chemoradiation (a). We can observe how the tumor disappeared after treatment (b).

Ultrasound for Assessing Treatment Response in Locally Advanced Cervical Cancer

One issue that has gained attention in the field of ultrasound and cervical cancer is the potential use of this technique to assess tumor response to neoadjuvant chemotherapy, radiotherapy, or chemoradiation in locally advanced cervical cancer.

Some reports have shown that transrectal ultrasound has a similar accuracy as MRI to evaluate tumor size reduction after neoadjuvant chemotherapy (34) (Figure 8.17).

There are also reports that show that tumor vascularization assessment using pulsed or power Doppler ultrasound can predict tumor response to treatment (35,36). However, recent reports have questioned this point (37). Additionally, the reproducibility of pulsed Doppler velocimetric indices and power Doppler mapping is questionable, making the clinical application of these findings difficult. The use of 3D power Doppler seems to have no role in predicting treatment response (37,38).

REFERENCES

1. Hillemanns P, Soergel P, Hertel H, Jentschke M. Epidemiology and early detection of cervical cancer. *Oncol Res Treat*. 2016;39:501–506.
2. Ries LAG, Melbert D, Krapcho M et al. *SEER Cancer Statistics Review, 1975–2004*. National Cancer Institute, Bethesda, MD, 2007.
3. Pecorelli S, Zigliani L, Odicino F. Revised FIGO staging for carcinoma of the cervix. *Int J Gynaecol Obstet*. 2009;105:107–108.
4. LaPolla JP, Schlaerth JB, Gaddis O, Morrow CP. The influence of surgical staging on the evaluation and treatment of patients with cervical carcinoma. *Gynecol Oncol*. 1986;24: 194–206.
5. Quinn MA, Benedet JL, Odicino F et al. Carcinoma of the cervix uteri. FIGO 26th annual report on the results of treatment in gynecological cancer. *Int J Gynaecol Obstet*. 2006;95(Suppl 1):S43–S103.

6. Colombo N, Carinelli S, Colombo A, Marini C, Rollo D, Sessa C; ESMO Guidelines Working Group. Cervical cancer: ESMO Clinical Practice Guidelines for diagnosis, treatment and follow-up. *Ann Oncol*. 2012;23(Suppl 7):vii, 27–32.
7. Narayan K, Lin MY. Staging for cervix cancer: Role of radiology, surgery and clinical assessment. *Best Pract Res Clin Obstet Gynaecol*. 2015;29:833–844.
8. Thomeer MG, Gerestein C, Spronk S, van Doorn HC, van der Ham E, Hunink MG. Clinical examination versus magnetic resonance imaging in the pretreatment staging of cervical carcinoma: Systematic review and meta-analysis. *Eur Radiol*. 2013;23:2005–2018.
9. Choi HJ, Ju W, Myung SK, Kim Y. Diagnostic performance of computer tomography, magnetic resonance imaging, and positron emission tomography or positron emission tomography/computer tomography for detection of metastatic lymph nodes in patients with cervical cancer: Meta-analysis. *Cancer Sci*. 2010;101:1471–1479.
10. Follen M, Levenback CF, Iyer RB et al. Imaging in cervical cancer. *Cancer*. 2003;98(9 Suppl):2028–2038.
11. Epstein E, Di Legge A, Måsbäck A, Lindqvist PG, Kannisto P, Testa AC. Sonographic characteristics of squamous cell cancer and adenocarcinoma of the uterine cervix. *Ultrasound Obstet Gynecol*. 2010;36:512–516.
12. Cheng WF, Lee CN, Chu JS et al. Power Doppler angiographic appearance and blood flow velocity waveforms in invasive cervical carcinoma. *Gynecol Oncol*. 2000;79:181–186.
13. Alcázar JL, Castillo G, Jurado M, López-García G. Intratumoral blood flow in cervical cancer as assessed by transvaginal color Doppler ultrasonography: Correlation with tumor characteristics. *Int J Gynecol Cancer*. 2003;13:510–514.
14. Testa AC, Ferrandina G, Distefano M et al. Color Doppler velocimetry and three-dimensional color power angiography of cervical carcinoma. *Ultrasound Obstet Gynecol*. 2004;24:445–452.
15. Jurado M, Galván R, Martinez-Monge R, Mazaira J, Alcázar JL. Neoangiogenesis in early cervical cancer: Correlation between color Doppler findings and risk factors. A prospective observational study. *World J Surg Oncol*. 2008;6:126.
16. Alcázar JL, Jurado M, López-García G. Tumor vascularization in cervical cancer by 3-dimensional power Doppler angiography: Correlation with tumor characteristics. *Int J Gynecol Cancer*. 2010;20:393–397.
17. Gaurilcikas A, Vaitkiene D, Cizauskas A et al. Early-stage cervical cancer: Agreement between ultrasound and histopathological findings with regard to tumor size and extent of local disease. *Ultrasound Obstet Gynecol*. 2011;38:707–715.
18. Chou CY, Hsu KF, Wang ST, Huang SC, Tzeng CC, Huang KE. Accuracy of three-dimensional ultrasonography in volume estimation of cervical carcinoma. *Gynecol Oncol*. 1997;66:89–93.
19. Epstein E, Testa A, Gaurilcikas A et al. Early-stage cervical cancer: Tumor delineation by magnetic resonance imaging and ultrasound—A European multicenter trial. *Gynecol Oncol*. 2013;128:449–453.
20. Pálsdóttir K, Fischerova D, Franchi D, Testa A, Di Legge A, Epstein E. Preoperative prediction of lymph node metastasis and deep stromal invasion in women with invasive cervical cancer: Prospective multicenter study using 2D and 3D ultrasound. *Ultrasound Obstet Gynecol*. 2015;45:470–475.
21. Innocenti P, Pulli F, Savino L et al. Staging of cervical cancer: Reliability of transrectal US. *Radiology*. 1992;185:201–205.
22. Fischerova D, Cibula D, Stenhova H et al. Transrectal ultrasound and magnetic resonance imaging in staging of early cervical cancer. *Int J Gynecol Cancer*. 2008;18:766–772.
23. Testa AC, Ludovisi M, Manfredi R et al. Transvaginal ultrasonography and magnetic resonance imaging for assessment of presence, size and extent of invasive cervical cancer. *Ultrasound Obstet Gynecol*. 2009;34:335–344.
24. Moloney F, Ryan D, Twomey M, Hewitt M, Barry J. Comparison of MRI and high-resolution transvaginal sonography for the local staging of cervical cancer. *J Clin Ultrasound*. 2016;44:78–84.
25. Huang WC, Yang JM, Yang YC, Yang SH. Ultrasonographic characteristics and cystoscopic correlates of bladder wall invasion by endophytic cervical cancer. *Ultrasound Obstet Gynecol*. 2006;27:680–686.
26. Mamsen A, Ledertoug S, Hørlyck A et al. The possible role of ultrasound in early cervical cancer. *Gynecol Oncol*. 1995;56:187–190.
27. Han XS, Ning CP, Sun LT, Li XY, Peng YQ, Dang MZ. Three-dimensional transvaginal tomographic ultrasound imaging for cervical cancer staging. *Ultrasound Med Biol*. 2015;41:2303–2309.
28. Byun JM, Kim YN, Jeong DH, Kim KT, Sung MS, Lee KB. Three-dimensional transvaginal ultrasonography for locally advanced cervical cancer. *Int J Gynecol Cancer*. 2013;23:1459–1464.
29. Chiappa V, Di Legge A, Valentini AL et al. Agreement of two-dimensional and three-dimensional transvaginal ultrasound with magnetic resonance imaging in assessment of parametrial infiltration in cervical cancer. *Ultrasound Obstet Gynecol*. 2015;45:459–469.
30. Arribas S, Alcázar JL, Arraiza M, Benito A, Minguez JA, Jurado M. Three-dimensional transvaginal sonography and magnetic resonance imaging for local staging of cervical cancer: An agreement study. *J Ultrasound Med*. 2016;35:867–873.
31. Sun LT, Ning CP, Liu YJ et al. Is transvaginal elastography useful in pre-operative diagnosis of cervical cancer? *Eur J Radiol*. 2012;81:e888–e892.
32. Ma X, Li Q, Wang JL, Shao J et al. Comparison of elastography based on transvaginal ultrasound and MRI in assessing parametrial invasion of cervical cancer. *Clin Hemorheol Microcirc*. 2017;66:27–35.
33. Mabuchi S, Sasano T, Kuroda H, Takahashi R, Nakagawa S, Kimura T. Real-time tissue sonoelastography for early response monitoring in cervical cancer patients treated with definitive chemoradiotherapy: Preliminary results. *J Med Ultrason*. 2015;42:379–385.
34. Pinkavova I, Fischerova D, Zikan M et al. Transrectal ultrasound and magnetic resonance imaging in the evaluation of tumor size following neoadjuvant chemotherapy for locally advanced cervical cancer. *Ultrasound Obstet Gynecol*. 2013;42:705–712.
35. Alcázar JL, Castillo G, Martínez-Monge R, Jurado M. Transvaginal color Doppler sonography for predicting response to concurrent chemoradiotherapy for locally advanced cervical carcinoma. *J Clin Ultrasound*. 2004;32:267–272.
36. Chen CA, Cheng WF, Lee CN, Su YN, Hsieh CY, Hsieh FJ. Power Doppler vascularity index for predicting the response of neoadjuvant chemotherapy in cervical carcinoma. *Acta Obstet Gynecol Scand*. 2004;83:591–597.

37. Testa AC, Ferrandina G, Moro F et al. Prospective multimodal imaging assessment of locally advanced cervical cancer patients administered by chemoradiation followed by radical surgery. The PRICE (PRospective Imaging of CErvical cancer and neo-adjuvant treatment) study: The role of ultrasound. *Ultrasound Obstet Gynecol*. 2017 Nov 8. doi: 10.1002/uog.18953.

38. Alcázar JL, Arribas S, Martinez-Monge R, Jurado M. Three-dimensional power Doppler ultrasound for predicting response and local recurrence after concomitant chemoradiation therapy for locally advanced carcinoma of the cervix. *Int J Gynecol Cancer.* 2016;26:534–538.

Taylor & Francis
Taylor & Francis Group
http://taylorandfrancis.com

9

Ultrasound Features of Gestational Trophoblastic Disease

Introduction

Gestational trophoblastic disease (GTD) comprises a group of disorders arising from uncontrolled growth of placental trophoblastic tissue, with a spectrum of placental lesions including premalignant hydatiform mole (complete and partial) and malignant invasive hydatiform mole, placental site trophoblastic tumor, epithelioid trophoblastic tumor, and choriocarcinoma (1,2). The malignant entities are known as gestational trophoblastic neoplasia (GTN).

Hydatiform mole accounts for 80% of all GTD, with a prevalence that varies significantly depending on the geographical area, from 0.05%–0.1% of pregnancies in Western countries to 0.8%–1.2% of pregnancies in Southeast Asia (1). Choriocarcinomas are rare, with an estimated incidence of one in 2000–40,000 pregnancies. About 50% of choriocarcinomas arise from hydatiform moles, 25% follow abortions, and 25% are associated with term or preterm gestations (1).

Placental site trophoblastic tumor (PSTT) is also a rare entity (<1% of all GTD), and most of them appear after a nonmolar pregnancy (1). Epithelioid trophoblastic tumor (ETT) is a rare variant of PSTT that simulates a carcinoma and may appear years after delivery (2).

Most hydatiform moles present with vaginal bleeding in the first trimester or early second trimester. In developed countries, other symptoms such as hyperemesis, thyrotoxicosis, and early onset preeclampsia are rare, due to an earlier diagnosis by ultrasound after bleeding.

The diagnosis of GTD is mainly based on the human chorionic gonadotropin (hCG) serum levels (2). However, ultrasound has also been shown to be very helpful. Since most GTN appear after a molar pregnancy, GTN is more frequently diagnosed biochemically with hCG serum levels (a plateaued or rising hCG). However, in some cases clinical symptoms such as vaginal bleeding, seizures, headache, and dyspnea or chest pain may be present, depending on the extent of metastases. According to the International Federation of Gynecology and Obstetrics (FIGO), staging is mainly clinical (1) (Table 9.1).

Treatment of molar pregnancies is based on uterine evacuation by suction (1). Hysterectomy may be an option if the patient has completed her family. Chemotherapy should be considered for all forms of GTN (3). The type of chemotherapy depends on the risk classification and stage at diagnosis (3).

In this chapter, we review the ultrasound features of GTD.

Hydatiform Mole

Ultrasound may be considered as the first-line imaging technique for the diagnosis of a clinically suspected molar pregnancy (4). Actually, with the advent of routine first trimester ultrasound scanning, many molar pregnancies are suspected by ultrasound before becoming symptomatic.

The typical ultrasound appearance of a complete hydatiform mole is an enlarged uterus with the uterine cavity filled with multiple sonolucent areas of varying size (1–30 mm) and shape, the "snowstorm" appearance, without any embryonic or fetal structure (Figure 9.1) (4,5). In the second trimester, a complete hydatiform mole will further expand the uterus, and the anechoic spaces will become more numerous and visible, even transabdominally (4).

Color Doppler shows no flow within these areas (Figure 9.2). However, flow velocity waveforms from arcuate or uterine arteries at pulsed Doppler interrogation usually show very high velocity and low resistance flow (Figure 9.3).

TABLE 9.1

International Federation of Gynecology and Obstetrics (FIGO) Anatomic Staging System

Stage	Description
I	Disease confined to the uterus
II	Gestational trophoblastic neoplasm (GTN) extends outside of the uterus, but is limited to the genital structures (adnexa, vagina, broad ligament)
III	GTN extends to the lungs, with or without known genital tract involvement
IV	All other metastatic sites

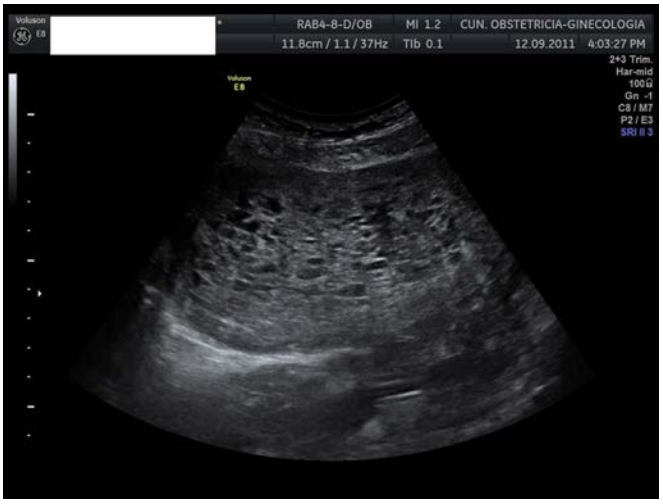

FIGURE 9.1 Transabdominal ultrasound in a 10-week pregnant woman presenting with vaginal bleeding. The typical "snowstorm" appearance of complete hydatiform is observed.

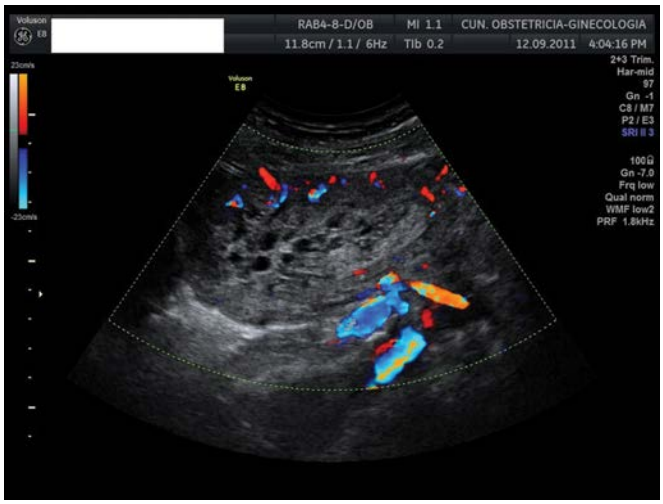

FIGURE 9.2 The same patient as in Figure 9.1. The cystic areas are avascular.

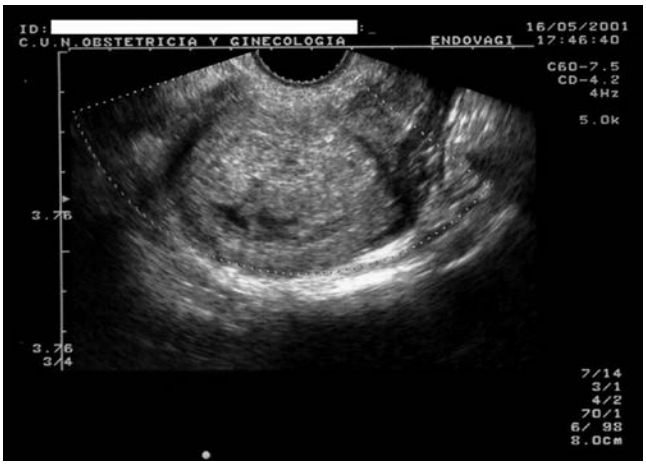

FIGURE 9.4 Transvaginal ultrasound in an 8-week pregnancy showing the absence of gestational sac. The uterine cavil is filled with an echogenic structure. Beta-hCG level was >100,000 IU/mL. After uterine evacuation, complete hydatiform mole was definitively diagnosed.

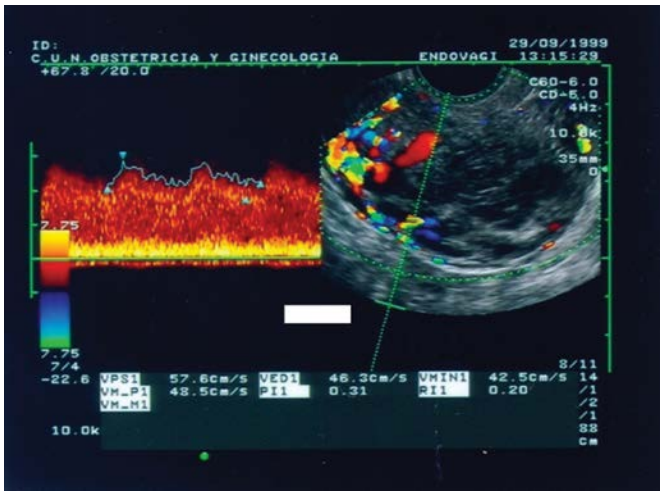

FIGURE 9.3 Flow velocity waveforms from arcuate artery in a case of complete hydatiform mole, showing high-velocity and low-resistance blood flow.

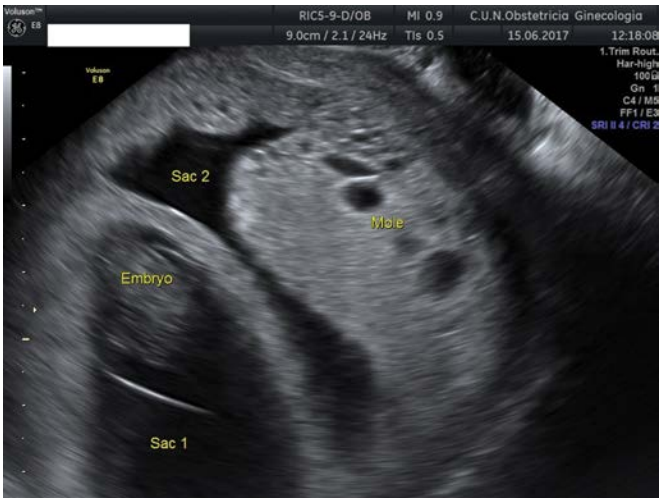

FIGURE 9.5 Transvaginal ultrasound in a case of twin pregnancy. One gestational sac (Sac 1) contains a normal embryo. However, the second sac (Sac 2) is empty, and the placenta shows cystic areas and increased thickening. Serum ß-hCG level was 560,000 IU/mL. Histology revealed a complete mole.

Typically, these findings are observed during late first trimester or early second trimester (9–14 weeks) but can also be found in the early first trimester (Figure 9.4). Unfortunately, in very early pregnancy, this appearance is nonspecific, and an incomplete miscarriage may appear identical (4). Betel et al. reported that the sonographic features that predicted GTD were a myometrial epicenter, depth of myometrial invasion of more than one-third, placental venous lakes, maximum mass dimensions of more than 3.45 cm, and maximum endometrial thickness of less than 12 mm (6).

Complete hydatiform mole may coexist with a twin viable pregnancy. The estimated incidence is 1 in 20,000 to 100,000 pregnancies (7). When this happens, usually a normal gestational sac with a living embryo or fetus next to an empty sac with cystic areas within the chorion frondosum (early pregnancy) or a complete hydatiform mole (late first trimester or early second trimester) will be found (Figure 9.5) (8).

Partial hydatiform mole implies the presence of a gestational sac with fetus and a placenta that suffers localized molar degeneration (5). Typically, this placenta presents on ultrasound examination as an enlarged placenta containing an area of multicystic avascular sonolucent spaces (the "Swiss cheese" appearance), part of the placenta may appear as normal (Figure 9.6). The fetus is visible and is alive most of the time. Partial hydatiform mole may be suspected in early pregnancy, although caution is advised because benign hydropic villous degeneration may also occur, and it is very difficult to discriminate between these two entities in early pregnancy. Another typical finding in hydatiform mole is the presence of theca-lutein cysts in the ovaries (Figure 9.7). These cysts are secondary to high levels of hCG.

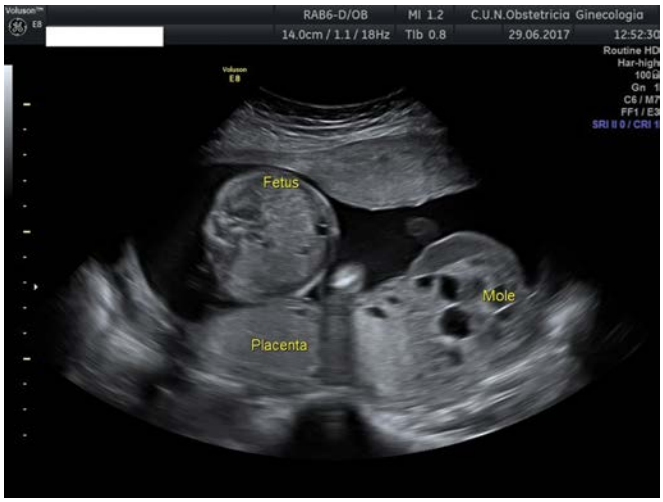

FIGURE 9.6 Transabdominal ultrasound in a case of partial mole. We can observe the fetus and the placenta, part of it with large cystic areas.

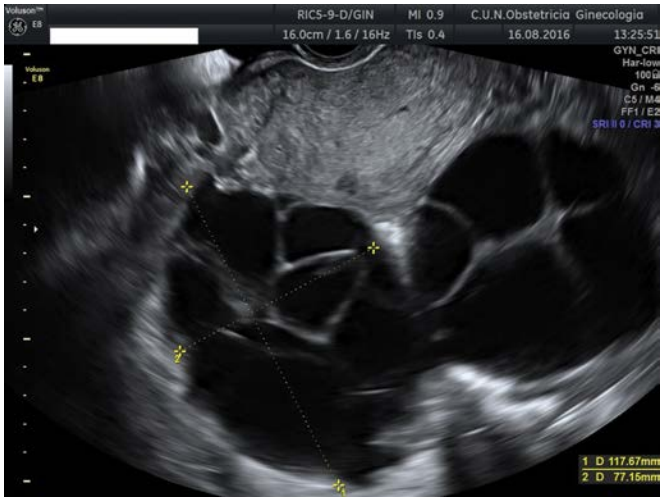

FIGURE 9.7 Transvaginal ultrasound showing theca-lutein cysts in a case of complete hydatiform mole.

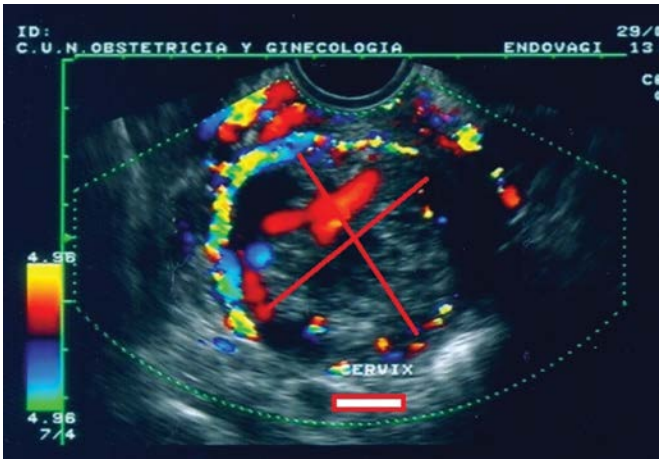

FIGURE 9.8 Transvaginal ultrasound showing a large cervical lesion in a 38-year-old woman. This woman had a miscarriage 2 months before this sonogram was performed. Beta-hCG level was 8700 IU/mL. An invasive mole was suspected and hysterectomy recommended. Histology confirmed this lesion as a choriocarcinoma.

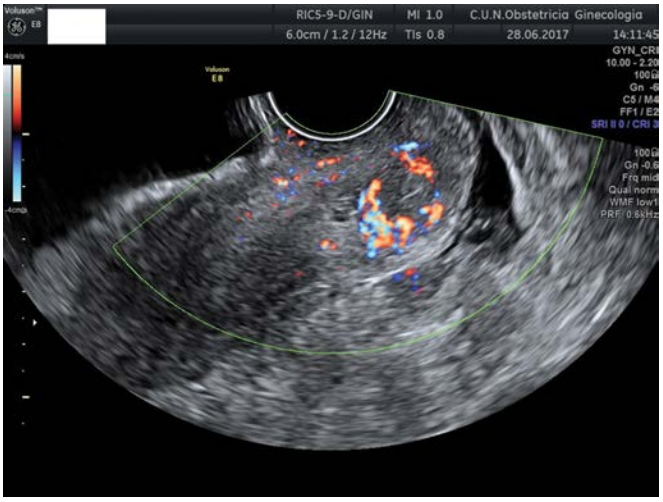

FIGURE 9.9 Transvaginal ultrasound showing a highly vascularized lesion in the cervix. This woman had a past history of complete hydatiform mole 3 years before. Beta-hCG monitoring was normal until this scan was performed. However, at this time ß-hCG was 204 IU/mL. The patient underwent hysterectomy, and permanent frozen section demonstrated a choriocarcinoma.

Gestational Trophoblastic Neoplasia

Invasive mole, PSTT, ETT, and choriocarcinoma are observed on grayscale ultrasound as nonspecific myometrial focal masses (4). All of them are indistinguishable from one another by ultrasound examination. The mass appears more frequently as a heterogeneous or hyperechogenic mass (Figures 9.8 and 9.9), with cystic areas (Figure 9.10). Color Doppler mapping is very rich, and pulsed Doppler reflects high-velocity and low-resistance flow (Figure 9.11).

Potential sources of confusion may be adenomyomas or fibroids (Figure 9.12). However, correlation with clinical history, hCG levels, and pulsed Doppler findings may aid in their differentiation (4).

Another potential cause for confusion is an arteriovenous malformation (AVM). AVMs may appear in the myometrium after a molar pregnancy or after normal delivery or miscarriage (9). Typically, they are seen as large vascular spaces with very high velocity and low-resistance flow (Figure 9.13). These findings may raise the suspicion of persistent GTN. However, AVM does not show a distinct mass within the myometrium. A negative hCG level in serum should provide the diagnosis of AVM. Classically, angiography has been considered as the technique of choice for diagnosing AVM (10). However, many authors consider that ultrasound should be the first-line technique for diagnosing AVM (11).

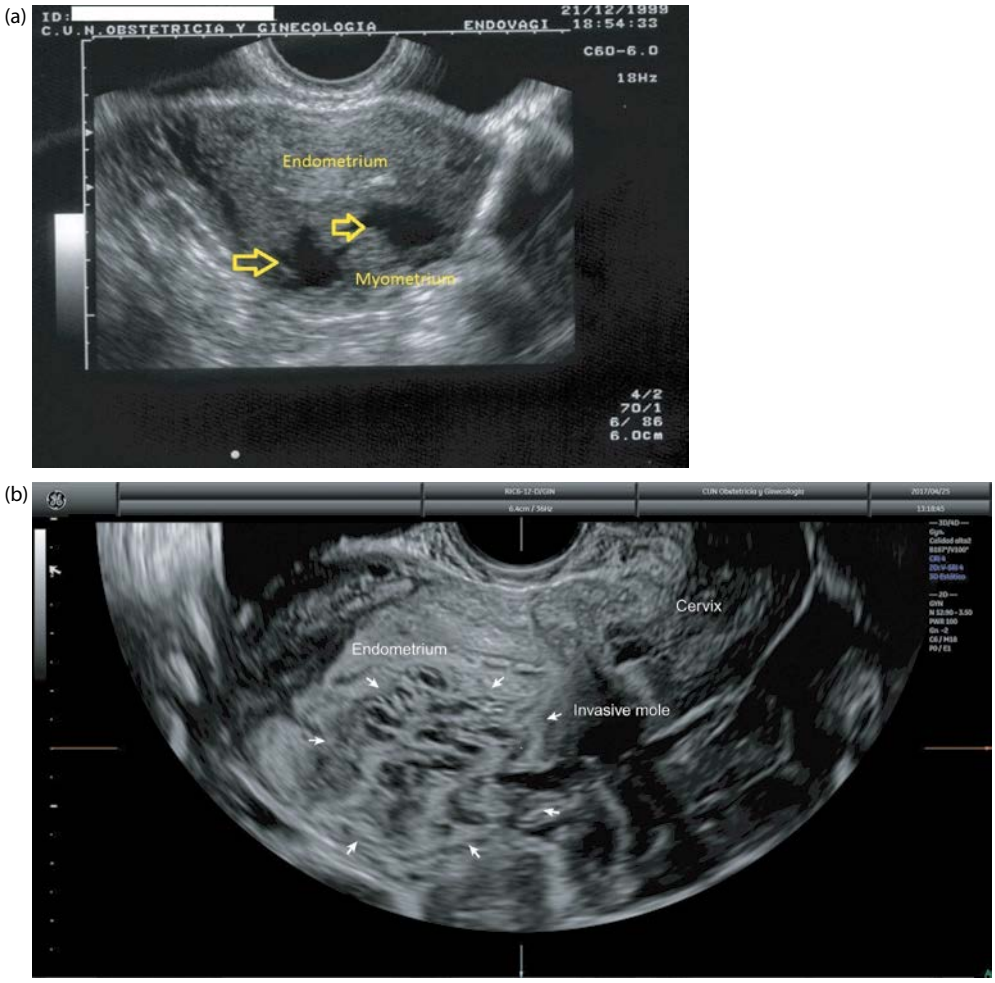

FIGURE 9.10 Transvaginal ultrasound showing two cases of invasive mole (a and b). An irregular mass with irregular cystic areas (arrows) is observed within the posterior myometrial wall.

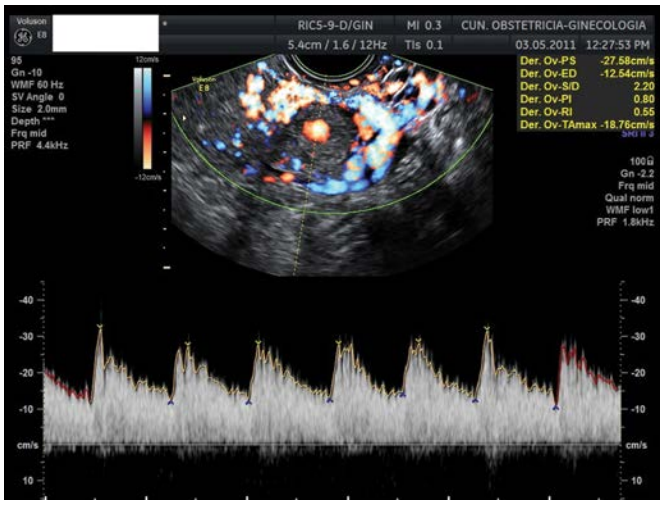

FIGURE 9.11 Transvaginal color ultrasound showing the characteristic blood flow (high velocity/low resistance) in gestational trophoblastic disease.

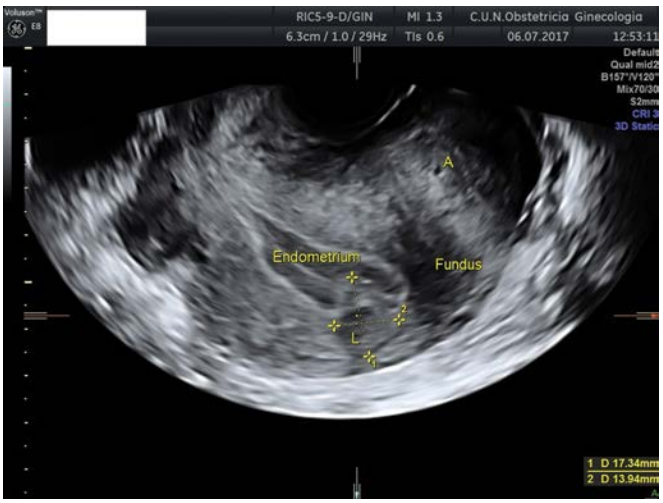

FIGURE 9.12 Transvaginal ultrasound from a 43-year-old woman with a past history of complete mole. We can observe an irregular heterogeneous lesion partially protruding into the endometrium. Beta-hCG was negative. A second nodule can be seen in the posterior myometrial wall (A). Differential diagnosis between gestational trophoblastic disease and adenomyosis was considered. Hysterectomy was advised. Pathologic analysis confirmed the presence of adenomyosis.

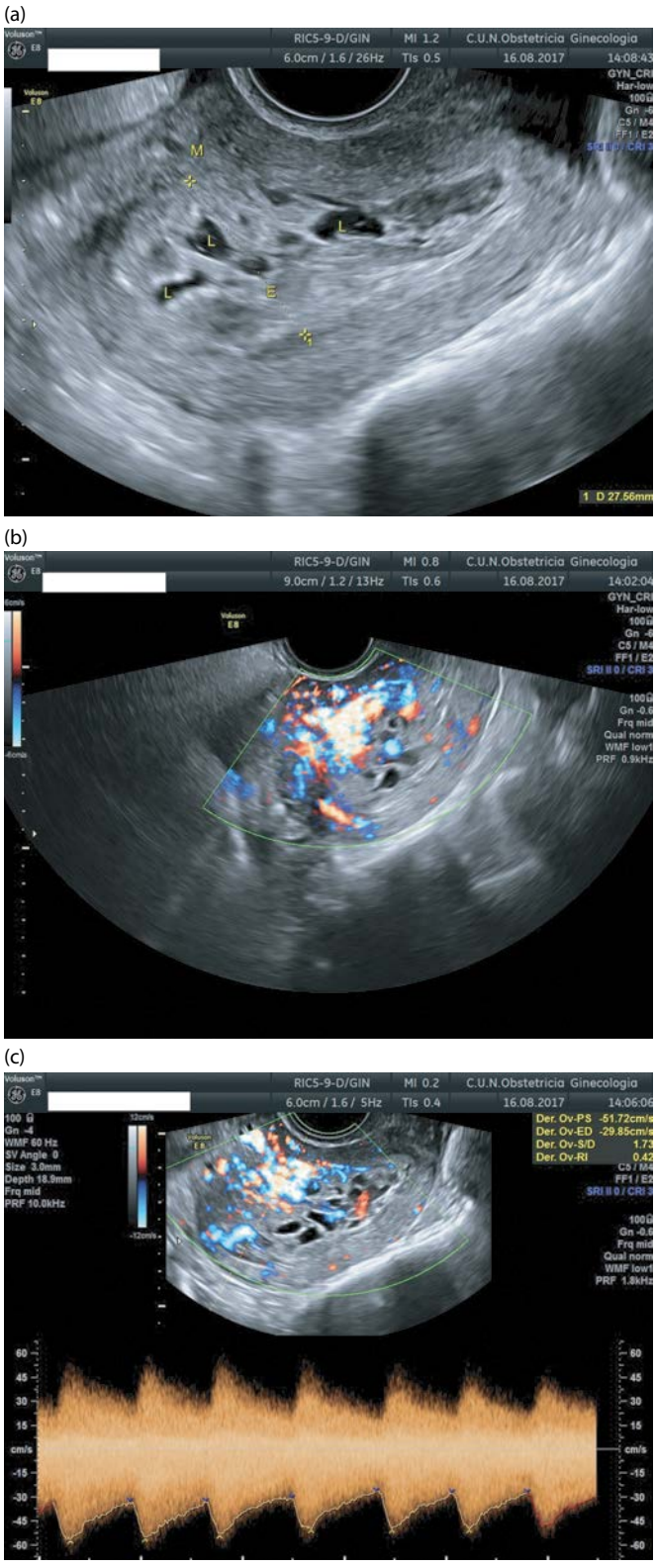

FIGURE 9.13 Transvaginal ultrasound showing a case of arteriovenous malformation after spontaneous first-trimester miscarriage. Large cystic areas (L) can be observed (a). With color Doppler, we can observe how most of these cystic areas are actually blood vessels (b) that exhibit high-velocity and low-resistance blood flow (c).

The Role of Doppler Ultrasound in GTD

A recent systematic review evaluated the role of Doppler ultrasound (pulsed and color Doppler) in the assessment of GTD (12). This systematic review found that Doppler does not help to discriminate between complete and partial moles.

Additionally, the use of Doppler to predict GTN after a molar pregnancy is controversial. Doppler may be used for assessing the response to chemotherapy in GTN (4,12). However, it cannot replace assessment of hCG levels.

Role of Other Imaging Techniques for Assessing GTD

Computed tomography (CT) has a main role for detecting metastatic disease, and it is not considered as a first-line imaging technique for diagnosis (4,13).

Thoracic CT scan should be performed to detect or rule out lung metastasis, the most common place for metastasis in GTN, and should be part of the metastatic workup. In women with lung metastasis, brain CT should also be performed to exclude brain metastasis.

Magnetic resonance imaging (MRI) does not have a role in routine assessment of GTN but may be a problem-solving tool in some cases of myometrial masses (4,13). It should be noted that MRI findings could be relatively nonspecific.

There are very limited data about the use of positron emission tomography–computed tomography (PET-CT) scan to draw meaningful conclusions regarding the role of this imaging technique in the assessment of GTN (4).

REFERENCES

1. Shanbhogue AK, Lalwani N, Menias CO. Gestational trophoblastic disease. *Radiol Clin North Am*. 2013;51:1023–1034.
2. Steigrad SJ. Epidemiology of gestational trophoblastic diseases. *Best Pract Res Clin Obstet Gynaecol*. 2003;17: 837–847.
3. Mangili G, Lorusso D, Brown J et al. Trophoblastic disease review for diagnosis and management: A joint report from the International Society for the Study of Trophoblastic Disease, European Organisation for the Treatment of Trophoblastic Disease, and the Gynecologic Cancer InterGroup. *Int J Gynecol Cancer*. 2014;24(9 Suppl 3):S109–S116.
4. Allen SD, Lim AK, Seckl MJ, Blunt DM, Mitchell AW. Radiology of gestational trophoblastic neoplasia. *Clin Radiol*. 2006;61:301–313.
5. Jauniaux E. Ultrasound diagnosis and follow-up of gestational trophoblastic disease. *Ultrasound Obstet Gynecol*. 1998;11:367–377.
6. Betel C, Atri M, Arenson AM, Khalifa M, Osborne R, Tomlinson G. Sonographic diagnosis of gestational trophoblastic disease and comparison with retained products of conception. *J Ultrasound Med*. 2006;25:985–993.

7. Steller MA, Genest DR, Bernstein MR, Lage JM, Goldstein DP, Berkowitz RS. Clinical features of multiple conception with partial or complete molar pregnancy and coexisting fetuses. *J Reprod Med*. 1994;39:147–154.
8. Wee L, Jauniaux E. Prenatal diagnosis and management of twin pregnancies complicated by a co-existing molar pregnancy. *Prenat Diagn*. 2005;25:772–776.
9. Touhami O, Gregoire J, Noel P, Trinh XB, Plante M. Uterine arteriovenous malformations following gestational trophoblastic neoplasia: A systematic review. *Eur J Obstet Gynecol Reprod Biol*. 2014;181:54–59.
10. Cura M, Martinez N, Cura A, Dalsaso TJ, Elmerhi F. Arteriovenous malformations of the uterus. *Acta Radiol*. 2009;50:823–829.
11. Timor-Tritsch IE, Haynes MC, Monteagudo A, Khatib N, Kovács S. Ultrasound diagnosis and management of acquired uterine enhanced myometrial vascularity/arteriovenous malformations. *Am J Obstet Gynecol*. 2016;214:731.e1-731.e10.
12. Lin LH, Bernardes LS, Hase EA, Fushida K, Francisco RP. Is Doppler ultrasound useful for evaluating gestational trophoblastic disease? *Clinics (Sao Paulo)* 2015;70:810–815.
13. Dhanda S, Ramani S, Thakur M. Gestational trophoblastic disease: A multimodality imaging approach with impact on diagnosis and management. *Radiol Res Pract*. 2014;2014:842751.

10

Ultrasound-Guided Procedures in Gynecologic Oncology

Introduction

Ultrasound-guided procedures in gynecologic oncology are a common practice. These procedures include Tru-Cut biopsy or fine needle aspiration biopsy for diagnosing primary carcinomas or pelvic recurrences, aspiration and drainage for pelvic or abdominal fluid collections, catheter placement for treatment, and intraoperative guidance for surgical or radiotherapy procedures.

This chapter reviews most of these procedures.

Tru-Cut Biopsy

The aim of Tru-Cut biopsy is to obtain a representative tissue sample that will allow for a valid histological diagnosis. Main indications for Tru-Cut biopsy are histological diagnosis of primary cancer or cancer recurrence in the pelvis or abdomen. Therefore, it may be indicated in any gynecological cancer.

An automatic bioptic gun should be used. There are different sizes and calibers. We usually use a disposable 14–16-gauge 150–250 mm long Tru-Cut needle (Figure 10.1).

The procedure can be performed using transabdominal (1), transvaginal (2–4), transrectal (5,6), or even transperineal (7) routes, depending on the location of the lesion. The placement of the needle and shot should be done under direct vision by ultrasound guidance, avoiding vessels, bowel, and bladder (Figure 10.2).

For transabdominal procedures, local anesthesia should be used and antibiotic prophylaxis may be advisable. Transvaginal and transperineal procedures should be performed with the patient in lithotomy position. The vagina and perineum should be cleaned with iodine povidone.

For transperineal procedures, local anesthesia should be used. However, for a transvaginal approach, local anesthesia is not usually needed. For a transperineal approach, either transvaginal or transabdominal probes may be used, depending on the depth of the lesion to be biopsied.

In any case, an adequate needle guide attached to the ultrasound probe is needed when using the transvaginal probe. A free-hand approach may be safely used when using the transabdominal probe. One to three tissue core samplings should be obtained (Figure 10.3).

Ultrasound is a good method for diagnosing pelvic recurrence of gynecological cancers (8,9). Tru-Cut biopsy may be indicated for definitive diagnosis of a primary cancer or a pelvic or abdominal relapse. The main indication for primary cancers is usually the presence of an abdominal mass, or carcinomatosis for diagnosing primary ovarian cancer of metastatic masses from nonovarian origin. It may be used in women with a history of cancer (e.g., from colon, rectum, stomach, breast) and in cases of a likely ovarian cancer in women who are predicted to have poor performance in undergoing surgery. The diagnosis of a pelvic or abdominal relapse of any type of gynecological cancer is another indication for ultrasound-guided Tru-Cut biopsy.

The sample was adequate for diagnosis in 83%–100% of the cases (1–5). The accuracy of Tru-Cut biopsy has been reported as high as 93%–100% (1–5). Complications may occur, such as hemorrhage, infection, or pain. However, the complication rate reported is low (1%) (1–5).

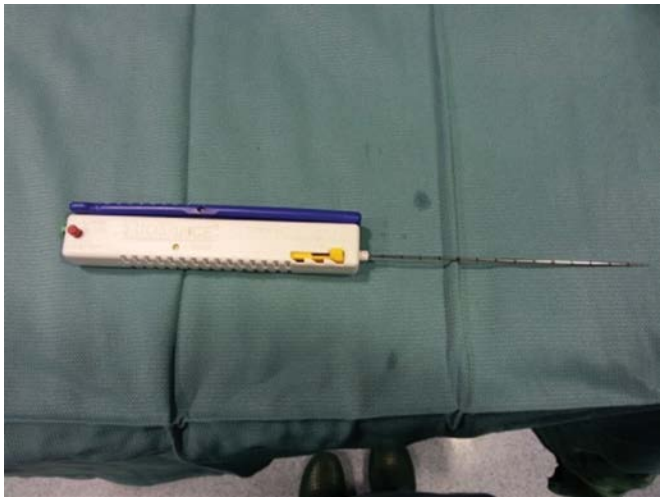

FIGURE 10.1 Tru-Cut biopsy device.

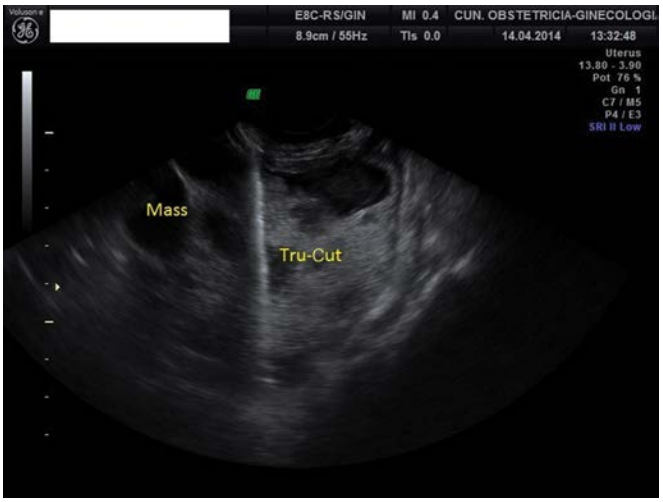

FIGURE 10.2 Transvaginal ultrasound showing the Tru-Cut needle passing through a cystic-solid lesion suspected as a pelvic recurrence from ovarian cancer.

FIGURE 10.3 Two tissue cylinders obtained after Tru-Cut biopsy.

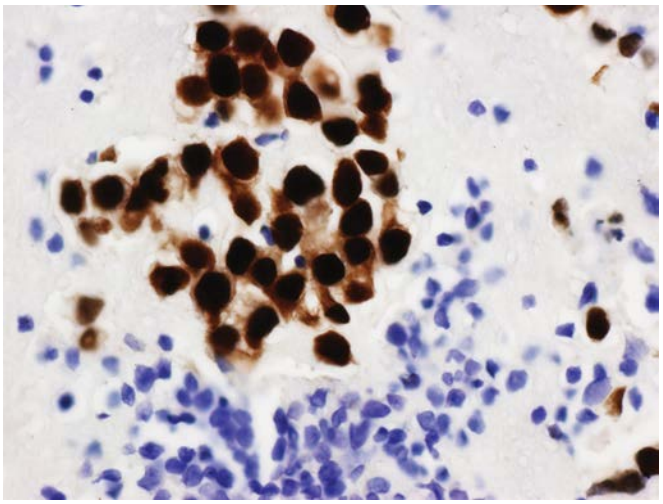

FIGURE 10.5 Cytologic smear obtained after FNA from a malignant lesion.

Fine Needle Aspiration (FNA) Biopsy

Fine needle aspiration biopsy is another approach for tissue sampling. In this case, a fine 15–25 mm long needle (20–25 gauge) is used. The procedure and technique are similar to Tru-Cut biopsy (Figure 10.4). However, the sample obtained allows cytopathologic and not histopathologic diagnosis (Figure 10.5). The main indications for FNA are the diagnosis of gynecologic cancers, pelvic relapses, or assessment of lymph node status (10,11).

Like Tru-Cut biopsy, FNA can be performed using transabdominal or transvaginal routes (Figures 10.4 and 10.6).

The sensitivity and specificity reported for FNA are 76% and 100%, respectively (10), for diagnosing pelvic relapse.

For assessing lymph node status, the figures reported are 61% sensitivity and 89% specificity for pelvic lymph nodes, and 75%

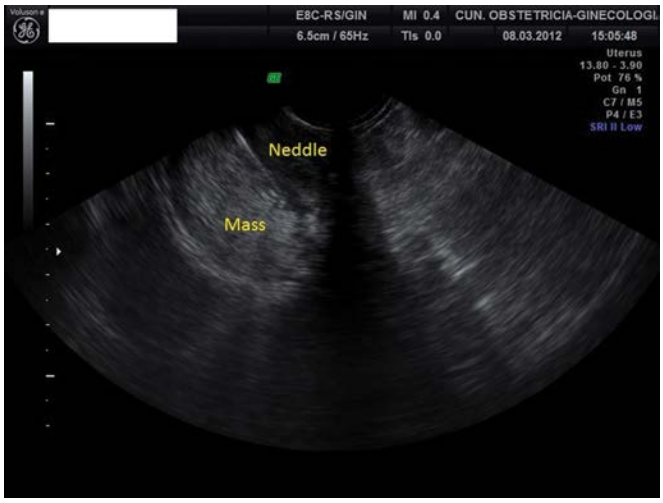

FIGURE 10.4 Fine needle aspiration from a lesion suspected as being a pelvic recurrence of a cervical carcinoma. The needle is observed passing through the mass. The transvaginal route is used.

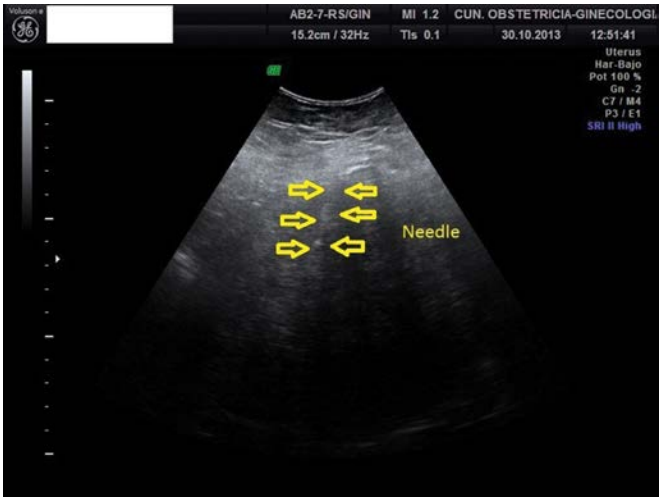

FIGURE 10.6 Transabdominal fine needle aspiration from a large abdominal mass suspected as being a recurrence of uterine leiomyosarcoma. The needle is seen in between the arrows.

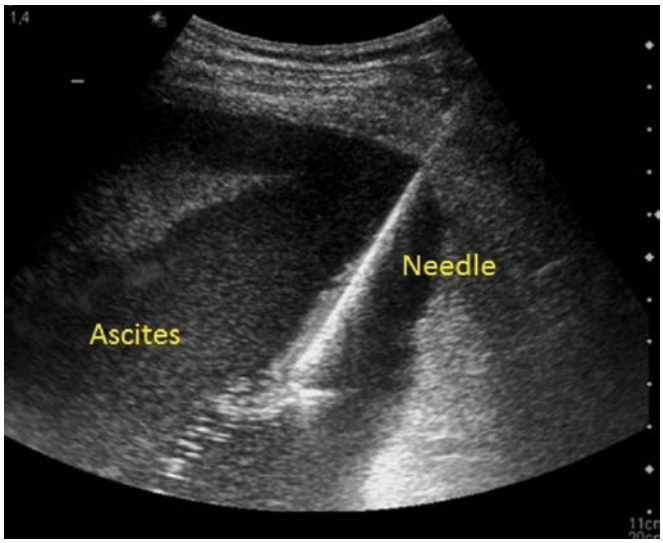

FIGURE 10.7 Transabdominal ultrasound-guided paracentesis for ascites drainage in a woman with advanced-stage ovarian cancer.

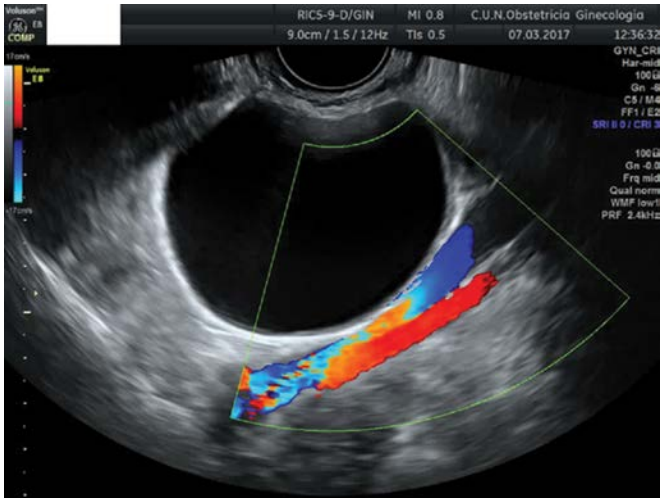

FIGURE 10.8 Transvaginal ultrasound showing the typical appearance of a pelvic lymphocele in a woman with a past history of radical hysterectomy plus pelvic lymphadenectomy for a cervical cancer.

sensitivity and 100% specificity for para-aortic lymph nodes (11). This procedure is safe with a very low complication rate (10,11).

Drainage

Ultrasound can also be used for drainage. The main indications in gynecologic oncology are ascites drainage and lymphocele drainage.

Ascites drainage (paracentesis) can be performed for patient symptom relief or for cytological diagnosis (Figure 10.7).

Lymphoceles are a complication occurring after lymphadenectomy (12). The incidence of postoperative lymphocele reported is wide, ranging from 1% to 58% (12). The diagnosis is relatively

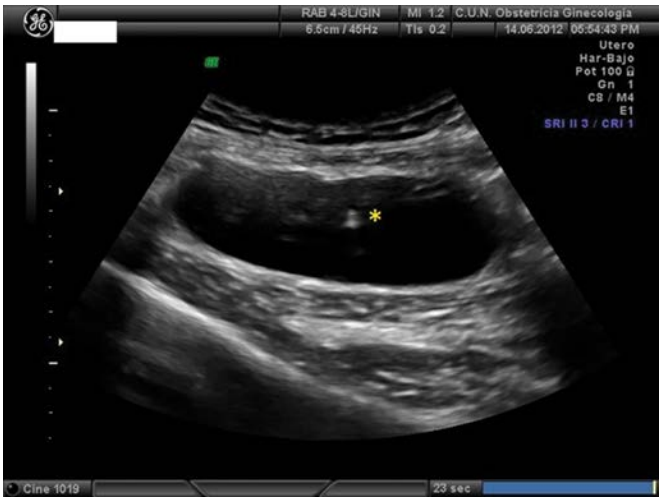

FIGURE 10.9 Transabdominal ultrasound depicting ultrasound-guided drainage of an inguinal lymphocele. The tip of the needle can be observed (*).

easy by ultrasound. A lymphocele is usually seen as a round or oval simple cyst running alongside pelvic iliac vessels or the aorta (Figure 10.8).

Most lymphoceles are asymptomatic, but sometimes the patient may complain of pain or pressure symptoms. Rarely, the lymphocele may become infected (12,13).

When symptoms appear, lymphocele drainage is indicated. Ultrasound guidance is the method of choice (13). Usually, a 15 cm long 18-gauge needle is used. Local anesthesia is advisable, and the complication rate is low (Figure 10.9).

Simple aspiration and drainage has a high recurrence rate (80%–90%) (12). For this reason, sclerotherapy with ethanol or iodide povidone is preferable (14). The success rate for the latter technique ranges between 88% and 97% with a recurrence rate of 3%–7% (12).

Surgery either via laparoscopy or via laparotomy remains an option in recurring, poorly accessible, or inflammatory lymphoceles (12).

Other Ultrasound-Guided Procedures

Ultrasound has also been used for guiding other procedures.

Benedetti-Panici reported that intraperitoneal chemotherapy delivered through an intraperitoneal catheter placed under transabdominal ultrasound guidance is feasible (15). Local anesthesia should be used. The success rate was 97%. No severe complications occurred, and mild complications (vagal reaction) were observed in 2.5% of the patients.

Ultrasound is also considered as a good technique for placing intravaginal tandem for delivering interstitial brachytherapy for either primary or recurrent cervical, endometrial, or vaginal cancer (16–18). Ultrasound guidance can be performed through transvaginal, transabdominal, or transrectal routes. The main advantage for using ultrasound guidance is more accurate, correct placement of brachytherapy tandem or needles and decreasing morbidity, such as uterine or vaginal perforation or bladder and rectal overdose.

Torné et al. also reported the use of transvaginal ultrasound guidance for myometrial injection of radiotracer for sentinel lymph node detection in endometrial cancer (19). They reported a success rate of 90.5%. No complications were reported, and patient tolerance was good in most cases.

REFERENCES

1. Zikan M, Fischerova D, Pinkavova I, Dundr P, Cibula D. Ultrasound-guided Tru-Cut biopsy of abdominal and pelvic tumors in gynecology. *Ultrasound Obstet Gynecol*. 2010;36:767–772.
2. Volpi E, Zola P, De Grandis T, Rumore A, Volpe T, Sismondi P. Transvaginal sonography in the diagnosis of pelvic malignant recurrence: Integration of sonography and needle-guided biopsy. *Ultrasound Obstet Gynecol*. 1994;4:135–138.
3. Dadayal G, Weston M, Young A et al. Transvaginal ultrasound (TVUS)-guided biopsy is safe and effective in diagnosing peritoneal carcinomatosis and recurrent pelvic malignancy. *Clin Radiol*. 2016;71:1184–1192.
4. Park JJ, Kim CK, Park BK. Ultrasound-guided transvaginal core biopsy of pelvic masses: Feasibility, safety, and short-term follow-up. *AJR Am J Roentgenol*. 2016;206:877–878.
5. Giede C, Toi A, Chapman W, Rosen B. The use of transrectal ultrasound to biopsy pelvic masses in women. *Gynecol Oncol*. 2004 Dec;95(3):552–556.
6. Roy D, Kulkarni A, Kulkarni S, Thakur MH, Maheshwari A, Tongaonkar HB. Transrectal ultrasound-guided biopsy of recurrent cervical carcinoma. *Br J Radiol*. 2008;81: 902–906.
7. Fleischer AC, Burnett LS, Jones HW 3rd, Cullinan JA. Transrectal and transperineal sonography during guided intrauterine procedures. *J Ultrasound Med*. 1995;14: 135–138.
8. Testa AC, Ciampelli M, Mastromarino C et al. Detection of central pelvic recurrent disease with transvaginal color Doppler ultrasound in women treated for gynecological malignancy. *Ultrasound Obstet Gynecol*. 2002;19:490–495.
9. Savelli L, Testa AC, Ferrandina G et al. Pelvic relapses of uterine neoplasms: Transvaginal sonographic and Doppler features. *Gynecol Oncol*. 2004;93:441–445.
10. Nagano T, Nakai Y, Taniguchi F et al. Diagnosis of paraaortic and pelvic lymph node metastasis of gynecologic malignant tumors by ultrasound-guided percutaneous fine-needle aspiration biopsy. *Cancer.* 1991; 68:2571–2574.
11. Zanetta G, Brenna A, Pittelli M, Lissoni A, Trio D, Riotta S. Transvaginal ultrasound-guided fine needle sampling of deep cancer recurrences in the pelvis: Usefulness and limitations. *Gynecol Oncol*. 1994;54:59–63.
12. Weinberger V, Cibula D, Zikan M. Lymphocele: Prevalence and management in gynecological malignancies. *Expert Rev Anticancer Ther.* 2014;14:307–317.
13. Zikan M, Fischerova D, Pinkavova I et al. A prospective study examining the incidence of asymptomatic and symptomatic lymphoceles following lymphadenectomy in patients with gynecological cancer. *Gynecol Oncol*. 2015;137:291–298.
14. Liu FS, Hung MJ, Hwang SF, Lu CH, Ke YM, Ho ES. Management of pelvic lymphocysts by ultrasound-guided aspiration and minocycline sclerotherapy. *Gynecol Obstet Invest*. 2005;59:130–133.
15. Benedetti-Panici P, Perniola G, Marchetti C et al. Intraperitoneal chemotherapy by ultrasound-guided direct puncture in recurrent ovarian cancer: Feasibility, compliance, and complications. *Int J Gynecol Cancer.* 2012;22:1069–1074.
16. Sahinler I, Cepni I, Oksuz DC et al. Tandem application with transvaginal ultrasound guidance. *Int J Radiat Oncol Biol Phys*. 2004;59:190–196.
17. Tharavichitkul E, Tippanya D, Jayavasti R et al. Two-year results of transabdominal ultrasound-guided brachytherapy for cervical cancer. *Brachytherapy.* 2015;14:238–244.
18. Sharma DN, Rath GK, Thulkar S, Kumar S, Subramani V, Julka PK. Use of transrectal ultrasound for high dose rate interstitial brachytherapy for patients of carcinoma of uterine cervix. *J Gynecol Oncol*. 2010;21:12–17.
19. Torné A, Pahisa J, Vidal-Sicart S et al. Transvaginal ultrasound-guided myometrial injection of radiotracer (TUMIR): A new method for sentinel lymph node detection in endometrial cancer. *Gynecol Oncol*. 2013;128:88–94.

11

Ultrasound in Vulvar and Vaginal Cancer

Introduction

Vulvar cancer is rare, accounting for 5% of all gynecologic malignancies (1). This cancer typically occurs in postmenopausal women, and it is diagnosed clinically by visual inspection, vulvoscopy, and directed biopsy (1). Approximately, 95% of cases are squamous cell carcinoma (1). Current International Federation of Gynecology and Obstetrics (FIGO) staging is based on surgical findings related to size and invasion as well as the type and number of lymph nodal involvement (2) (Table 11.1). Sentinel node assessment plays an important role in current management of vulvar cancer (3).

Cancer of the vagina is also rare, accounting for 2%–3% of all of gynecologic malignancies (4). Approximately 90% of vaginal cancers are squamous cell carcinomas. Most vaginal cancers occur in postmenopausal women, and diagnosis is mainly based on clinical findings and directed biopsy (4). Current FIGO staging of vaginal cancer is based on clinical findings (5) (Table 11.2).

Role of Ultrasound in Vulvar Cancer

In general, imaging in vulvar cancer has a limited role. It is mainly focused on the assessment of local extension of the tumor and for assisting surgical planning (6,7). The best imaging modality for evaluation of vulvar anatomy is magnetic resonance imaging (MRI) because of excellent soft-tissue contrast. On MRI the tumor shows intermediate signal intensity on T1-weighted MRI and high signal intensity on T2-weighted MRI sequences (6,7). The role for positron emission tomography–computed tomography (PET-CT) scan in vulvar cancer is undefined.

There are no descriptions of vulvar cancer by ultrasound, and currently it is considered that ultrasound has no role in the assessment of vulvar cancer, except for assessing groin lymph node status.

We have used high-frequency convex probes for assessing a small series of five primary or recurrent cases of vulvar cancer.

TABLE 11.2

FIGO Staging: Carcinoma of the Vagina

Stage	Description
Stage I	The carcinoma is limited to the vaginal wall.
Stage II	The carcinoma has involved the subvaginal tissue but has not extended to the pelvic wall.
Stage III	The carcinoma has extended to the pelvic wall.
Stage IV	The carcinoma has extended beyond the true pelvis or has involved the mucosa of bladder or rectum; bullous edema; such does not permit a case to be allotted to stage IV.
IVA	Tumor invades bladder and/or rectal mucosa and/or direct extension beyond the true pelvis.
IVB	Carcinoma has spread to distant organs.

TABLE 11.1

FIGO Staging of Carcinoma of the Vulva

Stage	Description
Stage I	Tumor confined to the vulva
IA	Lesions ≤2 cm in size, confined to the vulva or perineum and with stromal invasion ≤1 mm, no nodal metastasis
IB	Lesions >2 cm in size or with stromal invasion >1 mm, confined to the vulva or perineum, with negative nodes
Stage II	Tumor of any size with extension to adjacent perineal structures (one-third lower urethra, one-third lower vagina, anus) with negative nodes
Stage III	Tumor of any size with or without extension to adjacent perineal structures (one-third lower urethra, one-third lower vagina, anus) with positive inguino-femoral lymph nodes
IIIA (i)	With one lymph node macrometastasis (≥5 mm), or
IIIA (ii)	One to two lymph node micrometastasis or micrometastases (<5 mm)
IIIB (i)	With two or more lymph node macrometastases (≥5 mm) or
IIIB (ii)	Three or more lymph node micrometastases (<5 mm)
IIIC	With positive nodes with extracapsular spread
Stage IV	Tumor invades other regional (two-thirds upper urethra, two-thirds upper vagina) or distant structures
IVA	Tumor invades any of the following:
IVA (i)	Upper urethral and/or vaginal mucosa, bladder mucosa, rectal mucosa, or fixed to pelvic bone, or
IVA (ii)	Fixed or ulcerated inguino-femoral lymph nodes
IVB	Any distant metastasis including pelvic lymph nodes

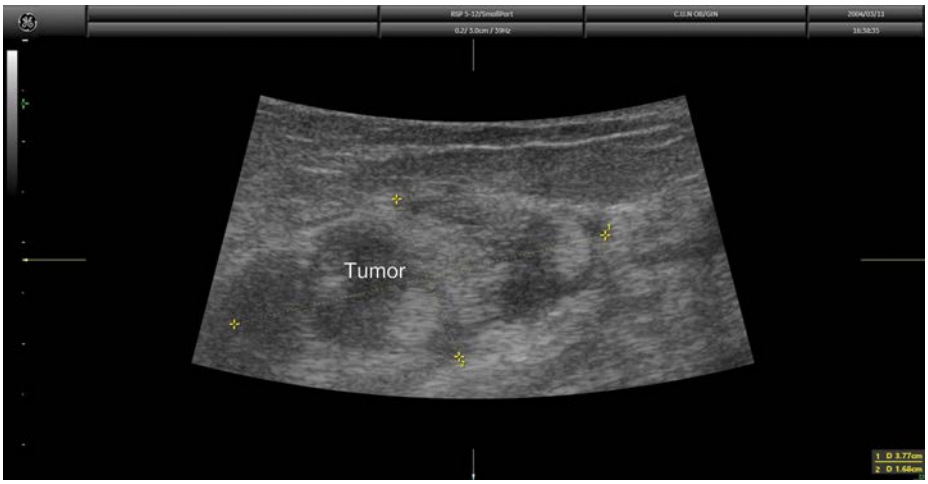

FIGURE 11.1 Ultrasound evaluation of a vulva carcinoma using a high-frequency transducer. The tumor appears as an irregular lesion with heterogeneous echogenicity.

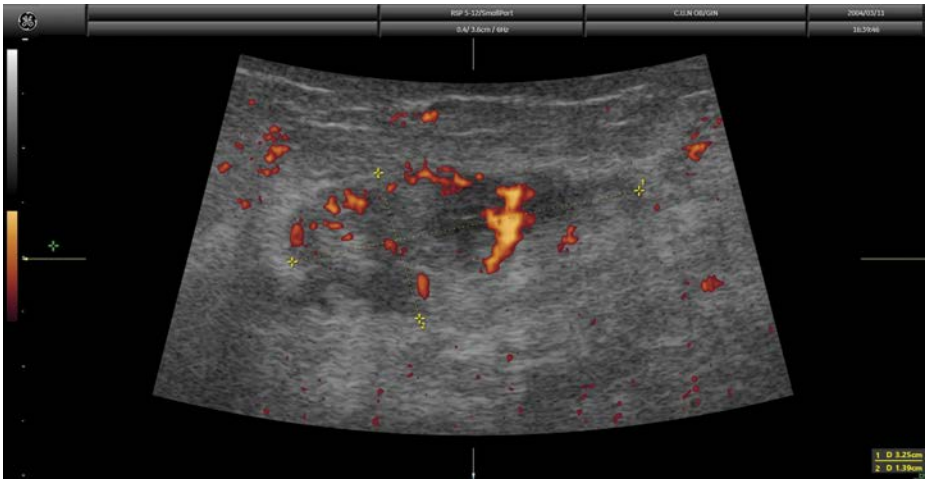

FIGURE 11.2 The same case as in Figure 11.1. Power Doppler allows the assessment of tumor vascularization.

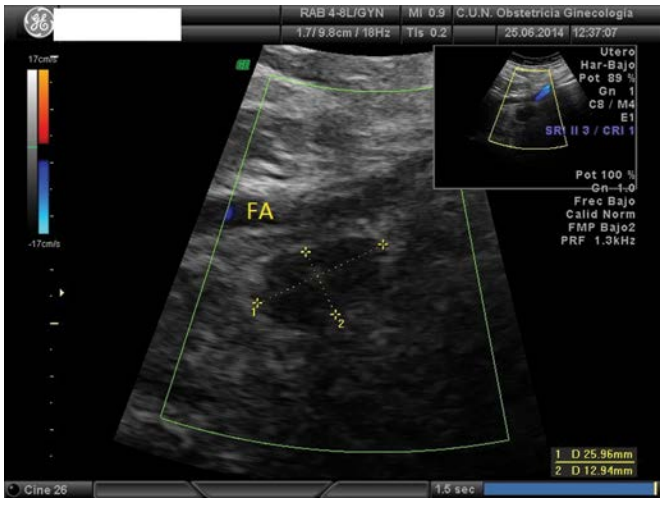

FIGURE 11.3 Inguinal ultrasound in a case of vulvar carcinoma. A suspicious lymph node can be detected behind the femoral artery.

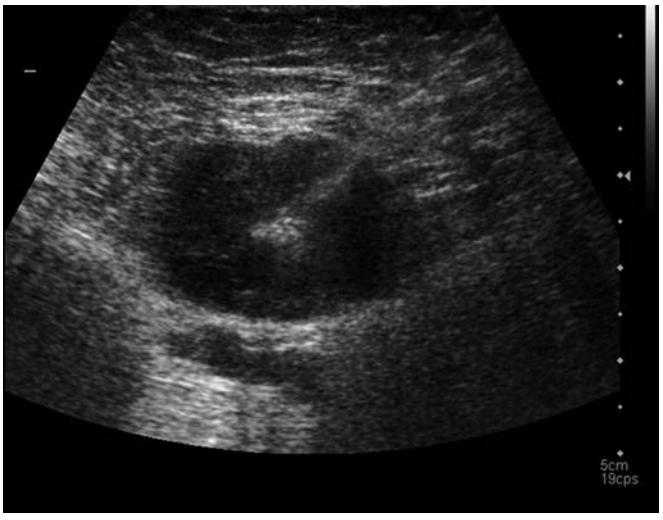

FIGURE 11.4 Ultrasound-guided fine needle aspiration from a lymph node in vulvar cancer.

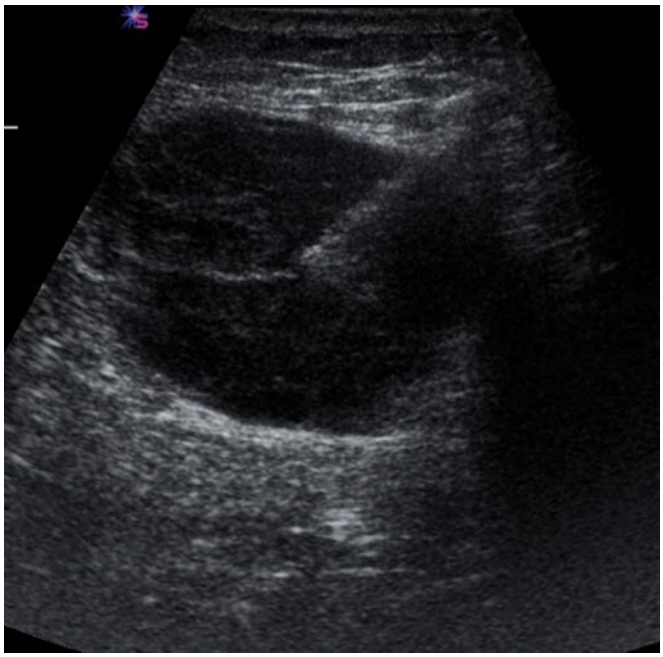

FIGURE 11.5 A similar case as in Figure 11.4.

In our experience, vulvar carcinomas appear as solid, irregular, heterogeneous lesions (Figure 11.1). Most tumors were vascularized (Figure 11.2).

Regarding the assessment of inguinal lymph nodes, the typical ultrasound features of lymph node involvement are increase in size, rounded shape, irregular contour, and loss of the fatty hilum (Figure 11.3) (8,9).

Ultrasound is also useful for guiding fine needle aspiration (FNA) of inguinal lymph nodes to detect metastatic disease (Figures 11.4 and 11.5). This technique is simple, cheap, and easy to perform. There is no need for anesthesia. Ultrasound-guided FNA offers a good sensitivity (72%–93%) with a high specificity (82%–100%) (10–12). However, Selman et al. reported a systematic review analyzing the diagnostic performance of five different techniques for evaluating inguinal lymph node status in vulvar cancer. They showed that ultrasound-guided FNA cannot replace sentinel node dissection (13).

Role of Ultrasound in Vaginal Cancer

In vaginal cancer, imaging techniques such as MRI or CT scan may have a role for local staging and preoperative assessment of the disease. MRI is more useful for assessing local spread, whereas CT scan is preferred for detecting lymph node and metastatic disease (8).

Similar to vulvar cancer, there are no reports about ultrasound in vaginal cancer, and it is considered that this technique has no role in the assessment of vaginal cancer.

In our experience, primary cancer of the vagina can be visualized on transvaginal or transrectal ultrasound as a solid irregular structure arising from the vaginal wall (Figures 11.6 and 11.7). Tumors are well vascularized (Figure 11.8). For lesions located in the lower two-thirds of the vagina, using some amount of gel in the vagina combined with a scan using the transperineal or transintroital route may increase visualization of the lesion (Figure 11.9). Infiltration of adjacent structures, such as the bladder or the paracolpium, can be observed in some cases (Figures 11.10 and 11.11). In some other cases, we have observed that lesions may appear as rounded and well defined with limited vascularization (Figure 11.12).

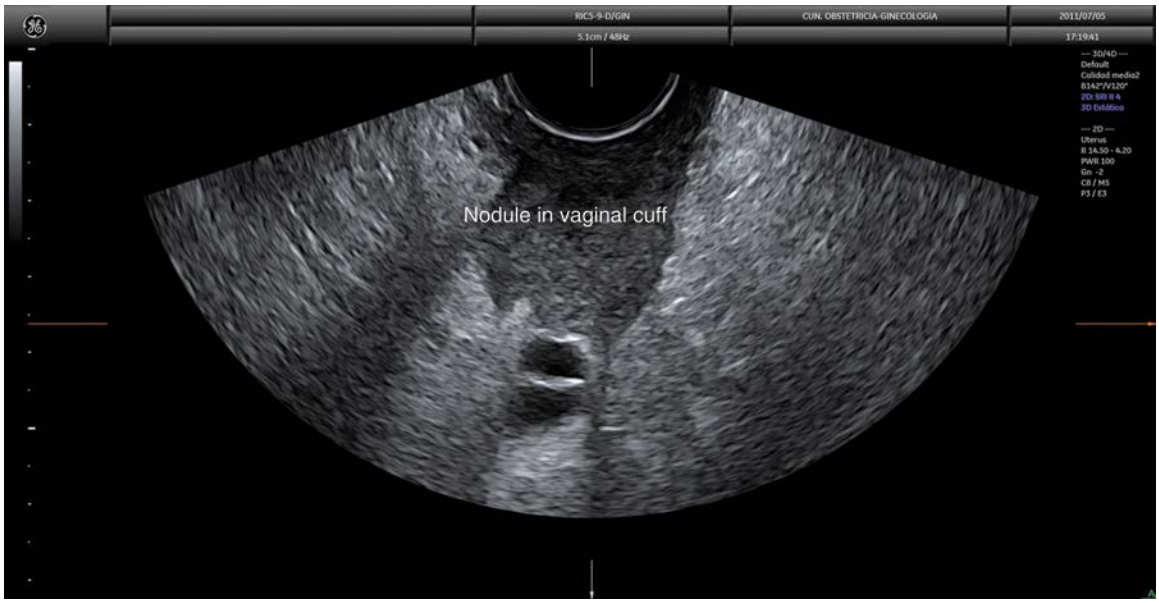

FIGURE 11.6 Transvaginal ultrasound depicting a solid irregular nodule in the vaginal cuff in a 72-year-old woman with a past history of simple hysterectomy for uterine fibroids. Biopsy revealed a squamous cell carcinoma from the vagina.

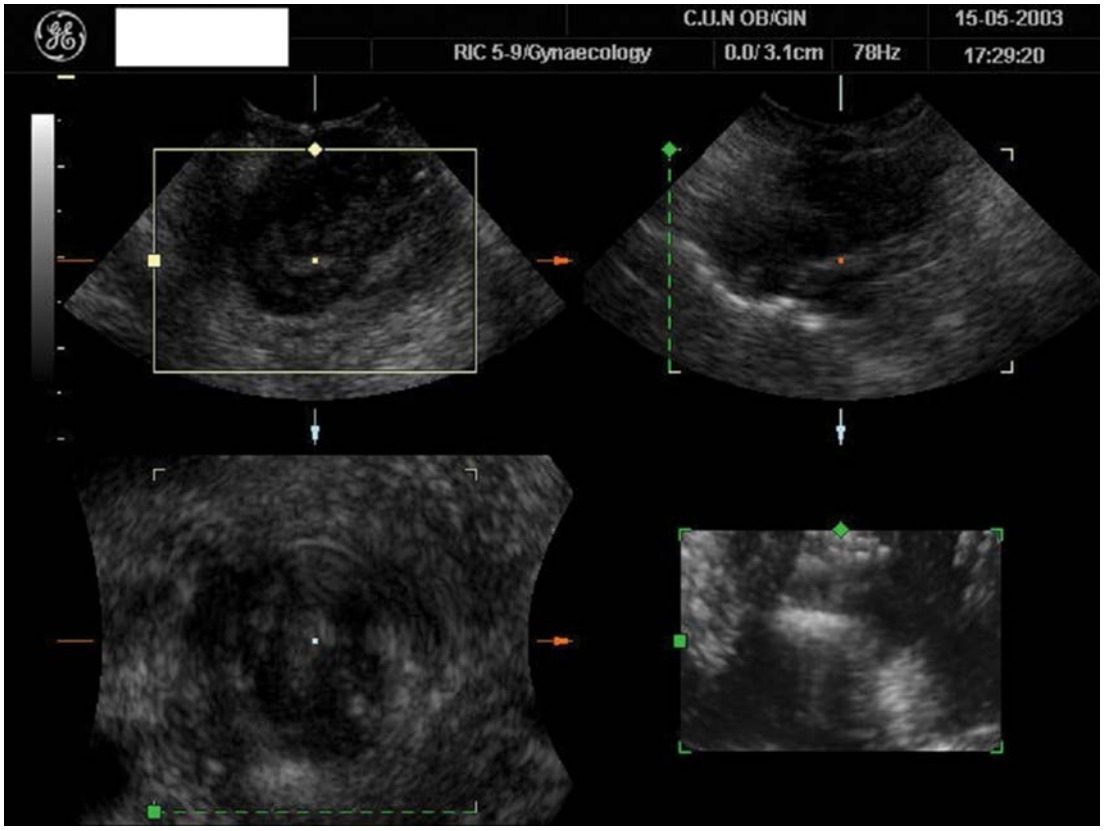

FIGURE 11.7 Three-dimensional ultrasound from a vaginal carcinoma. In this case, the lesion is hypoechoic with irregular contour.

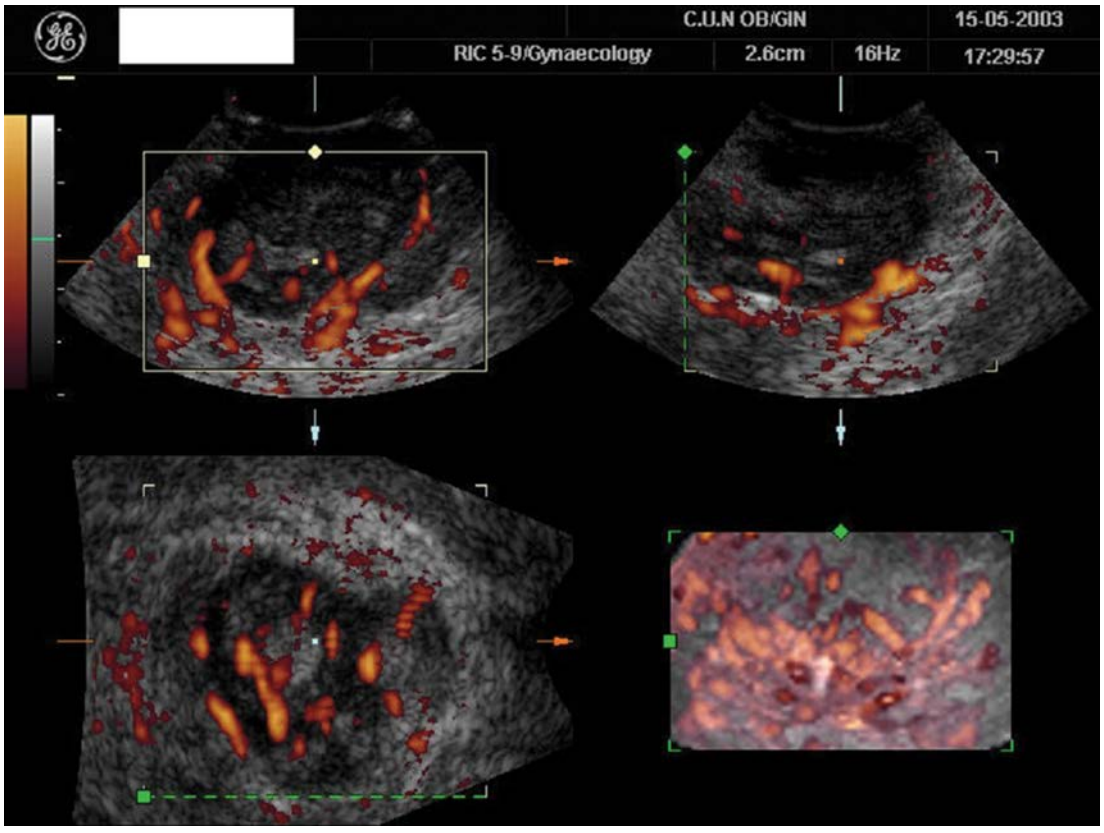

FIGURE 11.8 Same case as in Figure 11.7, and with power Doppler evaluation it can be observed that the lesion is highly vascularized.

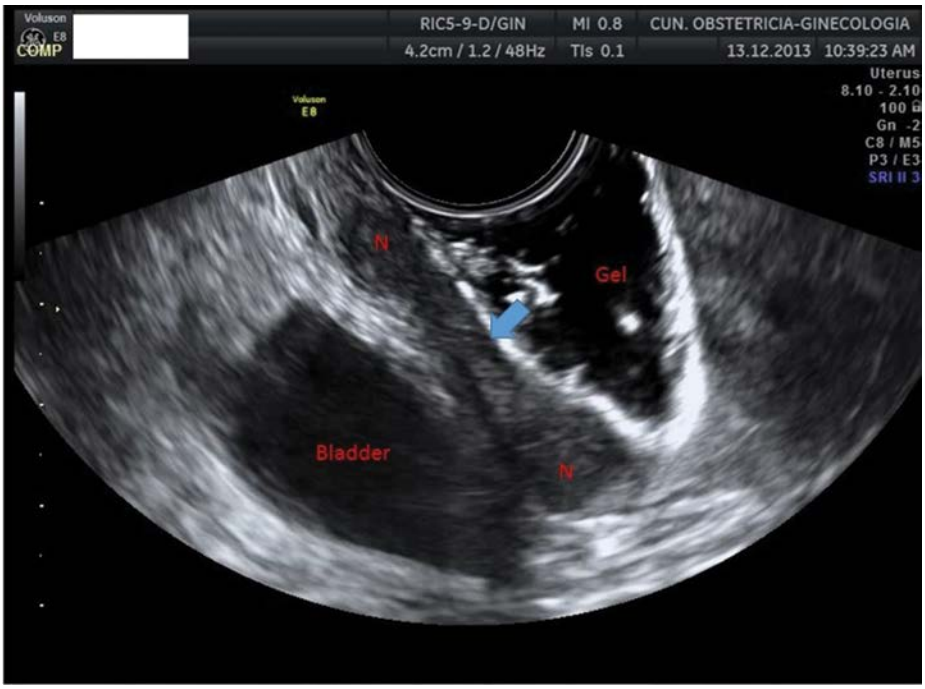

FIGURE 11.9 Transvaginal ultrasound using sonovaginography in a woman with a melanoma from the vagina. We can observe two different nodules (N) in the anterior vaginal wall.

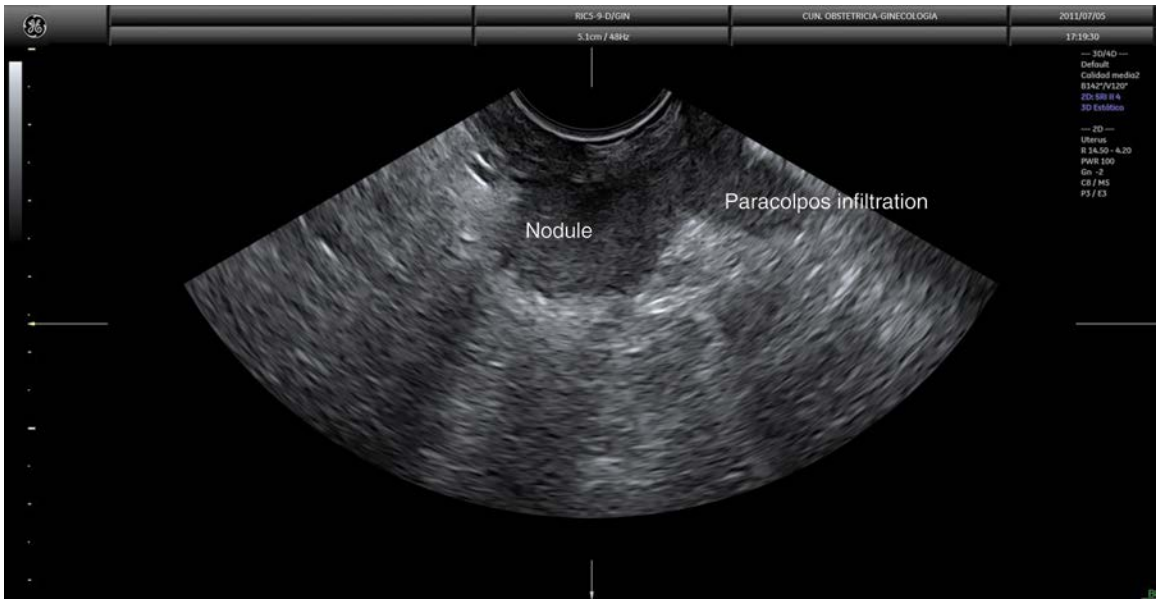

FIGURE 11.10 The same case as in Figure 11.6. In this view, we can observe that the lesion extends to the left paracolpium.

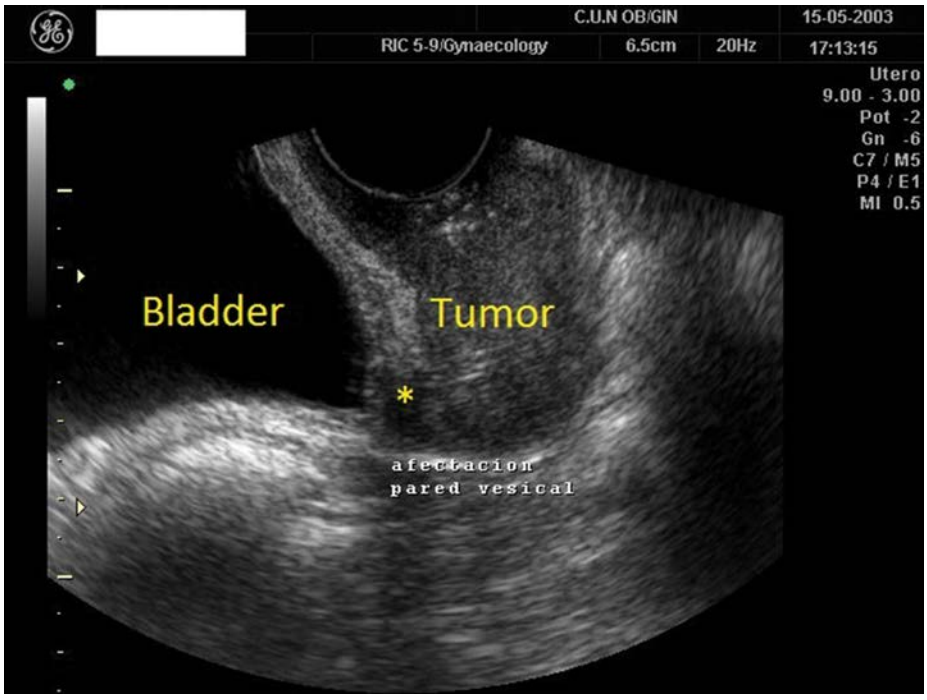

FIGURE 11.11 Transvaginal ultrasound in a case of vaginal carcinoma. Sagittal view. Bladder infiltration is suspected (*).

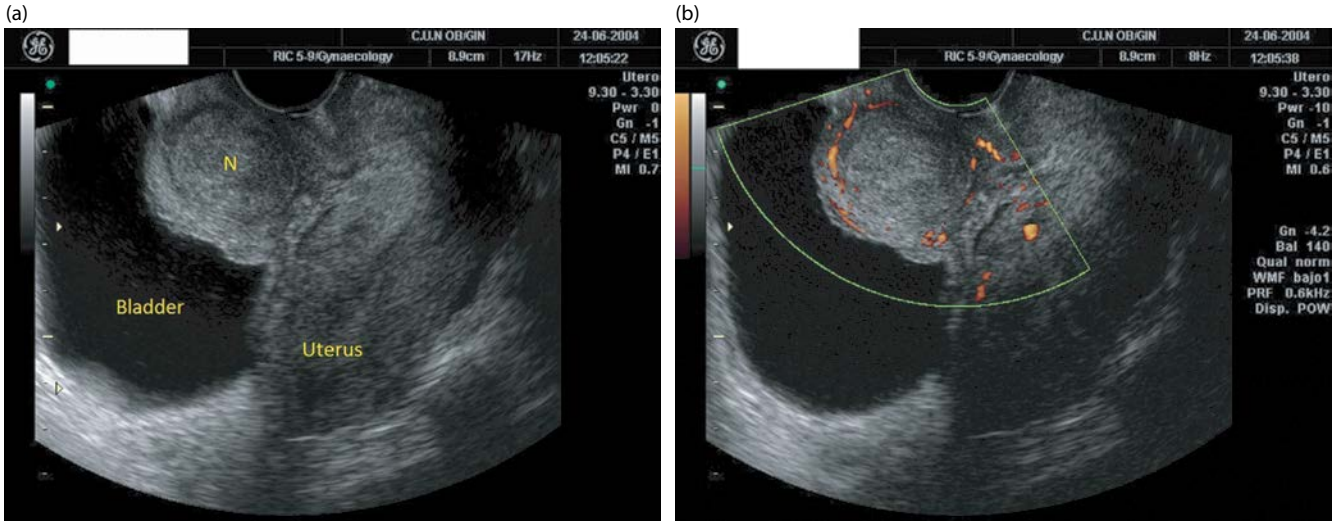

FIGURE 11.12 (a) A well-defined rounded nodule (N) arising from the anterior vaginal wall was detected during transvaginal ultrasound examination. (b) Power Doppler examination showed a circumferential flow around the lesion but no flow within the lesion. A benign lesion was suspected, but histology revealed a vaginal adenocarcinoma.

REFERENCES

1. Alkatout I, Schubert M, Garbrecht N et al. Vulvar cancer: Epidemiology, clinical presentation, and management options. *Int J Womens Health*. 2015;7:305–313.
2. Hacker NF, Barlow EL. Staging for vulvar cancer. *Best Pract Res Clin Obstet Gynaecol*. 2015;29:802–811.
3. Brincat MR, Muscat Baron Y. Sentinel lymph node biopsy in the management of vulvar carcinoma: An evidence-based insight. *Int J Gynecol Cancer*. 2017;27:1769–1773.
4. Siegel RL, Miller KD, Jemal A. Cancer statistics, 2017. *CA Cancer J Clin*. 2017;67:7–30.
5. Rajaram S, Maheshwari A, Srivastava A. Staging for vaginal cancer. *Best Pract Res Clin Obstet Gynaecol*. 2015;29:822–832.
6. Kim KW, Shinagare AB, Krajewski KM et al. Update on imaging of vulvar squamous cell carcinoma. *AJR Am J Roentgenol*. 2013;201:W147–W157.
7. Sohaib SA, Moskovic EC. Imaging in vulval cancer. *Best Pract Res Clin Obstet Gynaecol*. 2003;17:543–556.

8. Miccò M, Sala E, Lakhman Y, Hricak H, Vargas HA. Imaging features of uncommon gynecologic cancers. *AJR Am J Roentgenol*. 2015;205:1346–1359.
9. Abang Mohammed DK, Uberoi R, de B Lopes A, Monaghan JM. Inguinal node status by ultrasound in vulva cancer. *Gynecol Oncol*. 2000;77:93–96.
10. Hall TB, Barton DP, Trott PA et al. The role of ultrasound-guided cytology of groin lymph nodes in the management of squamous cell carcinoma of the vulva: 5-year experience in 44 patients. *Clin Radiol*. 2003;58:367–371.
11. Land R, Herod J, Moskovic E et al. Routine computerized tomography scanning, groin ultrasound with or without fine needle aspiration cytology in the surgical management of primary squamous cell carcinoma of the vulva. *Int J Gynecol Cancer*. 2006;16:312–317.
12. de Gregorio N, Ebner F, Schwentner L et al. The role of preoperative ultrasound evaluation of inguinal lymph nodes in patients with vulvar malignancy. *Gynecol Oncol*. 2013;131:113–117.
13. Selman TJ, Luesley DM, Acheson N, Khan KS, Mann CH. A systematic review of the accuracy of diagnostic tests for inguinal lymph node status in vulvar cancer. *Gynecol Oncol*. 2005;99:206–214.

Taylor & Francis
Taylor & Francis Group
http://taylorandfrancis.com

Index

A

ADC, *see* Apparent diffusion coefficient
Adnexal masses, 9
  diagnosis, 9
  GI-RADS, 13, 14
  hydrosalpinx, 10
  imaging for diagnosis of, 13, 15
  indeterminate masses, 15
  logistic regression models, 12
  malignant tumors, 10
  multilocular cyst, 10
  multilocular-solid mass, 15
  ovarian cyst, 9
  ovarian lesion, 9
  ovarian unilocular anechoic simple cyst, 9
  para-ovarian cyst, 10
  pattern recognition, 9–10
  reporting ultrasound findings of, 12–13
  scoring systems, 10
  sequential use of IOTA three-step strategy, 13
  simple rules, 10–12
  3D ultrasound in surface rendering mode, 14
  vascular tree reconstruction of ovarian tumor, 15
ADNEX model, 12
Apparent diffusion coefficient (ADC), 43
Arteriovenous malformation (AVM), 63
Ascites drainage, 68
AVM, *see* Arteriovenous malformation

B

Benign uterine leiomyoma, 39; *see also* Uterine sarcomas
BI-RADS, *see* Breast Imaging, Reporting and Data System
Bladder, 1, 2
Borderline tumors (BOTs), 17–18; *see also* Ovarian malignancies
BOTs, *see* Borderline tumors
Breast Imaging, Reporting and Data System (BI-RADS), 13

C

Cervix, 4, 5
CEUS, *see* Contrast-enhanced ultrasound
CL, *see* Corpus luteum
Computed tomography (CT), 15, 25
  to detect metastatic disease, 65
  for myometrial infiltration assessment, 49
  ovarian cancer spread detection, 25
Contrast-enhanced ultrasound (CEUS), 13
Corpus luteum (CL), 6
Corpus uteri, 4
CT, *see* Computed tomography

D

Diffusion-weighted imaging–magnetic resonance imaging (DWI-MRI), 42
Doppler ultrasound
  for cervical cancer, 54
  in GTD, 65
Drainage, 68–69
DWI-MRI, *see* Diffusion-weighted imaging–magnetic resonance imaging
Dysgerminoma, 20; *see also* Ovarian malignancies

E

Endometrial cancer, 31, 35–36, 46; *see also* Ultrasound assessment of spread of endometrial cancer
  color Doppler interrogation, 34
  color/power Doppler mapping, 33
  endometrial volume and 3D vascular indices calculation, 35
  heterogeneous and thickened endometrium, 33
  ill-defined, thickened endometrium, 36
  in perimenopausal woman, 33
  saline infusion sonohysterography, 35
  serous-papillary adenocarcinoma of endometrium, 32
  staging, 45
  thickened endometrium, 31, 32, 33
  tumor grade, 31
  types, 31
  ultrasound diagnosis of, 31–35
  vascularized endometrium, 34
Endometrial stromal sarcoma (ESS), 39, 40–42; *see also* Uterine sarcomas
Endophytic tumors, 51, 52; *see also* Uterine cervical cancer
EOC, *see* Epithelial ovarian cancer
Epithelial invasive ovarian carcinoma, 18–19, 20; *see also* Ovarian malignancies
Epithelial ovarian cancer (EOC), 19
Epithelioid trophoblastic tumor (ETT), 61
ESS, *see* Endometrial stromal sarcoma
ETT, *see* Epithelioid trophoblastic tumor
Exophytic tumors, 51, 52; *see also* Uterine cervical cancer

F

Fallopian tube, 6
Female pelvis, 1; *see also* Uterus
  bladder, 1, 2
  hypoechoic creeping structure, 2
  iliac vessels, 1
  nonreproductive organs, 1–2
  pelvic vessels, 1
  pelvic wall structures, 1
  recto-sigmoid, 2, 3
  reproductive organs, 1, 3–7
  sonovaginography, 7
Fine needle aspiration biopsy (FNA biopsy), 68
FNA biopsy, *see* Fine needle aspiration biopsy

G

Gestational trophoblastic disease (GTD), 61
  arteriovenous malformation after first-trimester miscarriage, 65
  characteristic blood flow in, 64
  cystic areas, 62
  diagnosis of, 61
  flow velocity waveforms from arcuate artery, 62
  gestational trophoblastic neoplasia, 63
  hydatiform mole, 61–62
  invasive mole, 64
  large cervical lesion, 63
  multicystic avascular sonolucent spaces, 62
  partial mole, 63
  role of Doppler ultrasound in, 65
  role of imaging techniques for assessing, 65
  symptoms, 61
  theca-lutein cysts, 63
  treatment of molar pregnancies, 61
Gestational trophoblastic neoplasia (GTN), 61, 63; *see also* Gestational trophoblastic disease
GI-RADS, *see* Gynecologic Imaging Reporting and Data System
Gordon's method, 46, 47
Granulosa cell tumors, 21; *see also* Ovarian malignancies
GTD, *see* Gestational trophoblastic disease
GTN, *see* Gestational trophoblastic neoplasia
Gynecologic Imaging Reporting and Data System (GI-RADS), 12, 13
  reporting system, 14
Gynecologic oncology, 67
  drainage, 68–69
  fine needle aspiration biopsy, 68
  pelvic lymphocele, 69
  transabdominal ultrasound-guided paracentesis, 69
  Tru-Cut biopsy, 67, 68
  ultrasound-guided procedures, 69

H

hCG, *see* Human chorionic gonadotropin
Human chorionic gonadotropin (hCG), 61
Hydatiform mole, 61–62
Hypoechoic creeping structure, 2

I

IFS, *see* Intraoperative frozen section
IGE, *see* Intraoperative gross examination

Iliac vessels, 1
Indeterminate masses, 15
International Federation of Gynecology and Obstetrics (FIGO), 17, 39
  anatomic staging system, 61
  endometrial cancer staging, 45
  staging for uterine sarcoma, 39
  uterine cervical cancer staging, 51
  vaginal carcinoma staging, 71
  vulva carcinoma staging, 71
International Ovarian Tumor Analysis (IOTA), 9
  sequential use of IOTA three-step strategy, 13
  simple descriptors, 13
  simple rules, 11–12
Intraoperative frozen section (IFS), 45
Intraoperative gross examination (IGE), 45
IOTA, *see* International Ovarian Tumor Analysis

K

Karlsson's method, 45, 46

L

Leiomyosarcoma (LMS), 39–40, 41; *see also* Uterine sarcomas
LMS, *see* Leiomyosarcoma
Logistic models, 12
Lymphoceles, 68

M

Magnetic resonance imaging (MRI), 15, 25
  to detect metastatic disease, 65
  to detect parametrial infiltration in cervical cancer, 55
  to detect spread of ovarian cancer, 25
  for myometrial infiltration assessment, 49
Malignant mixed Müllerian tumor (MMMT), 31; *see also* Endometrial cancer
Malignant struma ovarii, 22
Mesenchymal tumors, 39; *see also* Uterine sarcomas
Metastatic tumors to ovary, 22–23; *see also* Ovarian malignancies
MMMT, *see* Malignant mixed Müllerian tumor
MRI, *see* Magnetic resonance imaging
Multilocular cyst, 10
Multilocular-solid
  mass, 15
  ovarian lesion, 18
  tumor, 18

N

Nabothian cysts, 4
NACT, *see* Neoadjuvant chemotherapy
Neoadjuvant chemotherapy (NACT), 25
Nonepithelial ovarian malignancies, 19–20, 21–22; *see also* Ovarian malignancies
Nonreproductive organs, 1–2; *see also* Female pelvis

O

Ovarian cancer, 25; *see also* Ovarian malignancies
  abundant ascites, 27
  ascites surrounding uterus and tumoral carcinomatosis, 26
  bowel loops trapped within large tumor implants, 28
  carcinomatosis, 26
  computed tomography, 25
  contemporary management of, 25
  cytoreduction, 25
  liver metastases, 29
  lymph node, 28
  magnetic resonance imaging, 25
  metastatic nodule, 26
  omental cake, 28
  pelvic carcinomatosis, 26
  pelvic lymph node, 27
  positron emission tomography, 26
  tumoral implant, 26, 27, 28
  ultrasound, 26–29
Ovarian cyst, 9
Ovarian lesion, 9
Ovarian malignancies, 17; *see also* Ovarian cancer
  adnexal mass, 21
  borderline tumors, 17–18
  dysgerminoma, 20
  granulosa cell tumors, 21
  groups, 17
  immature teratoma, 22
  irregular solid tumor, 21
  metastatic tumors, 22–23
  multilocular-solid adnexal mass, 22
  multilocular-solid ovarian lesion, 18
  multilocular-solid tumor, 18
  nonepithelial ovarian tumors, 21–22
  primary epithelial invasive carcinoma, 18–19, 20
  primary nonepithelial, 19–20
  sertoli cell tumors, 20
  solid adnexal tumor, 20
  solid tumor from ovarian surface, 18
  type II epithelial ovarian cancer, 20
  ultrasound images of metastatic tumors, 23
  unilocular cyst, 19
  unilocular-solid ovarian lesion, 18
Ovary, 5, 6

P

Paracentesis, *see* Ascites drainage
Para-ovarian cyst, 10
Pelvic lymphocele, 69
Pelvic vessels, 1
Pelvic wall structures, 1; *see also* Female pelvis
PET, *see* Positron emission tomography
Placental site trophoblastic tumor (PSTT), 61
Positron emission tomography (PET), 15, 26
Pouch of Douglas, 6
PSTT, *see* Placental site trophoblastic tumor

R

Recto-sigmoid colon, 2, 3
Recto-vaginal septum, 7
Reproductive organs, 1, 3–7; *see also* Female pelvis; Uterus
Risk of Malignancy Index (RMI), 12
RMI, *see* Risk of Malignancy Index

S

Saline infusion sonohysterography, 35
  for assessing myometrial infiltration, 49
Sertoli cell tumors, 20; *see also* Ovarian malignancies
Simple rules (SRs), 10–12
Smooth muscle tumors of uncertain malignant potential (STUMP), 39
Solid tumor, 18
Sonovaginography, 7
SRs, *see* Simple rules
STUMP, *see* Smooth muscle tumors of uncertain malignant potential

T

TDS, *see* Tumor distance to serosa
Three-dimensional ultrasound (3D-US), 13, 49
  for cervical cancer using TUI display, 56
  endometrial volume and 3D vascular indices calculation, 35
  of multilocular-solid mass, 15
  ovarian tumor vascular tree reconstruction, 15
  power Doppler ultrasound, 14
  vaginal carcinoma, 74
3D-US, *see* Three-dimensional ultrasound
Tomographic ultrasound imaging (TUI), 56
Transabdominal ultrasound-guided paracentesis, 69
Transvaginal ultrasound (TVS), 1
  adnexal mass, 10, 20, 21, 22
  arteriovenous malformation after miscarriage, 65
  ascites, 26, 27
  bladder, 2
  blood flow in GTD, 64
  carcinomatosis, 26
  cervical cancer, 52, 53, 55, 56, 57
  cervical stromal infiltration, 54
  cervix, 4, 5, 54
  corpus luteum, 6
  corpus uteri, 4
  cystic areas, 62
  cysts, 9, 10, 19, 63
  endometrial cancer, 32, 33, 46, 48
  endometrial stromal sarcoma, 41, 42
  endometrium, 31, 32, 33, 34, 36
  fallopian tube, 6
  iliac vessels, 1
  inguinal lymphocele drainage, 69
  internal iliac and utero-ovarian vessels, 1
  lesions, 9, 18, 40, 41, 63
  liver metastases, 29
  lymph node, 27, 28, 55
  mass, 40, 41, 42, 43, 47
  melanoma from vagina, 75
  mole, 63, 64
  myometrial infiltration, 46, 47, 48
  nodule, 26, 73
  omental cake, 28
  ovarian carcinomas, 20
  ovary, 5, 6
  parametrial infiltration in cervical cancer, 55
  pelvic carcinomatosis, 26
  pelvic lymphocele, 69
  pouch of Douglas with free fluid, 6

recto-sigmoid colon, 3
recto-vaginal septum, 7
teratoma, 22
trapped bowel loops, 28
Tru-Cut needle passing through cystic-solid lesion, 67
tumor, 18, 21
tumoral implants, 27, 28
uterine arteries, 2
uterine leiomyosarcoma, 41
uterus, 2, 3, 5
for vaginal bleeding, 32
vaginal carcinoma, 76
vascularization, 41
Tru-Cut biopsy, 67
two tissue cylinders obtained after, 68
TUI, *see* Tomographic ultrasound imaging
Tumor distance to serosa (TDS), 49
TVS, *see* Transvaginal ultrasound
Two dimenssional ultrasound, 14

U

UAs, *see* Uterine arteries
Ultrasonography, 27; *see also* Transvaginal ultrasound
adnexal mass diagnosis by, 9
advantage, 69
to detect ovarian cancer spread, 29
diagnosis of endometrial cancer, 31–35
EES, 40
endometrial cancer, 35–36, 49
gestational trophoblastic disease, 61
images from metastatic tumors, 23
IOTA simple rules, 11–12
myometrial and cervical infiltration assessment, 45
3D ultrasound, 13, 15
treatment response assessment, 57
tumor spread assessment, 26–29
2D ultrasound, 14
uterine cervical cancer, 51–52
uterine LMS, 39
uterine sarcomas, 39
in vaginal cancer, 73–76
in vulvar cancer, 71–73
Ultrasound, 9
Ultrasound assessment of spread of endometrial cancer, 45
cervical involvement, 48
endometrial lesion, 46
imaging techniques, 49
intracavitary myoma, 47
myometrial infiltration, 48
myometrial infiltration assessment, 45, 46, 47
staging of endometrial cancer, 45
2D ultrasound, 45–49
3D ultrasound, 49
Ultrasound-guided procedures, 67, 69
for drainage, 68–69
fine needle aspiration biopsy, 68
transabdominal ultrasound-guided paracentesis, 69
Tru-Cut biopsy, 67, 68
Unilocular anechoic ovarian simple cyst, 9
Unilocular cyst, 19
Unilocular-solid ovarian lesion, 18
Uterine arteries (UAs), 2
Uterine cervical cancer, 51–52
bladder and rectum in, 55
cervical carcinoma, 52
cervical stromal infiltration, 54
cervix, 54
diagnostic performance of TVS and MRI, 55
Doppler findings in, 54
growth pattern, 51
irregular and hypoechoic lesion, 53
isoechoic cervical cancer, 53
lymph node assessment, 55
parametrial infiltration, 53–56
spread assessment, 52
staging, 51
3D ultrasound, 56
treatment response assessment, 57
tumor and stromal invasion, 52
Uterine sarcomas, 39
EES, 40–42
endometrial stromal sarcoma, 41, 42
ill-defined uterine mass, 40, 42
imaging for diagnosis of, 42–43
intracavitary lesion, 41
intracavitary mass, 43
pelvic mass with cystic areas, 40
uterine LMS, 39–40, 41
uterine mass, 41
vascularization, 41
Uterine vessels, 1
Utero-ovarian vessels, 1
Uterus, 3; *see also* Female pelvis
cervical canal, 4
endometrium, 3
fallopian tube, 6
in longitudinal plane, 2, 3
myometrium, 3
nabothian cysts, 4
ovaries, 5, 6
in postmenopausal woman, 5
pouch of Douglas with free fluid, 6

V

Vaginal cancer, 71
carcinoma staging, 71
FIGO staging of, 71
melanoma from vagina, 75
nodule from vaginal wall, 76
role of ultrasound in, 73–76
solid irregular nodule in vaginal cuff, 73
3D ultrasound, 74
Vulvar cancer, 71
carcinoma staging, 71
FIGO staging of, 71
fine needle aspiration from lymph node in, 72
inguinal ultrasound, 72
role of ultrasound in, 71–73
ultrasound evaluation of, 72

W

WHO, *see* World Health Organization
World Health Organization (WHO), 17, 39

Taylor & Francis
Taylor & Francis Group
http://taylorandfrancis.com